



Université de Liège – Académie Wallonie-Europe
Faculté des Sciences

Io's interaction with Jupiter's magnetosphere

Dissertation présentée par

Vincent Dols

en vue de l'obtention du grade

de
Docteur en Sciences

Année Académique 2011-2012

“Je commence à y croire”

Anonymous

REMERCIEMENTS

Ce travail est une étape d'un long périple. Il a débuté en 1990 avec Jean-Claude Gérard et l'analyse des premières images ultraviolettes des aurores de Jupiter prises par le Télescope Spatial Hubble. L' idée d'utiliser la camera FOC, qui n'était pas destinée à de telles observations, était ingénieuse. Longtemps après, elle m'impressionne toujours. Ces premières images ont initié une longue série d'observations des aurores à l'aide d'instruments de plus en plus sophistiqués. Depuis, j'ai retrouvé Jean-Claude avec grand plaisir au cours des innombrables conférences auxquelles il participe, toujours plein d'humour, toujours à la pointe de la recherche.

Le travail présenté dans cette thèse doit tout à Fran Bagenal et Peter Delamere. Peter, toujours disponible, à la créativité scientifique prodigieuse; Fran, son dynamisme légendaire, sa connaissance profonde du sujet et de son développement historique. Qu' ils sachent combien je leur suis reconnaissant.

Finalement, également très important, je remercie Nisou sans qui ce travail n'aurait jamais commencé, et bien sur Cécile, experte en tout, sans qui ce travail n'aurait pu être achevé.

Je remercie également les membres de mon jury, Denis Grodent, Viviane Pierrard et Francois Leblanc qui ont accepté de consacrer un peu de leur temps à la réalisation de ce projet.

RÉSUMÉ

Io, le premier satellite Galiléen de Jupiter, est le corps le plus volcanique du système solaire. Ce volcanisme alimente une atmosphère ténue, composée principalement d'atomes de soufre et d'oxygène et de molécules de SO₂. Cette atmosphère est constamment bombardée par les ions et électrons qui sont en co-rotation avec le champ magnétique de Jupiter. Ce bombardement produit de nouveaux ions et perturbe localement le champ magnétique. Cette perturbation est la cause première des émissions aurorales observées dans la haute atmosphère de Jupiter, au pied du tube de flux magnétique d'Io.

La sonde spatiale Galiléo a survolé Io à basse altitude (une centaine de kilomètres) à cinq reprises entre 1996 et 2001. Elle a fait des mesures des propriétés du plasma et du champ magnétique qui ont révélé la complexité de l'interaction entre Io et de Jupiter.

Cette interaction a été modélisée à maintes reprises dans le passé par des approches complémentaires, chacune éclairant le problème d'une lumière neuve, mais chacune se basant sur des simplifications qui limitent la portée des résultats proposés. Les modèles magnéto-hydrodynamiques (*Linker et al., 1998*) sont basés sur une paramétrisation a priori de l'ionisation de l'atmosphère. De plus, ils ne considèrent qu'un seul constituant représentatif de l'atmosphère d'Io et du plasma environnant, généralement un mélange d'atomes de soufre et d'oxygène. Les modèles dits "à deux fluides" (*Saur et al., 1999*) calculent très précisément l'ionisation et les collisions dans l'atmosphère d'Io mais reposent sur l'hypothèse d'un champ magnétique non-perturbé par l'interaction, ce qui limite la cohérence du modèle et peut introduire des erreurs quantitatives importantes.

Le travail que nous proposons combine un modèle de l'interaction chimique dans l'atmosphère d'Io et un modèle de l'interaction électro-magnétique. Le modèle chimique inclut les principaux constituants du plasma et de l'atmosphère; le modèle "Hall-hydro-magnétique" calcule les perturbations du flot de plasma et du champ magnétique. Ce modèle couplé permet de calculer les propriétés du plasma et les perturbations du flot et du champ magnétique de façon cohérente et de les comparer aux mesures de Galiléo.

ABSTRACT

Io, the innermost Galilean moon of Jupiter, is the most volcanic body of the solar system. This volcanism is responsible for a tenuous atmosphere composed mainly of S, O and SO₂. This atmosphere is constantly bombarded by the plasma that co-rotates with the magnetic field of Jupiter, producing new ions and perturbing locally the magnetic field. This local perturbation is responsible for auroral emissions in the atmosphere of Jupiter, at the foot of Io's flux tube.

The spacecraft Galileo made five flybys of Io between 1995 and 2001 at very low altitude (~100's km) and made plasma and magnetic field measurements that reveal the complexity of Io's interaction with Jupiter.

Past studies have tackled the modeling of this interaction using different complementary approaches, each shedding a new light on the issue but each involving some simplifications. The MHD models (*Linker et al., 1998*) are based on an a priori parameterization of the ionization in the atmosphere, generally assuming spherical symmetry and a single atmospheric and plasma species (representative of O and S). They ignore the important effect of the cooling of electrons as well as the multi-species composition of both the plasma and the atmosphere. The two-fluid approach (*Saur et al., 1999*) computes precisely the ionization and collisions in the atmosphere of Io but make the assumption of a constant magnetic field, limiting the self-consistency of the model and potentially introducing large quantitative errors.

We combine a multi-species chemistry model of the interaction that includes atomic and molecular species with a self-consistent Hall-MHD calculation of the flow and magnetic perturbation to model as self-consistently as possible the plasma variables along the different flybys of Io by the Galileo probe.

CONTENTS

1. INTRODUCTION	1
1.1 CONTEXT	1
1.2 WHY STUDY IO?	3
1.3 CONTRIBUTION OF THIS WORK	5
1.4 HOW THE THESIS IS ORGANIZED	6
2. IO IN THE JOVIAN MAGNETOSPHERE	7
2.1 JUPITER'S MAGNETIC FIELD, IO TORUS AND GIANT NEUTRAL CLOUDS.	7
2.2 THE LOCAL INTERACTION OF IO'S ATMOSPHERE WITH THE PLASMA TORUS	11
3. THE ATMOSPHERE OF IO	16
3.1 SULFUR AND OXYGEN ATOMIC CORONA	16
3.2 THE SO ₂ ATMOSPHERE	17
3.2.1 Geographic distribution of the SO ₂ atmosphere	18
3.2.2 Sustaining the atmosphere: direct volcanism or frost sublimation?	19
3.2.3 Radial distribution of SO ₂	21
3.3 OTHER ATMOSPHERIC COMPONENTS	23
4. GALILEO DATA	25
4.1 GALILEO FLYBYS OF IO	25
4.2 THE PLS AND PWS INSTRUMENTS	28
4.3 PLASMA DENSITY AND TEMPERATURE	28
4.4 OTHER PLASMA PROPERTIES	29
4.5 SUMMARY	30
5. PREVIOUS MODELS	34
5.1 MHD MODELS	34
5.2 TWO-FLUID MODEL (ELECTRON + SO ₂ ⁺)	37
5.3 HYBRID MODELS	39
6. OUR MODEL	40
6.1 THE MULTI-SPECIES CHEMICAL MODEL	40
6.1.1 Summary of the modeling of the J0 flyby in Dols et al. [2008]	43
6.2 THE HALL-MHD MODEL	68
6.2.1 Hall-MHD equations	68
6.2.2 Simulation parameters and code numerical scheme	70
6.2.3 Features of the Hall-MHD code	72

6.3	THE COUPLED MODEL	80
6.3.1	<i>Importance of including the electron cooling.</i>	80
6.3.2	<i>Importance of multi-species for temperature calculation</i>	83
6.3.3	<i>Limitation of our own Hall-MHD model</i>	83
6.3.4	<i>Coupling</i>	84
7.	ATMOSPHERIC SCENARIOS	85
8.	ATOMIC ATMOSPHERE: "KK-S&O"	86
8.1	<i>THE J0 FLYBY IN IO 'S WAKE</i>	86
8.2	<i>THE I24 FLYBY, UPSTREAM OF IO</i>	92
8.3	<i>THE I27 FLYBY, ON THE ANTI-JOVIAN FLANK</i>	96
8.4	<i>THE I31 FLYBY, ABOVE THE NORTH POLE</i>	100
8.5	<i>THE I32 FLYBY, UNDER THE SOUTH POLE</i>	104
8.6	<i>CONFIRMING THE EXISTENCE OF AN INDUCED DIPOLE AT IO.</i>	108
8.6.1	<i>Induced dipole for I24 and I27</i>	108
8.6.2	<i>Induced dipole for I31</i>	112
8.7	<i>SUMMARY OF THE" KK-S&O" ATMOSPHERE</i>	114
9.	A MULTI-SPECIES ATMOSPHERE	115
9.1	<i>AN ATOMIC CORONA (CORONA-S&O)</i>	117
9.2	<i>THE SO₂ ATMOSPHERE (ATM-SO₂)</i>	121
9.2.1	<i>Radial distribution</i>	121
9.2.2	<i>Latitudinal distribution</i>	122
9.3	<i>AN SO₂ CORONA (CORONA-SO₂)</i>	127
10.	DISCUSSION	133
10.1	<i>THE J0 FLYBY. GLOBAL RESULTS.</i>	133
10.2	<i>THE O1356 Å EMISSION</i>	135
10.3	<i>I27 AND I31: PROBLEMATIC FLYBYS</i>	138
10.4	<i>ATMOSPHERIC COMPOSITION</i>	140
10.5	<i>DAY/NIGHT ASYMMETRY OF IO'S ATMOSPHERE</i>	145
10.6	<i>LONGITUDINAL ASYMMETRY OF IO'S ATMOSPHERE</i>	147
10.7	<i>TIME VARIABILITY</i>	149
11.	CONCLUSIONS	155
	BIBLIOGRAPHY	158

LIST OF TABLES

Table 1: Parameters of the flybys. (1) Local time indicates the location of Io on its orbit around Jupiter. At 09:00 LT, Io is at its largest Eastern elongation (on the left of Jupiter see Figure 14) (2) Altitude and longitude at closest approach..... 27

Table 2: The two scenarios tested in the next sections: the atomic atmosphere KK-O&S and a multi-species atmosphere that includes three components..... 85

Table 3: Global results with plasma conditions typical of the J0 flyby. 134

Table 4: Mixing ratio of different ion species at the closest approach on J0 flyby for different atmosphere scenarios, compared to the published composition of Frank et al. [1996]. 142

LIST OF FIGURES

Figure 1: Left: a Galileo image of Io showing two of the many active volcanoes. Regions close to the right limb are covered with SO₂ frost, resulting from the condensation of atmospheric SO₂ at the low surface temperature. Right: the volcanic plumes of Tsvashtar, close to the north pole of Io observed by New Horizons en route to Pluto. 2

Figure 2: The structure of the inner magnetosphere of Jupiter and the Galilean satellites. The field lines of Jupiter are represented in green. Io is located at the left of Jupiter, embedded in a dark red annulus called the Io plasma torus. The magnetic flux tube crossing Io is represented in purple. Close to the foot of this flux tube, the UV cameras onboard the Hubble space telescope detected a specific auroral emission equatorward of the main aurora, structured as a spot (or multi-spots) followed by a long auroral tail (insert bottom left). Credit: John Spencer (SWRI) as shown by Clarke et al. [2002]. 3

Figure 3: The magnetosphere of Jupiter. Io is embedded in the inner part of the magnetosphere, where the field is mainly dipolar. The dipole moment of Jupiter is tilted by $\sim 10^\circ$ relative to the rotation axis. The field rotates with Jupiter in ~ 10 hours. 8

Figure 4: Left: the torus density and some of the Galileo flybys. Right: the composition of the plasma in the cold and warm torus. 9

Figure 5: Left: a vertical section with the giant cloud in Io's orbital plane while the torus lies approximately in the magnetic equator and wobbles around Io with the ~ 10 hour period. Right: the giant cloud seen from above is centered on Io but extends many R_J along Io's orbit. 10

Figure 6: The interaction of torus electrons and ions of the plasma torus with the atmospheric corona of Io. The electron-impact ionization and the charge exchange of a torus ion with an Io neutral create a new ion that is carried by the flow and starts a gyromotion at the local flow velocity, in a process called pickup. 12

Figure 7: Left: the slowing of the flow close to Io creates a perturbation of the background field line that propagates along the field line as Alfvén waves. The combined motion of the Alfvén wave along the field line and the flow creates a stationary structure downstream of Io called the Alfvén wing. A current flows from Io to Jupiter along these Alfvén wings. Right: The plasma flow is diverted around the whole Alfvén tube that extends to the ionospheres of Jupiter. 13

Figure 8: View of Io from above, Jupiter is on the right of the figure in the Y direction while the plasma impinges Io in the X direction. The Galileo flybys are represented as solid lines and the gray shading along the trajectories highlights the location of detection of field-aligned electron beams. The line segments represent the direction of the flow, diverted around the Alfvén tube (B. Paterson, private communication, 2009). 15

Figure 9: UV brightness radial profile of oxygen and sulfur lines observed with the STIS spectrometer onboard the Hubble Space Telescope (Wolven et al., 2001). The right top insert shows the location of Io on its orbit at the time of the observation; the left insert shows the aperture position. This observation confirms the presence of an extended thin atomic corona around Io. 17

Figure 10: Map of the vertical column density of atmospheric SO₂ in Io's atmosphere, inferred from the Lyman-alpha observations of Feaga et al. [2009]. Io's rotation is phase-locked with its orbital rotation so the same hemisphere always faces Jupiter. The anti-jovian hemisphere spans Io's longitudes from 90 to 270°. The atmosphere is concentrated around the equator. It is denser and more extended in latitude on the anti-Jovian side of Io. 19

Figure 11: SO₂ density vertical profile in daylight (plain line and squares) and in eclipse (dashed line and squares) modeled by Walker et al. [2010] for a sublimation-sustained atmosphere. The atmosphere is very dense close to the surface and the whole column collapses during eclipse. 22

Figure 12: Structures of the Na clouds. Right: the jets, stream and banana cloud as seen from above Jupiter. Top left: The giant nebula. 23

Figure 13: Trajectories of the Galileo flybys in the XY plane. The night-side is shaded in black. 26

Figure 14: Left: trajectories of the flybys in the YZ plane. Right: location of Io on its orbit (Local time) for each flyby. The night-time hemisphere is shaded in black. 27

Figure 15: Trajectory of the J0 flyby and its plasma observations (Bagenal, 1997) 31

Figure 16: The plasma density inferred from PLS and PWS measurements for each flyby. CA represents the closest approach. 32

Figure 17: Ion average temperature determined from PLS measurements for each flyby. CA indicates the closest approach. 33

Figure 18: Simulation of Linker et al. [1998]. Left from top to bottom: Plasma density and speed in Io's equatorial plane. Axes are in R_{Io} and the flow enters the simulation domain from the left side. Right: The plasma properties along the J0 flyby. The blue lines represent the observations and the red the model results. From top to bottom: the magnetic field, the plasma density, the plasma speed and the plasma temperature. 36

Figure 19: Electron flow lines in the equatorial plane of Io of Saur et al. [1999]. Because of the Hall conductivity in the dense ionosphere of Io, the flow of the electron is strongly twisted towards Jupiter. 38

Figure 20: The plasma density, ion temperature and pressure from observations along J0 (plain lines) and the model results (with dots). Note the empty wake in the model results. 39

Figure 21: Concept of the multi-species chemical model in Io's equatorial plane. The insert in the lower right corner recalls that the flow is diverted all along the Alfvén tube. 41

Figure 22: Illustration of the evolution of the composition and temperature (average ion energy) of the plasma flowing along a flow line on the flanks of Io in a multi-species atmosphere. 42

Figure 23: Physical chemistry reactions of the multi-species chemical model. 43

Figure 24: Whistler phase velocity, v_{ph} , for different wavelengths. The grid resolution selects what wavelength can be propagated in the code and the time step has to be defined accordingly to fulfill the Courant condition..... 72

Figure 25: A vertical cut through the Alfvén wing. The background jovian magnetic is parallel to Z, the flow comes from the left. Left: the speed of the plasma. Right: the magnetic perturbation in the X direction. The white solid line is the Alfvén characteristic, the white dashed line is the slow mode characteristic. 73

Figure 26: Propagation of the slow magnetosonic mode that forms a wing aligned with the slow mode characteristic (dashed line). For comparison, we have added the Alfvén mode characteristic (solid line). 75

Figure 27: Illustration of the Hall effect. Top: The flow of ions. Bottom: The electron flow lines. Initially, both electrons and ions started on the same flow lines but the Hall effect in the atmosphere of Io deflects the electrons more strongly towards Jupiter..... 76

Figure 28: A cut in the equatorial plane (XY). The magnetic field of Jupiter points into the page, the torus plasma enters the domain in $X=-3 R_{Io}$ and flows in the X direction. Left: The plasma density. Right: the ion temperature. 77

Figure 29: Vertical component of the magnetic field in the equatorial XY plane, where the background magnetic field of Jupiter points into the page and the torus plasma enters the domain from left to right. The field is compressed upstream of Io and depressed in the wake..... 78

Figure 30: Current through Io. Left: J_z in a vertical plan YZ, showing the vertical currents on the flanks of the Alfvén tube. Right: horizontal current J_y in the vertical XZ plane..... 79

Figure 31: Sketch of the current system in the Alfvén wing..... 79

Figure 32: Reaction rate coefficient K for ionization of S, O and SO₂ and SO₂ dissociation. 81

Figure 33: Ionization rate in Io's equatorial plane for an atmosphere composed of 1) Left: S and O. 2) Right: SO₂ only. Note that the scales of the ionization rates are different. The ionization rate is lower and more upstream for the SO₂ atmosphere because of the cooling of electrons, shown in the lower panels. 82

Figure 34: The plasma characteristics calculated with the chemical model in the XY plane parallel to Io's equatorial plane at distance $Z \sim -0.26 R_{Io}$. The dashed line represents the J0 trajectory. A) Plasma density. B) Neutral density. The night-side hemisphere is shaded in gray C) Flow speed extracted from the MHD simulation. D) Average ion temperature. 88

Figure 35: J0 flyby. Velocity and magnetic field perturbations. Black lines=observations, red lines= MHD model results..... 89

Figure 36: Plasma properties along the J0 flyby. The thin black lines represent the observations. For the plasma density, the solid black line is the PWS observations, the dashed one is PLS. The colored lines are the model results. A) speed, B) magnetic field strength. C) plasma density computed with the MHD model. D) ion temperature

calculated by the MHD model. E) plasma density calculated with the Chemical model. F) Average ion temperature calculated by the chemical model.	91
Figure 37: The I24 flyby (dashed line) in the XY plane parallel to Io's equatorial equator at $Z \sim 0.1 R_{Io}$	92
Figure 38: I24 flyby. Velocity and magnetic field perturbations from the MHD model. Observations in black, MHD results in red.	93
Figure 39: The I24 flyby, upstream of Io: Plasma characteristics. The observations are the black thin lines, the MHD results are in red, the chemical model results in blue.	95
Figure 40: The I27 flyby (dashed line) and plasma characteristics in the XY plane parallel to the equatorial plane at $Z \sim 0.4 R_{Io}$, calculated by the chemical model.	96
Figure 41: The I27 flyby, on the anti-jovian flank. Velocity and magnetic field perturbations.	97
Figure 42: The I27 flyby. Plasma characteristics. Black=observations, red= MHD results, Blue= Chemical model results.	99
Figure 43: The 31 flyby (dashed line) above the north pole. Plasma characteristics in the XY plane parallel to Io's equator at $Z \sim 1.1 R_{Io}$	100
Figure 44: The 31 flyby: Velocity and magnetic field perturbations. The observations are in black, the MHD results in red.	101
Figure 45: The 31 flyby: Plasma characteristics. Black=observations, red= MHD results, Blue= Chemical model results.	103
Figure 46: The I32 flyby (dashed line), under the south pole. Plasma properties calculated by the chemical model in the XY plane parallel to Io's equator at $Z \sim -1.1 R_{Io}$	104
Figure 47: The I32 flyby. Velocity and magnetic field perturbations. The observations are in black, the MHD results in red.	105
Figure 48: The 32 flyby. Plasma characteristics. Black=observations, red= MHD results, Blue= chemical model results.	107
Figure 49: Components of the magnetic perturbation at Io during the I24 flyby. Black is the observations, red is the modeled plasma, green is the prescribed induced dipole and blue is the combination of the modeled plasma interaction and the induced dipole.	110
Figure 50: Components of the magnetic perturbation at Io during the I27 flyby. Black is the observations, red is the modeled plasma, green is the prescribed induced dipole and blue is the combination of the modeled plasma interaction and the induced dipole.	111
Figure 51: Components of the magnetic perturbation at Io during the I27 flyby. black is the observations, red is the modeled plasma, green is the prescribed induced dipole and blue is the combination of the modeled plasma interaction and the induced dipole.	113

<i>Figure 52: The different components of the multi-species atmosphere. Top: the radial profile. For comparison we added the profile of the atomic “KK-S&O” atmosphere of the previous chapter. Bottom left: A meridian section of the lower atmosphere based on the Walker et al. [2010] model. Bottom right: a meridian section of the “Atm-SO₂ “ component.</i>	116
<i>Figure 53: Electron density and average ion temperature calculated with the chemical model along each flyby. Note that the figure is split over two pages.</i>	120
<i>Figure 54: Latitudinal variation of surface density of the KK-S&O and Atm-SO₂ atmospheres.</i>	122
<i>Figure 55: Electron density and average ion temperature calculated with the chemical model along each flyby for the “Atm-SO₂ “ atmospheric component. Note that this figure is split over two pages.</i>	125
<i>Figure 56: Comparison of the SO₂⁺ density along J0 inferred from ion cyclotron wave observation (dashed black) with the density calculated for different atmosphere scenarios (red line): Left: “Atm-SO₂” without SO₂ corona. Right: “Corona-SO₂.”</i>	127
<i>Figure 57: Electron density and average ion temperature calculated with the chemical model along each flyby for the “Corona-SO₂” atmospheric component. Note that this figure is split over two pages.</i>	130
<i>Figure 58: The exponential SO₂-corona. Top: the SO₂⁺ density along J0 compared to the density inferred from ion cyclotron wave detection. Bottom: the plasma properties along I32</i>	132
<i>Figure 59: Left: OI (1356 Å) auroral emissions observed by the STIS camera onboard the Hubble space telescope (Retherford [2002]). Right: simulation of these auroral emissions by Saur et al. [2000].</i>	136
<i>Figure 60. Right: the OI (1356 Å) volumic emission rate calculated with the chemical model. This emission is localized upstream of Io. Left: The brightness, integrated along the line of sight along the X axis, in Rayleighs. The emission follows the observed profile of Wolven et al. [2001] (dotted line, valid from 4 to 1.4 R_{Io}) and peaks at ~ 0.3 R_{Io} from Io’s surface.</i>	137
<i>Figure 61: The ion temperature along I31 for different rotations of the trajectory around the X axis.</i>	139
<i>Figure 62: Mixing ratio at CA on J0 for different atmospheric scenarios listed in the bottom right panel.</i>	143
<i>Figure 63: Two SO₂⁺ ions impinging on an SO₂ atmosphere of Io. They experience a cascade of charge exchange where fast neutrals are ejected on straight paths, away from Io (Fleshman, 2011).</i>	148
<i>Figure 64: The comparison of the I27 and J0 flyby. Their trajectories intersect on the downstream anti-jovian hemisphere, although not at the Z altitude relative to Io’s equatorial plane. On the bottom panels, we compare the observed plasma density and temperatures (dashed-star lines) with the model results (solid lines) for the “Atm-SO₂ + Corona-S&O” scenario.</i>	152

1. INTRODUCTION

In this introduction, we wish to motivate our work. We place it in the context of previous modeling of Io's interaction with Jupiter's magnetic field as well as in the context of available observations of Io.

1.1 Context

Io, the innermost Galilean moon of Jupiter, orbits at a distance ~ 6 Jovian radii ($R_J = 71,492$ km) from the planet. Its size is comparable to our inert Moon ($R_{Io} = 1821$ km), so it is rather surprising to discover that Io is the most volcanic body of the solar system, thanks to intense tidal heating caused by the combined gravitational pull of Jupiter and the other Galilean satellites. Io's surface is covered with active volcanic vents releasing plumes of mainly SO_2 molecules. The volcanic activity is very variable, the larger plumes can reach 100's of km in height as illustrated in Figure 1 by the unexpected and spectacular eruption of Tsvastar during the New Horizons flyby (*Spencer et al., 2007*). These plumes are ultimately the source of a tenuous atmosphere bound to Io, a neutral corona that extends farther away, to $\sim 6 R_{Io}$, and giant neutral clouds that extend to several R_J along Io's orbit. These atmosphere/corona/cloud feed a giant torus of S and O ions that encircles Jupiter at Io's orbit and co-rotates with the magnetic field of Jupiter with a period ~ 10 hours (Figure 2). As Io's orbital period is much longer (~ 42 hours), Io's atmosphere is constantly bombarded by the torus plasma at a relative velocity of ~ 57 km/s, which provides further electron impact ionization. Through a series of complex processes, Io stands as the main plasma source of Jupiter's inner magnetosphere, with an ion supply rate of $\sim 0.5-1$ ton/s. This large plasma supply is an important driver of the Jovian magnetosphere dynamics, which results, for example, in the main auroral emissions in Jupiter's upper atmosphere (Figure 2). This is unlike the Earth where the magnetospheric plasma supply and dynamics are dominated by the solar wind and ionospheric plasmas and by the interplanetary magnetic field.

Galileo Images:

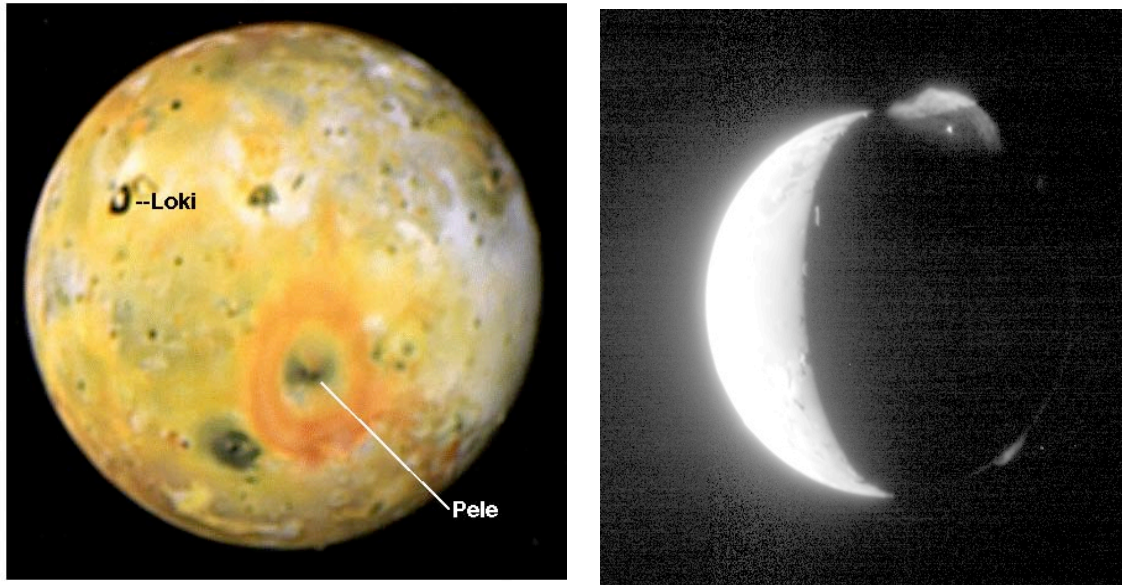


Figure 1: Left: a Galileo image of Io showing two of the many active volcanoes. Regions close to the right limb are covered with SO_2 frost, resulting from the condensation of atmospheric SO_2 at the low surface temperature. Right: the volcanic plumes of Tvashtar, close to the north pole of Io observed by New Horizons en route to Pluto.

The first evidence of a strong electromagnetic coupling between Io and Jupiter was the detection of decametric radio emissions from Jupiter, controlled by Io's location on its orbit (Bigg, 1964). This interaction was later spectacularly illustrated by the discovery of ultraviolet and infrared auroral emissions in the Jovian upper atmosphere, called the Io spot, located approximately at the foot of Jupiter field lines crossing Io (Clarke et al., 1996; Connerney and Satoh, 2000). Figure 2 shows an example of the Io spot, approximately 10° equatorward of the main auroral oval, followed by a long auroral tail that extends more than 100° from Io.

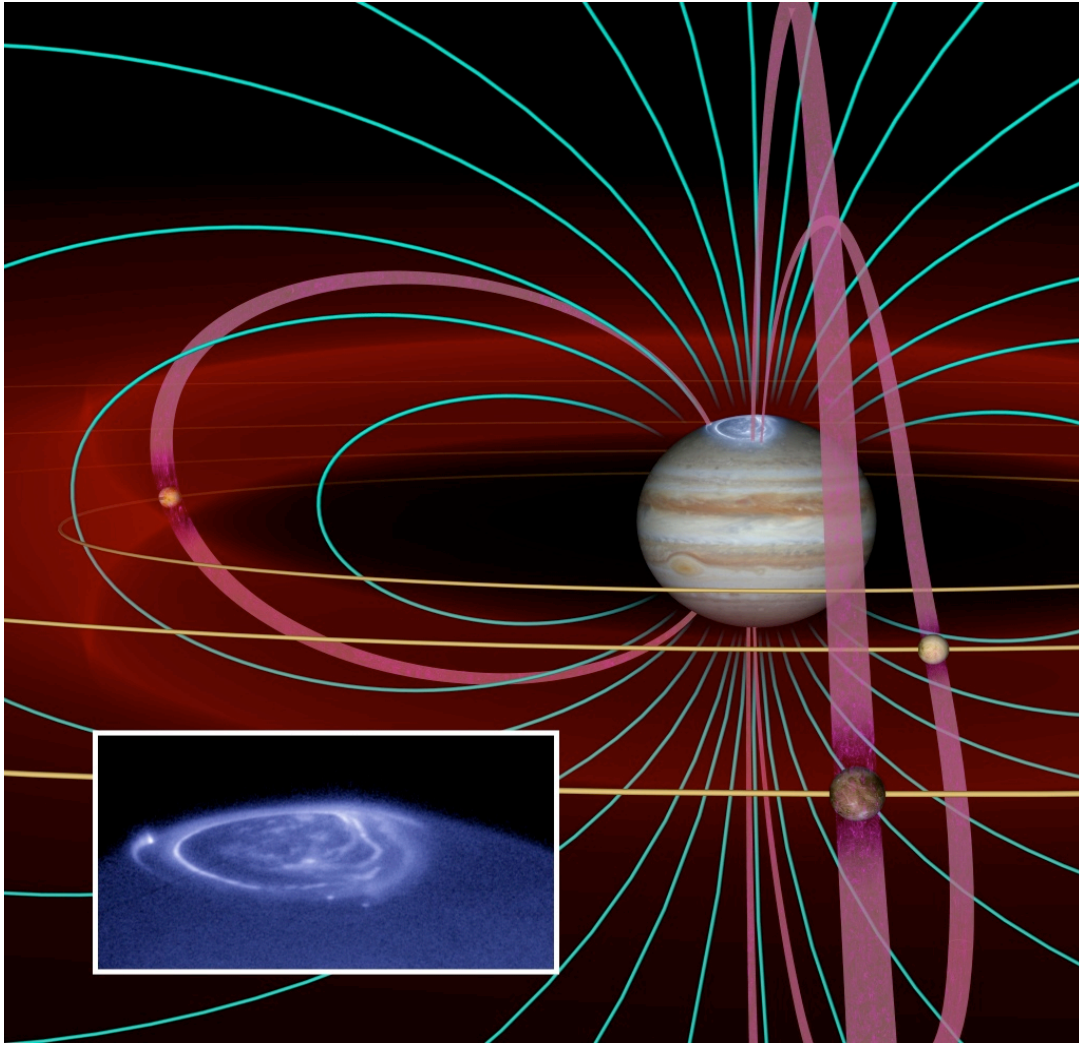


Figure 2: The structure of the inner magnetosphere of Jupiter and the Galilean satellites. The field lines of Jupiter are represented in green. Io is located at the left of Jupiter, embedded in a dark red annulus called the Io plasma torus. The magnetic flux tube crossing Io is represented in purple. Close to the foot of this flux tube, the UV cameras onboard the Hubble space telescope detected a specific auroral emission equatorward of the main aurora, structured as a spot (or multi-spots) followed by a long auroral tail (insert bottom left). Credit: John Spencer (SWRI) as shown by Clarke et al. [2002].

1.2 Why study Io?

Io's interaction is the prime example of the interaction of a moon with a tenuous atmosphere embedded in the magnetic field of a planet. Europa and Ganymede in Jupiter's magnetosphere, Enceladus and Titan in Saturn's magnetosphere are further applications of principles born from the study of Io. Io's interaction is also relatively well

constrained by in-situ measurements of the moon and its vicinity made by a series of probes (Pioneer 10 in 1975, Voyager 1 and 2 in 1979, Galileo (GLL) between 1996 and 2001) as well as remote observations by Earth or space-based telescopes and by the Cassini and New Horizons probes, in 2001 and 2007 respectively.

The study of the interaction is an interdisciplinary problem, which involves volcanology, surface chemistry, aeronomy and plasma physics in its full complexity. The first analytical models of Io's electromagnetic interaction with Jupiter, triggered by the discovery of Io-related radio emissions, can be traced back to *Piddington and Drake [1968]*, *Goldreich and Lynden-Bell [1969]* and *Goertz and Deift [1973]* to name just a few. The space probe Voyager 1 flew close to Io in 1979, and the discovery of Io's intense volcanic activity as well as its dense plasma torus triggered new modeling efforts by *Goertz [1980]* and *Neubauer [1980]*. Between 1996 and 2001, the Galileo probe made 5 flybys very close to Io at altitudes ranging from 100 km to 900 km (named J0, I24, I27, I31 and I32, based on the orbit number of Galileo around Jupiter). The plasma instruments and magnetometer provided detailed surprising observations that helped constrain the models. The most recent numerical models have tackled Io's local interaction using different complementary approaches, each providing important new insights of the interaction but also involving some important simplifications (see Chapter 4). The Magneto-HydroDynamic models (MHD) (*Linker et al., 1988*; *Combi et al., 1998*; *Khurana et al., 2011*) do not calculate the ionization around Io but prescribe its rate and location assuming a spherical symmetry and a single species (an average mass of O and S ~ 20 amu). Consequently, they ignore the important effect of the cooling of electrons in the atmosphere of Io, which limits the ionization of Io's neutral atmosphere. They also ignore the multi-species nature of the interaction, which changes the plasma composition and affects the plasma temperature close to Io. *Saur et al. [1999]* proposed a sophisticated two-fluid approach (electrons and one type of ion SO_2^+) with a detailed computation of the electric conductivity in Io's atmosphere but assumed an unperturbed magnetic field. The magnetic perturbation is an important aspect of the interaction and this assumption limits the self-consistency of their approach, leading to a possible $\sim 30\%$ error in the results (*Saur, private communication, 2011*). Finally, *Lipatov and Combi [2006]* published the first hybrid simulation (fluid electrons and single ions) of the interaction assuming an unrealistic ion mass to circumvent numerical limitations. Their results are difficult to interpret in terms of the real Io interaction.

In summary, a large data set of observations and multiple numerical models provide a good understanding of Io's local interaction but the difficulty of the data analysis (the remote observations of Io's atmosphere described in Chapter 3, and the plasma observation of Galileo reviewed in Chapter 4) and the limitations of current models keep a number of issues unresolved: to list a few, the atmospheric composition and distribution, the asymmetry of the interaction, the role of electron beams in the ionization and auroral emissions in Io's atmosphere, as well as the process of neutral escape from Io. This dissertation contributes to the effort of improving the numerical modeling of Io's local interaction.

1.3 Contribution of this work

In this thesis, we propose the most complete description of the Io/Jupiter local interaction to date. We combine a multi-species chemistry model of the interaction that includes atomic and molecular species (*Dols et al., 2008*) with a Hall-Magneto-HydroDynamic (Hall-MHD) calculation of the flow and magnetic perturbation. We then model, as self-consistently as possible, the plasma properties (plasma density, ion average temperature, composition, velocity, magnetic perturbation) along the Galileo flybys of Io. Currently, only 3 flybys (J0, I24, I27) have been modeled in the published literature, all close to the equatorial plane of Io (*Linker et al., 1998, Combi et al., 1998; Kabin et al., 2001, Saur et al., 1999; Saur et al., 2002; Khurana et al., 2011*). We will include the flybys above the poles (I31 and I32) to model the complete set of Galileo observations.

With this coupled model, we improve on the limitations of single-species, ionization-prescribed MHD and two-fluid models available so far. We run sensitivity experiments with different assumptions about the atmosphere/corona composition and distribution and compare to the observations. Although the proposed model is still a work in progress and has its own limitations, it illustrates the shortcomings of former models, confirms the existence of an induced dipole at Io, constrains the neutral corona distribution, shines a new light on the inaccuracies of the data analysis currently published and defines the questions that need to be resolved in the future.

We wish to emphasize that the core of the thesis work is actually the multi-species chemistry model. The description and results of the chemical model were

published in the Journal of Geophysical Research in 2008. We attach this article in its publication format as a substantial part of this dissertation. We will briefly describe the goal, method and main results but we refer the reader to the publication itself for detailed discussions.

1.4 How the thesis is organized

Chapter 2 covers the basics of Jupiter's inner magnetosphere and its interaction with Io.

Chapter 3 describes the atmosphere of Io.

Chapter 4 shows the observations of Galileo along its five close flybys.

Chapter 5 covers past modeling efforts of the interaction: MHD and two-fluid models.

Chapter 6 describes the model we propose: the multi-species chemistry model, the Hall-MHD model and their coupling. This chapter also includes one publication, based solely on the chemical model.

Chapter 7 describes briefly the two atmospheric scenarios that we consider in this work: an atomic atmosphere and an atmosphere that includes SO₂.

Chapter 8 shows the simulations for the first scenario, the atomic atmosphere. This chapter includes a detailed discussion of the MHD results and illustrates the presence of an induced dipole at Io.

Chapter 9 shows the simulations for the second atmospheric scenario, which includes SO₂.

Chapter 10 is a discussion of our results.

Chapter 11 presents our main conclusions.

2. IO IN THE JOVIAN MAGNETOSPHERE

2.1 *Jupiter's magnetic field, Io torus and giant neutral clouds.*

Here we describe briefly the Jupiter magnetic field characteristics relevant to the rest of this thesis. A detailed description of the magnetosphere of Jupiter can be found in “Jupiter, the Planet, Satellites and Magnetosphere” of *Bagenal et al. [2004]*. The pictures displayed in this chapter are extracted from this book, otherwise we add the proper reference in the caption.

Jupiter's magnetic moment is large ($\sim 4.3 \text{ Gauss } R_J^3$). The magnetosphere is gigantic: the sub-solar distance of the magnetopause is highly variable and extends to 40-100 R_J with $R_J = 71,492 \text{ km}$. From Earth, the magnetosphere has an angular size three times that of the sun although Jupiter is ~ 5 times farther away. Io's orbit, at 5.9 R_J , is deeply embedded in the inner magnetosphere of Jupiter. The dipole moment of Jupiter is not aligned with its rotation axis and is tilted by $\sim 9.6^\circ$ towards longitude 202 in the northern hemisphere (in the usual System III (1965), S_{III} , longitude system: *Dessler, 1983*). The internal field of Jupiter dominates the inner magnetosphere out to the distance of Io's orbit where it is approximately dipolar with a strength $\sim 2000 \text{ nT}$. The field rotates with Jupiter with a period of $\sim 9\text{h } 55 \text{ min}$.

Because of the dipole tilt and its fast rotation, the Galilean satellites experience a time-varying magnetic flux that can induce electric currents in the conducting layers of the moons and create an induced magnetic field. Induction was used to identify electrically conducting oceans under the surface of icy satellites like Europa (*Khurana et al., 1998*). A recent publication by *Khurana et al. [2011]* proposes that currents flowing in the conducting magma of Io create such an induced dipole, visible in the magnetometer measurements taken by Galileo. In this thesis, we will illustrate the contribution of this induced dipole on the magnetic perturbation created by the plasma flow around Io.

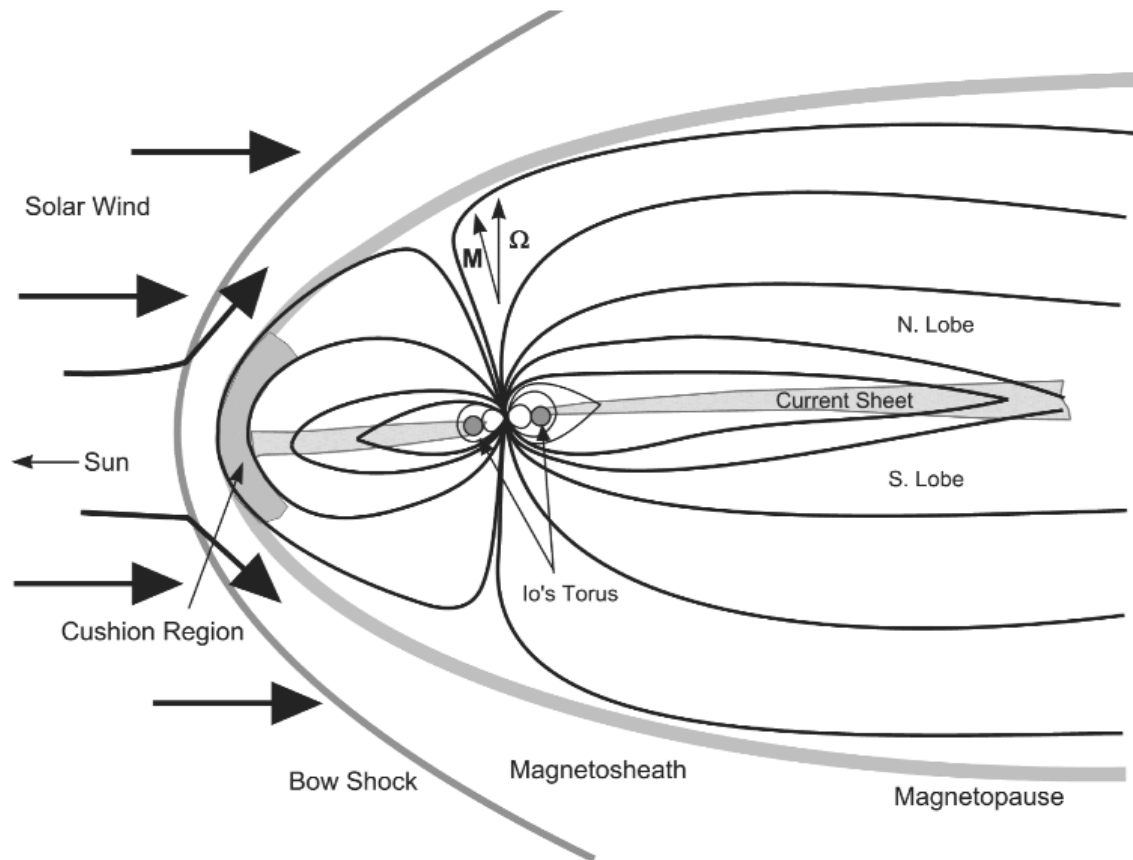


Figure 3: The magnetosphere of Jupiter. Io is embedded in the inner part of the magnetosphere, where the field is mainly dipolar. The dipole moment of Jupiter is tilted by $\sim 10^\circ$ relative to the rotation axis. The field rotates with Jupiter in ~ 10 hours.

When Voyager 1 approached Jupiter in 1979, the ultraviolet spectrometer detected powerful emissions of sulfur and oxygen ions in a toroidal region encompassing the orbit of Io called the Io torus (Figure 2). The Plasma Science instrument made local measurements of both electrons and various ionic species in this torus: O^+ , O^{++} , S^+ , S^{++} , SO_2^+ or S_2^+ . This collisionless plasma is frozen to the jovian magnetic field and co-rotates with it at a local velocity ~ 72 km/s at Io's orbit. The rapid rotation of Jupiter creates strong centrifugal forces that confine the plasma close to a region of the field line most distant from Jupiter's spin axis called the centrifugal equator. It is close but not identical to the magnetic equator: it is tilted ~ 7 deg relative to the orbital plane of Io. Vertically, the torus extends along the field lines to $\pm 1 R_{Io}$ from the centrifugal equator. Radially, it is structured in 3 main regions illustrated in Figure 4. The cold torus extends from $5.3 R_J$ to $5.6 R_J$ and the dominant ions are S^+ (70%) and O^+ (20%). The electron

density peaks at $10,000 \text{ cm}^{-3}$ and both electrons and ions temperatures are cold ($\sim 1 \text{ eV}$). Io's orbit ($5.9 R_J$) is embedded in the so-called warm torus, which extends from 5.6 to $8 R_J$. The electron temperature is $\sim 5 \text{ eV}$ and the composition is different from the cold torus. The major ion species are O^+ (40%), S^{++} (20%) and S^+ (10%). The electron density peak at the centrifugal equator varies between 2000 and 4000 cm^{-3} and the ion temperature is $\sim 60\text{-}100 \text{ eV}$. Between the warm and cold torus, Voyager detected a thin structure called the ribbon, with a high electron density ($\sim 3000 \text{ cm}^{-3}$). It is $\sim 0.2 R_J$ thick and $\sim 0.5 R_J$ high and its location varies with local time between 5.6 and $5.9 R_J$, potentially crossing the orbit of Io from time to time.

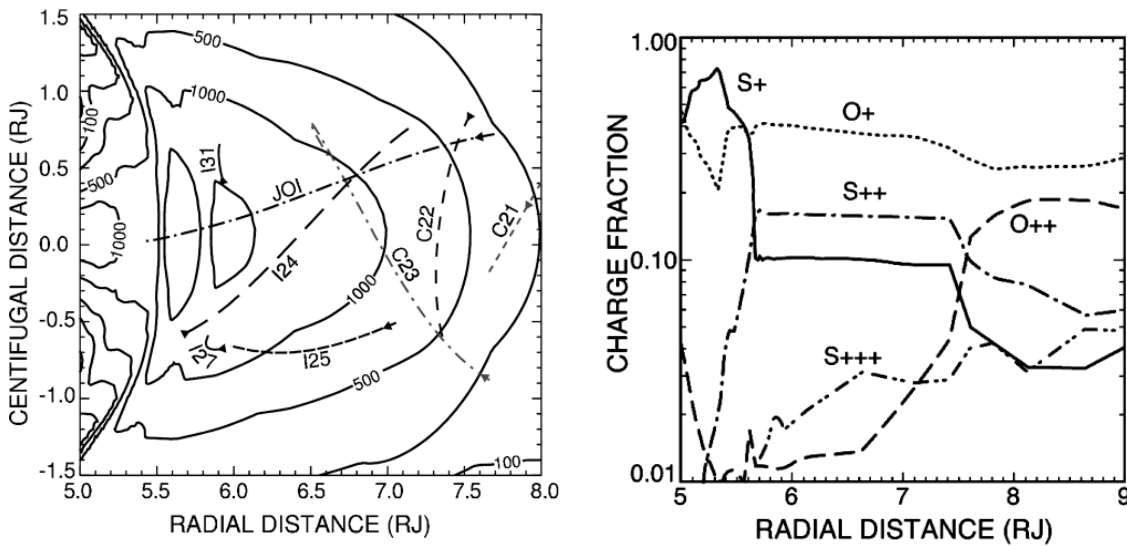


Figure 4: Left: the torus density and some of the Galileo flybys. Right: the composition of the plasma in the cold and warm torus.

UV observations of the torus help constrain its plasma and energy budget. At the time of Voyager 1, a total emission power $\sim 10^{12} \text{ W}$ was estimated from the UVS observations (Shemansky and Sandel, 1980). Delamere and Bagenal [2003] modeled the plasma and energy flow in the torus with a detailed chemical model, which we adapted to the local interaction at Io in this thesis. The UV emissions constitute the main loss of energy of the torus. They are triggered by thermal (5 eV) electron impact on the S and O ions of the torus. In this process, the electrons cool down and the torus emissions would dim and disappear rapidly if the electrons were not re-energized. A significant energy supply to the torus is the pickup process, where a new ion is created by ionization or charge exchange of a neutral coming from the atmosphere of Io. This

pickup takes place both in the atmosphere of Io and in the giant neutral clouds that extends several RJ along the orbit of Io (Figure 5).

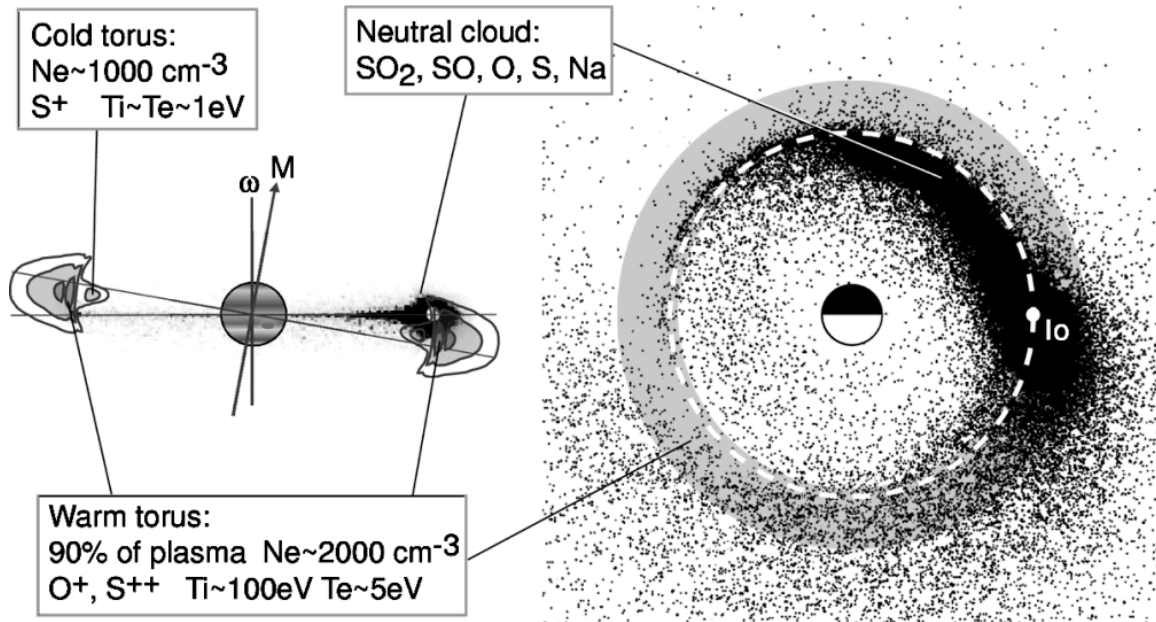


Figure 5: Left: a vertical section with the giant cloud in Io's orbital plane while the torus lies approximately in the magnetic equator and wobbles around Io with the ~ 10 hour period. Right: the giant cloud seen from above is centered on Io but extends many R_J along Io's orbit.

In the pickup process, the new ions initially at rest in the atmosphere of Io experience a typical $\vec{E} \times \vec{B}$ drift where \vec{E} is the co-rotation electric field in Io's frame (Figure 6). The new ions are entrained (picked-up) in the flow and start a gyro-motion at the local flow velocity. S^+ ions picked up at the co-rotation velocity (57 km/s) acquire a gyro-motion energy of 540 eV and SO_2^+ ions gain 1080 eV. Compared to the torus average ion temperature of ~ 60 -100 eV, this pickup process is a net energy supply to the torus. Ultimately, this energy is tapped from the rotation of Jupiter. Coulomb collisions transfer slowly this energy from the ions to the electrons, with a typical equilibration time ~ 10 days. These electrons then trigger the UV emissions of the torus ions through electron impact excitation. The new plasma created at each rotation amounts to 2% of the total amount of plasma in the torus and ultimately, the plasma will slowly diffuse radially outward (characteristic time ~ 30 days) and fill the magnetosphere of Jupiter with heavy ions. *Delamere and Bagenal [2003]* showed that, together with a small fraction of hot electrons, ~ 1 tons /s of neutral material has to be picked-up (the

canonical mass loading rate) to balance the UV radiative loss of the torus. It is not clear how Io's atmosphere contributes directly to the plasma and energy supply of the torus. Based on an analysis of the plasma fluxes observed by Galileo close to Io, *Bagenal [1997]* concluded that the atmosphere of Io contributes at most 20 - 60 % of the plasma supply to the torus and 15 - 30% of the energy supply so the rest of the plasma and energy supply probably comes from the giant neutral clouds. In this thesis, we will show that the specific molecular chemistry taking place in the atmosphere of Io suggests that most of the torus plasma and energy supply comes from the giant neutral clouds.

2.2 The local interaction of Io's atmosphere with the plasma torus

From the description above, we understand that Io, although small in size compared to the size of the magnetosphere, is a very important driver of the magnetospheric physics at Jupiter. Io is not only responsible for radio and auroral emissions in the Jovian ionosphere at the foot of its flux tube, but its volcanism is ultimately responsible for the supply of ions to the whole magnetosphere, for its inflated size, as well as for its main polar auroral emissions. The interaction at Io is complex and involves physics at every level from chemistry, MHD and kinetic plasma physics. We will briefly describe the electromagnetic interaction of the atmosphere /corona of Io with the plasma torus that will be better illustrated with the description of the Hall-MHD model in Section 6.2.3.

The plasma of the torus is collisionless and frozen to the magnetic field of Jupiter. It spins with the same period of ~ 10 hours. Io's orbital motion is much slower: it orbits Jupiter in ~ 42 hours so Io is constantly swept by the plasma of the torus and the field-lines of Jupiter at a relative velocity of 57 km/s. The electron-impact ionization and the charge exchange processes, followed by pickup in the atmosphere of Io are illustrated in Figure 6.

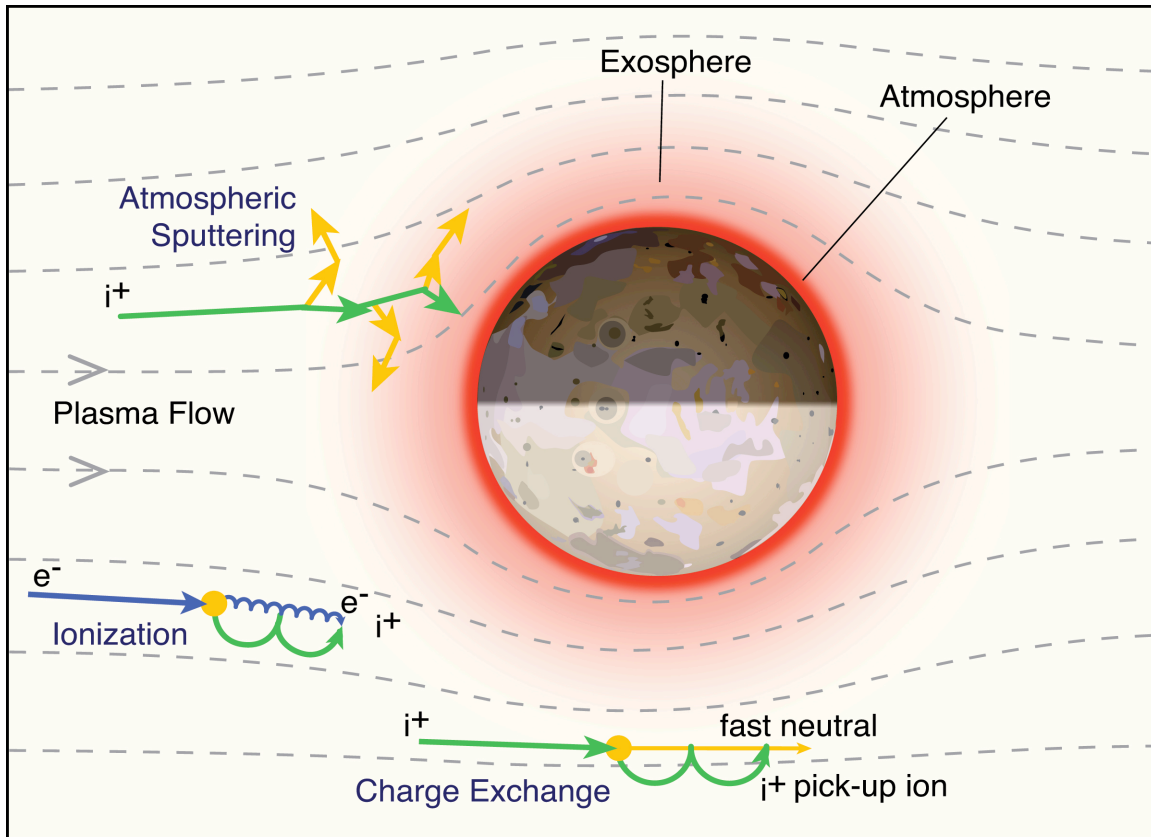


Figure 6: The interaction of torus electrons and ions of the plasma torus with the atmospheric corona of Io. The electron-impact ionization and the charge exchange of a torus ion with an Io neutral create a new ion that is carried by the flow and starts a gyromotion at the local flow velocity, in a process called pickup.

The ionization, charge exchange and ion/neutral collisions processes exert a frictional drag on the plasma flow close to Io while the field line above and under Io continue to move at the co-rotational velocity. This local deceleration of the plasma creates a disturbance in the magnetic field that propagates as Alfvén waves along the field lines, toward the south and north ionospheres of Jupiter (Figure 7). The Alfvén wave propagates at ~ 200 km/s in a plasma that flows at ~ 57 km/s relative to Io. The combination of these two velocities creates a stationary structure downstream of Io, similar to the bow wave of a boat moving on a river, called the Alfvén wing, which is the location of the propagating magnetic perturbation created at Io. A strong current (5 mega-amperes) flowing along this Alfvén tube was detected by Voyager 1. This current originates as a Pedersen current in the ionosphere of Io and, consistent with the wrapping of the field lines around Io and Ampere's law, flows in the anti-jovian direction. When this current reaches the anti-jovian boundary of Io's ionosphere, the conductivity

drops and the current is diverted along the Alfvén wing, towards both ionospheres of Jupiter.

The flow is slowed upstream of Io , diverted around the Alfvén tube (Figure 7), then reaccelerated almost to full co-rotation a few R_{Io} downstream of Io (Hinson *et al.*, 1998) by momentum transfer from the torus plasma above and under Io . Ultimately, after a few bounces back and forth from Jupiter to Io , the Alfvén wave system stabilizes and the plasma returns to full co-rotation (Delamere *et al.*, 2003). This slow recovery is illustrated by the long auroral tail that follows Io 's auroral spot on the ionosphere of Jupiter (Figure 2).

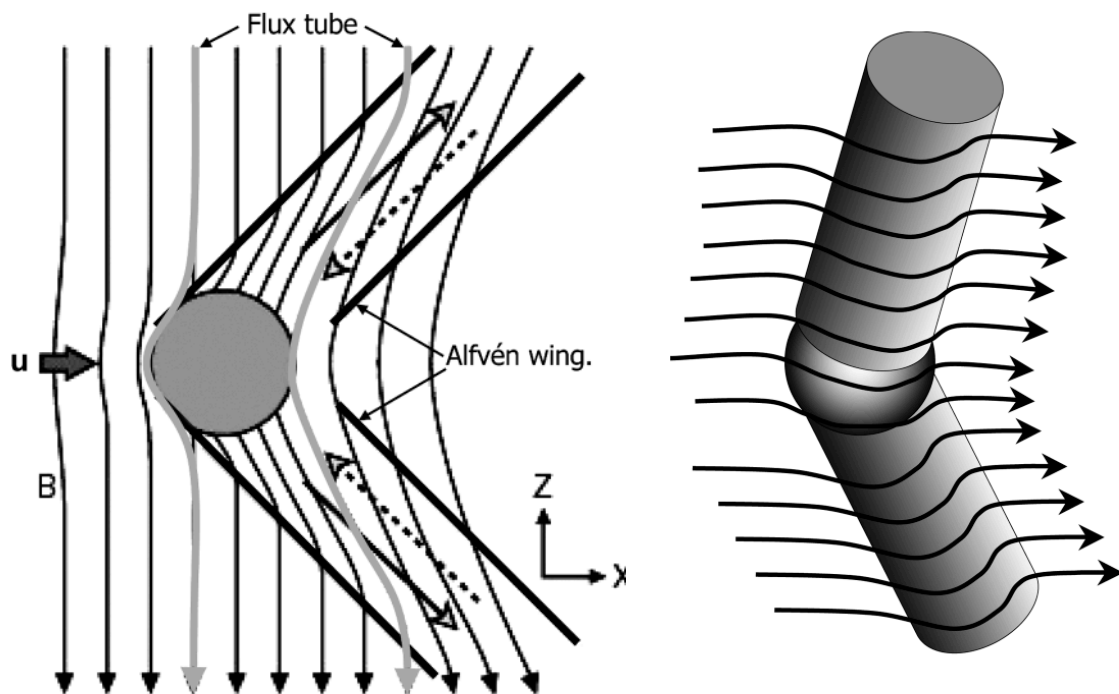


Figure 7: Left: the slowing of the flow close to Io creates a perturbation of the background field line that propagates along the field line as Alfvén waves. The combined motion of the Alfvén wave along the field line and the flow creates a stationary structure downstream of Io called the Alfvén wing. A current flows from Io to Jupiter along these Alfvén wings. Right: The plasma flow is diverted around the whole Alfvén tube that extends to the ionospheres of Jupiter

Finally, Galileo detected high-energy electron beams, aligned with the local magnetic field and flowing in both directions. These beams were detected in the wake of Io, along the flanks and above the pole by the PLS and EPD instruments (*Frank and Paterson, 1999; Williams et al., 1996*). We will show in this thesis that these beams contribute significantly to the dense plasma observed in the wake of Io. The average energy of the electrons in the beams is ~ 300 eV for an energy flux ~ 2 erg/cm² s in each direction. A consistent picture emerges whereby these electrons beams are a direct consequence of the Alfvénic perturbation at Io, provided that this perturbation is filamented in small perpendicular structures (inertial Alfvén wave). When the Alfvén wave reaches the ionosphere of Io, it develops a strong parallel electric field that accelerates the local hot electron population in both directions (*Hess et al., 2010*). The electrons accelerated towards Jupiter trigger the Io-related emissions shown on Figure 8 (*Bonfond et al., 2008*), the electrons accelerated upward form the parallel electron beams detected at Io.

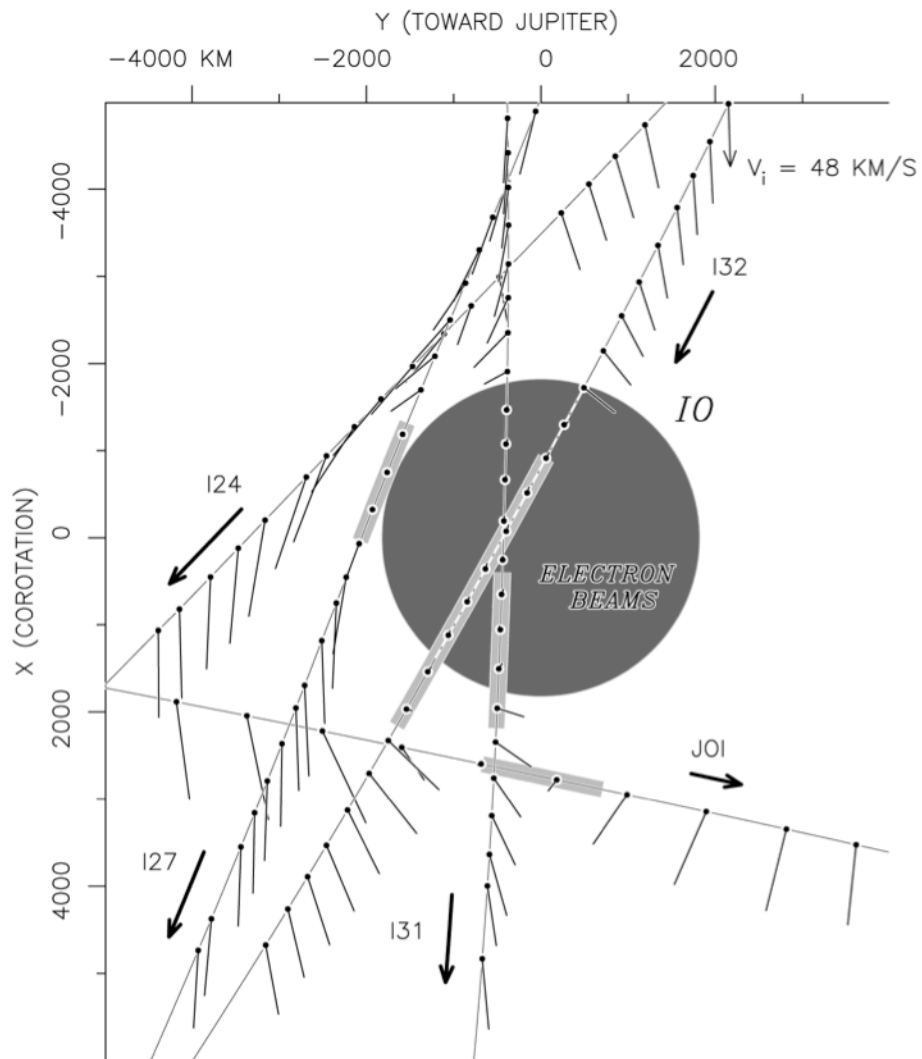


Figure 8: View of Io from above, Jupiter is on the right of the figure in the Y direction while the plasma impinges Io in the X direction. The Galileo flybys are represented as solid lines and the gray shading along the trajectories highlights the location of detection of field-aligned electron beams. The line segments represent the direction of the flow, diverted around the Alfvén tube (B. Paterson, private communication, 2009).

3. THE ATMOSPHERE OF IO

As illustrated previously, the complex phenomena triggered by Io start with ionization and charge exchange in its extended atmosphere. This section describes in detail the current knowledge about this atmosphere.

The first proof of the existence of Io's atmosphere was the radio-occultation experiment of the probe Pioneer 10 in 1973, which detected a dense ionosphere. The infrared spectrometer onboard Voyager 1 identified gaseous sulfur dioxide (SO₂) as the primary component of Io's dayside atmosphere (*Pearl et al., 1979*).

3.1 Sulfur and oxygen atomic corona

Atomic sulfur and oxygen coronae have been observed at ultraviolet wavelengths by *Wolven et al. [2001]* using the Space Telescope Imaging Spectrograph (STIS). They provide radial brightness profiles of S and O from 10 to 1 R_{Io}, where R_{Io} = 1821 km (Figure 9). These profiles are quite complex, revealing distinct emission regions near Io's equator: limb glow on the hemisphere facing Jupiter, equatorial spots under 1.4 R_{Io} (Io's aurora) and diffuse emissions beyond. The slopes of these power law profiles between 1.4 and 4 R_{Io} have indices ranging from -1.5 to -2.0, depending on the hemisphere (trailing/leading) and on Io's orbital phase. These emissions are difficult to interpret unequivocally in terms of neutral density profiles because they represent a line-of-sight brightness integration that depends on the neutral density, the electron density and the electron temperature. The excitation itself can result from direct electron impact on atomic species or dissociative excitation of molecular species. It is generally assumed that direct electron impact on atoms is the excitation mechanism and that the electron density and temperature are constant along the line of sight. All are questionable assumptions and the atomic neutral atmosphere very close to Io is thus poorly constrained.

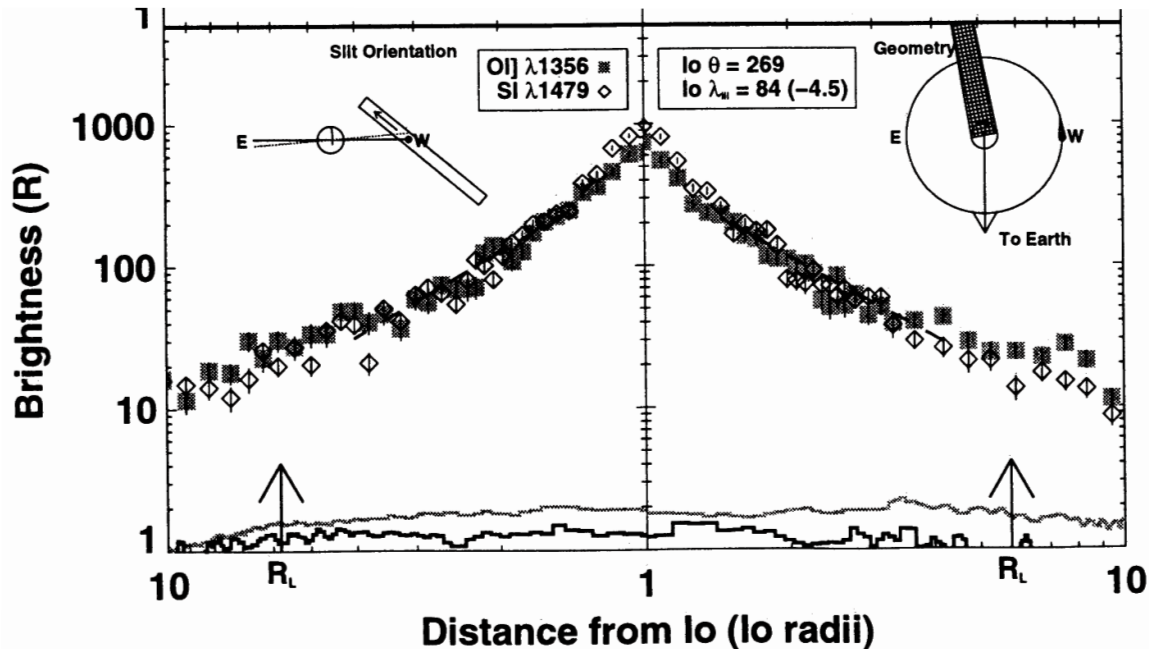


Figure 9: UV brightness radial profile of oxygen and sulfur lines observed with the STIS spectrometer onboard the Hubble Space Telescope (Wolven et al., 2001). The right top insert shows the location of Io on its orbit at the time of the observation; the left insert shows the aperture position. This observation confirms the presence of an extended thin atomic corona around Io.

Assuming nominal torus values for the electron density ($\sim 2000 \text{ cm}^{-3}$) and temperature (5 eV) and a spherically symmetric distribution of O emissions, Wolven et al., 2001 compute, from a 50 Rayleighs brightness at $2 R_{Io}$, a neutral O density at $2 R_{Io}$ of $\sim 1 \cdot 10^5 \text{ cm}^{-3}$. This O density at $2 R_{Io}$ is reasonable as the electron temperature and density are probably close to their background value at this distance. Wolven et al. [2001] also report a relatively constant O/S emission ratio that may reflect the stoichiometric ratio of the SO_2 parent molecule. The columns of S and O are poorly constrained. Ballester [1989] reports vertical columns ranging between $2.2 \cdot 10^{12} \text{ cm}^{-2} < n_S < 7 \cdot 10^{15} \text{ cm}^{-2}$, spanning 3 orders of magnitude and $n_O > (4-7) \cdot 10^{13} \text{ cm}^{-2}$.

3.2 The SO_2 atmosphere

Voyager Images of the surface of Io revealed a large coverage of SO_2 frost, concentrated in the equatorial latitudes, resulting from the condensation of SO_2 from the volcanic plumes (McEwen et al., 1988) (see Figure 1). The increased equatorial

coverage results from the larger number of vents at these locations. These vents are the primordial source of Io's atmosphere, but there remain questions about the relative importance of the volcanoes as direct source of SO₂ to deposition of the condensed SO₂ followed by sublimation when the frost is exposed to the sunlight (see below).

3.2.1 Geographic distribution of the SO₂ atmosphere

Numerous observations provide some information about the longitudinal and latitudinal distribution of the SO₂ sunlit atmosphere as well as its integrated radial column. *Lellouch et al. [2007]*, *Roesler et al. [1999]* and *Feldman et al. [2000]* observed solar Lyman-alpha (1216 Å) reflected from the surface of Io. At this wavelength, SO₂ is a continuum absorber with a large cross section, so a dense SO₂ column will strongly attenuate the reflected solar line. Based on some assumptions about the reflectivity of the surface, a vertical SO₂ column can be inferred. Their observations show that gaseous SO₂ is concentrated along the equator and is very thin at the poles. *Feaga et al. [2009]* proposed a global mapping of SO₂ in Lyman-alpha, at a 200 km spatial resolution (Figure 10). SO₂ was also observed in mid-UV absorption (*Jessup et al., 2004*), in infrared absorption (*Spencer et al., 2005*) and at millimeter wavelengths (*Moulet et al., 2008*).

All observations support an SO₂ atmosphere denser along the equatorial latitudes (under ~ 40°), with a vertical column density correlated to the SO₂ frost deposits and a denser and more latitudinally extended atmosphere on the anti-jovian side of Io. Nonetheless, the different wavelength observations differ considerably in their implied SO₂ vertical column: the longitudinally averaged SO₂ vertical column from each hemisphere at the equator deduced from Lyman-alpha observations is about 3×10^{16} cm⁻² and 1×10^{16} cm⁻² respectively (see Fig.15 in *Feaga et al., 2009*), while *Jessup et al. [2004]* and *Spencer et al. [2005]* report column densities as high as 15×10^{16} cm⁻². This discrepancy in SO₂ column is currently not resolved.

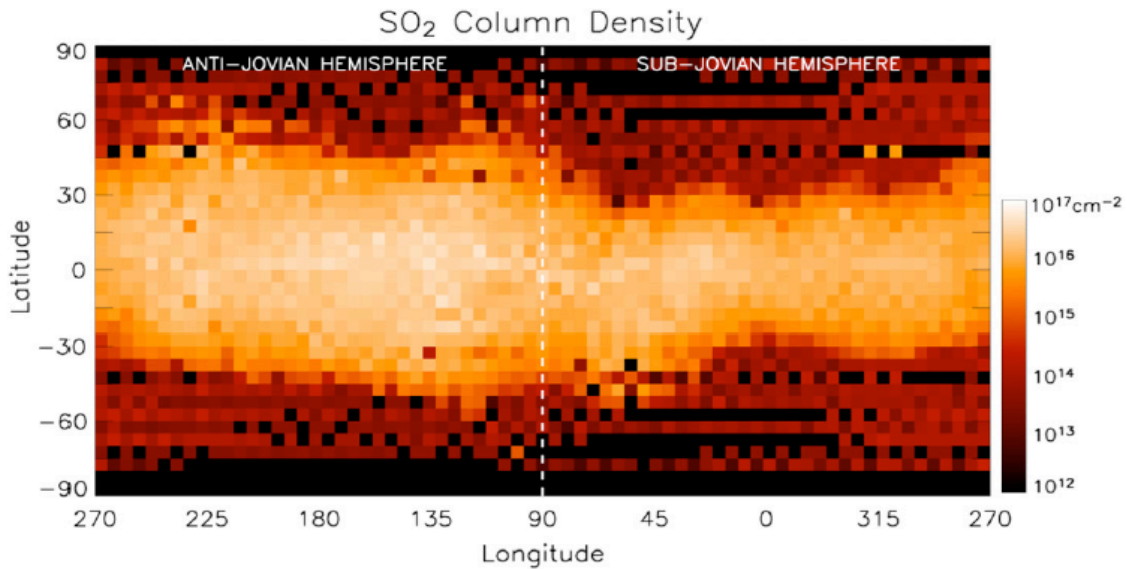


Figure 10: Map of the vertical column density of atmospheric SO_2 in Io's atmosphere, inferred from the Lyman-alpha observations of Feaga et al. [2009]. Io's rotation is phase-locked with its orbital rotation so the same hemisphere always faces Jupiter. The anti-jovian hemisphere spans Io's longitudes from 90 to 270°. The atmosphere is concentrated around the equator. It is denser and more extended in latitude on the anti-Jovian side of Io.

3.2.2 Sustaining the atmosphere: direct volcanism or frost sublimation?

It is still debated if the atmosphere is sustained by SO_2 frost condensation and sublimation or by direct volcanic ejection from the vents.

An atmosphere sustained by direct volcanism would be patchy as the volcanic plumes do not extend beyond 100 km and would be as variable as Io's volcanic activity. Furthermore, such an atmosphere would be insensitive to the variation of the solar zenith angle and would be maintained through eclipse.

On the other hand, an atmosphere sustained by SO_2 sublimation and condensation would be very sensitive to the variation of the solar zenith angle (the local time), denser close to the zenith at noon, collapsing at night and during eclipse, and its longitudinal and latitudinal distribution would be smoother.

The atmosphere is probably maintained by a combination of both mechanisms but available observations do not yet provide a consistent picture of their relative importance (see discussion by Spencer et al., 2005).

Feaga et al. [2009], using Lyman-alpha observations, studied the time variability of the global SO₂ atmosphere. They claim that the global atmosphere is surprisingly stable: the volcanic plumes appear as local variations on a background SO₂ atmosphere that is fairly constant between 1997 and 2001. This would favor an atmosphere sustained by sublimation of frost. On the other hand, Lyman-alpha images do not show variations of the absorption with the solar zenith angle (from terminator to sub-solar point), which suggests that the atmosphere is well developed from limb to limb. If the atmosphere is sustained by SO₂ sublimation, the absence of local time variation would imply a large thermal inertia of the SO₂ frost and the most recent model of an SO₂ sublimation-driven atmosphere (*Walker et al., 2010*) is unable to reproduce the insensitivity to the local zenith angle and the sharp decrease of density at mid-latitude. Recent infrared observations (*Tsang et al., 2010*), show a variation of the dayside column when Jupiter recedes from the Sun and the insolation decreases.

The UV observations of Io's atmosphere in eclipse confirm that insolation is a major driver in maintaining the atmosphere, which partially collapses in darkness. *Clarke et al. [1994]*, using the FOS spectrometer onboard the Hubble Space Telescope (HST), observed a factor of 3 variation of atomic sulfur and oxygen far ultraviolet (FUV) brightness when Io enters eclipse. Similarly, *Wolven et al. [2001]*, using STIS aboard HST observed an increase of FUV oxygen and sulfur lines when Io emerges from eclipse. *Retherford [2002]* shows that the response of the atmosphere depends on its altitude. They quantify the timescales for the atmosphere collapse after ingress: ~ 5 minutes for the molecular atmosphere, < 30 minutes for the atomic atmosphere and ~ 280 minutes for the corona. The condensation response was modeled by *Moore et al. [2009]*. They show that even a small amount of non-condensable gases would create a buffer close to the surface that limits the condensation of SO₂.

The eclipse has a short duration while the night on Io can be as long as ~ 20 hours. Modeling by *Wong and Johnson [1996]* suggests the possibility of a night-side atmosphere dominated by non-condensable gases (O₂ and possibly SO) as SO₂ condenses on the surface. Although the data are limited, it is reasonable to assume that the atmosphere is less dense on the night-side of Io.

3.2.3 Radial distribution of SO₂

If the dayside vertical column and its geographical variations are well constrained, (Strobel, 1994), its vertical structure is still unknown. As the surface temperature is very low (T=120K at day and 90K at night) the atmospheric scale height is very small (12 km) and most of the SO₂ column is probably concentrated at low altitude.

In this thesis, for convenience, we structure the radial distribution of SO₂ in four loosely defined regions: the **bound atmosphere (1)** up to 0.1 R_{Io} ~ 200 km where the scale height is a few 10's km. Plasma bombardment and Joule heating inflate the upper atmosphere (Strobel, 1994) to form a thin exosphere that we call the **extended atmosphere (2)** with a scale height of a few hundreds of km. This region reaches 6 R_{Io} where the gravity of Jupiter and Io counterbalance. The composition of the extended atmosphere is probably dominated by SO₂ close to the bound atmosphere but because of electron dissociation impact, it is probably enriched in S and O. Farther away, plasma sputtering and electron impact dissociation form an **atomic and molecular corona (3)**, which eventually form the "**giant neutral clouds**"(4) that span several R_J along Io's orbit. Let it be clear that we choose these definitions for convenience and that these regions overlap over large distances.

The vertical distribution in the bound atmosphere close to the surface is unknown but Walker et al. [2010] proposed an interesting model that is still in its early development but clarifies the structure of the bound atmosphere and its response to eclipse. They propose a Monte Carlo simulation of flow dynamics in a rarefied gas of pure SO₂. The atmospheric density is controlled by the local vapor pressure and the local surface coverage of SO₂ frost. They take into account the planetary rotation, the heating due to plasma bombardment, the inhomogeneous coverage of SO₂ frost and volcanic plumes, the SO₂ residence time on rocks and the thermal inertia of the frost. In general, their base model provides a vertical daylight column density and a geographic asymmetry that is consistent with the Lyman-alpha observations but they cannot model the steep drop of density with latitude and the insensitivity of the SO₂ column to the local solar zenith angle. Figure 11 illustrates their modeled SO₂ profile to an altitude of 200 km for daylight and night conditions. We approximate these profiles with two exponentials (scale height ~ 10 km close to the surface and ~35 km farther up). The first

evidence from their figure is that the bound atmosphere collapses at night as the surface density drops by 3 orders of magnitude. Let us note that their model does not include the buffer effect of a non-condensable component modeled by *Moore et al. [2009]* that we discussed above. On the other hand, the scale height of this collapsed atmosphere seems very similar to the scale height of the daylight atmosphere as the night temperature (90 K) is not very different from the daylight temperature (120 K). The second evidence is that the vertical integration of this low altitude profile yields a vertical column of $\sim 6 \cdot 10^{16} \text{ cm}^{-2}$ on the dayside. This suggests that most of the column inferred from UV observations is concentrated in the first 200 km. Thus the lower limit of the vertical column of the extended atmosphere (scale height of a few 100s km) is **not constrained by these observations but by its effect on the plasma density and ion temperature along the GLL flybys of Io.**

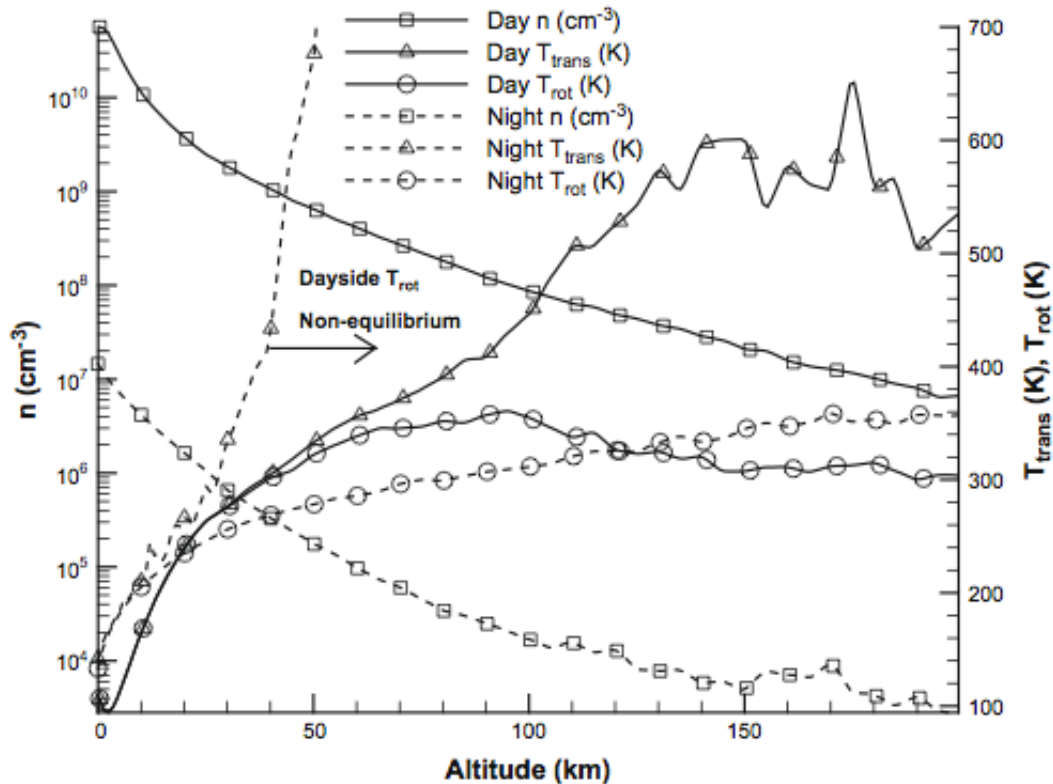


Figure 11: SO_2 density vertical profile in daylight (plain line and squares) and in eclipse (dashed line and squares) modeled by Walker et al. [2010] for a sublimation-sustained atmosphere. The atmosphere is very dense close to the surface and the whole column collapses during eclipse.

3.3 Other atmospheric components

Sodium (Na) is a very minor constituent (1%) of Io's atmosphere but its scattering cross section of solar visible light is very large. The structure of the Na extended atmosphere and corona and its variation have been extensively observed from the ground. Numerous structures of the Na clouds have been observed: fast jets from the anti-jovian flank of Io, the fast stream emitted far from Io all along its orbit, the large banana cloud that extends several R_J along the orbit of Io and the giant sodium nebula larger than Jupiter's magnetosphere itself (Figure 12). Na could be interpreted as a tracer of more abundant atmospheric components (SO_2 , S and O) that are less visible because of smaller scattering cross sections or cross sections peaking in the UV where the solar flux is low.

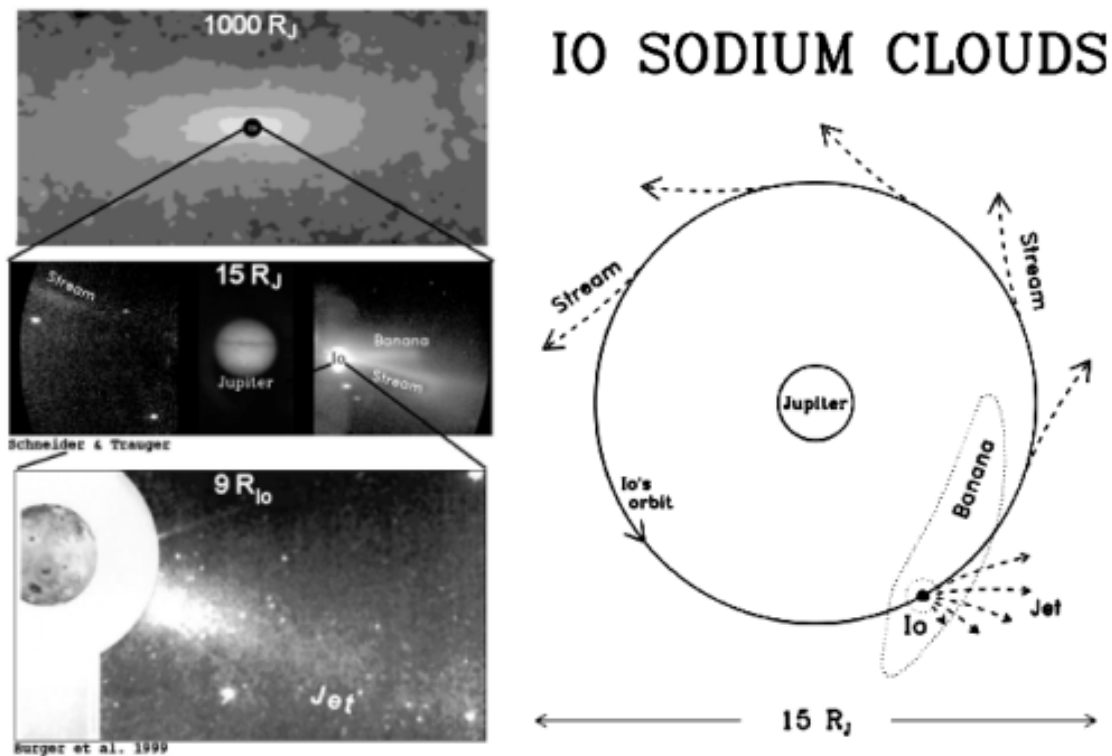


Figure 12: Structures of the Na clouds. Right: the jets, stream and banana cloud as seen from above Jupiter. Top left: The giant nebula.

Sulfur monoxide (SO): SO was detected in mm-wave observations (Lellouch *et al.*, 1996). Global coverage and column of SO is uncertain (see review McGrath *et al.* [2004] and references within). The interpretation of the observations is ambiguous,

consistent either with a very low column hemispheric SO atmosphere or a SO column mixed with SO₂ on a restricted fraction of Io's surface with a SO/ SO₂ mixing ratio ~ 10%. Ion cyclotron waves at the SO local gyro-frequency were detected along some Galileo flybys mainly downstream of Io (*Russell and Kivelson, 2001*).

Other minor species have been reported (S₂, NaCl, H₂S⁺, Cl⁺ etc.) and we refer to *McGrath et al. [2004]*'s review for details.

4. GALILEO DATA

4.1 *Galileo flybys of Io*

Galileo (GLL) was a spacecraft sent by the National Aeronautics and Space Administration (NASA) to study Jupiter and its moons. It was launched in October 1989 and arrived at Jupiter in December 1995. It ended its mission in September 2003 when it was sent into Jupiter's atmosphere. During its cruise to Jupiter, the high-gain antenna could not deploy and the transmission of the data back to Earth relied on the backup antenna, which had a transmission rate 1,000 times lower than the high-gain antenna. The planned observations had to be modified to decrease the data volume to be transmitted and the data set had to be limited. Consequently, the interpretation of this limited data in terms of plasma characteristics (density, velocity, composition etc.) is difficult and sometimes questionable.

Between 1995 and 2001, Galileo made 6 flybys of Io at altitudes ranging from 100 to 900 km. Figure 13 and Figure 14 show the Galileo trajectories in the reference frame of Io, the X axis pointing to the unperturbed co-rotation flow (the downstream direction), Y toward the center of Jupiter (the jovian direction) and Z completing the right-handed frame, almost anti-parallel to Jupiter's magnetic field. Galileo's trajectory is called "inbound" when Galileo approaches Io, and "outbound" when the spacecraft moves away from Io, after the closest approach. The upstream, anti-jovian flank and wake of Io were directly observed. Most of the upstream flybys sampled the night side of Io or were close to the terminator. There was unfortunately no direct observation of the jovian flank. Table 1 shows the orbital parameters of each flyby.

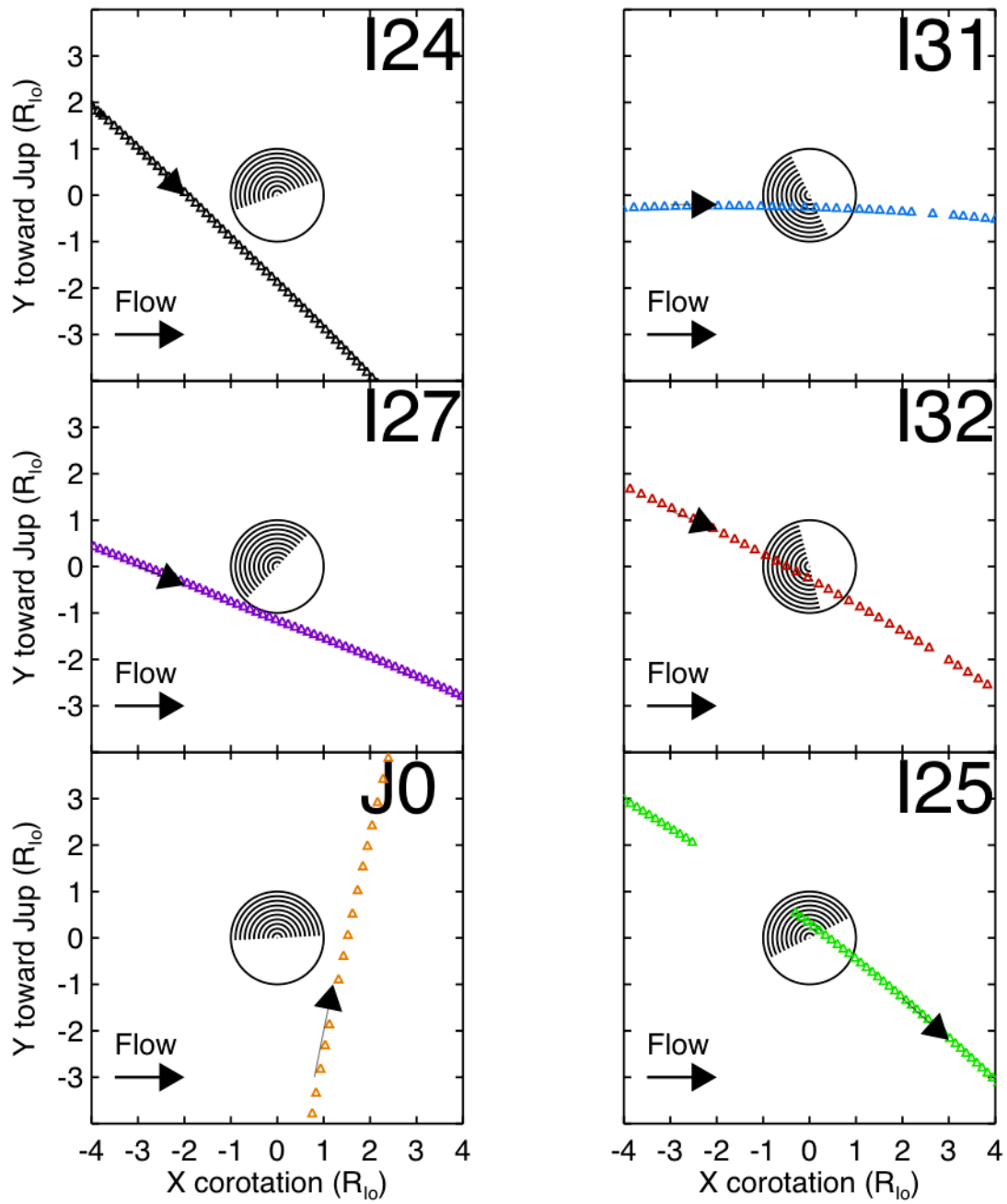


Figure 13: Trajectories of the Galileo flybys in the XY plane. The night-side is shaded in black.

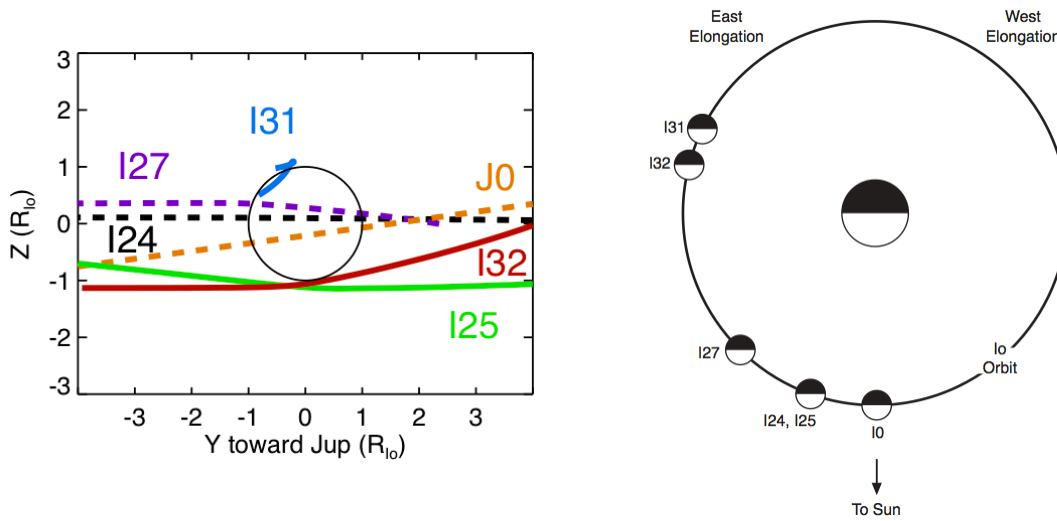


Figure 14: Left: trajectories of the flybys in the YZ plane. Right: location of Io on its orbit (Local time) for each flyby. The night-time hemisphere is shaded in black.

Flyby name	Local time ¹	Altitude ²	Jovian longitude ²	S _{III}	Date
J0	11.8 h	897 km	272.4		Dec 1995
I24	10.7 h	611 km	80.3		Oct 1999
I27	8.91 h	198 km	81.1		Feb. 2000
I31	4.33 h	193 km	159.6		Aug. 2001
I32	5.04 h	184 km	260.5		Oct. 2001

Table 1: Parameters of the flybys.

(1) Local time indicates the location of Io on its orbit around Jupiter. At 09:00 LT, Io is at its largest Eastern elongation (on the left of Jupiter see Figure 14)

(2) Altitude and longitude at closest approach.

4.2 The PLS and PWS instruments

The Plasma Wave Subsystem instrument (PWS) on board Galileo measured the electric fields in the plasma, detecting plasma and radio waves. The electron density can be inferred from the electrostatic emission at the upper hybrid resonance frequency (*Gurnett et al., 2001*). The emission is thought to be locally excited so the observed frequency reflects the electron density close to the spacecraft. As illustrated in *Gurnett et al. [2001]*, the upper hybrid frequency is often clearly identified in the frequency-time spectrograph. But there are also occasions when the identification is less clear.

The PLasma Subsystem instrument (PLS) (also called the PLasma Spectrometer) collected charged particles for energy and mass analysis. The spinning of the instrument and the field of view of the detectors provided coverage in almost all directions. The instrument measured ion count rates for different incoming angles and different energy/mass ratios from 0.9 eV to 52 keV. Ion density, bulk velocity, average ion temperature and composition can be derived from these measurements through computation of numerical moments of the measured velocity distribution function (*Frank et al., 1996*). PLS ion measurements rely on either substantial flow speeds or significant thermal energies to bring the ions into the sensors. When the plasma is cold and/or stagnant (such as in or close to Io's ionosphere) the PLS moment calculations can underestimate the total plasma density. Calculation of the total charge density from these ion measurements relies on the assumption of charge state of the ions, assumed to be constant along the spacecraft trajectory. The limited data transmission rate of Galileo and the limited sensitivity of the instrument lead to poorly sampled distribution functions both in energy and direction. Consequently, the calculation of the moments is difficult and relies on many assumptions about the composition of the plasma as well as extrapolations of the distribution function.

4.3 Plasma density and temperature

The plasma density profiles from PLS and PWS along the 6 Galileo flybys are shown in Figure 16. On the J0 flyby downstream of Io, PLS and PWS deduced very similar plasma densities. The density profiles on the I27, I31 and I32 flybys are fairly similar in shape with PLS underestimating the total charge density by about a factor of

two for most of the region except around closest approach where the spacecraft probably encountered dense, cold, ionospheric plasma and PWS shows significantly higher densities. Due to problems on the spacecraft there were no PLS measurements on I25 and there is a data gap in the PWS plasma density measurements of I25 just before closest approach, between $X = -3$ and $-0.5 R_{Io}$. For these reasons, we decided to ignore the I25 measurements in our analysis. On the I24 flyby, the differences in the profiles are more difficult to explain. Inconsistency of two simultaneous observations by two different instruments is a challenge for the modeler. We chose to compare our model results with the PWS electron density values and hope that re-analysis of the PLS and PWS data might reconcile these data sets in the future.

Figure 17 shows the plasma temperature deduced from PLS observations (with no observations obtained on I25). This variation of temperature is caused by Io's neutral material, newly ionized or charge exchanged, picked-up by the flow at the local flow velocity. The constant temperature upstream of Io is an indication of little ionization or charge exchange, and implies little neutral material along the GLL trajectory, the deep dip at the location of closest approach is an indication of pick-up at a very slow flow velocity very close to Io and the abrupt increase of T_i downstream farther from Io is a sign of accumulation of fresh ions (from ionization or charge exchange) picked up along the flow line crossing the trajectory. The constant increase of temperature on the outbound leg of the wake flyby J0 is too far from Io to be caused by the torus-atmosphere interaction and might be related to gradients in the torus, although it is difficult to explain such an increase in temperature inside the orbit of Io, in the direction of the cold torus.

4.4 Other Plasma properties

We summarize here the other plasma properties deduced from the data that are relevant to this thesis: the plasma velocity, the magnetic perturbation and the plasma composition. They will be shown in Section 8 with the model results.

The plasma velocities are deduced from the PLS measurements. We could not obtain the PLS files so we estimated the velocity based on figures published in the literature, which limits their accuracy. We have subtracted a background velocity determined from measurements far from Io.

The magnetometer data were extracted from the Planetary Data System archives. Because of the tilt of Jupiter's magnetic field, Io experiences a background magnetic field in the X,Y,Z directions that depends on Io's longitude at the time of the observation. As we are interested in the magnetic perturbation caused by Io's plasma interaction, we remove this background field from the observations. We used the model of Jupiter's magnetic field of *Khurana and Tsyganenko [2002]* to calculate the Jovian field along each GLL trajectory. This field combines a model of Jupiter's internal magnetic field (*Connerney, 1981*) and the field created by the current sheet. We shifted each component of the background field independently so the modeled field matches the data far from Io and we removed it from the observations.

Another interesting observation is the detection by the magnetometers, in the wake of Io along J0 (and also along other flybys) of ion cyclotron waves at the gyro-frequency of SO_2^+ and SO^+ (*Huddleston et al., 1997*). Ion cyclotron waves are produced when the distribution function is highly non-Maxwellian, which is the case of picked-up ions as they acquire a velocity perpendicular to the magnetic field direction (i.e. a ring beam distribution). The S and O gyro-frequencies are not observed because the emission is rapidly quenched by a thermal background of S and O ions in the torus. Close to the wake of Io, the ion cyclotron wave instability is masked by the mirror mode instability that develops when there is a large pressure gradient, which happens in the wake because it is very dense, even if it is also very cold. A lower limit on SO_2^+ densities ($1\text{-}100\text{ cm}^{-3}$) along this flyby was deduced from the modeling of cyclotron emission. The absolute density is uncertain as it is model dependent, but this observation somewhat constrains the SO_2^+ density resulting from Io's interaction and also supports the presence of an SO_2 corona extending (at least) to distances as far as $10 R_{\text{Io}}$. The density profile along J0 inferred from the ion cyclotron wave observations along J0 will be presented in Section 9.3.

4.5 Summary

Even with its limited capabilities, Galileo revealed the complexity of the physics involved in the interaction. Figure 15 summarizes one of the main results of the J0 flyby: The wake of Io is dense ($\sim 40,000\text{ cm}^{-3}$), cold ($T_i \sim 2\text{ eV}$) and stagnant ($V_x \sim 2\text{ km/s}$). The magnetic field in the wake is strongly depressed ($\sim 30\%$) and the flux of new ions from

this local interaction is small compared to the canonical flux needed to sustain the torus emission (Bagenal, 1997) (see Section 2.1). We refer to *Saur and Strobel [2004]* and the review of *Chust et al. [2005]*, for a more detailed description.

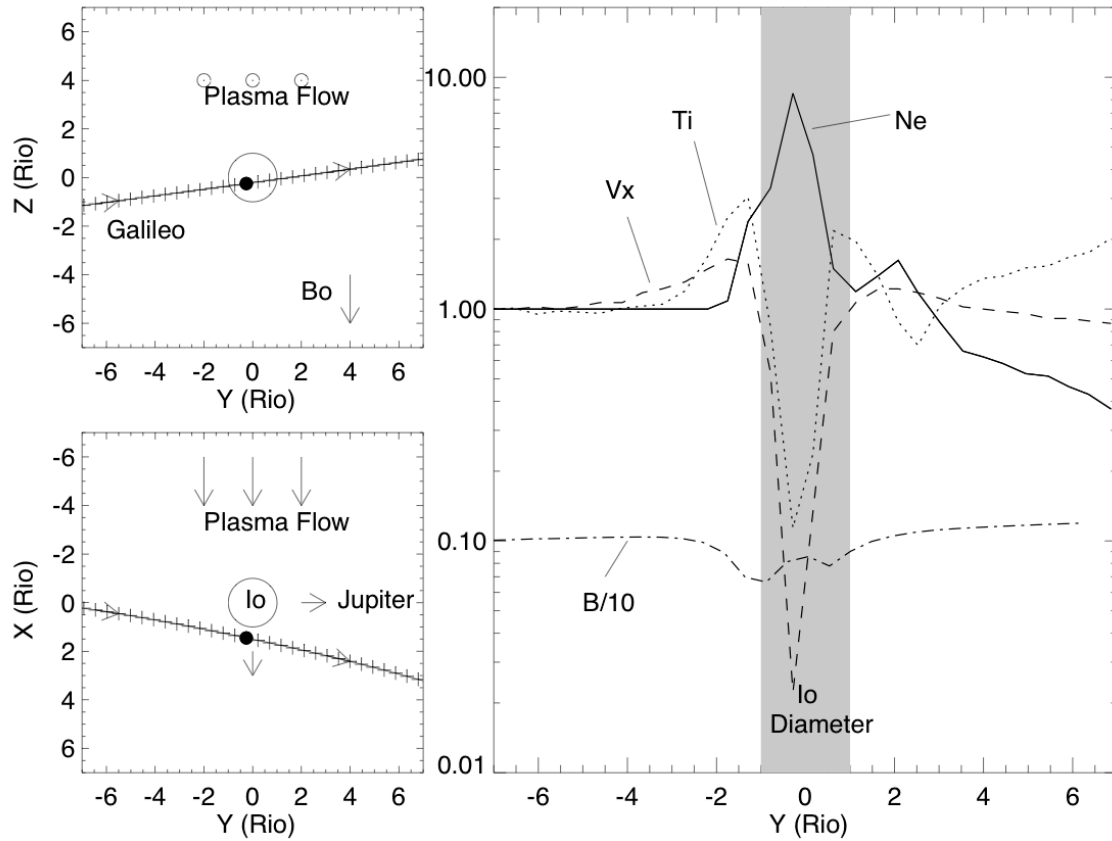


Figure 15: Trajectory of the J0 flyby and its plasma observations (Bagenal, 1997)

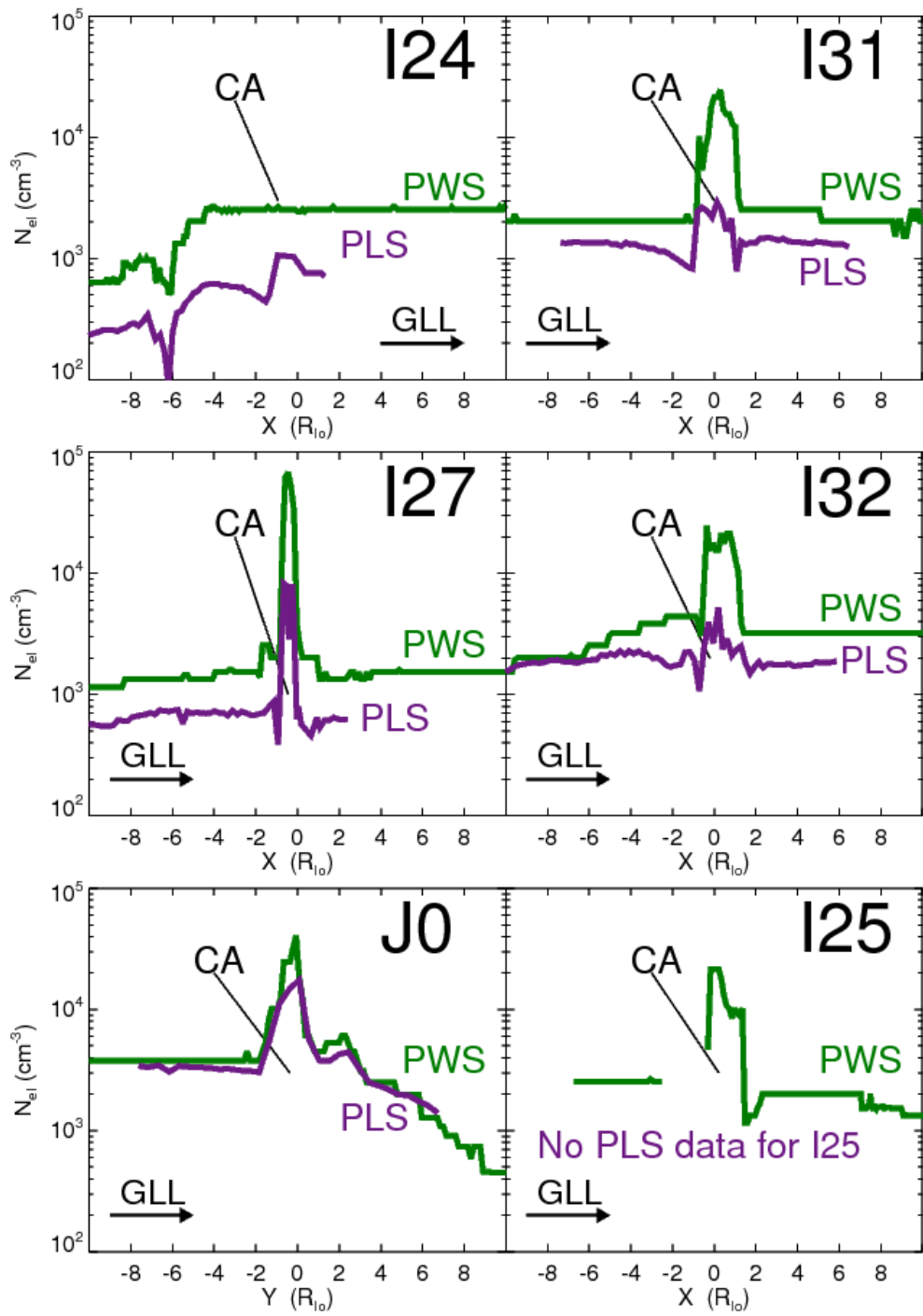


Figure 16: The plasma density inferred from PLS and PWS measurements for each flyby. CA represents the closest approach.

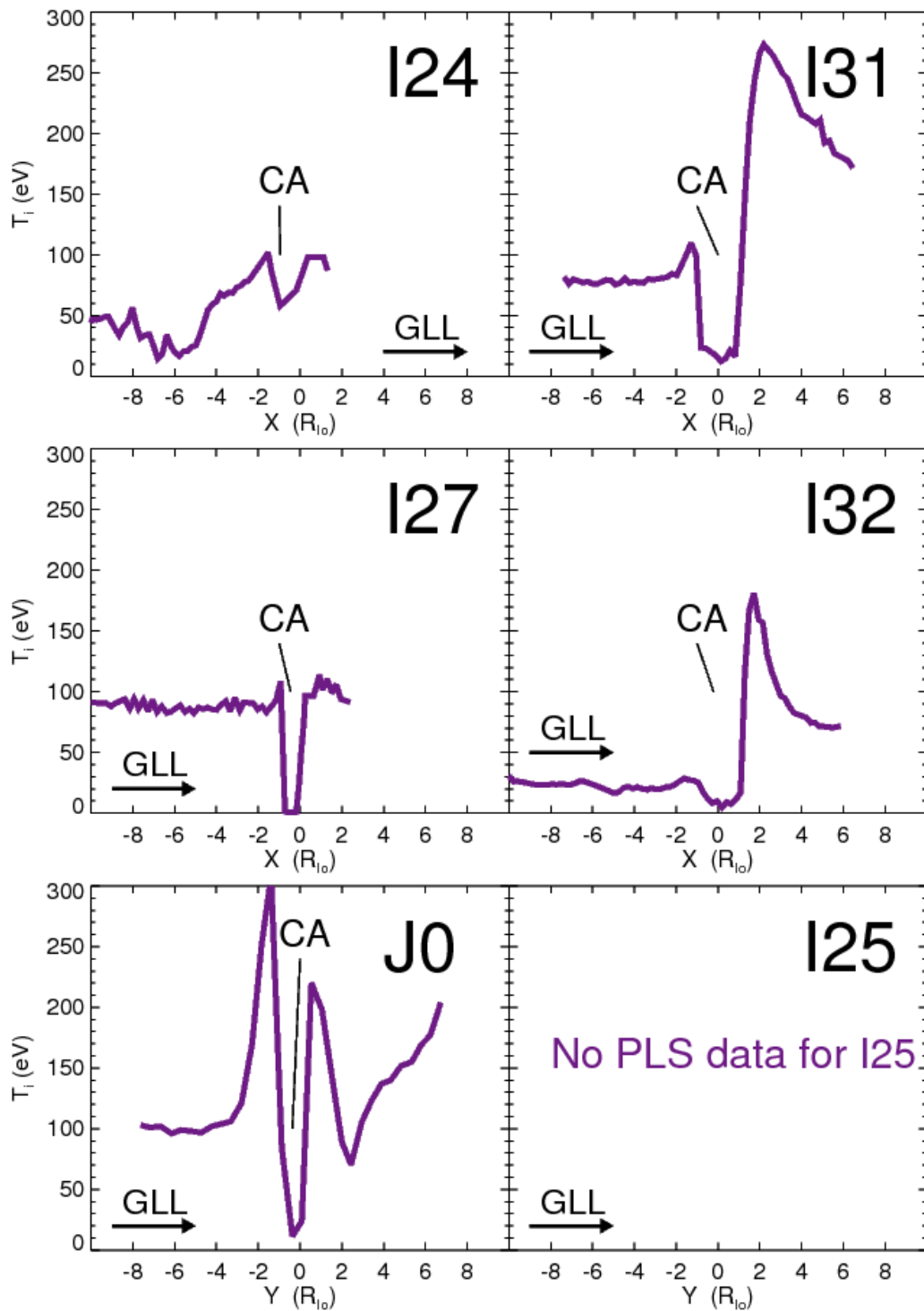


Figure 17: Ion average temperature determined from PLS measurements for each flyby. CA indicates the closest approach.

5. PREVIOUS MODELS

As summarized in the introduction, many models of the plasma-Io interaction were proposed in the past. We classify them in three categories: the MHD, the two-fluid and the multi-species chemical models. Each approach assumes simplifications to focus on different aspects of the interaction. We will summarize the two first methods. The multi-species chemical approach that we have developed (*Dols et al., 2008*) will be described in Section 6.1.

5.1 MHD models

The MHD numerical models self-consistently solve the 3-D fluid MHD equations (*Linker et al., 1988; Linker et al., 1989; Linker et al., 1991; Linker et al., 1998; Combi et al., 1998; Kabin et al., 2001*). Such models simulate the flow of a magnetized plasma encountering a conducting sphere representing Io and its dense ionosphere. In general, they are able to reproduce the gross features of the interaction, showing the propagation of the MHD plasma waves. Recently, *Khurana et al. [2011]* used this MHD approach to show convincingly that Io, like Europa, develops an induced dipole when Jupiter's magnetic field sweeps by it.

The focus of the MHD codes is mainly the description of the flow and magnetic perturbations. The plasma density, ion temperature and neutral distribution are less reliably addressed. MHD codes do not solve an energy equation for electrons and do not compute the electron temperature, although the ionization cross sections are known to be extremely sensitive to this parameter (see Section 6.3.1). Ionization, molecular dissociation as well as atomic and molecular excitations cool the electrons down and limit the ionization. Usually, MHD codes prescribe ionization and charge exchange rates that are proportional to the local neutral density, assuming implicitly that the ionization cross sections are independent of the local electron temperature. Thus, the plasma density computed in MHD is approximate.

Generally, MHD models assume a single species (some MHD models are multi-species but are not yet developed to model the close Io interaction). The evolution of the plasma temperature is driven by the pickup of new ions and the energy gained is

proportional to their mass. Usually, the MHD codes assume an ion mass ~ 20 amu, corresponding to a mixture of S and O ions typical of the torus. The interaction involves heavier ions like S (32 amu) or SO_2 (64 amu), for which the energy gain would be 1.5 to 3 times larger. We will show in the next section that, due to the charge exchange and ionization cross sections, S or SO_2 ions dominate the interaction. Thus the gain of energy in the MHD models and the resulting ion temperature are probably underestimated.

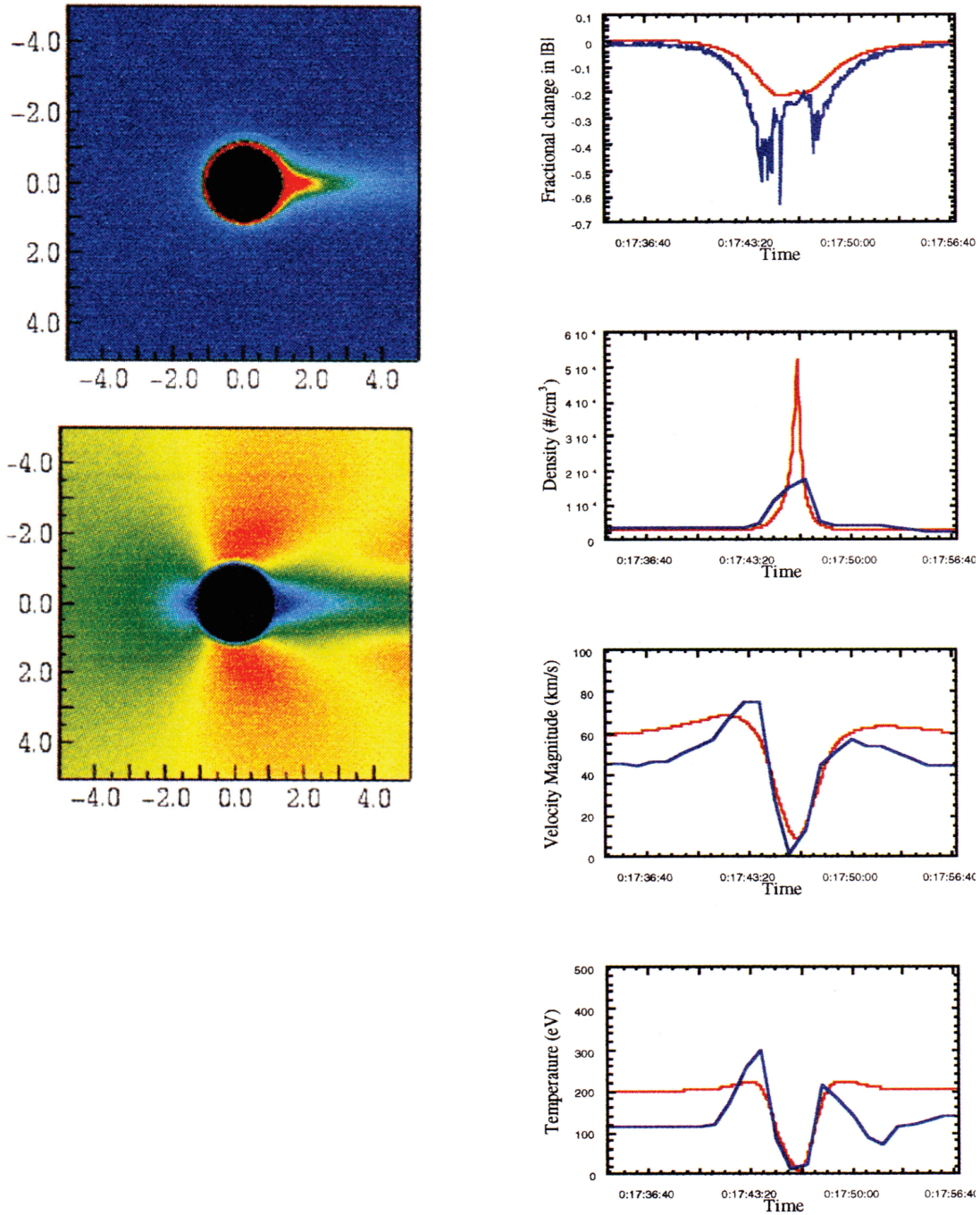


Figure 18: Simulation of Linker et al. [1998]. Left from top to bottom: Plasma density and speed in Io's equatorial plane. Axes are in R_{Io} and the flow enters the simulation domain from the left side. Right: The plasma properties along the J0 flyby. The blue lines represent the observations and the red the model results. From top to bottom: the magnetic field, the plasma density, the plasma speed and the plasma temperature.

5.2 Two-fluid model (electron + SO₂⁺)

An alternative approach is the (Saur *et al.*, 1999; Saur *et al.*, 2002; Saur *et al.*, 2003) two-fluid model. These authors were the first to focus on the SO₂ physical chemistry. They solve the 3D steady-state equations for the electrons and for one type of ion (SO₂⁺) with a prescribed SO₂ atmosphere. This approach focuses mainly on the current, the electric field and the plasma density. The authors compute in detail the conductivities based on ionization, charge exchange and elastic collisions as well as the evolution of the electron temperature. The simplification of this approach is the assumption that the magnetic field is unperturbed by the interaction. The magnetic perturbation observed by GLL is ~ 600 nT for a ~ 2000 nT background Jovian field at Io, thus the magnetic perturbation is a strong feature of the interaction. This simplification may account for a 30% error in their results (Saur, personal communication, 2011) but this description led to important new insights in the understanding of the interaction.

Saur *et al.* [1999] showed that photo-ionization of Io's atmosphere is negligible and most of the ionization comes from the electron impact from the torus plasma. They also show that the Hall conductivity in the deep atmosphere of Io "twists" the electron flow towards Jupiter while the ion flow does not experience such a strong twist (Figure 19). This separation of the electron and ion flows leads to strong currents in the ionosphere that are eventually diverted along the Alfvén wing. They claim that this asymmetry of the electron flow explains the asymmetry of Io's auroral emissions, on the flanks of Io (Saur *et al.*, 2000) (see Section 10.2).

They compute explicitly the cooling of the electrons by inelastic collisions on molecular SO₂. A molecular ion is much more efficient at cooling the electrons than an atomic ion. Under electron impact, SO₂ can be ionized (threshold= 13.1 eV), dissociated (threshold 5.7 eV) and excited in higher ro-vibrational levels. This efficient loss of electron energy limits the ionization of the atmosphere to the upstream hemisphere of Io.

They claim that their boundary conditions are more physical than the ones used by Linker *et al.* because, they argue, when a flow line hits the surface of Io, it ends up empty of plasma. The direct effect of this boundary condition and the upstream location of the ionization is a wake devoid of plasma, unlike the MHD results and unlike the observations. Their plasma density profile along the GLL/J0 trajectory presents two peaks on the flanks and a large 'bite out' in the center, see Figure 20. Saur *et al.* [2002]

showed that this empty wake could be filled by another ionization process in Io's downstream atmosphere, provided by energetic electron beams flowing along the magnetic field lines, which were detected by Galileo in the wake of Io (Figure 8). We note that our modeling presented in Section 8 and 9 will have the same empty wake for the same reasons.

Although they do not compute the magnetic perturbation self-consistently, they use Ampere's law and their calculated currents to compute it a posteriori. They show that the doubled peak magnetic perturbation observed in the wake of Io results from diamagnetic currents along the flanks of the wake.

In summary, the main issue with this sophisticated model is its lack of self-consistency since the magnetic field is kept constant during the calculation. We note that the multi-species chemical model that we propose in this thesis (Section 6.1) uses the same description of the electron cooling (*Strobel, personal communication, 2009*).

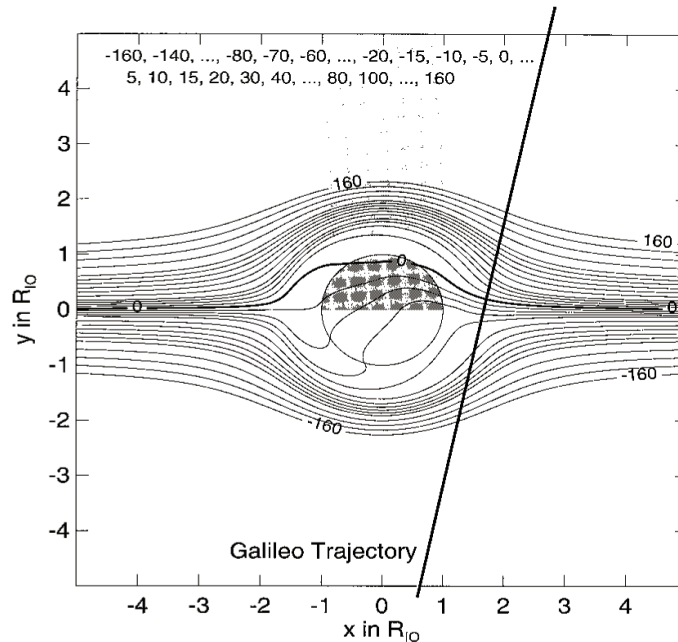


Figure 19: Electron flow lines in the equatorial plane of Io of Saur et al. [1999]. Because of the Hall conductivity in the dense ionosphere of Io, the flow of the electron is strongly twisted towards Jupiter.

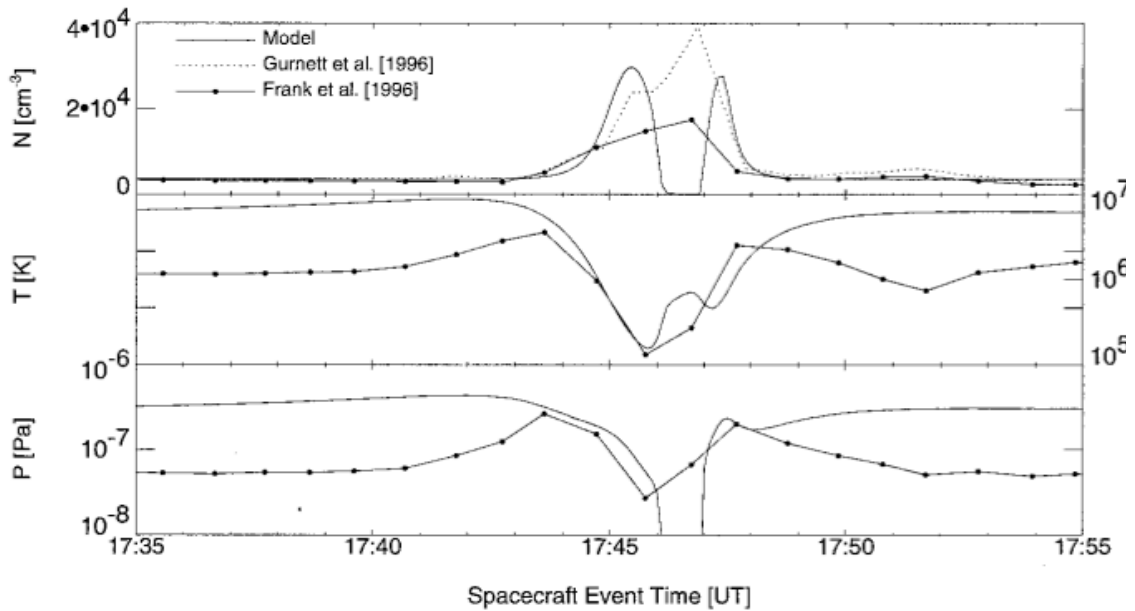


Figure 20: The plasma density, ion temperature and pressure from observations along J0 (plain lines) and the model results (with dots). Note the empty wake in the model results.

5.3 Hybrid models

Hybrid models have been intensively developed for Titan and Mars. *Lipatov and Combi [2006]* developed a hybrid simulation of Io where the electrons are described as a fluid and the ions as particles. Because of computer limitation, their simulation assumes very heavy ions (~ 30 times the mass of oxygen ions) and their results are difficult to interpret.

We explored extensively this approach with the hybrid code of *Delamere et al. [1999; 2000; 2006; 2009]*. The difficulty of this approach is the spatial resolution needed to resolve the gyro-radius of the ions. An oxygen ion at co-rotation velocity in the magnetic field of Jupiter at Io has a gyro-radius ~ 5 km. Considering that the simulation domain should extend to $\sim 10 R_{Io}$ to capture the whole interaction (10,000s grid points required in each direction) and avoid the difficulties of the boundary conditions, a hybrid model demands a lot of computer resources and is practically difficult to achieve. Nonetheless, it might be the next relevant step in the effort of modeling Io.

6. OUR MODEL

Studies of the local interaction have been limited, therefore, to two main approaches: MHD models with parameterized ionization and charge exchange in the corona (i.e., no explicit chemistry) and 2-fluid models, ignoring the magnetic perturbation and assuming a plasma composition described by only one ion (SO_2^+) interacting with only one type of neutral (SO_2). Yet, the torus plasma is composed of multiple ionization states of S and O. This multi-species plasma interacts with Io's neutral corona, which is composed of S, O, SO_2 , SO to cite only some of the observed neutrals around Io. The ionization of the neutrals provides fresh plasma to the torus and ions resulting from both ionization and charge exchange are picked-up by the flow, altering considerably the composition and the energy of the plasma of the torus close to Io.

In this thesis, we will combine and extend both approaches. We have developed a multi-species chemical model, based on the chemical model of *Delamere and Bagenal [2003]*. The multi-species chemical model includes detailed atomic and molecular cross sections and computes the time evolution of the plasma composition, the gain of energy through pickup of ions with different mass and the cooling of electrons through inelastic collisions.

We describe first the multi-species chemical model. Then, we describe the Hall-MHD model to compute self-consistently the flow and magnetic perturbations including the “twist” of the electron flow by the Hall conductivity. Finally we couple both models.

6.1 *The multi-species chemical model*

The physical chemistry model used in this analysis was explained in detail in the attached article (*Dols et al., 2008*). We give below a succinct description of the model concepts sketched on Figure 21.

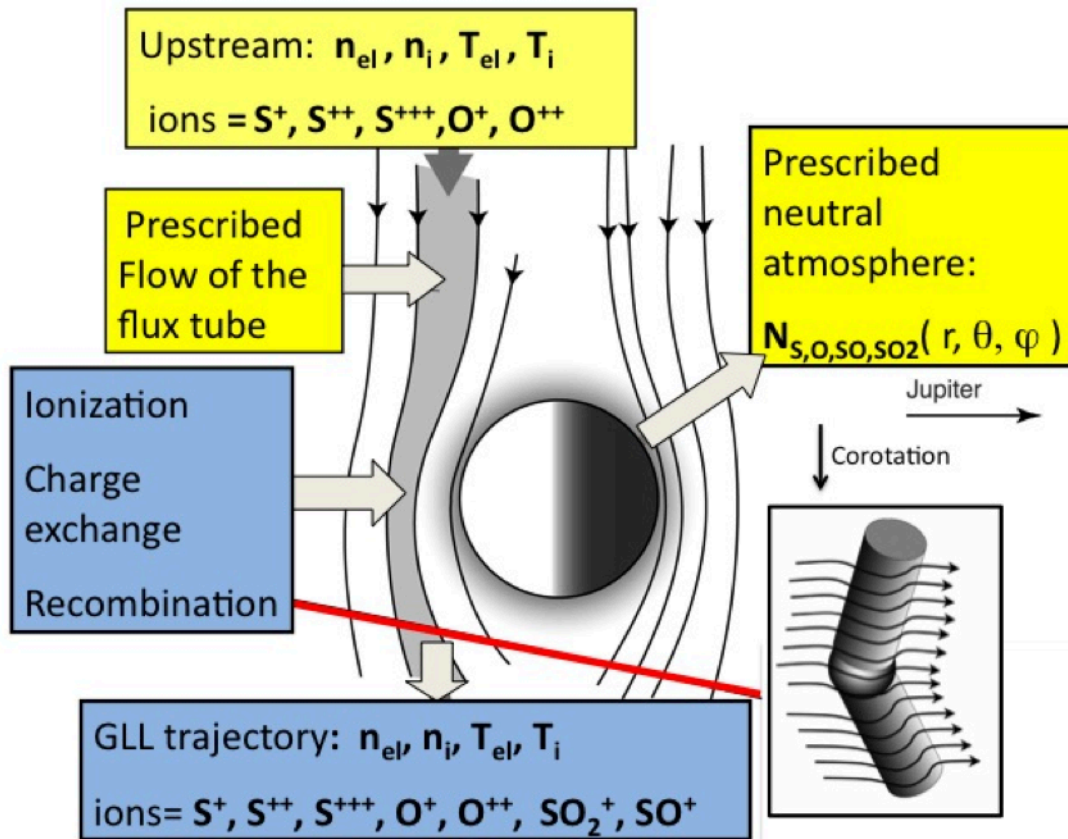


Figure 21: Concept of the multi-species chemical model in Io's equatorial plane. The insert in the lower right corner recalls that the flow is diverted all along the Alfvén tube.

A parcel of plasma of known composition and temperature, based on the Galileo observations upstream of Io, is carried along prescribed flow-lines around the moon. The parcel encounters a prescribed atmosphere of S, O, SO₂ and SO around Io. Its composition and energy are modified by ionization, charge exchange and electron recombination (see an illustration in Figure 22). The plasma density and average ion temperature are then collected along a Galileo flyby and compared to the observations. We solve the time-dependent equations for ion mass and ion energy of each species along prescribed flow-lines, taking into account the ionization and charge exchange reactions involving neutrals, electrons and ions of S, O, SO₂ and SO (see reactions in Figure 23) and equations in *Dols et al. [2008]*). The energy equation for electrons is also solved for the convected parcel, taking into account ionization, dissociation, Coulomb collisions with the ions and atoms and molecules excitation. Since the electrons are very mobile along the flux tube, the electron temperature that we compute is the flux

tube average temperature, based on electron density profile from Voyager (*Sittler and Strobel, 1987*), implicitly assuming instantaneous energy conduction in the flux tube. We assume that the torus plasma density, temperature and composition upstream of Io are spatially uniform. The prescription of the flow is 2-D (X and Y) and we make the simplifying assumption that Galileo flew at constant Z equal to the altitude of the closest approach. This is a reasonable approximation, especially given the uncertainties in the data with which we are comparing our model output. The neutral density is then calculated at each point of the 2-D trajectory of Galileo.

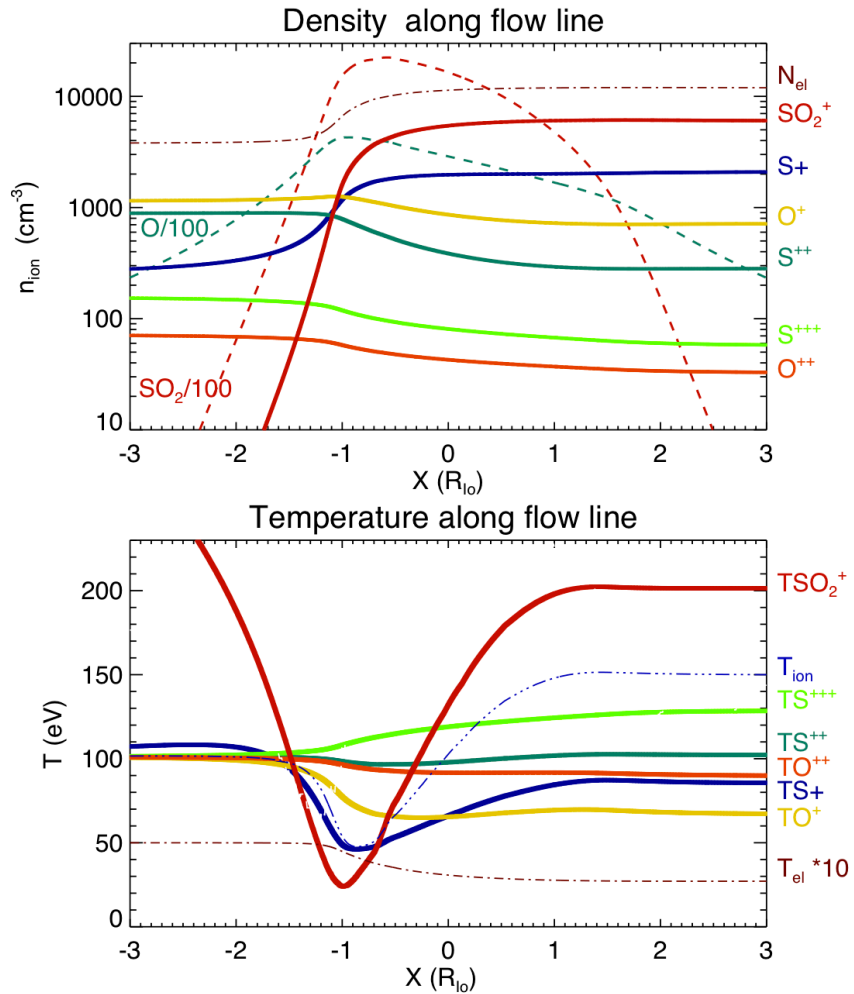


Figure 22: Illustration of the evolution of the composition and temperature (average ion energy) of the plasma flowing along a flow line on the flanks of Io in a multi-species atmosphere.

Molecular reactions		Atomic reactions	
$\text{SO}_2 + e^- \rightarrow \text{SO} + \text{O} + e^-$	Electron-impact dissociation ^a	$\text{S} + e^- \rightarrow \text{S}^+ + 2 e^-$	Ionization
$\text{SO}_2 + e^- \rightarrow \text{S} + \text{O}_2 + e^-$		$\text{S}^+ + e^- \rightarrow \text{S}^{++} + 2 e^-$	
$\text{SO}_2 + e^- \rightarrow \text{SO}_2^+ + 2 e^-$	Ionization	$\text{S}^{++} + e^- \rightarrow \text{S}^{+++} + 2 e^-$	
$\text{SO}_2 + e^- \rightarrow \text{SO}^+ + 2 e^-$			$\text{O} + e^- \rightarrow \text{O}^+ + 2 e^-$
$\text{SO}_2 + e^- \rightarrow \text{S}^+ + 2 e^-$		$\text{O}^+ + e^- \rightarrow \text{O}^{++} + 2 e^-$	
$\text{SO}_2 + e^- \rightarrow \text{O}^+ + 2 e^-$		$\text{S}^{+++} + e^- \rightarrow \text{S}^{++}$	Recombination
$\text{SO}_2^+ + e^- \rightarrow \text{SO} + \text{O}$	Dissociative-recombination	$\text{S}^{++} + e^- \rightarrow \text{S}^+$	
		$\text{O}^{++} + e^- \rightarrow \text{O}^+$	
$\text{SO}_2 + \text{SO}_2^+ \rightarrow \text{SO}_2^+ + \text{SO}_2$	Resonant charge exchange	$\text{S}^+ + \text{S}^{++} \rightarrow \text{S}^{++} + \text{S}^+$	Charge-exchange
$\text{SO}_2 + \text{O}^+ \rightarrow \text{SO}_2^+ + \text{O}$	Charge exchange	$\text{S} + \text{S}^+ \rightarrow \text{S}^+ + \text{S}$	
$\text{SO}_2 + \text{S}^{++} \rightarrow \text{SO}_2^+ + \text{S}^+$		$\text{S} + \text{S}^{++} \rightarrow \text{S}^+ + \text{S}^+$	
		$\text{O} + \text{O}^{++} \rightarrow \text{O}^+ + \text{O}^+$	
$\text{SO} + e^- \rightarrow \text{SO}^+ + 2 e^-$	Electron-impact ionization	$\text{O} + \text{O}^{++} \rightarrow \text{O}^{++} + \text{O}$	
$\text{SO}^+ + e^- \rightarrow \text{S} + \text{O}$	Dissociative-recombination	$\text{O} + \text{S}^+ \rightarrow \text{O}^+ + \text{S}$	
		$\text{S} + \text{O}^{++} \rightarrow \text{S}^{++} + \text{O}^+ + e^-$	
$\text{SO} + \text{S}^+ \rightarrow \text{SO}^+ + \text{S}$	Charge exchange	$\text{S} + \text{O}^+ \rightarrow \text{S}^+ + \text{O}$	
		$\text{S} + \text{O}^{++} \rightarrow \text{S}^+ + \text{O}^+$	
		$\text{O} + \text{S}^{++} \rightarrow \text{O}^+ + \text{S}^+$	
		$\text{O}^{++} + \text{S}^+ \rightarrow \text{O}^+ + \text{S}^{++}$	
		$\text{O} + \text{S}^{+++} \rightarrow \text{O}^+ + \text{S}^{++}$	
		$\text{O}^{++} + \text{S}^{++} \rightarrow \text{O}^+ + \text{S}^{+++}$	
		$\text{O} + \text{O}^+ \rightarrow \text{O}^+ + \text{O}$	
		$\text{S}^{+++} + \text{S}^+ \rightarrow \text{S}^{++} + \text{S}^{++}$	
		$\text{S} + \text{S}^{++} \rightarrow \text{S}^{++} + \text{S}$	
		$\text{S} + \text{S}^{+++} \rightarrow \text{S}^+ + \text{S}^{++}$	

^a used for the electron energy equation only

Figure 23: Physical chemistry reactions of the multi-species chemical model.

6.1.1 Summary of the modeling of the J0 flyby in *Dols et al. [2008]*

The goal of this article is to model the J0 flyby in the wake of Io. We give here a summary of the assumptions and results of the chemical model published in *Dols et al. [2008]* and refer the reader to the article attached to this thesis for a detailed discussion.

We prescribe the radial profile of the oxygen and sulfur atmosphere based on *Wolven et al. [2001]* UV observations shown in Figure 9 (see Section 3.1 for more details). We prescribe a radial profile of SO_2 based on the model of *Saur et al. [1999]*. This profile describes an SO_2 atmosphere in hydrostatic equilibrium with a scale-height at the surface ~ 100 km, increasing with altitude to ~ 300 km and an SO_2 atmosphere vanishing at a distance $\sim 3.5 R_{\text{Io}}$ where the S and O corona becomes dominant. We recognized that this profile is not derived self-consistently but it is reasonable: The scale

height of a few hundred km in the high atmosphere is consistent with the modeling of *Strobel [1994]*. With limited observations, it is sufficient for our purposes.

We show that for this prescribed multi-species atmosphere, the interaction is dominated by the SO₂ chemistry. The atomic chemistry, based on the Wolven profile, is a minor player. All incoming O and S ions are rapidly charge exchanged with SO₂ and the plasma composition in the center of the wake is dominated by SO₂⁺. We recognize that this result is not consistent with the plasma composition published by *Frank et al. [1996]* (see further discussion in Section 10.4). If the conclusion that SO₂ ions are the main output of the interaction is correct, the consequences for the plasma and energy supply to the torus are important: Molecular ions recombine rapidly and this recombination is followed by rapid dissociation in neutral fragments (atoms and molecules). We will explain in detail in Section 10.4 that the local interaction provides little plasma and energy to the torus and the source of its energy has to be found in the giant neutral clouds.

We show that the thermal electrons of the torus (5 eV) cannot provide enough ionization to fill the wake of Io. Molecules like SO₂ are very efficient at cooling the electrons, because of the numerous inelastic collision processes that they experience (ionization, dissociation and ro-vibrational excitation). When the electrons are cold, they are not able to provide further ionization. We include a simple description of the ionization of the atmosphere by the bi-directional electron beams discovered by Galileo in the wake, on the flanks and above the poles of Io (Figure 8). We used a formalism for auroral electrons on Earth described in *Rees [1989]*, where the energy deposition at altitude Z is calculated based on an effective stopping range and on the common assumption, that, whatever the nature of the atmosphere, electrons lose ~ 35 eV per ionization. Although the calculation proposed is a simplification of a complex electron transport code (*Grodent et al., 2001*), our estimation demonstrates that, for an SO₂ atmosphere consistent with our hypothesis, electron beams play a major role in the ionization around Io. This confirms the hypothesis proposed by *Saur et al. [2002]* although their formalism is different.

We compute a plasma production rate that is consistent with the plasma and energy flux in the wake of Io analyzed by *Bagenal [1997]*. We calculate the so-called pickup current, based on the rate of pickup in Io's corona and estimate it at 5 mega-amps. The rest of the current flows in the deep ionosphere as Pedersen and Hall

currents. This region is not covered by our model as the flow lines are diverted around it but the conclusion is that pickup currents are strong and thus might contribute substantially to the dynamics of the plasma flow around Io.

The limitation of this approach is the lack of self-consistent description of the flow. We first assume that the flow around Io is an incompressible flow around a solid obstacle (the Alfvén tube). This flow is accelerated along the flanks of Io to 114 km/s, twice the upstream flow velocity. When heavy ions such as SO_2^+ are picked up at this local velocity, the energy gain is about 2100 eV, leading to a high flank ion temperature inconsistent with the observations. In reality, the flow is slowed by the ionization and charge exchange processes close to Io and the momentum transfer from the torus plasma is limited (*Delamere et al.*, 2003). We then prescribe an “ad hoc” slowing of the flow close to Io to get reasonable flow velocities (a few km/s) in the deep atmosphere of Io and show that the ion temperature consistently decreases to match the observations.

To summarize the scientific contribution of this work:

- We demonstrate the importance of the SO_2 chemistry in the multi-species chemical interaction, calculating a plasma flux, a plasma density along the flanks of the wake and an ion average temperature consistent with the Galileo observations along the J0 flyby.
- We emphasize the consequences of a SO_2 -dominated chemistry: the plasma and energy supply to the torus coming directly from Io are very limited. The supply of energy and plasma probably comes from the extended neutral clouds.
- We demonstrate that the bi-directional field-aligned electrons beams provide enough ionization to account for the dense plasma in Io’s wake.
- The pickup process contributes significantly (~ 50%) to the Alfvén wing current.

A multispecies chemistry model of Io's local interaction with the Plasma Torus

V. Dols,¹ P. A. Delamere,¹ and F. Bagenal¹

Received 7 September 2007; revised 11 April 2008; accepted 22 April 2008; published 5 September 2008.

[1] We model the local interaction between the plasma in the torus and Io's neutral corona (inside $\sim 6 R_{Io}$), focusing on the multispecies chemistry outside the collision-dominated ionosphere. We include a detailed chemistry of S, O, SO₂, SO under ionization, charge exchange, and recombination processes in a parcel of plasma that follows a prescribed flow field around Io's ionosphere and interacts with the neutral density profiles in the corona, as constrained by available observations. We compare the model results to the Galileo plasma observations in Io's wake (GLL/J0). We conclude the following: (1) The plasma characteristics along GLL/J0 require a dense SO₂ corona confined close to Io ($< 2 R_{Io}$). (2) Molecular SO₂ chemistry dominates the interaction, with atomic chemistry playing a negligible role. (3) SO₂⁺ is the main output ion of the local interaction, but it recombines and dissociates rapidly so that the contribution of the local interaction to the global mass and energy supply of the torus is very small. (4) The high density of plasma observed in the wake requires a supplemental ionization source beyond the thermal electrons of the torus, and we estimate the ionization due to the (~ 350 eV) field-aligned electron beams observed around Io. (5) Assuming a SO₂ atmosphere/corona with a vertical column of 6×10^{16} cm⁻² and a prescribed deceleration of the flow around Io, we estimate a local ion mass production rate of ~ 200 kg/s. We also compute a neutral loss rate of ~ 2400 kg/s and a pick-up current of ~ 5.2 MAmp, both dominated by the SO₂ resonant charge exchange reaction.

Citation: Dols, V., P. A. Delamere, and F. Bagenal (2008), A multispecies chemistry model of Io's local interaction with the Plasma Torus, *J. Geophys. Res.*, 113, A09208, doi:10.1029/2007JA012805.

1. Introduction

[2] Our motivation for studying Jupiter's enigmatic moon Io is primarily to characterize the supply of plasma and energy to the Jovian magnetosphere taking place close to Io. However the nature of the plasma-atmosphere interaction also has important implications for the heating of Io's atmosphere and for electrodynamic coupling to Jupiter's ionosphere (see review by Saur *et al.* [2004]). For example, the detection of a UV auroral spot near the foot of the magnetic flux tube that connects to Io is a dramatic illustration of the long-range influence of the Io interaction (see review by Clarke *et al.* [2004]). The processes initiated near Io accelerate electrons toward both ionospheres of Jupiter and excite the UV auroral spots. A better understanding of the local interaction is thus needed as a first step to understand how and where the power is supplied to the Io/Jupiter system. Moreover, this local interaction is well constrained by data obtained on the several occasions that the Galileo spacecraft passed close to Io (see summary of flyby geometries by Bagenal *et al.* [2004]). While there remains some debate about the relative importance of direct

escape from volcanic geysers vs. sublimation of volcanic material deposited as frosts on Io's surface, there is no question about volcanic activity being the ultimate source of a patchy and variable bound atmosphere [reviewed by McGrath *et al.*, 2004]. Heated by the plasma interaction, Io's upper atmosphere extends as a corona to the Hill radius of $\sim 6 R_{Io}$ and subsequently feeds the neutral clouds that span several Jovian radii (R_J) along Io's orbit (see review by Thomas *et al.* [2004]). Plasma trapped in Jupiter's magnetosphere bombards these clouds with a relative velocity of ~ 57 km/s triggering reactions of dissociation, ionization, charge exchange, recombination as well as elastic collisions, which change the composition and energy of the incoming plasma. Io supplies about 1 ton/s of neutral material, about half of which becomes ionized to supply additional material to the torus of plasma surrounding Jupiter. The remaining neutral material undergoes charge exchange reactions in which energy is supplied to the torus plasma and energetic neutral atoms are lost from the jovian system. It is not clear, however, if the new plasma is supplied by ionization of the corona, close to Io, or by the extended neutral clouds far from Io. In this work, we focus on the local interaction at Io, defined as the interaction of torus plasma and the neutrals in Io's corona (or exosphere) within $\sim 6 R_{Io}$. The interaction of torus plasma with the extended neutral clouds is reviewed by Thomas *et al.* [2004] and recently modeled by Delamere *et al.* [2004].

¹Laboratory for Atmospheric and Space Physics, University of Colorado, Boulder, Colorado, USA.

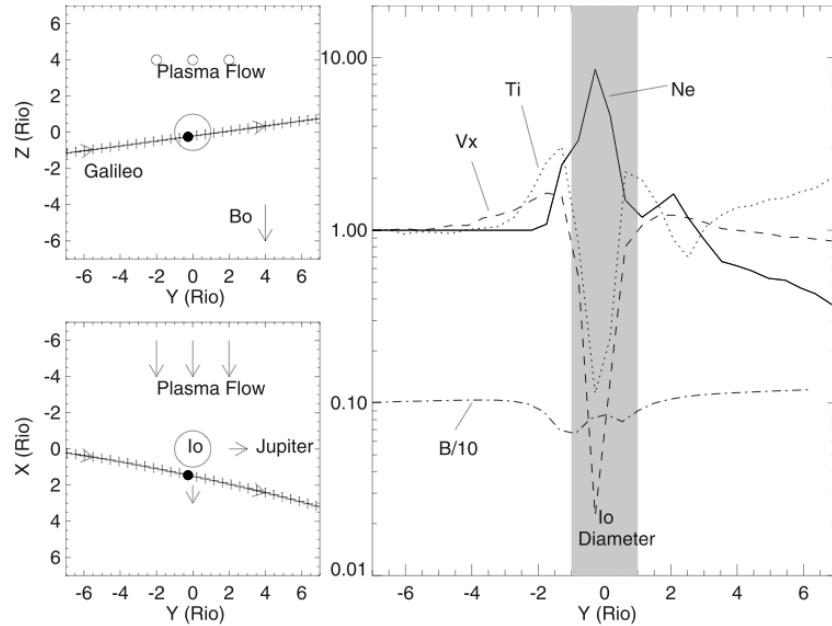


Figure 1. The J0 trajectory of the Galileo spacecraft and plasma measurements made along the trajectory [Bagenal, 1997].

[3] On December 1995, Galileo flew about 900 km from the surface of Io on the side downstream of the corotating plasma flow (this flyby is called GLL/J0 in the rest of the paper). Later, Galileo made several close flybys on the flanks and over the poles of Io. In this paper, we use the GLL/J0 observations in Io's plasma wake as the major constraints of our model. The plasma characteristics along the GLL/J0 trajectory have been described by Bagenal [1997] and are shown on Figure 1 together with the probe trajectory. Galileo observed a dense wake of cold plasma. In the center of the wake, the electron density peaked at $\sim 30,000 \text{ cm}^{-3}$ and the flow slowed down to almost stagnation at $\sim 2 \text{ km/s}$. The average ion temperature rose to $\sim 300 \text{ eV}$ on the flanks then dropped to $\sim 10 \text{ eV}$ in the core of the wake. The magnetic field was depressed by an amplitude of $\sim 600 \text{ nT}$. Far from Io, Galileo observed a background plasma that was denser and hotter than observed by Voyager 1 in 1979, with a plasma density $\sim 4000 \text{ cm}^{-3}$ (compared with the Voyager 1 value of $\sim 2000 \text{ cm}^{-3}$) and an average ion temperature $\sim 100 \text{ eV}$ (compared with Voyager's $\sim 60 \text{ eV}$). The background GLL/J0 plasma flow $\sim 45 \text{ km/s}$, rather slower than the relative velocity of the plasma in Io's reference frame (57 km/s) but, according to Frank *et al.* [1996] uncertainties in the ion composition introduce uncertainties in the flow speeds of $\sim 15\%$ which do not rule out the possibility of full corotational flow. Figure 1 shows an asymmetry in the plasma characteristic along the GLL/J0 trajectory relative to Io's location which may result of several factors. First, there is an effect of Galileo's slanted trajectory relative to the flow direction. Second, the flow around Io is probably asymmetric as Saur *et al.* [1999] showed with 2-fluid modeling. Third, there might be some effect of the relatively large gyroradius of heavy ions

($\sim 20 \text{ km}$ for an SO_2 ion at 60 km/s) that may affect the plasma density profile in the wake. This study does not address the asymmetry of the plasma parameters and for the rest of the paper we will compare the model results and the GLL/J0 data for only the inbound trajectory, on the anti-Jupiter side of Io.

[4] Since the local interaction has been extensively studied in the past (see review by Saur *et al.* [2004]), we briefly summarize the previous results that are particularly relevant to our study. There has been considerable study of the plasma-Io interaction with numerical models that self-consistently solve the 3-D MHD equations for a one-fluid plasma [Linker *et al.*, 1988, 1989, 1991, 1998; Combi *et al.*, 1998]. Such models simulate the flow of a magnetized plasma encountering a conducting sphere representing Io and its dense ionosphere. They model the ionization and charge exchange taking place in the corona by prescribing the rates of these reactions in a spherical cloud around Io. These rates are parameterized by the lifetime of each reaction. The model parameters are then adjusted to fit the plasma characteristics observed along the GLL/J0 trajectory. In general, such models are able to reproduce the gross features of the plasma observed in the wake. An alternative approach is to assume a steady state 3-D 2-fluid to study the interaction of electrons and of one type of ion (SO_2^+) with a prescribed SO_2 atmosphere that extends down to the surface of Io [Saur *et al.*, 1999, 2002, 2003]. These authors compute effective conductivities based on ionization, charge exchange and elastic collisions. They then self-consistently compute the electric field, the electric current, the electron and ion velocities, the electron and ion temperature and plasma density around Io. Although they do not self-consistently compute the magnetic field perturbation

tion, they are able to evaluate it a posteriori through the application of Ampere's law from the calculated current. Their plasma flow is comparable to the MHD flow far from Io, but becomes strongly decelerated and highly asymmetrical in the collisional ionosphere. Because of a strong Hall effect, the electron flow is strongly twisted toward Jupiter while the ion flow is slightly diverted in the anti-jovian direction. This separation of the electron and ion flows leads to high currents in the ionosphere that are eventually diverted along the magnetic field in the Alfvén wing. *Saur et al.* [1999] compute an Alfvén wing current of 5 MAmp. They claim that their boundary conditions are more physical than the ones used by Linker et al. because, they argue, when a flow line hits the surface of Io it ends up empty of plasma. The direct effect of this boundary condition is that Io's wake becomes devoid of plasma and their plasma density profile along the GLL/J0 trajectory presents two peaks on the flanks and a large "bite out" in the middle. *Saur et al.* [1999] state that this "bite-out" is due to the simplification of their model whereby there is no electron flow along the field lines to fill the wake. In further publication, *Saur et al.* [2002] fill their empty wake with a new ionization source in Io's downstream atmosphere, provided by energetic electron beams (detected by Galileo in the wake) flowing along the magnetic field lines. In general, *Saur et al.* [2002] were able to address many detailed features of the GLL/J0 measurements, such as the double-peaked magnetic perturbation.

[5] Studies of the local interaction have been limited, heretofore, to 2 main approaches: MHD models which parameterized ionization and charge exchange rates in the corona (i.e., no explicit chemistry); or through 2-fluid modeling assuming a plasma composition described by only one ion (SO_2^+) interacting with only one type of neutral (SO_2). Yet we know the torus plasma is composed of multiple ionization states of S and O. This multispecies plasma interacts with Io's neutral corona that is composed of S, O, SO_2 , SO to cite only some of the observed neutrals around Io. The ionization of the neutrals provides fresh plasma to the torus and ions resulting from both ionization and charge-exchange are picked-up by the flow, altering considerably the composition and the energy of the plasma of the torus close to Io. We focus on the multispecies chemistry of the interaction in Io's corona, outside of the collision-dominated ionosphere. Thus we do not consider the elastic collisions and the resulting conduction current through Io that *Saur et al.* [1999] address. Because of the complexity of the chemical reactions assumed in this work, we necessarily simplify the electrodynamic description of the interaction.

[6] This work addresses the following issues:

[7] (1) Can a multispecies model match the observed plasma parameters along the GLL/J0 trajectory? We show that, assuming prescribed neutral densities described in section 2.2, the model provides a reasonable fit to the wake observations.

[8] (2) What is the dominant chemistry of the local interaction? We show that molecular (SO_2) chemistry dominates over the atomic (S, O) chemistry.

[9] (3) How much fresh plasma is globally supplied to the torus by the local interaction? We show that the supply of plasma very close to Io is relatively minor (200–300 kg/s)

and that this fresh plasma is delivered as molecular ions that recombine and dissociate rapidly as atomic neutrals. We conclude that the local interaction at Io contributes very little to the global mass and energy supply of the torus. The bulk of the plasma delivered to the torus is thus probably supplied by the extended neutral clouds far from Io.

[10] (4) What is the rate of neutral removal from Io's corona as ions? We show that about 2–3 tons/s of neutral material are removed from the corona but almost all escape rapidly from the torus system as fast neutrals.

[11] (5) What is the contribution of currents generated in the pick-up process (subsequent to ionization or charge exchange) to the currents propagating along the Alfvén wing? We show that the pick-up current (2–3 MAmp) contributes significantly to the Alfvén wing current and thus to the dynamics of the plasma flow around Io.

[12] (6) We show that the $\sim 350\text{eV}$ parallel electron beams observed by Galileo in Io's wake could contribute significantly to the plasma production if also present in the dense atmosphere of Io.

2. Model

[13] The basic idea of the model is to follow a parcel of the torus plasma in its motion around Io. We impose plasma properties upstream of Io as observed in the torus (i.e., density, temperature, and composition). The motion of the plasma parcel is prescribed as an incompressible flow around a solid obstacle representing Io and its collision-dominated ionosphere. As the parcel approaches Io, it encounters the neutral corona where ionization, charge exchange, pick-up and recombination take place, changing the ion composition and temperature of the parcel. The plasma characteristics of the parcel are then collected along the GLL/J0 trajectory and compared with the observations. The plasma production rate, the neutral loss rate, the ion mass production rate and the pick-up currents are computed over the whole simulation box for a range of different assumptions about the distribution of neutrals and flow velocity around Io. The simulation box is centered on Io and extends from $-10 R_{\text{Io}}$ to $+10 R_{\text{Io}}$ in the flow direction and $-5 R_{\text{Io}}$ to $+5 R_{\text{Io}}$ in the Io-Jupiter direction.

[14] In order to fully explore the plasma chemistry we keep the electrodynamics simple and make several assumptions that are justified in each sections of the model description. A summary of the simplifications and assumptions of the present modeling can be found in section 2.5.

[15] The model is not dynamically self-consistent in the sense that the velocity of the parcel is prescribed and does not include any effects of collisions, charge exchange or ionization on the flow [e.g., see *Linker et al.*, 1998]. The model is also not electromagnetically self-consistent. Elastic collisions in Io's ionosphere, ionization and charge exchange are sources of currents through Io's corona that are eventually the cause of the diversion of the flow around Io. Here the flow diversion will be prescribed without calculating the effects of ionization and charge exchange on the flow. Finally, the model is not completely chemically self-consistent in the sense that the neutral densities of the major neutral species are prescribed and not consistently computed from the primordial SO_2 volcanic and sublimation sources. Nevertheless, these simplifications allow us to

elucidate the role of multispecies physical chemistry on the interaction of the torus plasma with Io's extended atmosphere.

2.1. Chemical Model

[16] The physical and chemical interactions of the plasma in the torus with the neutrals around Io is based on the multispecies physical chemical model by *Delamere and Bagenal* [2003]. This model (hereafter referred to as the "homogenous torus" model) is initially a homogenous 0-D time-dependent torus model that includes the atomic chemistry of S and O and ions thereof. The model solves equations of conservation of mass and energy for each ion species and electrons. It incorporates experimental data for coulomb collisions, ionization, recombination, charge exchange and UV radiative losses and has proved to be successful at investigating variability of torus properties. We have adapted the model to describe the local chemistry that takes place in the plasma parcel along its path through Io's neutral corona. We have added the molecular chemistry of SO₂ and SO and have used the electron energy equation by *Saur et al.* [1999]. It includes cooling due the inelastic collisions between electrons and ions, which is particularly important close to Io where the neutral density is very high. We will not consider the effects of the small hot electron population in the incoming torus plasma. *Saur et al.* [2003] calculated that this population accounts for a mere 2% of the total ionization close to Io. We also ignore photo-ionization, which contributes less than 15% of the total ionization rate *Saur et al.* [2003]. We have listed in Appendix A all the chemical reactions considered in this work and in Appendix B the mass and energy equations as well as references for their reaction rate coefficients. Here we summarize a few noteworthy features of this large ensemble of chemical reactions:

[17] (1) Electron impact dissociation of SO₂ is the fastest reaction. *Smyth and Marconi* [1998] computed the characteristic lifetime of an SO₂ molecule experiencing a Voyager plasma conditions and computed a dissociation lifetime of a few hours, much faster than any other electron impact reaction. We do not include electron impact dissociation in the chemistry because it is implicitly accounted for by taking prescribed neutral atomic profiles (shown in section 2.2.2) based on observations which result from the fast dissociation. However we include it in the electron energy equation as an energy loss process. The atomic distributions implicitly result from the fast dissociation, which, together with the elastic collisions eventually feed the extended neutral clouds.

[18] (2) New ions resulting from ionization or charge exchange are picked up by the flow: they acquire a gyrocenter drifting velocity as well as a gyromotion velocity equal to the local flow velocity. The average energy of the gyromotion is an essential heating source for the plasma of the torus: An SO₂⁺ ion picked up at a local flow velocity of 60 km/s acquires a gyromotion energy ~1080 eV, which is large compared with the average ion thermal energy upstream ~100 eV. We show, however, that this energy source is less effective than one might initially suppose.

[19] (3) The atomic ion recombination rate is small while the molecular ion dissociative recombination is very fast because each particle resulting from the dissociation can

carry the extra energy of the incoming electron. In Io's wake, the electrons are cold and numerous. The dissociative recombination is thus very efficient at removing molecular ions before they can be added to the torus (as discussed further in section 3.4).

2.2. Neutral Density Profiles in Io's Corona

[20] SO₂ is the dominant species of Io's bound atmosphere. By-products of the fast SO₂ dissociation (S, O and SO) have been observed close to Io, extending to several R_{Io} . In our model, we will prescribe the neutral profiles of S, O, SO₂ and O in Io's corona, constrained as best as possible by the available observations. The profiles applied in this work are shown on Figure 2. The SO₂ profile represents a dense atmosphere bound to Io with a corona whose radial extent is sharply cut off by the fast dissociation processes. At about 2 R_{Io} from the surface, the atomic products of the dissociation process (S and O) dominate and their profiles extend smoothly to far distances consistently with the UV observations of S and O emissions described below.

2.2.1. Neutral SO₂ and SO Radial Density Profiles

[21] The SO₂ atmosphere has been extensively studied in the last two decades but some fundamental questions about its source and distribution remain unanswered. It is probably patchy and variable due to its volcanic and sublimation sources. As extensively reviewed by *McGrath et al.* [2004] and *Lellouch et al.* [2007], the emerging picture is an SO₂ atmosphere covering 50–70% of Io's dayside, concentrated at low latitudes with an average density column $\sim [1-10] \times 10^{16} \text{ cm}^{-2}$. The SO₂ radial profile is poorly determined. To describe a localized dense SO₂ atmosphere/corona, we will use the very simplified SO₂ radial density profile by *Saur et al.* [1999]. These authors propose a radial hydrostatic atmosphere with a surface scale height of 100 km, vanishing at a distance of 3.5 R_{Io} above the surface. Although a rigorous physical basis for such a profile is lacking, it simulates the removal of the neutral atmosphere by the torus plasma flow and will be sufficient for our purposes. We use this radial profile to prescribe the density in Io's equatorial plane. Since observations suggest Io's atmosphere seems to be confined to the equator, we assume that this radial profile extends uniformly along the Jovian magnetic field line crossing Io with a thickness = $1R_{Io}$. This radial density profile of SO₂ is scaled to produce a vertical column $\sim 6 \times 16 \text{ cm}^{-2}$, which falls in the range of the observations cited by McGrath. In the rest of the paper, we will call this profile, the "Nominal SO₂" profile (case 3 of Table 1). We will also scale the SO₂ profiles to a "Reduced SO₂" (case 4) and an "Enhanced SO₂" column (case 5) to roughly span the observed range.

[22] SO has been detected both in millimeter observations and infrared spectroscopy [reviewed by *McGrath et al.*, 2004]. SO is a by-product of SO₂ dissociation but it was also observed as direct ejection from a volcanic vent. The interpretation of the observations is still ambiguous, consistent either with a very low column hemispheric SO atmosphere or a SO column mixed with SO₂ on a restricted fraction of Io's surface with a SO/SO₂ mixing ratio ~10%. In this work, we will make the simplifying assumption that SO and SO₂ are collocated and thus assume an SO radial density profile similar to the SO₂ profile with a radial column of 10% of the SO₂ column.

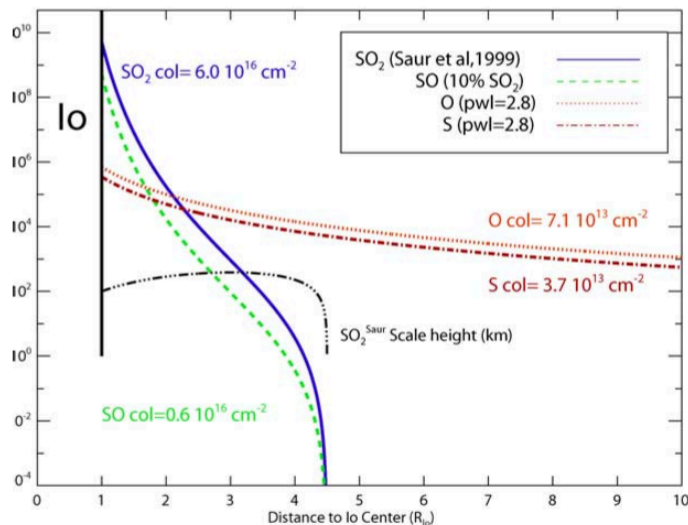


Figure 2. Nominal neutral density profiles and their vertical density columns. “Col” means vertical column density and “pwl” is the powerlaw index. The three-dot dashed line represents the scale height in kilometers of the SO_2 atmospheric model from *Saur et al.* [1999].

2.2.2. Radial Density Profiles of Neutral Sulfur and Oxygen

[23] Atomic sulfur and oxygen emissions have been extensively observed near Io and in the torus. *McGrath et al.* [2004] explain that these emissions are difficult to interpret unequivocally in terms of neutral density profiles because they represent a line-of-sight brightness integration that depends on the neutral density, the electron density and the electron temperature. The excitation itself can result from direct electron impact on atomic species or dissociative excitation of molecular species. *McGrath et al.* [2004] state that it is generally assumed that direct electron impact on atoms is the excitation mechanism and that the electron density and temperature are constant along the line of sight. All are questionable assumptions and the atomic neutral atmosphere very close to Io is thus poorly constrained. *Wolven et al.* [2001] observe O and S emissions around Io at very high spatial resolution, using the Space Telescope Imaging Spectrograph. They provide radial brightness profiles from ~ 1 to ~ 10 Io radii. These profiles are quite complex, revealing distinct emission regions near Io’s equator: limb glow on the hemisphere facing Jupiter, equatorial spots under $1.4 R_{\text{Io}}$, and diffuse emissions beyond.

The slopes of these powerlaw profiles between 1.4 and $4 R_{\text{Io}}$ have indices ranging from -1.51 to -1.97 , depending on the hemisphere (trailing/leading) and on Io’s orbital phase. Assuming nominal torus values for the electron density ($\sim 2000 \text{ cm}^{-3}$) and temperature (5 eV) and a spherically symmetric distribution of O emissions, the authors compute a neutral O density at $2 R_{\text{Io}}$ of $\sim 1-2 \times 10^5 \text{ cm}^{-3}$. This O density at $2 R_{\text{Io}}$ is reasonable as the electron temperature and density are probably close to their background value at this distance. In this work, for simplicity, we assume an oxygen brightness power law slope of -1.8 in Io’s equatorial plane, in the range of *Wolven et al.*’s [2001] analysis. The electron density and temperature certainly vary strongly close to Io, but, as these two effects cannot be untangled by the observations, we will make the simplification that the increase in brightness toward Io is caused only by the radial increase of only neutral density and that the electron density and temperature are constant and equal to their nominal Voyager’s values ($T_{el} = 5 \text{ eV}$ and $n_{el} = 2000 \text{ cm}^{-3}$).

[24] The brightness profile powerlaw can then be used to infer an oxygen density profile power law index of -2.8 , assuming a spherically symmetric atmosphere. We extend this O profile from Io’s surface to $10 R_{\text{Io}}$ and scale it to

Table 1. Atmospheric Properties Used in Each Sensitivity Experiment

Experiment	Name	SO_2 Column, cm^{-2}	SO Profile	S Column, cm^{-2}	O Column, cm^{-2}
Case 1	nominal O, S			3.7×10^{13}	7×10^{13}
Case 2	dense O, S			3.7×10^{14}	7×10^{14}
Case 3	nominal SO_2	6×10^{16}	10% SO_2		nominal S and O
Case 4	reduced SO_2	2×10^{16}	column, profile		profiles—same
Case 5	enhanced SO_2	30×10^{16}	collocated with		as Case 1
Case 6	slowed SO_2	6×10^{16}	SO_2 profile		
Case 7	electron beams	6×10^{16}			

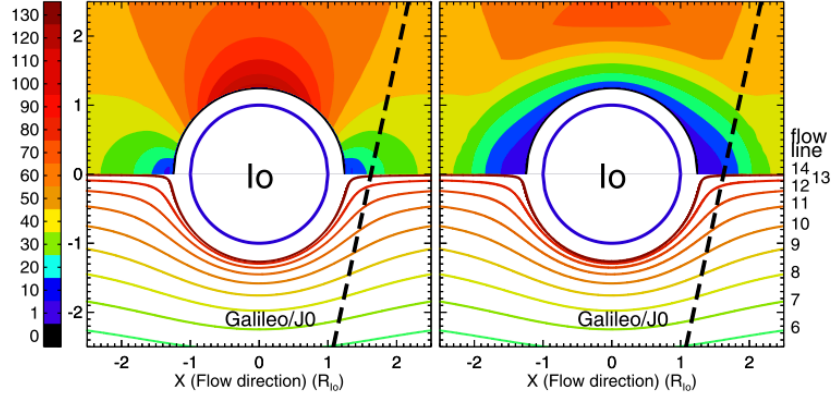


Figure 3. Flow velocities (km/s) and flow lines for the prescribed nonslowed and slowed flow. The colored upper half refers to the color scale on the left and shows the speed of the flow. Each flow line is assigned a number on the right and a color not related to the color scale that will help identify the flow line intersections with GLL/J0 on the next figures. The full simulation box extends from -10 to $+10 R_{10}$ along the flow direction and from -5 to $+5 R_{10}$ in the jovian direction.

match the density of 10^5 cm^{-3} at $2 R_{10}$. *Wolven et al* [2001] also report a relatively constant O/S emission ratio that may reflect the stoichiometric ratio of the SO_2 parent molecule. We will assume a neutral S density profile similar to the O profile with a O/S ratio of 2. The columns of S and O are poorly constrained. *Ballester* [1989] report vertical columns ranging between $2.2 \times 10^{12} \text{ cm}^{-2} < N_S < 7 \times 10^{15} \text{ cm}^{-2}$, spanning 3 orders of magnitude and $N_O > (4-7) \times 10^{13} \text{ cm}^{-2}$. From the profiles described above, we get a vertical column of $7.1 \times 10^{13} \text{ cm}^{-2}$ for atomic oxygen and $3.7 \times 10^{13} \text{ cm}^{-2}$ for sulfur consistent with the observational range. In the rest of this paper, these O and S profiles will be called the “Nominal O and S” neutral density profiles. They are shown on Figure 2. We explore the sensitivity of the model to O and S densities by increasing these columns by a factor of 10 in section 3.1.

2.3. Two-Dimensional Flow Around Io

[25] In this work, we idealize the flow of the plasma around Io as an incompressible flow around a perfectly conducting obstacle representing Io and its collision-dominated bound ionosphere. We thus model the interaction in the corona itself and not deep down in the ionosphere where conduction currents dominate the dynamics. Although the bound ionosphere is critical for the self-consistent computation of the flow [*Saur et al.*, 1999], this flow is almost stagnated as confirmed by Galileo flow measurements on a polar flyby through the Alfvén wing (flow velocity $< 2 \text{ km/s}$ [see *Chust et al.*, 2005] for a summary of the flybys and references herein). The plasma is also very cold. These two factors imply that ionization and charge exchange rates are very small and thus little chemistry takes place in the bound ionosphere (see discussion in section 3.7). As stated in the introduction section, our focus is actually the computation of the plasma and the energy supplied locally to the torus and we can thus reasonably ignore the small contribution of the bound ionosphere.

[26] We use a flow description based on the work by *Neubauer* [1980]. *Barnett* [1986] used *Neubauer*’s model to fit the flow measured by *Voyager* during the Io flyby

deriving an obstacle size of $1.26 R_{10}$. This larger obstacle represents the size of the current distribution close to Io. The component of the flow used in this model are listed in Appendix C. The extension of the collision-dominated ionosphere (the obstacle) can be estimated by computing the neutral density where the ion/neutral collision frequency is approximately equal to the ion gyrofrequency [*Linker et al.*, 1998].

$$n_n \sigma_{i,n} v = \frac{\Omega_i}{2\pi} \quad (1)$$

where n_n is the neutral density, $\sigma_{i,n}$ the ion/neutral collision cross-section, v the relative velocity of ions and neutrals and Ω_i the gyrofrequency of the main ion involved in the collision. At Io, assuming SO_2 ions and a magnetic field = 2000 nT, $\Omega_i \sim 1 \text{ s}^{-1}$. Assuming a $\text{SO}_2^+/\text{SO}_2$ collision cross-section varying between 4 and $20 \cdot 10^{-16} \text{ cm}^2$ (for induced dipole attraction or SO_2^+ resonant charge exchange [*Saur et al.* 1999]) and a flow velocity varying between 10 and 57 km/s, the boundary of the collision-dominated ionosphere is reached when the neutral density is between 4.4×10^7 and $1.2 \times 10^9 \text{ cm}^{-3}$. For the SO_2 density profile shown on Figure 2, this neutral density is reached between 1.1 and $1.35 R_{10}$ from Io’s center. *Barnett*’s obstacle size falls in this range, so for simplicity, we will use his $1.26 R_{10}$ obstacle’s size and argue that this simplification is sufficient for the limited purpose of assessing the effects of the multispecies chemistry. The flow speed assumed in this model is shown on the left-hand side of Figure 3. Close to Io, the flow is slowed down to $\sim 10 \text{ km/s}$ upstream and diverted along the flanks where it is accelerated to $\sim 114 \text{ km/s}$ (twice the upstream velocity [*Neubauer*, 1980]). The flow is then slowed again in the wake to $\sim 10 \text{ km/s}$ before reaching the 57 km/s background flow velocity farther downstream. We assume that the flow is similar above and below Io’s orbital plane so that there is no flow passing above or under Io.

[27] We emphasize that this flow pattern was deduced from observations far from Io’s neutral corona ($\sim 10 R_{10}$ south of Io, upstream of the Alfvén wing). Close to Io,

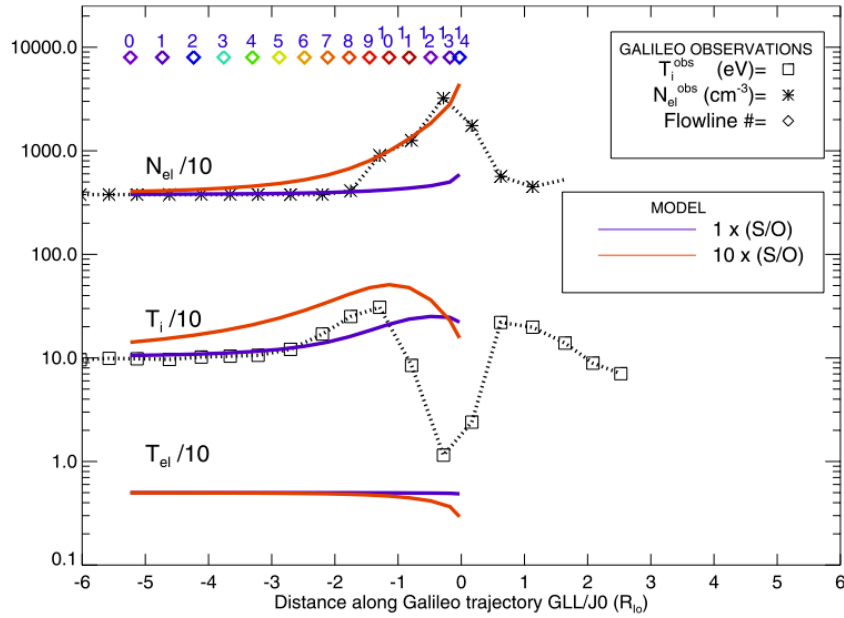


Figure 4. Plasma parameters along the GLL/J0 trajectory for an atmosphere of atomic S and O without any molecular components (Cases 1 and 2). The numbers and colors on top of this figure and the following ones represent the intersection of the flow lines shown on Figure 3 with the GLL/J0 trajectory.

ionization, charge exchange and elastic collisions slow the flow, as shown by the self-consistent simulations by *Linker et al.* [1989] or *Saur et al.* [1999]. We address the importance and rationale of the slowing of the flow in section 3.3

where we prescribe a slowing factor. This decelerated flow is shown on the right-hand side of Figure 3. On the same figure, we show some of the 15 flow lines (numbered from 6 to 14 and colored) that cover half of the simulation box

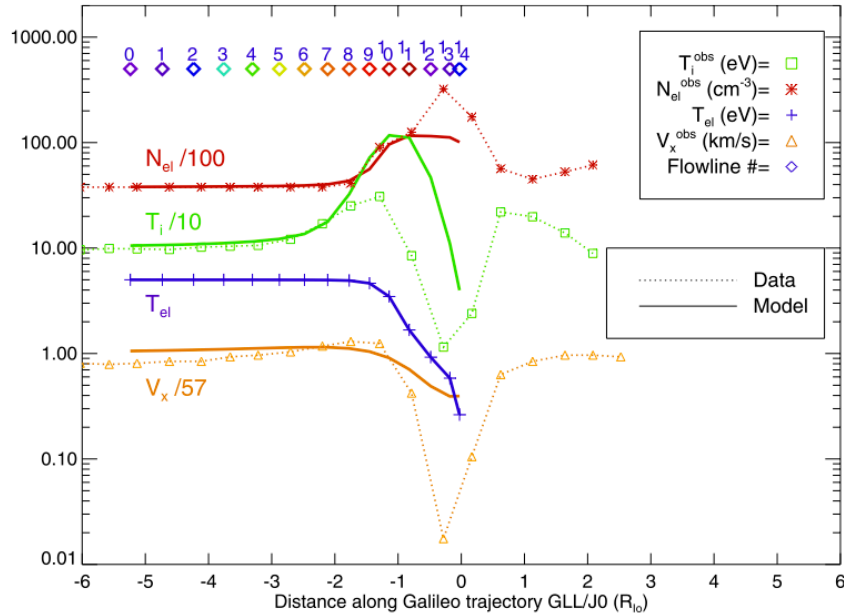


Figure 5. Plasma parameters along the GLL/J0 trajectory for a nominal atmosphere of O, S, SO, and SO₂ (Case 3).

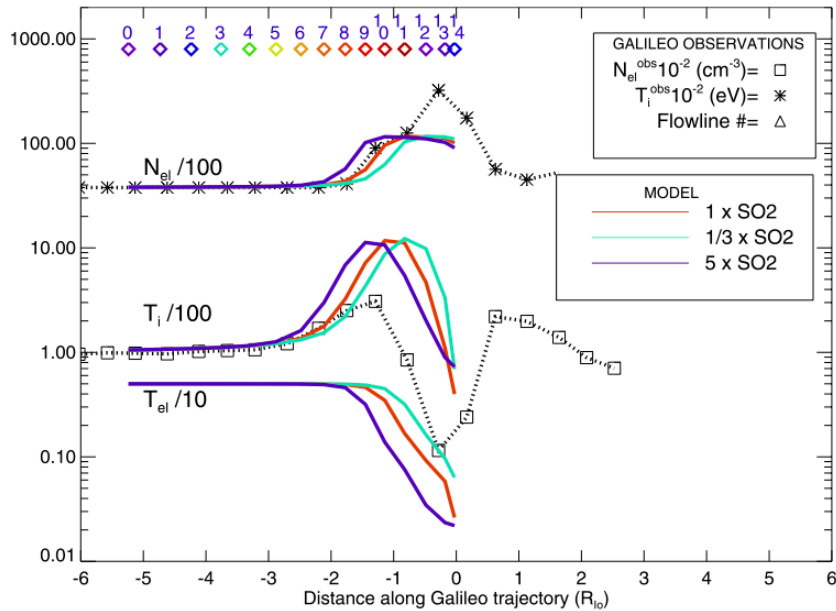


Figure 6. Plasma parameters along the GLL/J0 trajectory for the three sensitivity experiments on SO₂ column density: the nominal (1 × SO₂) Case 3, an enhanced (5 × SO₂) Case 5, and a reduced (1/3 × SO₂) Case 4.

($Y < 0$). The intersection of the 15 flow lines with the inbound Galileo trajectory GLL/J0 will appear on top of all the following figures showing our modeled plasma characteristics (Figures 4, 5, 6, 7, 8 and 11) with the same

numbering and color coding. By focusing on the neutral corona, the stretch that goes through the bound ionosphere is not being covered in the inbound leg of our plots. This stretch is very small because most of the flow is diverted

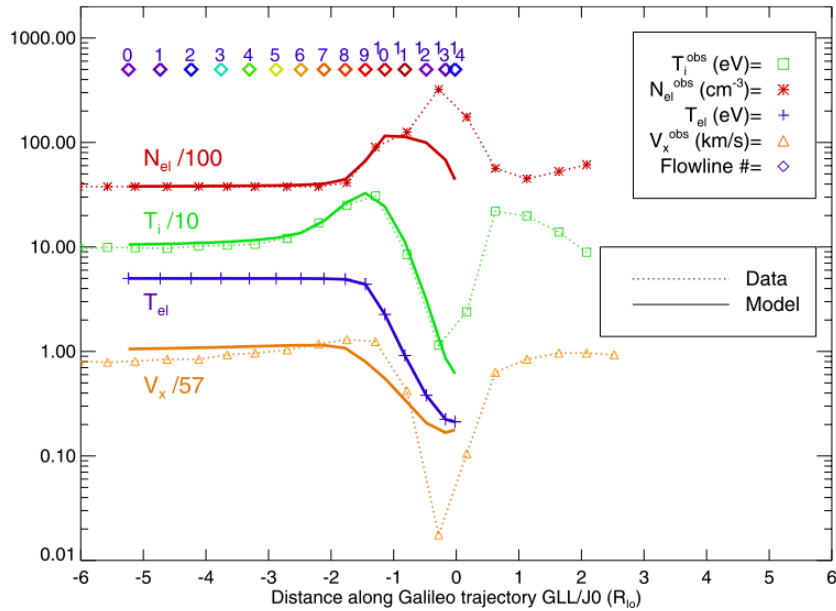


Figure 7. Plasma characteristics along the GLL/J0 trajectory for a nominal atomic and molecular atmosphere, with a prescribed slowing of the flow around Io shown on Figure 3 (Case 6).

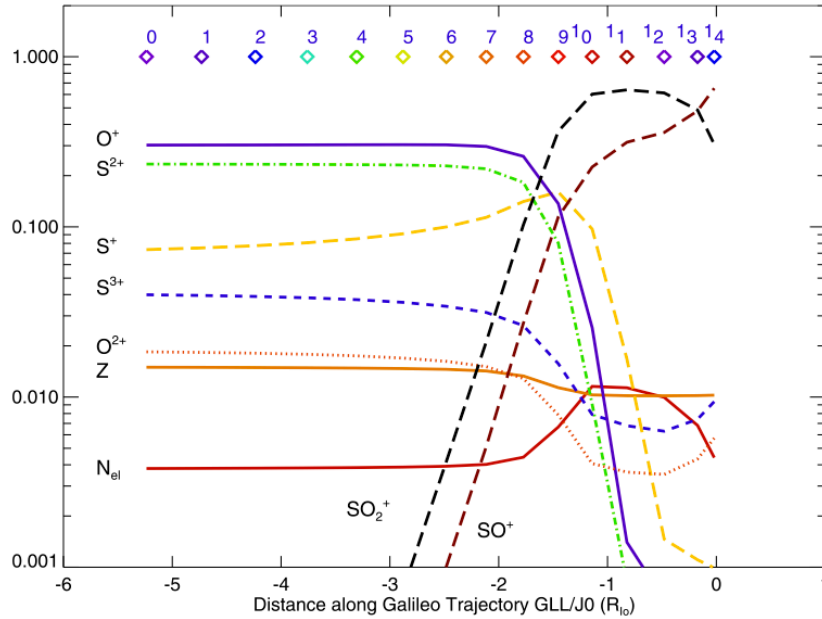


Figure 8. Mixing ratio for each ion along the GLL/J0 trajectory using the nominal atomic and molecular atmosphere and a slowed flow (Case 6 of Table 2). N_{el} is the electron density scaled by 10^{-6} .

around the bound ionosphere and it therefore does not have an effect on the results of this paper.

2.4. Upstream Plasma Description

[28] The upstream plasma characteristics used in this study are based on observations along the GLL/J0 trajectory far from Io. We use an upstream electron density $n_{el} = 3778 \text{ cm}^{-3}$, electron temperature $T_{el} = 5 \text{ eV}$ and ion temperature $T_i = 101 \text{ eV}$ [Bagenal, 1997; Cray et al., 1998]. Because the plasma composition is poorly constrained by in situ measurements, we base the ion composition of the upstream plasma in our model on the homogeneous, steady state simulations of Delamere et al., 2004. Based on an electron density of 3778 cm^{-3} , the respective ion upstream densities used in the model are as follows: $n(S^+) = 253 \text{ cm}^{-3}$, $n(S^{++}) = 886 \text{ cm}^{-3}$, $n(S^{+++}) = 156 \text{ cm}^{-3}$, $n(O^{++}) = 72 \text{ cm}^{-3}$, $n(O^+) = 1140 \text{ cm}^{-3}$, $n(SO_2^+) = 0 \text{ cm}^{-3}$.

2.5. Summary of Model Assumptions

[29] Because of the complexity of the chemical reactions assumed in this work, we made several working assumptions and simplify the electrodynamic description of the interaction. Some assumptions are based on the available observations, such as the radial profiles and columns of S and O. Some assumptions are simplifications that do not alter the conclusions of this work, such as considering the chemistry outside the collisional ionosphere. We argued that the ionosphere does not contribute much to the plasma and energy supply to the torus, which is the focus of this work so that the quantitative results of this modeling under this simplification are still relevant. Some assumptions are working hypothesis that we test in this paper, such as the column and profile of SO_2 and the prescribed flow velocity. We will show that the prescribed velocity field (called the

“non-slowed flow” in the rest of this article) as described in section 2.3 is not a good hypothesis but that some adaptation of this flow is needed in order for the model to match the ion temperature along the GLL/J0 trajectory. This adapted flow (“slowed flow” in the rest of the paper) and the quantitative results deduced from it (such as the plasma production rate, the neutral loss mass etc.) will be validated by computing a total Alfvén wing current that is reasonably consistent with Voyager observations and other modeling results published in the literature. We will show that the hypothesis of an SO_2 profile displaying a dense localized atmosphere close to Io is supported by the match of the modeled plasma density and ion temperature profiles along GLL/J0.

3. Model Results Along the Galileo/J0 Trajectory

[30] In this section, we present 7 sensitivity study cases (Table 1) and compare them to the GLL/J0 observations. These sensitivity studies represent a first step to allow us to determine the important characteristics of the neutral density profiles, flow velocity and dominant chemistry.

3.1. Considering Atomic Chemistry Alone

[31] We start our study of multispecies chemistry with the simplest assumption: we consider the O and S chemistry alone and ignore all molecular reactions. The rationale for this experiment is to explore the possibility that the plasma density and ion temperature profiles observed by Galileo in Io’s wake can be matched by the smooth atomic neutral clouds (extending to $\sim 10 R_{Io}$), even with increased column density but without the contribution of the dense SO_2 atmosphere that is localized very close to Io’s surface. In Case 1, we use the nominal S and O density profiles and in

Case 2, we explore the uncertainty in these profiles with a ten-fold scaling of the nominal profiles. Results for Cases 1 and 2 are presented in Figure 4. We have added the modeled electron temperature along the GLL/J0 trajectory although it was not observed at this high spatial resolution. In Case 1, the model does not reproduce the steep increase both in plasma density and average ion temperature, observed around flow line number 8, which samples Io's atmosphere at a distance $\sim 1 R_{10}$ from the surface. Case 1 does not provide much ionization. While increasing the neutral S and O columns does increase the ionization (Case 2), the profiles are still smoother than the data because the neutral profiles are themselves smooth. Obviously, the steep profiles of plasma density and ion temperature deduced from the data call for an additional process close to the flanks of Io. A possible way to increase ionization close to the flanks of Io could be a local denser atmosphere very close to Io's surface, such as SO₂. We will explore this possibility in the next section.

3.2. Adding a Molecular Neutral Atmosphere: SO₂ and SO

[32] In the following experiments, we use the S and O nominal profiles and add the SO₂ and SO profiles with variable column densities. Case 3 uses the nominal SO₂ column described on Figure 2. Case 4 uses a reduced SO₂ column density = 30% of the nominal column, Case 5 simulates an enhanced SO₂ corona where the column is 5 times the nominal one. Figure 5 shows the plasma conditions along the GLL/J0 trajectory for the nominal SO₂ profile of Case 3. Comparison with the atomic neutrals (cases 1 and 2 in Figure 4) demonstrates how the steeper profile of molecules produces a better fit to the observations but still does not match the core of the wake. Figure 6 compares Cases 3, 4, and 5. For all experiments, we obtain a steep increase in electron density and ion temperature at $\sim 2 R_{10}$ along the GLL/J0 trajectory (see flow line 8, skimming Io at a distance $< \sim 2 R_{10}$ from Io's center). This is in striking contrast to Cases 1 and 2 (Figure 4) where we use the flatter profiles of S and O. The reduced column of Case 4 and the enhanced column of Case 5 show that by increasing the overall density of the neutral SO₂ atmosphere the location of the density enhancement moves radially outward while the peak density is limited by electron cooling in the denser region close to Io. This important stabilizing effect will be re-emphasized in section 5.2. In all experiments the modeled plasma density at their peak is about 1/3 the observed value ($\sim 30,000 \text{ cm}^{-3}$) in the center of the wake. The flow lines beyond number 11 probe Io's atmosphere at distance closer than $0.4 R_{10}$ above the surface, where the neutral density is high. The inelastic collisions between electrons and neutrals cool the electrons down to a temperature lower than 1 eV, which inhibits any further ionization. These experiments suggest that the locally dense SO₂ atmosphere and the SO₂ chemistry are essential in order to explain the steep plasma density increase observed along the GLL/J0 trajectory at $\sim 2 R_{10}$ on the flanks of the wake. However to explain the dense center of the wake an additional mechanism needs to provide further ionization. As a test, we ran the model while bypassing completely the atomic chemistry and obtained essentially the same results. The chemistry of O and S, assuming the neutral density

profiles shown on Figure 2, plays a minor role both in shaping the plasma characteristics along the GLL/J0 trajectory as well as in contributing to the total neutral loss rate (see section 5.2). We emphasize that it is not the nature of SO₂ and its chemical reactions that matter but the fact that the neutral density is very high and localized close to Io. While we could have increased arbitrarily the S and O densities close to Io, where they are poorly constrained by observations, we recall that SO₂ has been observed close to Io with a high vertical column and is thus the main component of this dense localized atmosphere. The density of SO₂⁺ ions along GLL/J0 was deduced from the observations of ion cyclotron waves by the Galileo magnetometer [Huddleston *et al.*, 1997]. The data cover the flanks of the wake and no SO₂⁺ density could be computed right behind Io, from $-2R_{10}$ to $+2R_{10}$ along the GLL/J0 trajectory. The modeled SO₂⁺ density computed at $2 R_{10}$ along the GLL/J0 trajectory (flow line 7) for Case 5 is about $\sim 300 \text{ cm}^{-3}$. This result is in agreement with the Huddleston's inference of the minimum SO₂⁺ density at the same location on the inbound trajectory ($\sim 200\text{--}300 \text{ cm}^{-3}$) better illustrated in Figure 3 of Smyth and Marconi [1998] supporting a dense SO₂ atmosphere close to Io.

[33] Figures 5 and 6 illustrate two problems with the models so far:

[34] (1) The average ion temperature profile displays a steep increase around $2 R_{10}$ along the GLL/J0 trajectory. In all experiments, inward of flow lines $\sim \#8$, the average temperature is much higher than observed. This is the direct consequence of the flow field we assumed. Close to Io, the modeled flow is fast (twice the upstream velocity) and heavy ions such as SO₂⁺ and SO⁺ are picked-up at this high velocity. In the pick-up process, the heavy ions gain a large amount of energy in their gyromotion. SO₂⁺ ions picked-up at 57 km/s gain 1080 eV in thermal energy and about 4 times more at 114 km/s.

[35] (2) Even with a dense SO₂ atmosphere we are not able to produce the peak of the electron density in the center of the wake. This lack of plasma in the center of the wake may have several causes. We do not have any plasma flow above the poles, which could increase the plasma density in the wake. Another hypothesis is that we might be missing an alternative source of ionization. Saur *et al.* [2002] showed that electron beams parallel to the magnetic field, which were detected along the GLL/J0 trajectory can provide further ionization. We will address these two problems in the next sections.

3.3. Slowing the Flow

[36] The results of the above simulations lead us to investigate the limitation of our non self-consistent flow. The ionization and charge-exchange reactions extract momentum from the surrounding plasma. This should slow the flow around Io relative to that of an incompressible fluid moving past a cylindrical object. The first effect of such deceleration of the flow would be to decrease the average ion temperature as the new ions are picked-up at a slower flow velocity. Intuitively, the second effect of slowing the flow would be an increase of the plasma production (total ionization) as a parcel of plasma would spend more time in the dense atmosphere of Io. However, as we will show, this is not the case.

[37] Slowing the flow self-consistently is beyond the scope of this work. Nevertheless, we estimate the effect by forcing the flow to slow down close to Io. We introduce a prescribed deceleration that produces a reasonable match to the average ion temperature. In this simulation (Case 6), we keep the nominal neutral density of Case 3 but the flow velocity around Io is slowed by factor that ranges linearly from 100% at $\sim 1R_{Io}$ to $\sim 10\%$ at a distance of $0.26 R_{Io}$ above the surface. Thus at $1.26 R_{Io}$ on the flanks, the flow velocity is reduced from 114 km/s to ~ 10 km/s (see Figure 3). The slowing function is shown in Appendix C.

[38] The results of decelerating the flow are shown in Figure 7 and should be compared with Case 3 illustrated in Figure 5. The average ion temperature decreases drastically as the ions are picked-up at a slower flow velocity and the plasma density actually decreases on flow lines that pass in the dense part of Io's corona (flow lines 11 to 14). The cooling of electrons through inelastic collisions shuts down the ionization and counterbalances the longer time the plasma parcel is spending in Io's atmosphere. Figure 7 shows that this prescribed slowing of the flow, adjusted to roughly match the average ion temperature along the GLL/J0 trajectory, does not provide a good fit to the observed plasma velocity in the wake. As shown also in Figure 3, the prescribed slowed flow is symmetrical upstream and downstream. It does not describe the long wake of slowed flow that has been observed to extend downstream further than $7 R_{Io}$ [Hinson *et al.*, 1998]. The long wake consists of a dense and cold plasma, the flow is almost stagnated [Bagenal, 1997] and the dense SO₂ atmosphere vanishes rapidly with distance to Io. Its far-distance contribution to the plasma and energy supply to the torus is thus negligible. A self-consistent calculation of the flow, including the momentum transfer from the plasma in the torus, is needed to address the formation of a long wake but this detailed description of the flow is not the focus of this work. Our goal is to provide a reasonable flow where the SO₂ atmosphere is still dense ($< 2 R_{Io}$) and where the chemistry matters. The prescribed "slowed flow" is an attempt to prescribe such a flow, using the only constraint of the average ion temperature along GLL/J0. This slowed flow is a simplification of the flow close to the boundary of the stagnated ionosphere. A self-consistent flow calculation like Saur *et al.* [1999] shows that in this region, the flow lines have a geometry different from the one described here: the flow in the ionosphere is strongly slowed and the flow lines are straight lines tilted toward Jupiter. Like Saur *et al.* [1999], we show that the plasma density in the center of the wake cannot be explained by the ionization provided by the thermal plasma of the torus. We address this issue in section 3.5.

[39] In section 5.2, we will use our prescribed "slowed flow" to compute the total current along Io's Alfvén wing and claim that the reasonable results obtained give a posteriori support to this simplified slowing of the flow.

3.4. Flux Tube Composition After the Interaction with Io's Neutral Corona

[40] Figure 8 shows the mixing ratio of ions along the GLL/J0 trajectory, downstream of Io, computed for Case 6 with slowed flow. On flow lines that pass far from Io (i.e., flow lines 0 to 5), the downstream flux tube composition is similar to the upstream composition where O⁺ and S⁺⁺ are

dominant. On flow lines that pass through the dense atmosphere (i.e., flow lines 9 to 14), the composition is radically changed. The flux tube is almost depleted of all atomic ion species due to charge exchange of O⁺ and S⁺⁺ with SO₂ and S⁺ with SO (see Appendix A). Consequently, the downstream composition of the flux tubes that interacted strongly with the SO₂ corona is dominated by SO₂⁺ and SO⁺ ions and the average ion charge state ~ 1 (compared with ~ 1.5 in the upstream flow). This result has important consequences. Molecular ions recombine more rapidly than atomic ions because the molecular recombination is followed by quick dissociation and the resulting neutrals can carry the extra energy of the incoming electron. The dissociative recombination rate of molecular ions increases when the electron temperature drops and when the electron density increases, which are the plasma conditions in the dense cold wake. For example, if we assume an electron temperature in the wake of ~ 1 eV and a density of $\sim 10,000$ cm⁻³, we compute a characteristic time for dissociative recombination of ~ 1 hour (based on the reaction rate coefficients referred in Appendix B). This recombination time is very small compared to characteristic timescales of the torus like the torus period (~ 10 hours), or the coulomb interaction equilibration time (several days) or plasma radial transport (~ 30 days). Consequently, SO₂ and SO ions recombine, dissociate and most of them leave the torus system as fast neutrals before exchanging energy with background ions in the torus. This implies that Io's SO₂ corona provides very little mass and energy to the torus but does produce a huge source of fast neutrals. We discuss the issue further in section 3.7.

3.5. Field-Aligned Electron Beams

[41] Intense energetic (hundred eV to several keV) electron beams, aligned along Jupiter's magnetic field were observed in the wake, on the flanks and over the poles of Io. If field-aligned electrons are present where the neutral atmosphere is collisionally thick, they are likely very efficient at ionizing neutrals. Like auroral electrons on Earth, each electron of the beam is capable of many ionizations along its path through the atmosphere, losing a few tens of eV per ionization. We propose here to simply illustrate the effect of field-aligned electrons on Io's plasma production.

[42] Williams *et al.* [1996] detected bi-directional electron beams along the GLL/J0 trajectory with energy > 15 keV and a low energy flux ~ 0.03 ergs cm⁻² s⁻¹ (0.03×10^{-3} Watts m⁻²) in each direction [Williams *et al.*, 1999]. Similar beams were also detected on another flyby, along the anti-jovian flank of Io, ~ 200 km above the surface and potentially in the very dense part of the atmosphere [Mauk *et al.*, 2001]. Frank and Paterson [1999] report the detection of electron beams along the GLL/J0 trajectory in the range ~ 100 eV to ~ 1 keV. These beams have a lower average energy (i.e., ~ 350 eV) and a larger total energy flux ~ 4 erg cm⁻² s⁻¹ (4×10^{-3} Watts m⁻²), including both field-aligned directions. The ~ 350 eV electron beams were not observed along the flanks because of instrument failure but there is no reason to believe that they were not present as well [W.R. Paterson, personal communication, 2006].

[43] The ionization efficiency of these electron beams depends on two crucial elements: the incoming energy of

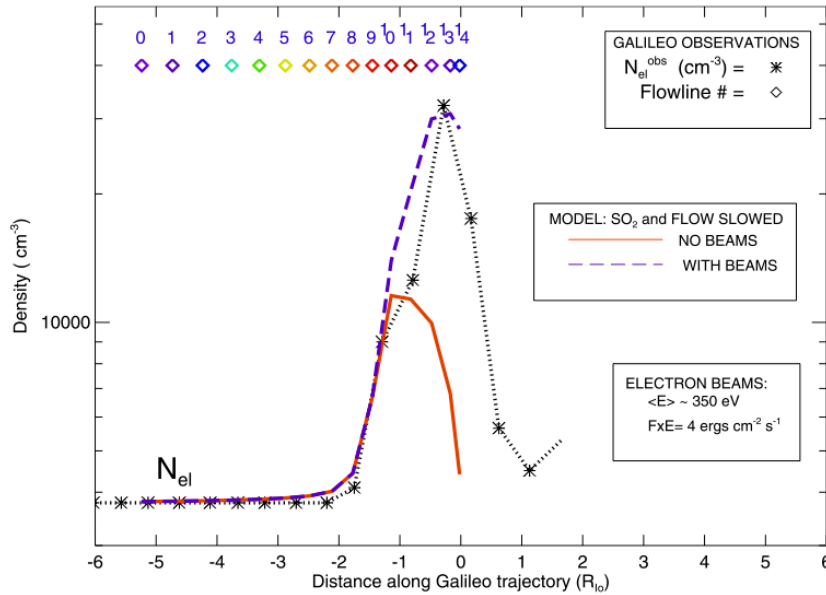


Figure 9. Plasma density along the GLL/J0 trajectory for a slowed flow. The solid line represents the modeled plasma density without the field-aligned electron beams of Case 6. The dashed line represents the plasma density computed with the supplemental contribution of the beams.

these electrons and the atmospheric column they encounter. If the electrons are too energetic or if the atmosphere is too thin, the electrons may go through the entire Io's corona without losing much of their energy. We will show that >15 keV electron beams provide negligible ionization even when they go through the dense part of Io's corona. The ~ 350 eV electron beams will be the most efficient at providing extra-ionization in Io's corona. The global distribution of these beams is not well known. It is constrained by Galileo observations along a few flybys (see *Chust et al. [2005]* for a summary) with very little flux upstream. In a simplified experiment, we assume a uniform flux of field-aligned electrons over the entire interaction region. The contribution of the field-aligned electrons to ionization is dependent on the column of neutral atmosphere, so little ionization is generated where the corona neutral density is low. In Appendix D, we estimate the ionization rate of the ~ 350 eV electron beams following the empirical formulation of *Rees [1989]* for the energy deposition of monoenergetic auroral electrons in the terrestrial atmosphere. We average this ionization rate, q_{beam} ($\text{cm}^{-3} \text{s}^{-1}$), on a cylindrical atmosphere $1 R_{10}$ high in the field-aligned direction using the nominal SO_2 densities along the profile of Figure 2. The electron density provided by this particular ionization process, assuming a typical characteristic time for the flow to go around the flanks of Io of $\tau \sim 60$ s, is

$$n_{el,beam} = \langle q_{beam} \rangle \tau \quad (2)$$

[44] We simply add this contribution to the plasma density calculated along the GLL/J0 trajectory that was provided by the thermal electron ionization. Figure 9 shows the electron density profile along the GLL/J0 trajectory of

Case 6 (Nominal SO_2 with slowed flow) with and without the 350 eV electron beams. The beams provide significant additional ionization for flow line numbers 10 to 14. Farther out, the atmosphere is tenuous and the ~ 350 eV electrons go through the density column without depositing much energy. We note that τ for flow lines very close to the bound ionosphere could be much longer for the slowed flow. That is why Figure 9 should be understood as a mere illustration of the efficiency of the beams.

[45] Finally, we illustrate the sensitivity of the results to the energy of the incident electrons. The electrons follow a convoluted path through the atmosphere and can eventually stop in the atmosphere after losing all their energy. The stopping distance for primary auroral electrons in the terrestrial atmosphere is described by an effective range (from *Rees [1989]*, see Appendix D)

$$R(E) = 4.3 \times 10^{-7} + 5.35 \times 10^{-6} E^{1.67} \quad (3)$$

where E is the incident energy in keV and the effective range, $R(E)$, is given in units of gm cm^{-2} . The effective range is an experimentally derived parameter and varies strongly with the incident energy (as $E^{1.67}$) but is practically independent of the nature of the target (S.C. Solomon, private communication). If the incident energy is too high, the stopping distance can be larger than the neutral mass column along the path of the electron. This means that the electron does not stop in Io's corona, loses little energy and provides little ionization. For flow line 14, the ~ 350 eV/4 erg $\text{cm}^2 \text{s}^{-1}$ (4×10^{-3} Watts m^{-2}) electron beam provided an extra electron density $\sim 4,000 \text{ cm}^{-3}$. As an illustration, the 15 keV electron beams, for the same energy flux (the observed energy flux of these beams is actually 2 orders of

magnitude smaller) provide an extra electron density of only $\sim 200 \text{ cm}^{-3}$, much less than the lower energy electron beams.

[46] Acknowledging the limited observational constraints on the location, full energy spectrum and source mechanism of the beams, as well as the very simplified treatment of the ionization they provide in our modeling, the main conclusion of our simple study is that the low-energy ($\sim 350 \text{ eV}$) electron beams could contribute considerably to the plasma density observed downstream of Io. *Saur et al.* [2002] reached a similar conclusion with different assumptions about the location and ionization mechanism of such electron beams. They computed an ionization rate coefficient for the energetic beam electrons in the same way as for thermal electrons (see Appendix B). They use the experimental ionization cross-section and a non-Maxwellian distribution function derived from the energy flux of the energetic electrons of *Williams et al.* [1996] extrapolated down to 2 keV. The main simplification of this approach is the assumption that this non-Maxwellian energetic population is permanently embedded in the torus and never loses energy. The authors assume that these beams exist mainly on the downstream side of Io. In the present work, we assume a uniform flux of field-aligned electrons over the entire interaction region covered by our flow lines.

[47] Our empirical formulation of the beam simplifies the calculation of the ionization provided by the beams by using laboratory deduced parameters in lieu of cross-sections. It addresses the ionization provided by the primary electrons impinging Io's atmosphere and ignores the effect of the secondary electrons on the plasma production and on the electron thermal content of the flux tube. Our approach also takes into account the multiple ionizations provided by each primary electron on its path through the neutral density and the subsequent energy loss of the beams through the process. In this sense, it is the first step toward the treatment of the beams with a full electron energy transport calculation where the energy deposition of both the primary and secondary electrons is computed self-consistently (see *Grodent and Gérard* [2001] for an example of such a code in Jupiter's atmosphere).

3.6. Definitions

[48] First, we define the concepts of neutral loss rate, plasma production rate and pick-up currents that we show in Tables 2 and 3. We think that these concepts are sometimes confusing in the literature. These definitions are the one we adopt for this specific paper, acknowledging that it is sometimes difficult to find simple names to describe complex processes. The neutral loss rate (s^{-1}) is the number of neutrals removed from Io's corona by ionization and charge exchange, integrated on the whole simulation box. We compute these rates by integrating along each flow line the local rate of the neutral loss multiplied by the volume of the cell at each time step of the flow motion. *Delamere and Bagenal* [2003] define this rate as a source rate in their homogenous torus model. We emphasize that this definition does not include other neutral loss processes like thermal Jeans escape, atmospheric sputtering or electron impact dissociation.

[49] The ion mass production rate (kg s^{-1}) is the mass of ions locally added to or subtracted from the torus plasma. In

the literature, this rate is also called the mass loading rate [*Saur et al.*, 2002]. Because of the complexity of the multispecies chemistry, we compute it by calculating, for each ion separately, the mass flux difference between the upstream side and the downstream side of our simulation box where the flow velocity is close to the corotation velocity.

[50] The plasma production rate (s^{-1}) is the rate of electrons added locally to the torus. It is computed as an electron flux difference on each side of the simulation box as well.

[51] The power added is also computed as a difference of energy fluxes at the ends of the simulation box. The energy flux is computed as the product of the ion temperature, density and velocity for each ion as in *Bagenal* [1997].

[52] Ion pick-up is a process of reacceleration of the new ions created at rest in Io's reference frame by ionization and charge exchange. The new ion acquires a guiding center drift as well as a gyrospeed around the guiding center equal to the local flow velocity in Io's reference frame. Because the electron and the ion resulting from ionization have very different gyroradii, a slight separation of charge, in the direction of Io's electric field occurs and is the source of a perpendicular (to Jupiter's magnetic field) current called the pick-up current [e.g., *Thomas et al.*, 2004]. Usually the name pick-up refers to reacceleration after ionization, but conceptually, the same process takes place after a charge exchange reaction where the new ion is created at rest in Io's reference frame. In this paper we compute the local pick-up current separately for the electron impact ionization and charge exchange reactions with all neutrals. The expression of the local pick-up current density can be found in *Goertz* [1980]

$$j_{pu} = \sum_i q_i \dot{n}_i r_L E / |E| = \sum_i m_i \dot{n}_i E / B_0^2 = \sum_i m_i \dot{n}_i V_{flow} / B_0 \quad (4)$$

where the subscript i represents each ion species, q_i is the charge of the new ion created by ionization or charge exchange, m_i is its mass, \dot{n}_i is the rate of new ions created, r_L is the gyroradius of the ion in Jupiter's local magnetic field B_0 , E is the local electric field and V_{flow} is the local flow velocity, both in Io's reference frame.

[53] The pick-up current is not the only current that flows through Io's corona/atmosphere. The conduction currents flow through the dense ionosphere of Io as a result of elastic collisions between ions and neutrals (i.e., induced dipole attraction). These currents are not considered in our calculations. The induced dipole attraction cross-sections are much smaller than the resonant charge exchange cross-sections at corotational flow speed and become comparable for very slow flow speed deep in the collisional ionosphere [*Saur et al.*, 1999], which we do not model here. Therefore the pick-up current resulting from ionization and charge exchange dominate in the corona beyond $1.26 R_{Io}$ which was defined as the limit of the collisional ionosphere.

[54] The Alfvén wing current is the current propagating along the Alfvén wing (see review in *Kivelson et al.* [2004] and *Saur et al.* [2004]). This current was deduced from Voyager magnetometer data and the diversion of the flow around Io's Alfvén wing [*Acuna et al.*, 1981; *Belcher et al.*, 1981]. In this work, we only calculate the pick-up contri-

Table 2. Volume-Integrated Rates Using a Nominal SO₂ Density Profile for Case 3 (Nonslowed Flow) and Case 6 (Slowed Flow) of Table 1

Process		Species	Nonslowed Flow	Slowed Flow
Neutral Loss Rate, kg s ⁻¹	Ionization	SO ₂	190	216
		SO	22	26
		S and O	18	20
		Total	231	262
	Chex	SO ₂	2580	2056
		resonant others	74	74
SO		31	33	
S and O		20	20	
Net Mass Production Rate, kg s ⁻¹	Total		2705	2183
	SO ₂ ⁻		207	191
	SO ⁺		69	72
	S ⁺		21	22
	S ⁺⁺		-14	-14
	S ⁺⁺⁺		-3	-3
	O ⁺		-6	-6
	O ⁺⁺		-1	-1
	Total		272	280
	Power Added, Watts			43 × 10 ¹⁰
Plasma Production Rate, s ⁻¹	Ionization + Recombination	All species	2.3 × 10 ²⁷	2.1 × 10 ²⁷
Alfvén Wing Current, Amp	Ionization + Charge exchange		4.3 × 10 ⁶	0.9 × 10 ⁶
			203 × 10 ⁶	2.6 × 10 ⁶

bution to the Alfvén wing current and we do this separately for the current resulting from ionization and from charge exchange reactions. We obtain the Alfvén wing current by computing the local divergence of the local pick-up current density and spatially integrate this Alfvén wing current density on one side of Io (i.e., anti-jovian northern side of Io's atmosphere) to isolate one branch of the Alfvén wing current system. The total pick-up current through Io is diverted along the Alfvén wings toward both ionospheres of Jupiter and is thus twice the pick-up contribution of the Alfvén wing current.

3.7. Discussion

[55] After concluding that the molecular SO₂ chemistry is dominant and that the slowing of the flow is critical, we illustrate in Figure 10 and Figure 11 the 2-D distribution in Io's equatorial plane of some SO₂ chemical processes as well as some plasma characteristics both for the non-slowed and for the slowed flow. From left to right and top to bottom, we show the flow speed, the electron temperature, the SO₂⁺ temperature, the ionization, charge exchange and recombination production/loss rates (in cm⁻³ s⁻¹), the SO₂⁻ and the electron density. The panels showing the ionization

rate in Figures 10 and 11 confirm that the plasma production inside the bound ionosphere can be ignored. By extrapolating the resonant charge exchange rate inside the bound ionosphere, for an almost stagnated flow (<2 km/s), we computed that the neutral loss rate by resonant charge exchange inside the bound ionosphere ~10 percent of the total neutral loss rate out of the bound ionosphere (see also Table 2) and can thus be ignored as well. We thus confirm, a posteriori, that the bound ionosphere can be neglected while focusing on the chemistry as stated in section 2.3. Figure 10 and Figure 11 also show the pick-up (ionization and charge exchange) current represented by the vector field and the Alfvén wing current density. As we do not model the conduction current in the bound ionosphere, the computation of the divergence of the horizontal current that we use to compute the Alfvén wing current should result in a strong vertical current at the boundary of the bound ionosphere (1.26 R_{Io}). This current is an artifact caused by ignoring the ionospheric current in the present work and has been purposely deleted in these figures. As shown in *Saur et al.* [1999], the pick up current actually connects continuously with the conduction current in the bound ionosphere. Table 2 shows the rates of neutral loss, ion mass production

Table 3. Rates for All Sensitivity Experiments Described in Table 1 and Rates Deduced From Plasma Observation in Io's Wake^a

SO ₂ Experiments	SO ₂ Column 10 ¹⁶ , cm ⁻²	SO ₂ Loss Rate, kg s ⁻¹		Mass Production Rate ^b , kg s ⁻¹	Plasma Production Rate, 10 ²⁷ s ⁻¹	Alfvén Wing Current ^c , 10 ⁶ Amp	
		Ionization	Resonant Chex ^d			Ionization	Resonant + Chex
Case 3 (nominal)	6	190	2,580	270	2.2	4.3	200
Case 4 (reduced)	2	140	800	210	1.8	3.9	70
Case 5 (enhanced)	30	280	13,000	360	2.9	4.6	930
Case 6 (slowed)	6	215	2,055	260	2.1	0.9	2.6
<i>Bagenal</i> [1997] ^e					2.7		

^aWe emphasize here the reactions involving the main contributor, SO₂. The rates have been rounded.

^bThe total ion mass production rate: it includes the S, O, and SO contributions, although they are not shown in the table.

^cThe ionization and charge exchange (Chex) contribution to the current flowing along one Alfvén wing. It does not include the contribution of the conduction current through Io's ionosphere.

^dResonant charge exchange = SO₂ + SO₂⁻.

^eThe plasma production rate deduced from the Galileo observation in Io's wake by *Bagenal* [1997], considering her rectangular geometry, corrected under the assumption that the atmosphere is 1R_{Io} high along the Jupiter field lines.

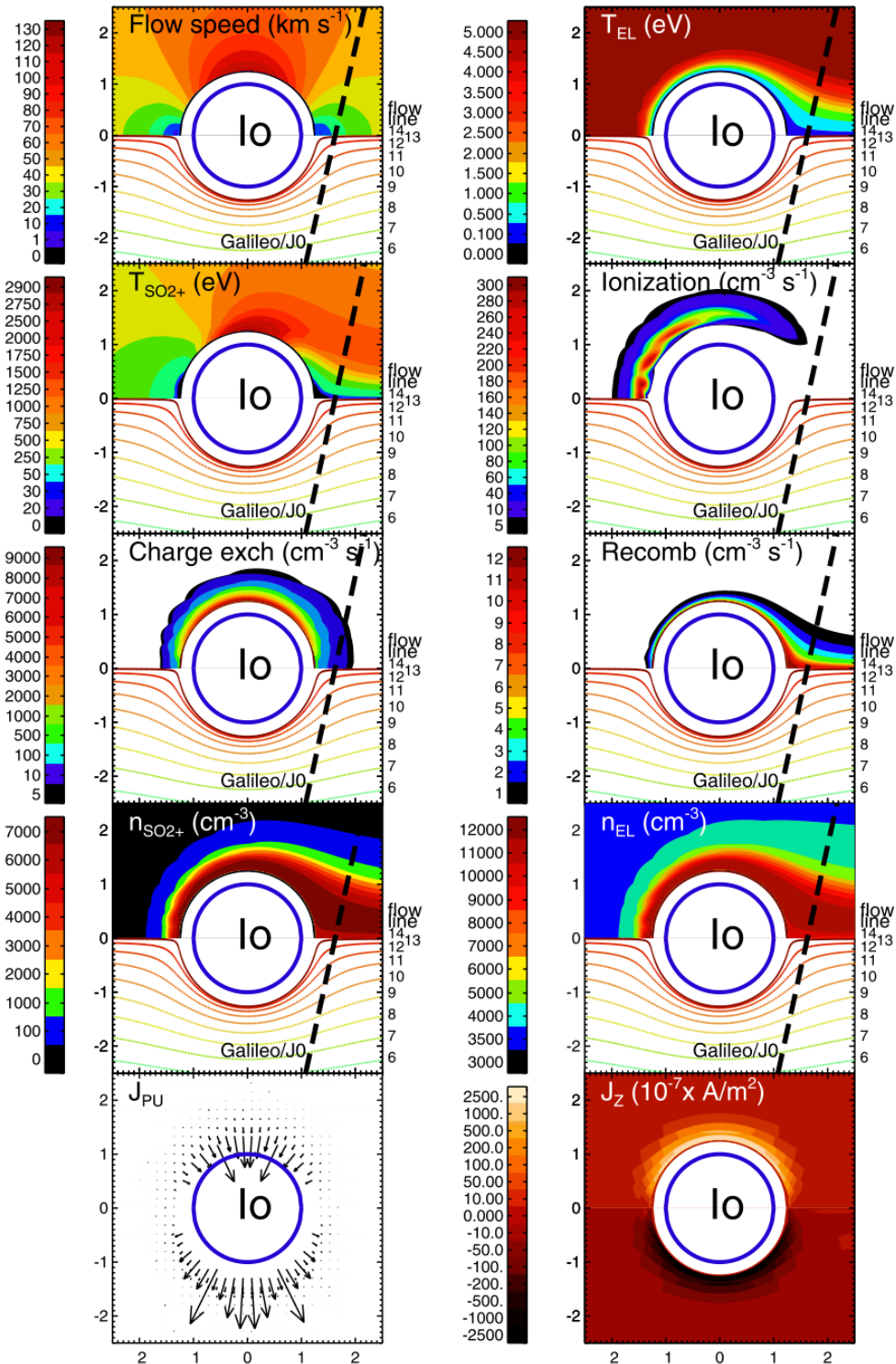


Figure 10. Mapping in Io's equatorial plane (in R_{Io}) of the plasma parameters for a nominal atomic and molecular atmosphere with the flow prescribed as incompressible flow around a cylinder as illustrated in the top left (Case 3 of Table 2).

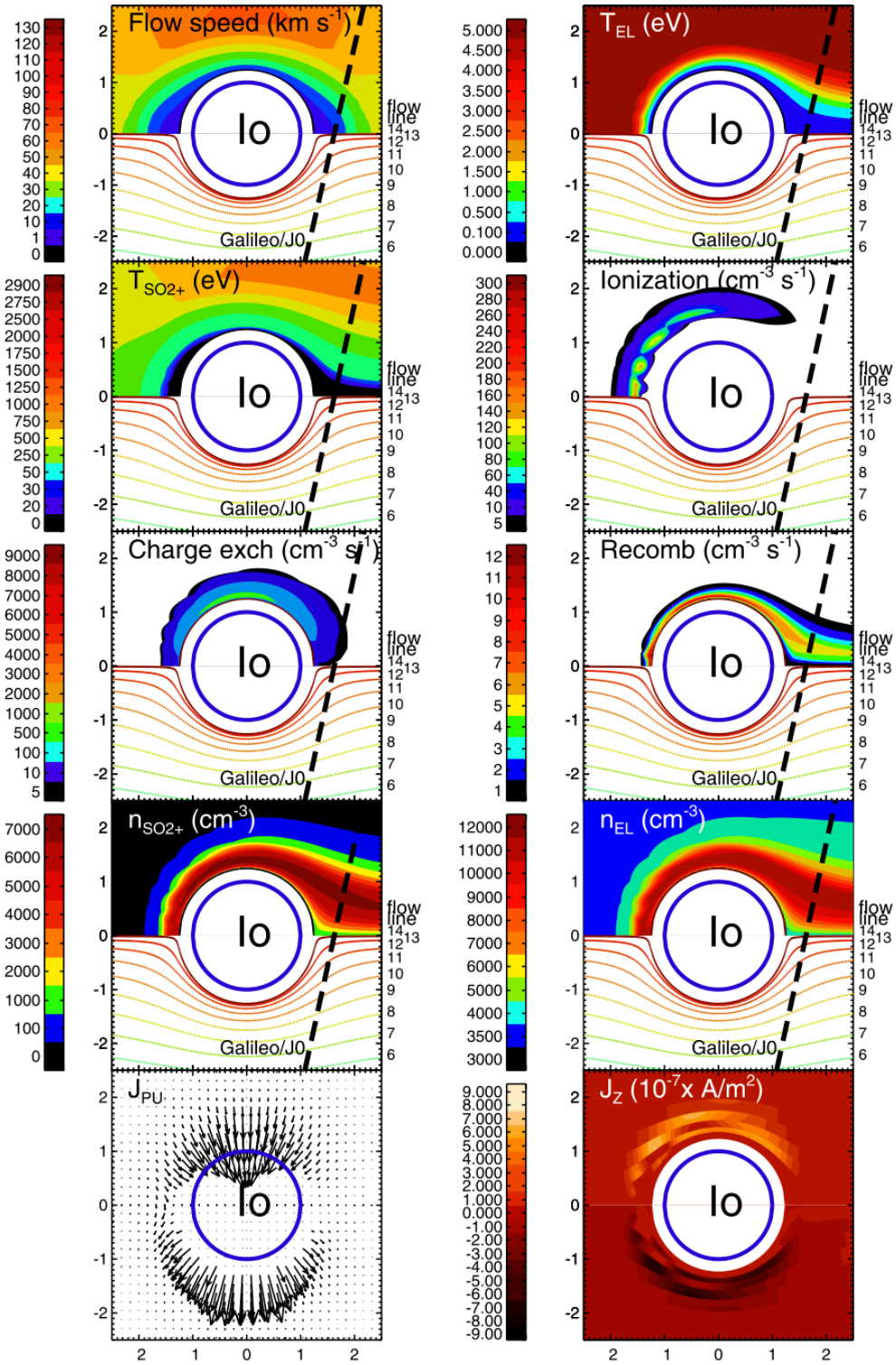


Figure 11. Mapping in Io's equatorial plane (in R_{Io}) of the plasma parameters for a nominal atomic and molecular atmosphere with a prescribed slowing of the flow as illustrated in the top left (Case 6 of Table 2).

and plasma production rates as well as the amount of currents generated in the interaction calculated for a $1 - R_{I_0}$ extension of the equatorial atmosphere along the jovian magnetic field direction.

3.7.1. Validating the Prescribed Slowing the Flow with the Current Calculation

[56] Some of the quantitative results that will be presented in this section (neutral loss rate by resonant charge exchange, Alfvén wing current) are very sensitive to the velocity field, it is thus very important to assess the validity of the flow we use in order to show that these results are relevant. Our first hypothesis for the description of the flow was the “non-slowed flow”, our second was the “slowed flow” prescribed with the only constraint of yielding an ion temperature along GLL/J0 that fits the data. The computation of the Alfvén wing current will give a convincing support to the second description of the flow and the quantitative results inferred from it. The Alfvén wing current that we compute for the two flow hypotheses are shown in Table 2. We compute for the non-slowed flow a 200 MAmp current solely because of pick-up while the Voyager canonical current (including contribution from the pickup and ionospheric conduction currents) was reported close to 2.8 MAmp [Acuna *et al.*, 1981]. There is no net Alfvén wing current estimate from the Galileo observations because the flybys were not at distant high latitude like that of Voyager 1 where the measurements are sensitive only to the Alfvén wing current. This largely overestimated current demonstrates that the non-slowed flow hypothesis cannot yield credible quantitative results when they depend on the flow velocity. The current computed for the “slowed-flow” shows a pick-up contribution to the Alfvén wing current ~ 2.6 MAmp. Noting the extreme sensitivity of the current to the flow velocity, it is remarkable that the current we compute with the slowed flow is in the range of the Voyager estimation. It is also consistent with the total current (5 Mamps, including pickup and ionospheric conduction) modeled self-consistently by Saur *et al.* [1999] for Galileo conditions. Our current is expected to be less than Saur's as we do not include the conduction current in the collisional ionosphere. The important point is that the ion temperature along GLL/J0 and the current computation as well as the quantitative results shown in Table 2 validate the “slowed flow”. Our calculation also suggests that the pick-up current contributes substantially to the flow dynamics, which seems contradictory to Saur *et al.*'s [2003] claim that the elastic collisions alone generate Io's electric system and slowing of plasma flow. Our results are actually consistent, but we differ in semantics. We elected to include charge exchange as a pick-up process while Saur *et al.* include the resonant charge exchange in the elastic collision term.

3.7.2. Electron Cooling Limits the Ionization

[57] Figure 10 and Figure 11 display the electron temperature and electron density around Io. The electrons cool on their way along the flanks of Io (from 5 eV down to ~ 0.1 eV in the core of the wake). The ionization rate region is upstream of Io, extending on the flanks in a boomerang shape because the electrons become too cold downstream to provide any further ionization. The cooling of the electrons limits the plasma (and mass) production rate both when the flow is slowed and when the neutral column density is increased. Intuitively, slowing the flow would increase the

interaction time and force the flux tube to remain in regions of high neutral density and the plasma density could build up to extremely high level as suggested by Kivelson *et al.* [2004]. Table 2 shows that the plasma production rate is actually quite similar for slowed and non-slowed flow: the electron cooling counter-balances the longer-interaction time effect and limits the plasma density in the wake. This cooling limits also the ionization when the neutral column density is increased. Table 3 experiments shows the results of the different sensitivity experiments where we vary the SO₂ column. When the column is increased by a factor 15 (Case 4 compared with Case 5), the neutral loss rate by ionization, ion mass production, and plasma production rates increase only by a factor 1–2. This stabilization effect was illustrated as well in Saur *et al.* [2003] in their Figure 3, where the electron-impact ionization and dissociation plateau for large SO₂ densities.

3.7.3. Role of SO₂ Resonant Charge Exchange

[58] In Figure 10 and Figure 11, the location of the SO₂⁺ production rate by resonant charge exchange is roughly circular, as it depends mainly on the SO₂ distribution. This rate is larger on the flanks where the flow velocity is large because the reaction rate is also proportional to the flow velocity. Consequently, the charge exchange rate is slightly lower for the case where the flow is slowed down. We immediately note that the local rates of charge exchange are about a factor of 10 larger than the ionization rates (note the different color scales for the panels of ionization and resonant charge exchange). Table 3 experiments illustrates further that the resonant SO₂ charge exchange dominate the neutral loss rate and the Alfvén wing current, whatever the corona neutral density.

[59] The SO₂⁺ temperature is an indicator of the energy extracted from the plasma flow and supplied to Io's plasma environment. The SO₂⁺ picked-up on the flanks (after an ionization or resonant charge exchange) where the flow velocity is fast will experience additional resonant charge exchange all along its downstream path. After a cascade of resonant charge exchanges, the last ion created by this process will be picked-up at the slower flow velocity downstream and end up cooler. This result is even stronger when the flow is slowed. The pickup of heavy SO₂⁺ ions close to Io is thus not a large energy supply as commonly supposed, it is mainly a process that creates a large supply of fast neutrals. This also explains the apparent contradiction with Bagenal [1997]. The author developed a simple model of the energy flux along the GLL/J0 trajectory to conclude that there is probably very little charge exchange reactions in Io's corona. We actually show that there is a lot of charge exchange taking place in the corona but the local pickup of heavy ions energizes the plasma only locally and, because of the cascade, does not provide much increased energy flux along GLL/J0 as confirmed by the observations.

3.7.4. Ion Mass and Plasma Production Rates

[60] The plasma production rates derived in this study are comparable to those estimated by Bagenal [1997] from Galileo observations in Io's wake, assuming a similar geometry for the interaction regions. Bagenal [1997] reported a plasma production rate $\sim 5.3 \times 10^{57} \text{ s}^{-1}$, assuming a rectangular geometry of the interaction region extending $2 R_{I_0}$ along the field lines. As discussed in section 2.2.1, the SO₂ atmosphere seems confined to the equatorial

latitudes. We follow *Saur et al.* [2003] by assuming a $1 R_{Io}$ -high rectangular geometry and get a revised-Bagenal plasma production rate $\sim 2.7 \times 10^{27} \text{ s}^{-1}$, close to our computed rate $\sim 2.1\text{--}2.3 \times 10^{27} \text{ s}^{-1}$. As noted before, our model is short on plasma density in the core of the wake and we claimed that the parallel electron beams are needed to account for the large plasma density in the center of the wake. The local mass production rate in the wake of Io is small. We compute a SO_2^+ -dominated local mass production rate $\sim 200\text{--}300 \text{ kg/s}$ comparable to the one deduced by *Bagenal* [1997] or computed by *Saur et al.* [2003]. In the literature, this ion mass production rate is usually compared to the canonical value $\sim 1 \text{ ton/s}$. We think that this comparison is misleading. Firstly, the canonical value is not a mass production rate but a neutral loss rate. *Delamere and Bagenal* [2003] and *Delamere et al.* [2004] clarified this issue. Their model computed a neutral loss rate $\sim 1 \text{ ton/s}$ (called "neutral source rate" in their publications) but about half of it leaves the torus as fast neutrals and only about 400 kg/s of fresh ions is actually supplied to the torus. Moreover, the derived neutral loss rate changes with epoch, from $\sim 0.5 \text{ tons s}^{-1}$ (Cassini) to $\sim 1.5 \text{ ton s}^{-1}$ (Voyager 2). Secondly, we claim in section 3.4 that these SO_2^+ fresh ions recombine and dissociate rapidly so they are mainly a local mass production in the wake of Io but do not contribute to the global torus ion supply. We argue that it makes little sense to compare this local mass production rate to the canonical mass loading rate provided by the extended neutral clouds.

[61] The location of the ion supply to the torus is an outstanding and controversial issue, as reviewed by *Thomas et al.* [2004]. Our conclusion opposes *Hill and Dessler's* [2004] assumption that a significant fraction of the torus plasma is injected very near Io ($< 1 R_{Io}$ of the surface), which is the key for their explanation of the low perpendicular temperature of S^+ in the ribbon. Our conclusion of an ion supply to the torus is consistent with the modeling of *Delamere et al.* which requires a pickup of fresh S and O ions at full corotation, far from Io.

3.7.5. Neutral Loss Rate

[62] The loss rate of neutrals in the corona is very large. Table 2 shows that the corona loses $\sim 2\text{--}3 \text{ tons/s}$ from SO_2 resonant charge exchange and $\sim 200\text{--}300 \text{ kg/s}$ from ionization. Even without electron impact dissociation and sputtering, these results are much larger than the neutral source rate of *Delamere et al.* [2004], which range from 0.5 to 1.5 ton s^{-1} . We recall that the charge exchange does not provide fresh plasma to the torus but merely neutrals. Some of the neutrals, created at very slow flow velocity ($< 2 \text{ km/s}$) will eventually feed the extended neutral cloud together with the sputtering and the electron-impact dissociation processes but most of them will be fast enough to leave the torus environment entirely.

4. Conclusions

[63] We have coupled a model of an incompressible flow around a conducting obstacle (Io and its ionosphere) with a chemical model that includes a detailed chemistry of S, O, SO and SO_2 to study the local (inside $\sim 6 R_{Io}$) interaction of Io's neutral corona and the plasma torus. We have prescribed the neutral density profiles in the corona, implicitly assuming that the atomic profiles are the result of fast

electron impact dissociation of SO_2 . We have also prescribed the plasma flow around the obstacle. We have not addressed the processes taking place in the collision-dominated ionosphere, where elastic collisions (induced dipole attraction) dominate, the flow is stagnated and little chemistry takes place. We have tested the sensitivity of this coupled model to different compositions and column densities of the neutrals species around Io as well as to a prescribed slowing of the flow around Io. We have validated the prescribed slowing of the flow and the quantitative results inferred from it by computing an Alfvén wing current consistent with the Voyager observation or self-consistent modeling of other authors. We have compared the model results to the GLL/J0 observations in Io's wake. We have also estimated the ionization provided by the $\sim 350 \text{ eV}$ field-aligned electron beams similar to those detected by Galileo in Io's wake. We summarize the main conclusions of this paper as follows:

[64] (1) To explain the plasma density and ion temperature profiles observed by Galileo along the J0 flyby trajectory, a dense and localized neutral density close to Io is required ($< 2 R_{Io}$). The natural candidate of such a dense atmosphere is SO_2 . We used a density such as that derived by *Wolven et al.*, 2001 at $2 R_{Io}$, i.e., a column density of $1\text{--}2 \times 10^{14} \text{ cm}^{-2}$ or a local density of $1\text{--}2 \times 10^5 \text{ cm}^{-3}$ at $2 R_{Io}$.

[65] (2) S and O neutral atoms (assuming density profiles and columns deduced from observations) are minor players when modeling the local chemistry. The whole interaction can be reasonably described with a single-species model (SO_2) including the three main reactions: the electron impact ionization, resonant charge exchange of SO_2 and SO_2^+ dissociative recombination. Molecular SO is assumed to be a minor species and does not play a major role in the chemical interaction.

[66] (3) The flux tubes that interact with Io's corona become rapidly devoid of almost all atomic ions and leave Io's vicinity dominated by SO_2^+ and SO^+ . These molecular ions recombine and dissociate rapidly and leave the corona as atomic neutrals. Consequently, the local interaction contributes very little to the ion supply and energy fluxes into the torus. The mass and energy supply to the torus plasma are presumably provided by the extended neutral clouds far ($> 10 R_{Io}$) from Io.

[67] (4) The high plasma density observed in Io's wake requires a supplemental ionization mechanism beyond the ionization provided by the torus thermal electrons. The $\sim 350 \text{ eV}$ field-aligned electrons beams detected around Io by Galileo could be this supplemental ionization source, provided they are also present in the dense part of Io's neutral corona. The $> 15 \text{ keV}$ parallel electron beams do not contribute much to the plasma production because they can pass through the entire Io neutral atmosphere/corona without depositing much energy.

[68] (5) The cooling of the torus thermal electrons by inelastic collisions with the neutrals provides a self-regulating mechanism that limits the ionization even when the neutral density is increased. Because of this, we compute (not including the effect of the electron beams) for a 15-fold variation of the SO_2 density, relatively constant local mass production ($200\text{--}300 \text{ kg/s}$) and plasma production rate ($1.8\text{--}2.9 \times 10^{27} \text{ s}^{-1}$). These results are close to the *Bagenal* [1997]

Table A1. Reactions of the Multispecies Chemistry Model^a

Molecular Reactions		Atomic Reactions	
$\text{SO}_2 + e^- \rightarrow \text{SO} + \text{O} + e^-$	Electron-impact dissociation ^b	$\text{S} + e^- \rightarrow \text{S}^+ + 2 e^-$	Ionization
$\text{SO}_2 + e^- \rightarrow \text{S} + \text{O}_2 + e^-$		$\text{S}^+ + e^- \rightarrow \text{S}^{++} + 2 e^-$	
$\text{SO}_2 + e^- \rightarrow \text{SO}_2^+ + 2 e^-$	Ionization	$\text{S}^{++} + e^- \rightarrow \text{S}^{+++} + 2 e^-$	
$\text{SO}_2 + e^- \rightarrow \text{SO}^+ + 2 e^-$		$\text{O} + e^- \rightarrow \text{O}^+ + 2 e^-$	
$\text{SO}_2 + e^- \rightarrow \text{S}^+ + 2 e^-$		$\text{O}^+ + e^- \rightarrow \text{O}^{++} + 2 e^-$	
$\text{SO}_2 + e^- \rightarrow \text{O}^+ + 2 e^-$		$\text{S}^{+++} + e^- \rightarrow \text{S}^{++}$	Recombination
$\text{SO}_2^+ + e^- \rightarrow \text{SO} + \text{O}$	Dissociative recombination	$\text{S}^{++} + e^- \rightarrow \text{S}^+$	
		$\text{O}^{++} + e^- \rightarrow \text{O}^+$	
$\text{SO}_2 + \text{SO}_2^+ \rightarrow \text{SO}_2^+ + \text{SO}_2$	Resonant charge exchange	$\text{S}^+ + \text{S}^{++} \rightarrow \text{S}^{++} + \text{S}^+$	Charge exchange
$\text{SO}_2 + \text{O}^+ \rightarrow \text{SO}_2^+ + \text{O}$	Charge exchange	$\text{S} + \text{S}^+ \rightarrow \text{S}^+ + \text{S}$	
$\text{SO}_2 + \text{S}^{++} \rightarrow \text{SO}_2^+ + \text{S}^+$		$\text{S} + \text{S}^{++} \rightarrow \text{S}^+ + \text{S}^+$	
		$\text{O} + \text{O}^{++} \rightarrow \text{O}^+ + \text{O}^+$	
$\text{SO} + e^- \rightarrow \text{SO}^+ + 2 e^-$	Electron-impact ionization	$\text{O} + \text{O}^{++} \rightarrow \text{O}^{++} + \text{O}$	
$\text{SO}^+ + e^- \rightarrow \text{S} + \text{O}$	Dissociative recombination	$\text{O} + \text{S}^+ \rightarrow \text{O}^+ + \text{S}$	
		$\text{S} + \text{O}^{++} \rightarrow \text{S}^{++} + \text{O}^+ + e^-$	
$\text{SO} + \text{S}^+ \rightarrow \text{SO}^+ + \text{S}$	Charge exchange	$\text{S} + \text{O}^+ \rightarrow \text{S}^+ + \text{O}$	
		$\text{S} + \text{O}^{++} \rightarrow \text{S}^+ + \text{O}^+$	
		$\text{O} + \text{S}^{++} \rightarrow \text{O}^+ + \text{S}^+$	
		$\text{O}^{++} + \text{S}^+ \rightarrow \text{O}^+ + \text{S}^{++}$	
		$\text{O} + \text{S}^{+++} \rightarrow \text{O}^+ + \text{S}^{++}$	
		$\text{O}^{++} + \text{S}^{++} \rightarrow \text{O}^+ + \text{S}^{+++}$	
		$\text{O} + \text{O}^+ \rightarrow \text{O}^+ + \text{O}$	
		$\text{S}^{+++} + \text{S}^+ \rightarrow \text{S}^{++} + \text{S}^{++}$	
		$\text{S} + \text{S}^{+++} \rightarrow \text{S}^{++} + \text{S}$	
		$\text{S} + \text{S}^{+++} \rightarrow \text{S}^+ + \text{S}^{++}$	

^aWe use the reactions with the largest cross-sections or those that involve a major torus ion (O^+ and S^{++}).

^bUsed for the electron energy equation only.

value $\sim 2.7 \times 10^{27} \text{ s}^{-1}$, computed for a rectangular geometry of the interaction region when it is corrected under the assumption that the atmosphere is $1 R_{\text{Io}}$ high along the Jupiter field lines. They are also close to *Saur et al.* [2003] results of a plasma production rate $\sim 1.6 \times 10^{17} \text{ s}^{-1}$ for an SO_2 atmospheric column comparable to our nominal atmospheric column of $6 \times 10^{20} \text{ m}^{-2}$.

[69] (6) The neutral loss rate is large and dominated by the SO_2 resonant charge exchange, which provides fast neutrals, most of them able to leave the torus system. Assuming an SO_2 atmosphere/corona with a $6 \times 10^{16} \text{ cm}^{-2}$ vertical column and prescribing a slowing of the flow around Io, we estimate a neutral loss rate through ionization and charge exchange $\sim 2,400 \text{ kg/s}$ ($22 \times 10^{27} \text{ s}^{-1}$). Other neutral loss processes, including electron impact dissociation and atmospheric sputtering, are not considered here.

[70] (7) The resonant charge exchange and ionization reactions on SO_2 contribute substantively to the current in Io's Alfvén wing and to the dynamics of the plasma flow around Io. We compute a pick-up current contribution to the Alfvén wing current (ionization and charge exchange) of $\sim 2.6 \text{ MAmp}$ at the time of Galileo flyby ($\sim 5.2 \text{ MAmp}$ for the pick-up current). The conduction currents flowing in the collision-dominated ionosphere are not computed in this work but will also contribute to the total Alfvén wing current.

Appendix A: Chemical Reactions

[71] Table A1 lists the set of reactions we considered in this model. The references for each reactions are listed with the model equations in Appendix B. The atomic chemistry is similar to *Delamere and Bagenal* [2003]. Recombination of S^+ and O^+ are ignored because the reaction rate coefficients are very small. We limit the list of charge exchange

reactions with SO_2 to those displaying large cross-sections or involving a major ion of the torus (S^{++} or O^+).

[72] The SO_2 electron impact dissociation reactions are not included in the mass and energy ions equations as we prescribe the atomic composition of Io's corona, assuming that this composition results from the fast dissociation. Nevertheless, the dissociation reactions are included as energy losses in the equation of electron energy. The SO reactions are limited to the reactions that have large cross-sections for electron temperatures of $\sim 5 \text{ eV}$ and below: the electron impact ionization, charge exchange with S^+ and dissociative-recombination.

Appendix B: Model Equations

B1. Ion Equations

[73] These equations are adapted from the work of *Delamere and Bagenal* [2003]. Some terms of their model have characteristic times of tens of days (coulomb interaction equilibration time, radial transport, UV emission of ions). The characteristic time for the plasma to flow in Io's corona is of the order of minutes to tens of minutes, so these long time scale terms can be neglected here. The basic equations for mass and energy for each ion species, α are

$$\frac{d}{dt}[n_\alpha] = S_m - L_m \quad (\text{B1})$$

$$\frac{d}{dt} \left[\frac{3}{2} n_\alpha T_\alpha \right] = S_E - L_E \quad (\text{B2})$$

[74] We compute the time variation of density and energy in the plasma blob on its way around Io by calculating, at each timestep, the sources and losses of density and energy

in the blob as it encounters the neutral densities. The source rate for the density of each ion species, n_{α} , is

$$S_m = K_{Ioz}^{\alpha_-} n_{\alpha_-} n_{el} + K_{recomb}^{\alpha_+} n_{\alpha_+} n_{el} + \sum_{\gamma,\beta} K_{cx}^{\gamma,\beta} n_{\gamma} n_{\beta} \quad (B3)$$

where K_{Ioz} is the electron impact ionization rate coefficient for the thermal electron populations, K_{recomb} is the recombination rate coefficient, α_- and α_+ are the lower and higher ionization states of species α , and K_{cx} symbolically represents all charge exchange reaction rate coefficients between ions and neutrals which produce species α given in Table A1. The loss rate for the density of each species, n_{α} , is

$$L_m = K_{Ioz}^{\alpha} n_{\alpha} n_{el} + K_{recomb}^{\alpha} n_{\alpha} n_{el} + \sum_{\alpha,\beta} K_{cx}^{\alpha,\beta} n_{\alpha} n_{\beta} \quad (B4)$$

[75] The energy input rate for a given species is

$$S_E = K_{Ioz}^{\alpha_-} n_{el} n_{\alpha_-} T_{\alpha_-} + K_{recomb}^{\alpha_+} n_{\alpha_+} n_{el} T_{\alpha_+} + \sum_{\gamma,\beta} K_{cx}^{\gamma,\beta} n_{\gamma} n_{\beta} T_{\beta} \quad (B5)$$

[76] The temperatures are expressed in eV. In the case of ionization or charge exchange involving neutrals, the input temperature is determined from the pick-up energy given by

$$\frac{3}{2} T_{pu} = \frac{1}{2} m_{\alpha} V_{flow}^2 \quad (B6)$$

where V_{flow} is the local prescribed flow velocity. The energy loss for a given species is

$$L_E = K_{Ioz}^{\alpha} n_{el} n_{\alpha} T_{\alpha} + K_{recomb}^{\alpha} n_{\alpha} n_{el} T_{\alpha} + \sum_{\alpha,\beta} K_{cx}^{\alpha,\beta} n_{\alpha} n_{\beta} T_{\alpha} \quad (B7)$$

[77] The electron impact ionization and recombination rate coefficients are given by D.E. Shemansky [personal communication, 2006]. They depend on the electron temperature. Their general analytical form for each process is

$$K_{process}^{\alpha}(T_{el}) = \int dv^3 v f_{Maxwell} \sigma_{process}(E) \quad (B8)$$

where $f_{Maxwell}$ is the normalized Maxwell electron distribution function at temperature T_{el} and σ the process cross-section. The charge exchange rate coefficients are computed as

$$K_{cx}^{\alpha,\beta} = \sigma_{cx} V_{flow} \quad (B9)$$

[78] Although σ_{cx} depends slightly on the relative velocity between the ions/neutrals involved in the charge exchange, we use a fixed charge exchange cross-section at 60 km/s from McGrath and Johnson [1989] for all charge exchange reactions and a $10 \times 10^{-16} \text{ cm}^2$ for the SO₂ resonant charge exchange [R.E. Johnson, personal communication, 2006]

B2. Electron Equations

[79] The electron density is computed with the ion densities assuming charge neutrality. *Delamere and Bagenal's* [2003] electron equation had to be revised completely as these electrons encounter locally a large neutral density. They are cooled down by inelastic collisions (ionization, recombination, dissociation, vibrational and rotational excitation) with neutrals. We limit our calculation to the inelastic collisions with SO₂ as we showed that it dominates the chemistry. We adopt the thermal electron energy description of *Saur et al.* [1999] of instantaneous electron heat conduction in the flux tube. The electrons in each flux tube adjust to one common temperature instantaneously so that the temperature calculated in the model is the average temperature of the whole flux tube electrons. We compute the time variation of the electron total energy content (W) of a flux tube of the torus (extending from $-1R_J$ to $+1R_J$ along the magnetic field line)

$$W = \int_{-R_J}^{+R_J} dz \frac{3}{2} n_{el} T_{el} \quad (B10)$$

$$\frac{d}{dt}[W] = - \int_{-R_J/2}^{+R_J/2} dz EL(T_{el}) n_{el} n_{SO_2} + F_{heating} \quad (B11)$$

with n_{el} = electron density, n_{SO_2} = SO₂ neutral density, and $EL(T_{el})$ = energy loss in units of eV cm³ s⁻¹

$$EL(T_{el}) = \delta E_{diss} K_{diss} + \delta E_{Ioz} K_{Ioz} + \delta E_{vib} K_{vib} + \delta E_{rot} K_{rot} + \frac{3}{2} T_{el} K_{recomb} \quad (B12)$$

where for each inelastic process (dissociation, ionization, rotational and vibrational excitation of SO₂), $\delta E_{process}$ is the energy lost in each process (13.1 eV for ionization, 5.7 eV for dissociation, 0.012 eV for vibrational excitation, 0.064 eV for rotational excitation) and K are the rate coefficients defined previously. We note that the energy losses and cross-sections for rotational and vibrational excitations are effective values adopted here to avoid the computation of the full rotational and vibrational excitation [D.F. Strobel, personal communication, 2006]. $F_{heating}$ represents the heating of electrons by ions and neutrals. Its analytical formulation is taken from *Saur et al.* [1999]. This term becomes important when the electrons cool down to 0.2 eV. The average flux tube electron temperature is then computed as

$$T_{el} = \frac{W}{\int_{-R_J}^{+R_J} dz n_{el}} \quad (B13)$$

Appendix C: Velocity Field

[80] We describe here the formulation of the velocity field use in section 2.2. The velocity field is based on the model of *Neubauer* [1980]. *Barnett* [1986] writes explicitly the velocity components of Neubauer's model and fit the model to velocity measurements along the Voyager flyby of Io.

The velocity field is similar to a uniform plasma flow around a long cylindrical perfect conductor slightly larger than Io ($R_c = 1.26 R_{Io}$), implying that the region of high conductivity is the ionosphere of Io rather than the satellite itself. We further simplify Barnett's formulation to get the flow in the equatorial plane of Io by neglecting the Hall current effect as well as the bent of the Alfvén wing ($\phi_0 = 0$ and $\theta_a = 0$ in Barnett's formulation) and describe the flow as

$$V_x = V_0 - V_0 \frac{R_c^2}{r^2} \cos(2\phi) \quad (C1)$$

$$V_y = -V_0 \frac{R_c^2}{r^2} \sin(2\phi) \quad (C2)$$

$$V_z = 0 \quad (C3)$$

where V_0 is the flow velocity far from Io (57 km/s) in the X direction,

$$r^2 = x^2 + y^2 \quad (C4)$$

$$\tan(\phi) = \frac{y}{x} \quad (C5)$$

[81] In section 3.3, we slow this flow (and call it the "slowed-flow") by multiplying the X component of the flow here above by the cylindrically symmetrical correction factor γ

$$\gamma(r) = 1. + 1.3(r - 1.91) \quad (C6)$$

in order to get a good fit of the average ion temperature computed by the model and the average ion temperature inferred from the observations along GLL/J0.

Appendix D: Field-Aligned Electron Beams

[82] We describe hereafter an empirical formulation from Rees [1989] of energy deposition of monoenergetic auroral electrons in the Earth atmosphere. The impinging electrons follow a convoluted path through the atmosphere, losing ~ 35 eV per ionization. The stopping distance for primary auroral electrons in the terrestrial atmosphere is described by an effective range

$$R(E) = 4.3 \times 10^{-7} + 5.35 \times 10^6 E^{1.67} \quad (D1)$$

where E is the incident energy in keV and the effective range, $R(E)$, is given in units of gm cm^{-2} . The effective range is an experimentally derived parameter and applies to incident auroral electrons with energies in the range $200 \text{ eV} < E < 50 \text{ keV}$. The electron energy is not dissipated uniformly along its range. The normalized energy dissipation distribution is a function of the fractional range $\Lambda(s/R)$ where $s(z)$ is the atmospheric scattering depth (gm cm^{-2}) given by

$$s(z) = \int_z^{R_{Io}} \rho(z) dz \quad (D2)$$

where $p(z)$ is the mass density. Several energy dissipation distribution functions for Earth's atmosphere are shown in

Figure 3.3.2 in [Rees, 1989]. Although these curves depend on the composition of the atmosphere, we use the 300 eV distribution as a first approximation for Io's atmosphere as well.

[83] For the terrestrial atmosphere, each electron loses an average energy, $\Delta\epsilon_{ion}$, of 35 eV per ionization for $E > 70$ eV. For our estimate we will use the same average energy loss. This includes the ionization energy itself (13.1 eV for SO_2) plus the kinetic energy of the secondary electron and excitation energy of the resulting ion. At lower energies, the loss per ionizing reaction increases sharply as more energy is lost in excitation of the resulting ion. For simplicity, we will assume that the electron loses a constant 35 eV amount until it stops in Io's atmosphere. The total ionization rate is given as

$$q_{beam} = \frac{1}{\Delta\epsilon_{ion}} F_E \Lambda(s/R) \frac{\rho(z)}{R(E)} \quad (D3)$$

where F_E is the energy flux observed by Galileo.

[84] **Acknowledgments.** We thank D.E. Shemansky for providing the electron impact reaction rates on SO_2 and SO , R.E. Johnson for the SO_2 resonant charge exchange cross-section, D.F. Strobel for providing the electron energy equation, N.M. Schneider, S.C. Solomon, J. Saur for fruitful discussions, and R.E. Ergun for suggesting the formulation of the field-aligned electron beam ionization.

[85] Wolfgang Baumjohann thanks Matthew Burger and Joachim Saur for their assistance in evaluating this paper.

References

- Acuña, M. H., F. M. Neubauer, and N. F. Ness (1981), Standing Alfvén wave current system at Io: Voyager 1 observations, *J. Geophys. Res.*, *86*, 8513–8521.
- Bagenal, F. (1997), The ionization source near Io from Galileo wake data, *Geophys. Res. Lett.*, *24*(17), 2111–2114.
- Bagenal, F., T. Dowling, and W. McKinnon (Eds.) (2004), *Jupiter*, Cambridge Univ. Press, Cambridge, UK.
- Ballester, G. E. (1989), Ultraviolet observations of the atmosphere of Io and the plasma torus, Ph.D. thesis, AA Johns Hopkins Univ., Baltimore, Md.
- Barnett, A. (1986), In situ measurements of the plasma bulk velocity near the Io flux tube, *J. Geophys. Res.*, *91*(A3), 3011–3019.
- Belcher, J. W., C. K. Goertz, J. D. Sullivan, and M. H. Acuña (1981), Plasma observations of the Alfvén wave generated by Io, *J. Geophys. Res.*, *86*(A10), 8508–8512.
- Chust, T., A. Roux, W. S. Kurth, D. A. Gurnett, M. G. Kivelson, and K. K. Khurana (2005), Are Io's Alfvén wings filamented? Galileo observations, *Planet. Space Sci.*, *53*, 395–412, doi:10.1016/j.pss.2004.09.021.
- Clarke, J. T., D. Grodent, S. W. H. Cowley, E. J. Bunce, P. Zarka, J. E. P. Connerney, and T. Satoh (2004), Jupiter's aurora, in *Jupiter: The Planet, Satellites and Magnetosphere*, pp. 639–670, Cambridge University Press, Cambridge, UK.
- Combi, M. R., K. Kabin, T. I. Gombosi, D. L. De Zeeuw, and K. G. Powell (1998), Io's plasma environment during the Galileo flyby: Global three-dimensional MHD modeling with adaptive mesh refinement, *J. Geophys. Res.*, *103*(A5), 9071–9081.
- Crary, F. J., F. Bagenal, L. A. Frank, and W. R. Paterson (1998), Galileo plasma spectrometer measurements of composition and temperature in the Io plasma torus, *J. Geophys. Res.*, *103*(A12), 29,359–29,370.
- Delamere, P. A., and F. Bagenal (2003), Modeling variability of plasma conditions in the Io torus, *J. Geophys. Res.*, *108*(A7), 1276, doi:10.1029/2002JA009706.
- Delamere, P. A., A. Steffl, and F. Bagenal (2004), Modeling temporal variability of plasma conditions in the Io torus during the Cassini era, *J. Geophys. Res.*, *109*, A10216, doi:10.1029/2003JA010354.
- Frank, L. A., and W. R. Paterson (1999), Intense electron beams observed at Io with the Galileo spacecraft, *J. Geophys. Res.*, *104*(A12), 28,657–28,669.
- Frank, L. A., W. R. Paterson, K. L. Ackerson, V. M. Vasyliunas, F. V. Coroniti, and S. J. Bolton (1996), Plasma observations at Io with the Galileo spacecraft, *Science*, *274*, 394–395.
- Goertz, C. K. (1980), Io's interaction with the plasma torus, *J. Geophys. Res.*, *85*(A6), 2949–2956.

- Grodent, D., J. H. Waite Jr., and J.-C. Gérard (2001), A self-consistent model of the Jovian auroral thermal structure, *J. Geophys. Res.*, *106*(A7), 12,933–12,952.
- Hill, T. W., and A. J. Dessler (2004), Longitude variation of ion temperature in the Io plasma torus, *J. Geophys. Res.*, *109*, A04206, doi:10.1029/2003JA010218.
- Hinson, D. P., A. J. Kliore, F. M. Flasar, J. D. Twicken, P. J. Schinder, and R. G. Herrera (1998), Galileo radio occultation measurements of Io's ionosphere and plasma wake, *J. Geophys. Res.*, *103*(A12), 29,343–29,357.
- Huddleston, D. E., R. J. Strangeway, J. Warnecke, C. T. Russell, M. G. Kivelson, and F. Bagenal (1997), Ion cyclotron waves in the Io torus during the Galileo encounter: Warm plasma dispersion analysis, *Geophys. Res. Lett.*, *24*(A17), 2143–2146.
- Kivelson, M. G., F. Bagenal, W. S. Kurth, F. M. Neubauer, C. Paranicas, and J. Saur (2004), Magnetospheric interactions with satellites, in *Jupiter: The Planet, Satellites and Magnetosphere*, pp. 513–536, Cambridge University Press, Cambridge, UK.
- Lellouch, E., M. A. McGrath, and K. L. Jessup (2007), Io's atmosphere, in *Io After Galileo*, edited by R. M. C. Lopes and J. R. Spencer, pp. 231–264, Springer, Chichester, UK.
- Linker, J. A., M. G. Kivelson, and R. J. Walker (1988), An MHD simulation of plasma flow past Io—Alfvén and slow mode perturbations, *Geophys. Res. Lett.*, *15*(11), 1311–1314.
- Linker, J. A., M. G. Kivelson, and R. J. Walker (1989), The effect of mass loading on the temperature of a flowing plasma, *Geophys. Res. Lett.*, *16*(7), 763–766.
- Linker, J. A., M. G. Kivelson, and R. J. Walker (1991), A three-dimensional MHD simulation of plasma flow past Io, *J. Geophys. Res.*, *96*(A12), 21,037–21,053.
- Linker, J. A., K. K. Khurana, M. G. Kivelson, and R. J. Walker (1998), MHD simulations of Io's interaction with the plasma torus, *J. Geophys. Res.*, *103*(E9), 19,867–19,877.
- Mauk, B. H., D. J. Williams, and A. Eviatar (2001), Understanding Io's space environment interaction: Recent energetic electron measurements from Galileo, *J. Geophys. Res.*, *106*(A11), 26,195–26,208.
- McGrath, M. A., and R. E. Johnson (1989), Charge exchange cross sections for the Io plasma torus, *J. Geophys. Res.*, *94*(A3), 2677–2683.
- McGrath, M. A., E. Lellouch, D. F. Strobel, P. D. Feldman, and R. E. Johnson (2004), Satellite atmospheres, in *Jupiter: The Planet, Satellites and Magnetosphere*, pp. 457–483.
- Neubauer, F. M. (1980), Nonlinear standing Alfvén wave current system at Io: Theory, *J. Geophys. Res.*, *85*(A3), 1171–1178.
- Rees, M. H. (1989), *Physics and Chemistry of the Upper Atmosphere*, Cambridge University Press, Cambridge, UK.
- Saur, J., F. M. Neubauer, D. F. Strobel, and M. E. Summers (1999), Three-dimensional plasma simulation of Io's interaction with the Io plasma torus: Asymmetric plasma flow, *J. Geophys. Res.*, *104*(A11), 25,105–25,126.
- Saur, J., F. M. Neubauer, D. F. Strobel, and M. E. Summers (2002), Interpretation of Galileo's Io plasma and field observations: I0, I24, and I27 flybys and close polar passes, *J. Geophys. Res.*, *107*(A12), 1422, doi:10.1029/2001JA005067.
- Saur, J., D. F. Strobel, F. M. Neubauer, and M. E. Summers (2003), The ion mass loading rate at Io, *Icarus*, *163*, 456–468, doi:10.1016/S0019-1035(03)00085-X.
- Saur, J., F. M. Neubauer, J. E. P. Connerney, P. Zarka, and M. G. Kivelson (2004), Plasma interaction of Io with its plasma torus, in *Jupiter: The Planet, Satellites and Magnetosphere*, pp. 537–560.
- Smyth, W. H., and M. L. Marconi (1998), An explanation for the east-west asymmetry of the Io plasma torus, *J. Geophys. Res.*, *103*(A5), 9091–9100.
- Thomas, N., F. Bagenal, T. W. Hill, and J. K. Wilson (2004), The Io neutral clouds and plasma torus, in *Jupiter: The Planet, Satellites and Magnetosphere*, pp. 561–591.
- Williams, D. J., B. H. Mauk, R. E. McEntire, E. C. Roelof, S. M. Krimigis, T. P. Armstrong, B. Wilken, J. G. Roederer, T. A. Fritz, and L. J. Lanzerotti (1996), Electron beams and ion composition measured at Io and in its Torus, *Science*, *274*, 401–403.
- Williams, D. J., R. M. Thorne, and B. Mauk (1999), Energetic electron beams and trapped electrons at Io, *J. Geophys. Res.*, *104*(A7), 14,739–14,753.
- Wolven, B. C., H. W. Moos, K. D. Retherford, P. D. Feldman, D. F. Strobel, W. H. Smyth, and F. L. Roesler (2001), Emission profiles of neutral oxygen and sulfur in Io's exospheric corona, *J. Geophys. Res.*, *106*(A11), 26,155–26,182.

F. Bagenal, P. A. Delamere, and V. Dols, Laboratory for Atmospheric and Space Physics, CB 392 Duane Physics, University of Colorado, Boulder, CO 80309-0391, USA. (dols@lasp.colorado.edu)

6.2 The Hall-MHD model

6.2.1 Hall-MHD equations

The equations that describe a magnetohydrodynamic fluid are composed of five magneto-fluid equations for the ions (the continuity, the momentum and the pressure) and 10 equations for the evolution of the electric and magnetic fields. Below are the 5 magneto-fluid equations for a single species fluid, in Io's rest frame where the neutrals are at rest and where we ignore the dissipation terms (resistivity and viscosity)

$$\frac{\partial \rho}{\partial t} + \nabla \cdot (\rho \bar{v}) = \dot{\rho}$$

$$\rho \left(\frac{\partial \bar{v}}{\partial t} + \bar{v} \cdot \nabla \bar{v} \right) = -\nabla P + \bar{J} \times \bar{B} - \dot{\rho} \bar{v} - \dot{Q} \bar{v}$$

$$\frac{\partial P}{\partial t} + \nabla \cdot (P \bar{v}) = (\gamma - 1) \left(-P(\nabla \cdot \bar{v}) + \frac{\dot{\rho} v^2 + \dot{Q} v^2}{2} \right) - \frac{\dot{Q} v^2}{\rho}$$

where

The time variable is t (s), ρ is the plasma mass density (kg m^{-3}), \bar{v} is the bulk flow velocity (m s^{-1}), \bar{B} the magnetic field (T), \bar{J} the current density ($\text{amp m}^{-2} \text{s}^{-1}$).

Ionization and collision processes, represented by $\dot{\rho}$ and \dot{Q} terms in the momentum equation, exert a drag on the co-rotating plasma, which results in momentum loss.

The ion mass-loading rate per unit volume $\dot{\rho}$ is the rate per unit volume of mass addition to the plasma ($\text{kg m}^{-3} \text{s}^{-1}$).

The rate of momentum transfer per unit volume is \dot{Q} ($\text{kg m}^{-3} \text{s}^{-1}$). This rate is expressed as $\dot{Q} = \rho v_{coll}$ where $v_{coll} = n_n \sigma_{coll} \bar{v}$ is the collision frequency of an ion in a neutral atmosphere of number density n_n (m^{-3}) and a neutral-ion collision cross section σ_{coll} (m^2). Ion-neutral collision processes include the induced dipole attraction, where the clouds of electrons of the neutral and the ion interact. This cross section is large at very low velocity (*Banks and Kockarts, 1973, Saur et al., 1999*), but at the velocities considered in this work, charge exchange is the main collision process. A typical charge

exchange cross section is of the order of $20 \cdot 10^{-16} \text{ m}^2$ while the induced dipole attraction cross section is ~ 4 times smaller.

The isotropic pressure is represented by P , and γ is the adiabatic index ($= 5/3$). Acceleration of new ions after ionization and charge exchange (pickup) at the local flow velocity are sources of energy but the third term on the right hand side of the equation represents a loss of energy density for the plasma as the incoming ion is transformed into a neutral after the charge exchange.

The field equations are the usual Maxwell's equation in the MHD approximation of large scales compared to the gyro-radius (the gyro-radius of O^+ ions for a plasma temperature of 100 eV is ~ 3 km) and low temporal variations compared to the gyro-frequency (the gyro-frequency of an O^+ ion in the field of Jupiter ~ 1 Hz).

$$\nabla \cdot \vec{B} = 0$$

$$\vec{J} = \frac{1}{\mu_0} (\nabla \times \vec{B}) \quad (\text{Ampere's law})$$

$$\frac{\partial \vec{B}}{\partial t} = -\nabla \times \vec{E}$$

$$\frac{\partial \vec{E}}{\partial t} = -\nabla \times \vec{B} \quad (\text{Faraday's law})$$

The generalized Ohm law becomes, after neglecting the term with small mass ratios $m_e/m_i \ll 1$.

$$\vec{E} = -\vec{v} \times \vec{B} + \frac{1}{ne} (\vec{J} \times \vec{B}) - \frac{1}{ne} \nabla P_e$$

where n is fluid number density ($n = n_e = n_i$ assuming quasi-neutrality) and $P_e =$ the electron pressure.

The second term on the left hand side of the equation is the Hall term, this term will provide some asymmetry of the plasma and we neglect the electron pressure gradient as our estimation based on the plasma conditions at l_0 shows that this term is three orders of magnitude lower than the Hall term.

The equations can be re-written in different forms to better illustrate the characteristics of the Hall MHD approach. Starting with the electron velocity

$$\vec{v}_e = \vec{v} - \frac{\vec{J}}{ne}$$

Ampere and Faraday's laws can be rewritten in the general induction law

$$\frac{\partial \vec{B}}{\partial t} = \nabla \times \left(\vec{v} \times \vec{B} - \frac{1}{ne} \vec{J} \times \vec{B} \right)$$

Or

$$\frac{\partial \vec{B}}{\partial t} = \nabla \times (\vec{v}_e \times \vec{B})$$

which shows that in the Hall-MHD approximation, the magnetic field is frozen to the electron flow and not to the ion flow like in ideal MHD.

6.2.2 Simulation parameters and code numerical scheme

The Hall-MHD code is the fluid part of the Hybrid code developed by *Delamere et al. (1999; 2000; 2002; 2003; 2006)*.

The numerical scheme is explicit and the density and pressure equations are solved with a 2-step Lax-Wendroff scheme that is second order accurate. The momentum equation is solved with an 2-step predictor-corrector (*Swift, 1995; Swift, 1996*) scheme that proved to be very robust in the hybrid version of the code.

The treatment of the boundary conditions is a difficult problem because of the propagation of waves: When they reach the boundaries, they bounce back and perturb the results inside the simulation domain. We chose to extend the simulation domain as much as reasonably possible considering the computer memory needed to simulate a large domain, the computer time and the time needed to transfer the results. The boundary conditions in the Z and Y directions are periodic, which means that when the Alfvén wave reaches the boundary, it comes back in the simulation box from the opposite boundary. The conditions in X are inflow and outflow boundary conditions (derivatives of field in terms of X equal zero), where the plasma is coming in on the

upstream side of Io and going out on the downstream side. These boundary conditions allow the waves to reflect back into the simulation domain when they reach the upstream and upper and lower boundaries, perturbing the results.

The simulation grid is Cartesian and extends from $-9 R_{Io}$ to $+9 R_{Io}$ in X and Y and $-25 R_{Io}$ to $+25 R_{Io}$ in Z with a spatial resolution of 60 km. The code is parallelized and the vertical dimension is split in 128 processors, running on the high performance cluster resource at the University of Colorado.

Io is modeled as a very dense cloud of neutrals with no boundary conditions set on its surface. Because of the repeated collisions inside the cloud, the flow is almost stagnant. The background plasma density is set to the upstream plasma density observed far from Io by Galileo, including in the body of Io to ensure no steep gradient at the start of the simulation, which can drive the code unstable. It is the simplest way to simulate Io but some consequences of these simplifications will be addressed in Section 6.3.3. We postpone to future work a more accurate treatment of Io's body that would insure that no plasma penetrates inside Io.

Because of the Hall term in Ohm's law, the code can propagate whistler plasma waves, which are very rapid (Figure 24). The time step has to be chosen small so that the Courant condition, $C = v_{ph} \frac{\Delta t}{\Delta x} \leq 1$, is fulfilled for the chosen grid resolution and the scheme is stable. For a 60 km-grid resolution, we found that a time step= 0.01 sec was needed.

For the plasma conditions typical of the torus, the Alfvén wave velocity is ~ 150 - 250 km/s and the wave reaches the vertical boundaries in $\sim 20,000$ time steps or 6 minutes of real flow. Then the simulation is stopped. Such a simulation is completed in ~ 40 hours. At the co-rotation velocity (57 km/s), the flow travels a distance= $2 R_{Io}$ in 1 minute. As a consequence of such a short real time simulation, the plasma that enters at the inflow boundary does not have time to reach the outflow boundary. Nevertheless, we verify that the velocity and magnetic perturbations close to Io reach a stationary state in 6 min. On the other hand, the plasma density in the wake of Io does not, as the flow close to Io is very slow.

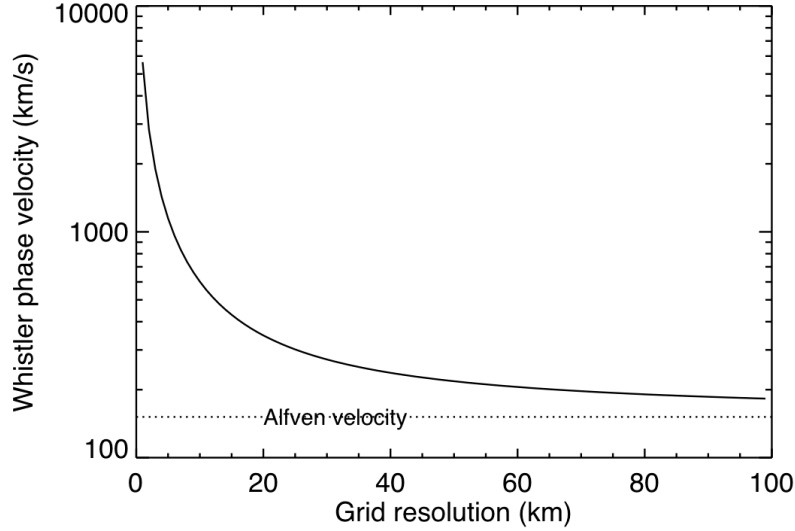


Figure 24: Whistler phase velocity, v_{ph} , for different wavelengths. The grid resolution selects what wavelength can be propagated in the code and the time step has to be defined accordingly to fulfill the Courant condition.

As the Hall-MHD code is a single-species model, we follow *Linker et al. [1998]* and assume that both the neutral and ions have a mass = 20 amu, the average mass of oxygen and sulfur atoms in the torus and the charge exchange cross section is 15 \AA^2 .

The background Jovian magnetic field is defined along the Z direction, perpendicular to the co-rotation velocity with a magnitude based on the GLL magnetometer measurements at the time of closest approach.

6.2.3 Features of the Hall-MHD code

We show here a few sections through the simulation domain (in Io's equatorial plane and along the background field lines) to illustrate the interaction physics that we described in Section 2.2.

The three following figures are vertical sections XZ of the simulation box, X is the flow direction and Z is along Jupiter's magnetic field. They illustrate the propagation of the three MHD waves: the fast magnetosonic mode, the Alfvén mode and the slow magnetosonic mode. The simulation is stopped at an early stage (3000 time-steps) to

illustrate the development of the features so in these figures, the interaction has not yet reached a stationary state.

The fast magnetosonic wave is a compressional mode that propagates in all directions with roughly spherical fronts (Figure 25, left). The restoring force responsible for its propagation is the combination of plasma and magnetic pressures. The fast mode slows the flow and diverts it around I_0 . The fast mode phase velocity perpendicular to the field lines is ~ 250 km/s. The torus plasma flow, at 57 km/s, is subsonic so there is no shock formation.

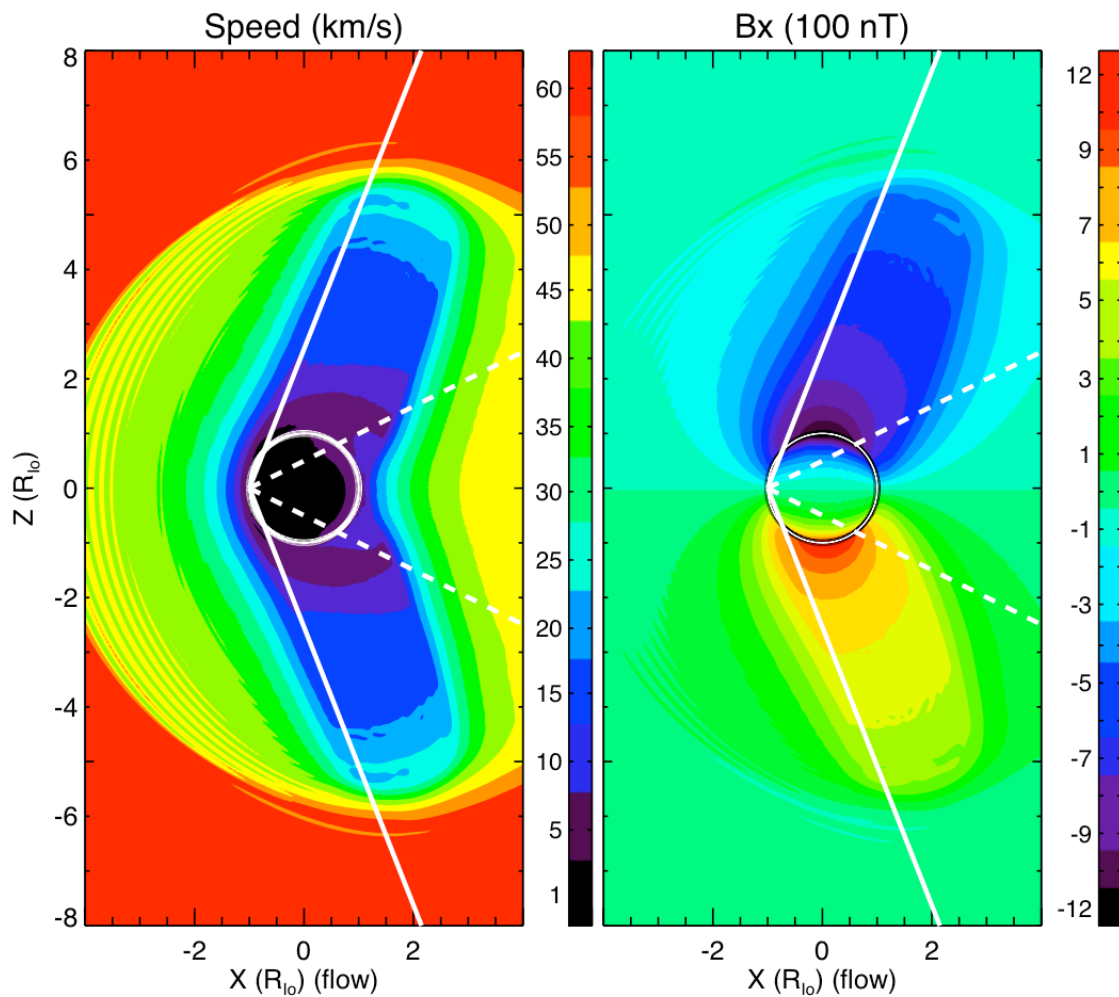


Figure 25: A vertical cut through the Alfvén wing. The background jovian magnetic is parallel to Z , the flow comes from the left. Left: the speed of the plasma. Right: the magnetic perturbation in the X direction. The white solid line is the Alfvén characteristic, the white dashed line is the slow mode characteristic.

The Alfvén wave is a transverse incompressible mode and the magnetic tension is responsible for its propagation, strictly along field lines. For the torus plasma conditions, the Alfvén phase velocity ~ 200 km/s. As the field line is carried downstream at the flow velocity (57 km/s), the magnetic and velocity perturbations form a wing, stationary in Io's frame (Figure 25). The wing angle calculated with the model is perfectly consistent with the analytical calculation of the Alfvén characteristic

represented by the solid white line at an angle α where $tg(\alpha) = \frac{1}{M_A}$ and $M_A = \frac{v_{flow}}{v_{Alfven}}$ is

the Mach number (Saur *et al.*, 2004). This cylindrical wing propagates toward Jupiter in both directions. The flow is diverted around it and, inside, the flow is very slow. In the Alfvén tube, the field lines, originally parallel to Z, are bent as illustrated by a B_x component positive above Io and negative under Io, typical of Alfvén wave propagation

where $\frac{\partial v}{v_{Alf}} = \pm \frac{\partial B_x}{B_z}$.

Figure 26 shows the propagation of the third MHD wave: the slow magnetosonic mode. This mode is guided by the field lines, and propagates at a much smaller velocity ($V_s \sim 20$ km/s) than the Alfvén wave. The slow mode perturbation creates a wing, tilted

to the Z axis by a much smaller angle with $tg(\alpha) = \frac{1}{M_s}$ and $M_s = \frac{v_{flow}}{C_s}$

In this slow mode wing, the plasma temperature, the density and the pressure are low. The white dashed line shows the analytical calculation of the slow mode characteristic based on the upstream plasma conditions. It is consistent with the model results as well.

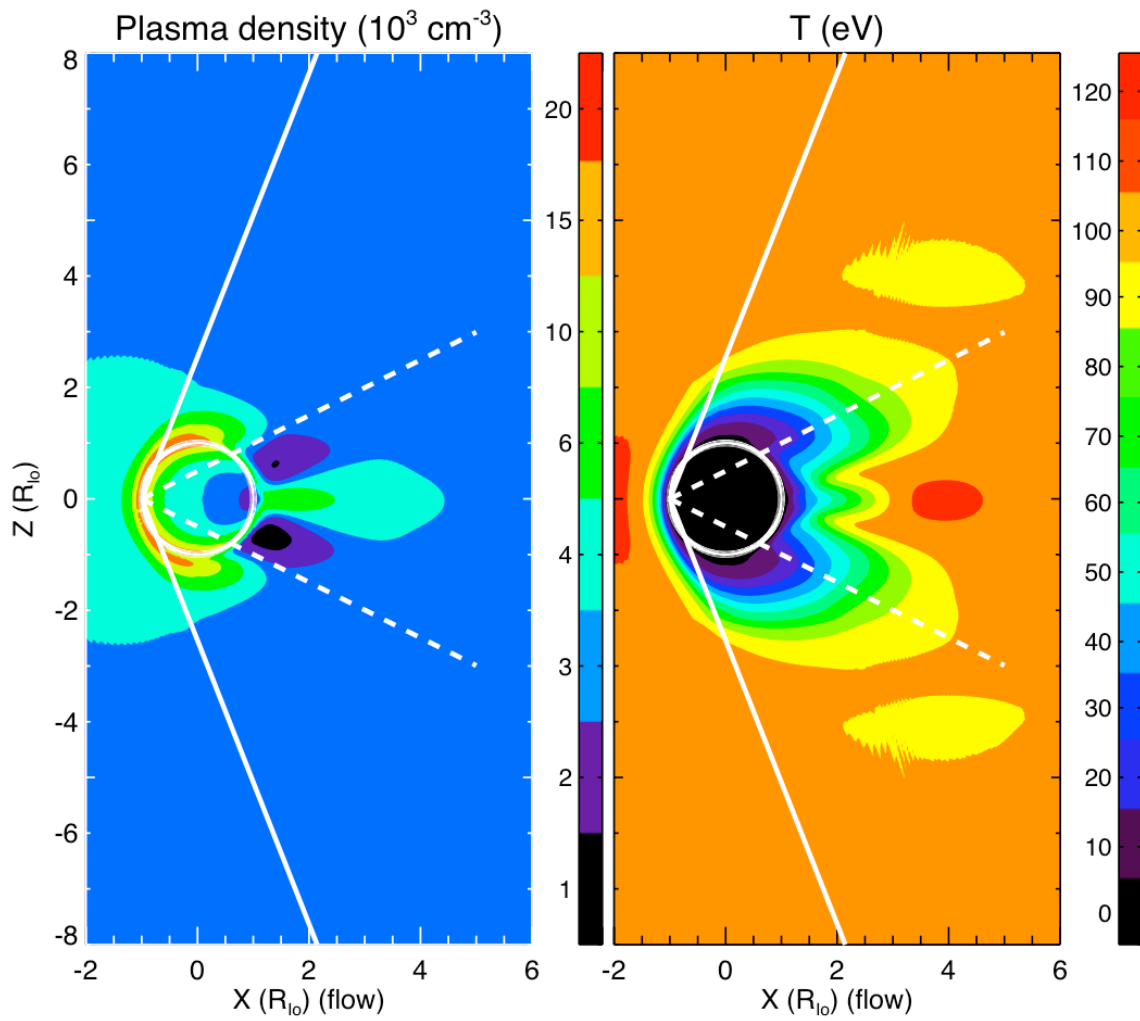


Figure 26: Propagation of the slow magnetosonic mode that forms a wing aligned with the slow mode characteristic (dashed line). For comparison, we have added the Alfvén mode characteristic (solid line).

We now present sections in Io equatorial plane XY. Io is seen from above and the flow enters the domain from $X = -3 R_{Io}$ in the X direction.

Figure 27 shows a comparison between the ion and electron flows. It illustrates the effect of the Hall term in the generalized Ohm's law. The flow is slowed in front of Io, diverted on the flanks where it is accelerated and slowed back in the wake. Electrons and ions enter the simulation domain at $x = -3 R_{Io}$. Far from Io, electrons and ions flow along the same flow lines. As Io is treated as a dense cloud of neutral gas, the plasma penetrates Io. This serendipitously illustrates the Hall effect. Flow lines of electrons are strongly diverted towards Jupiter while ions, which were initially flowing on the same lines, are less diverted. These flow lines are similar to the flow lines calculated by *Saur et al. [1999]* and shown in Figure 19.

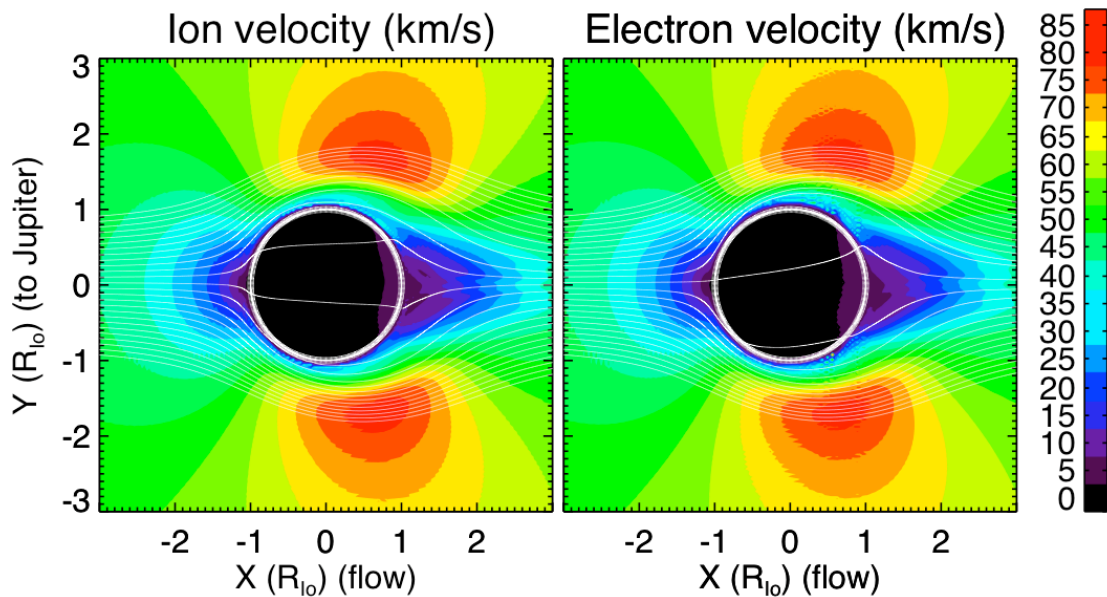


Figure 27: Illustration of the Hall effect. Top: The flow of ions. Bottom: The electron flow lines. Initially, both electrons and ions started on the same flow lines but the Hall effect in the atmosphere of Io deflects the electrons more strongly towards Jupiter.

Figure 28 shows the plasma density and the ion temperature. The plasma density increases along the downstream flanks and in the wake. It also increases inside Io because we treated the solid moon as a cloud of neutrals and the flow can penetrate Io's body. The ion temperature is low in front of Io and high on the flanks because of the pickup of new ions at the local flow velocity.

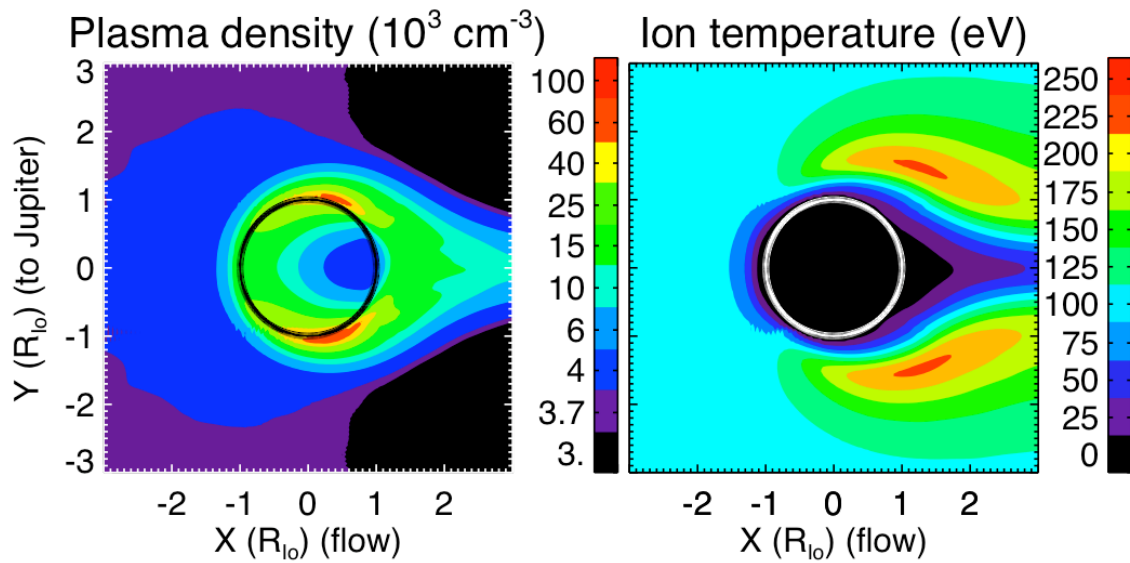


Figure 28: A cut in the equatorial plane (XY). The magnetic field of Jupiter points into the page, the torus plasma enters the domain in $X=-3 R_{Io}$ and flows in the X direction. Left: The plasma density. Right: the ion temperature.

Figure 29 shows the Z component of the magnetic field. In front of I_0 , the flow is slowed and the field piles up: it is compressed and is stronger. Then the field diffuses slowly through I_0 and is weaker in the wake. This magnetic perturbation is consistent with a current flowing through I_0 in the anti-jovian direction (Figure 30).

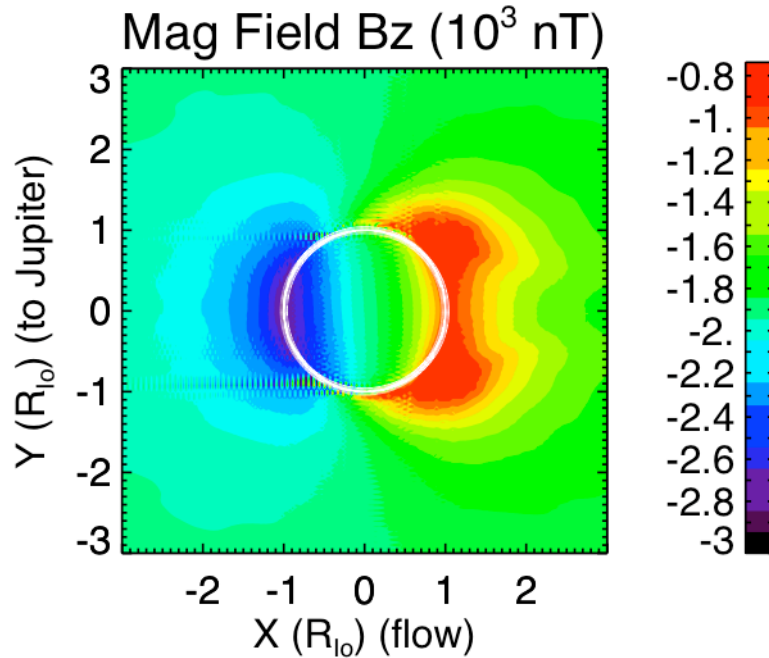


Figure 29: Vertical component of the magnetic field in the equatorial XY plane, where the background magnetic field of Jupiter points into the page and the torus plasma enters the domain from left to right. The field is compressed upstream of I_0 and depressed in the wake.

Using this magnetic perturbation in Ampere's law, we compute the currents around I_0 , shown in Figure 30. Figure 31 sketches the current system shown in Figure 30. The current flows down to I_0 along the northern Alfvén wing on the jovian side (blue in Figure 30 left panel), crosses I_0 as horizontal currents across the field (green in Figure 30 right panel), exit I_0 on the anti-jovian hemisphere and is diverted as vertical current back toward the northern hemisphere of Jupiter (red in Figure 30 left panel). The same current system exists along the southern Alfvén wing. Note that in these simulations, the Alfvén wave has not yet reached Jupiter and the current closes in front of the Alfvén wave (Neubauer, 1980). When it reaches Jupiter's ionosphere, the current along the Alfvén wing closes as horizontal currents (Pedersen current). The $\vec{J} \times \vec{B}$ force in the

ionosphere associated with this Pedersen current slows the Jovian ionosphere and ultimately its atmosphere. The current system described here explains how Io taps the rotation energy of Jupiter to accelerate its plasma.

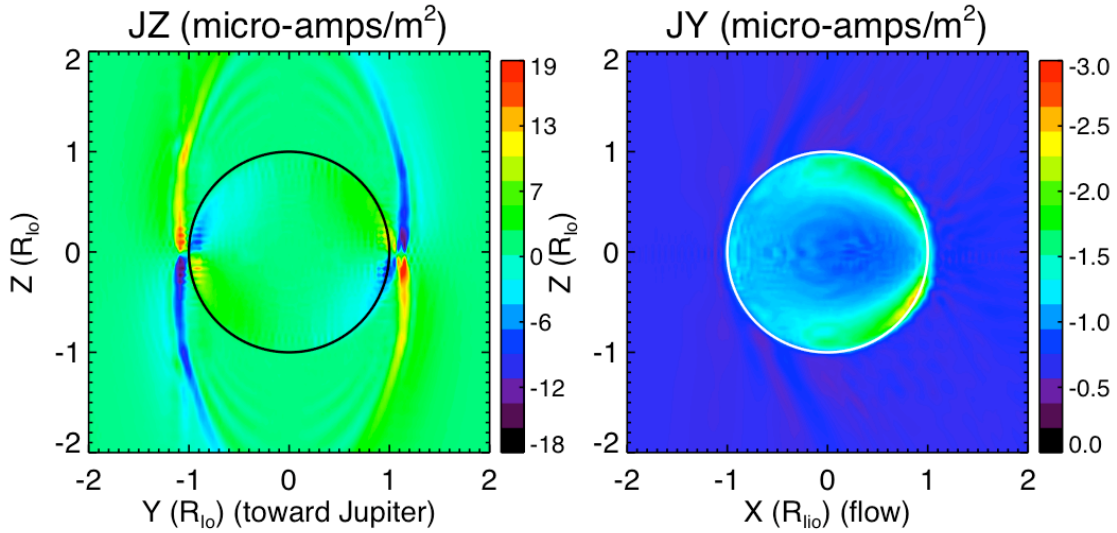


Figure 30: Current through Io. Left: J_z in a vertical plan YZ, showing the vertical currents on the flanks of the Alfvén tube. Right: horizontal current J_y in the vertical XZ plane.

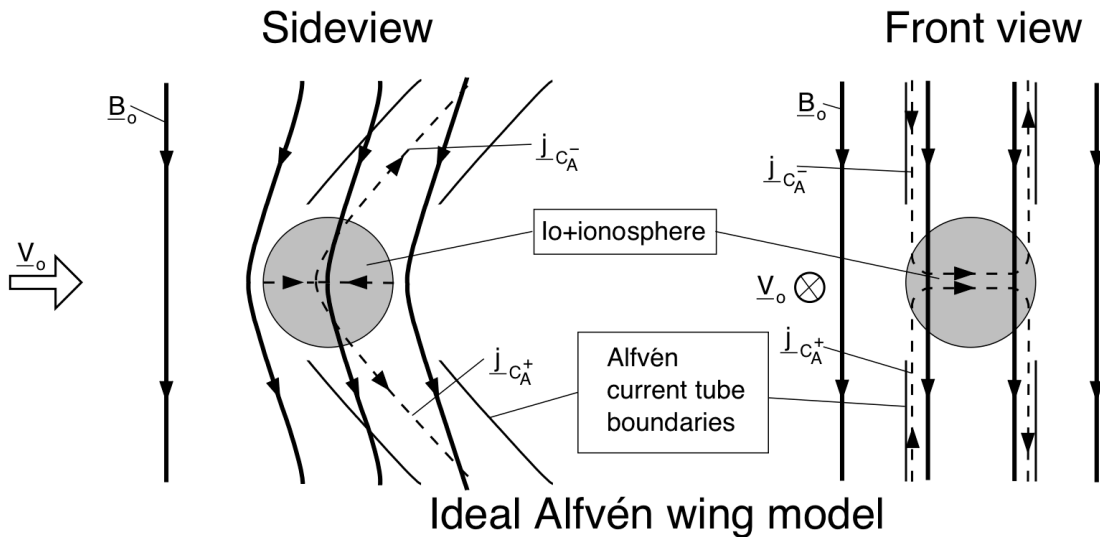


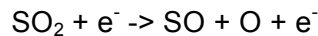
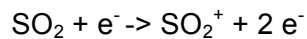
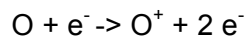
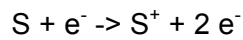
Figure 31: Sketch of the current system in the Alfvén wing

6.3 The Coupled Model

In this section, we illustrate the limitations of previous MHD simulations addressed in Section 5 in more detail as well as the limitation of our own Hall-MHD model and demonstrate that the chemical model circumvents them.

6.3.1 Importance of including the electron cooling.

In general, the quantitative results of MHD models are limited by the prescription of the ionization rate, inconsistent with the cooling of electrons (Section 5.1). Figure 32 shows the ionization rate coefficients of sulfur and oxygen (*Becker and Tarnovsky, 1995*), and the coefficient of the main ionization and dissociation reactions of SO₂ (*Shemansky, private communication, 2005*).



The reaction rate coefficients (K_{reac} in cm^3s^{-1}) are determined by convolving a limited number of measured cross sections above the ionization (dissociation) potential by a Maxwellian electron energy distribution at temperature T , so the ionization (dissociation) at an electron temperature under the potential threshold (13.1 eV and 5.7 eV respectively for ionization and dissociation of SO₂) comes from the high energy Maxwellian tail of this population. These reaction rate coefficients are very sensitive to electron temperature. They decrease by ~ 4 orders of magnitude when the electron temperature drops from 5 eV to 1 eV. The molecular dissociation is one of the most important mechanisms that cool the electrons. The other mechanisms are ionization, the rotational and vibrational excitations, which are included in the chemical model's electron energy equation.

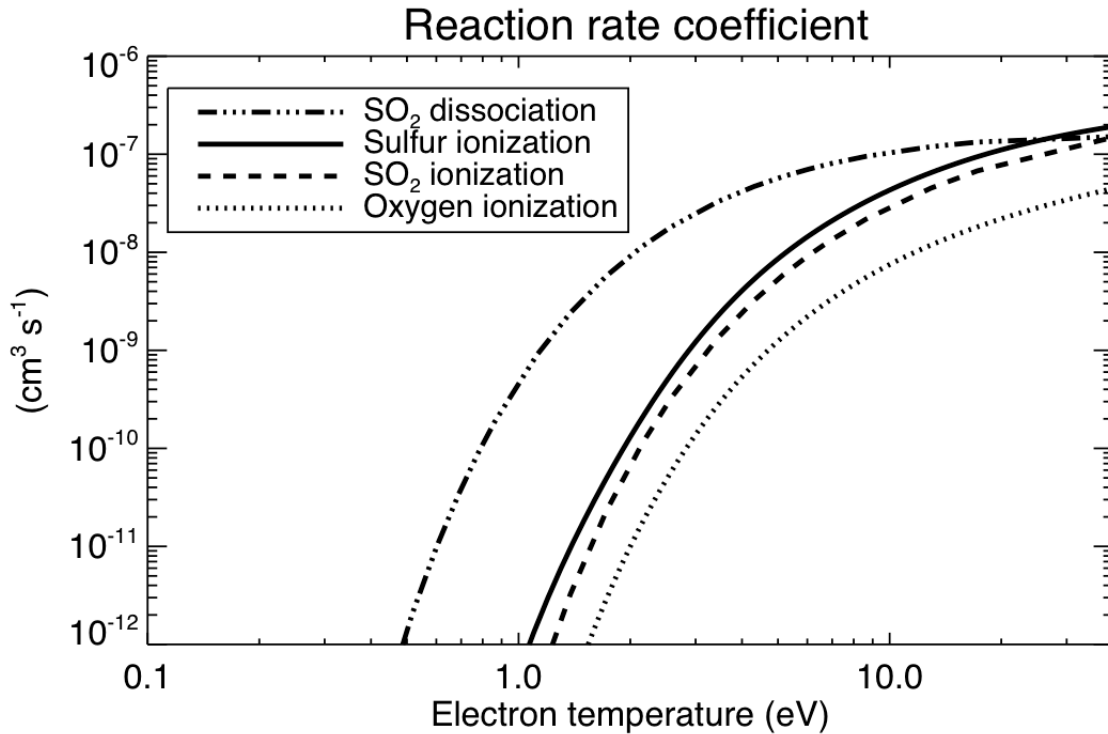


Figure 32: Reaction rate coefficient K for ionization of S, O and SO_2 and SO_2 dissociation.

We illustrate the effect of the electron cooling in the atmosphere of Io with a simple experiment using the multi-species chemical model. We run two cases where we prescribe the same neutral distribution (radial and latitudinal density) and the same flow. In the first case, the atmosphere is composed of S and O and the cooling processes are limited to ionization; in the second case, the atmosphere is composed entirely of SO_2 , which is much more efficient at cooling the electrons. Figure 33 shows the ionization rate ($K \times n_{\text{atm}} \times n_{\text{el}}$ in $\text{cm}^{-3} \text{s}^{-1}$) and the electron temperature around Io for each atmospheric case. When the electron temperature drops under ~ 2 eV (the green areas on the electron temperature contour), the ionization shuts down. The ionization is mainly located upstream of Io, especially for the molecular atmosphere, and the SO_2 maximum rate is 4 times lower than the S and O rate (note that the scales of the contour plots are different). As the ionization rate coefficients of S and SO_2 are similar on the range of temperature from 0.1 to 5 eV, the difference between the two cases is caused mostly by the molecular cooling of the electrons.

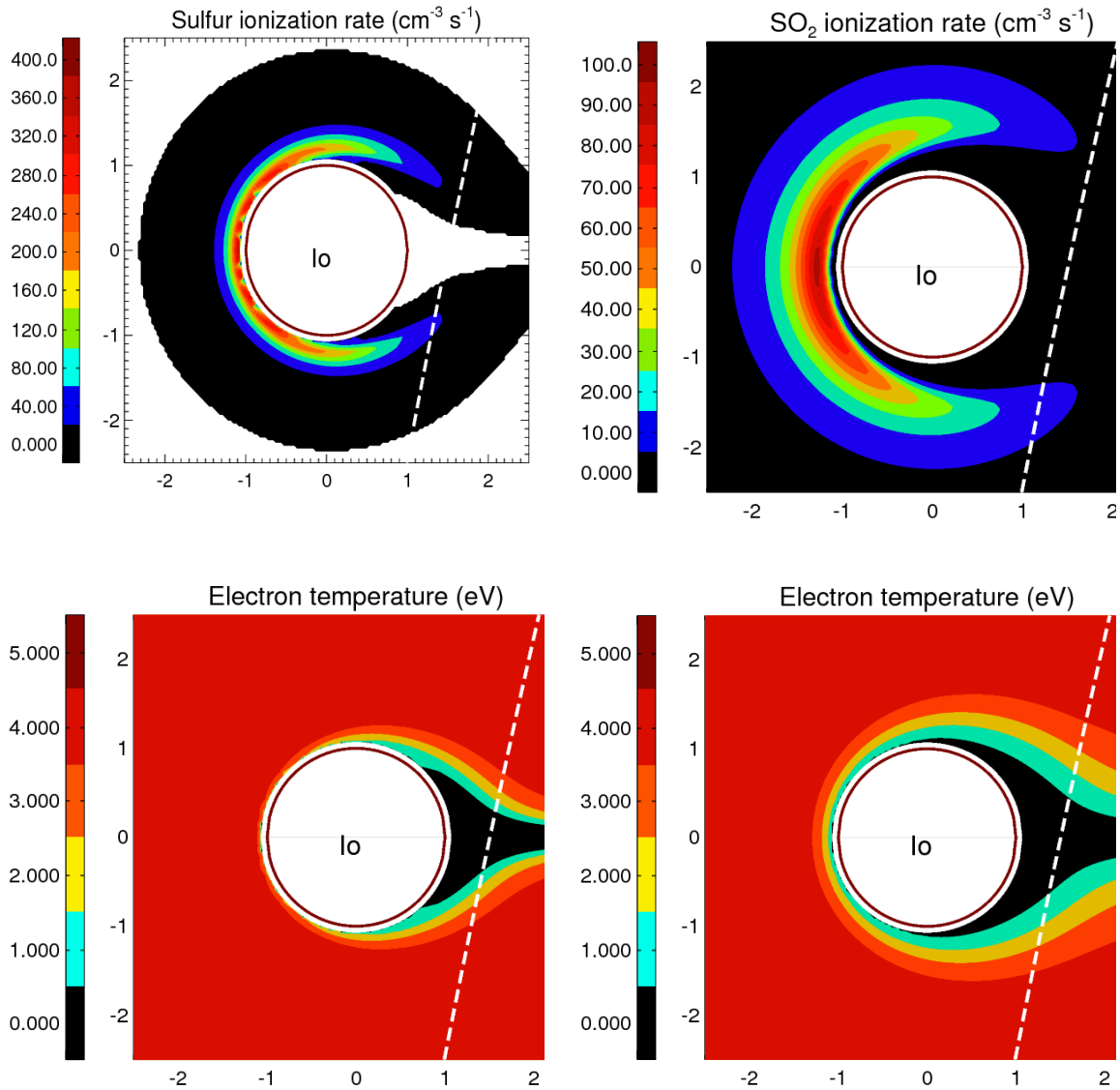


Figure 33: Ionization rate in Io's equatorial plane for an atmosphere composed of
 1) Left: S and O.
 2) Right: SO₂ only.
 Note that the scales of the ionization rates are different. The ionization rate is lower and more upstream for the SO₂ atmosphere because of the cooling of electrons, shown in the lower panels.

This experiment leads to two conclusions.

- 1) Whatever the atmosphere composition, the ionization by thermal electrons is limited to the upstream hemisphere of Io. The MHD codes, with an ionization rate prescribed spherically around Io overestimate the plasma production volume and thus overestimates the plasma density they compute.

- 2) A molecular atmosphere will cool the electrons more rapidly and the ionization and plasma production will be more limited and more confined to the upstream region than for an atomic atmosphere.

In summary, the multi-species chemistry takes into account the cooling of the electrons consistent with the composition of the prescribed atmosphere.

6.3.2 Importance of multi-species for temperature calculation

The second limitation of MHD has been discussed previously. The MHD model assumes a single species with a mass = 20 amu. As the plasma picked up could be heavier (S= 32 amu and SO₂= 64 amu), the temperature calculated by the MHD code may not be compared quantitatively to the data. On the other hand, the chemical model calculates precisely the average ion temperature by weighting the pickup energy of each ion species with their local density.

6.3.3 Limitation of our own Hall-MHD model

Our MHD simulations are limited by two other factors:

- 1) The short run-time of our model: the simulation is stopped when the MHD waves reach the simulation domain boundary. In the short run (6 min of real flow), the plasma close to Io does not have time to accumulate in the wake.
- 2) As Io is not defined with a solid sharp boundary but as a dense cloud of neutrals, the flow penetrates the moon and drags plasma downstream in the wake. The consequence is that the plasma density calculated by our own Hall-MHD code, although qualitatively correct, could be quantitatively imprecise.

The chemical model circumvents these issues. As the model has no electromagnetic description, it does not propagate waves and the boundary conditions are thus not an issue. The code can be run as long as needed for the plasma to cross the simulation domain (15 min of real flow) and accumulate in the wake. Following *Saur et al. [1999]*, when a flow line hits the solid body of Io, it is stopped and no further chemistry is calculated. So the plasma cannot penetrate Io.

6.3.4 Coupling

We verified that the Hall-MHD calculation of the flow and magnetic perturbations reach very rapidly a stationary state. Our method is to iterate between the MHD and multi-species chemical codes.

The MHD code is used with an initial estimate of the ionization rate to compute a velocity field. The calculated MHD flow is then implanted in the multi-species chemical model to compute an improved ionization rate that is implanted in the MHD model and so on. At the end of the iteration process, the plasma density and temperature are calculated with the chemical model and compared to the GLL observations, the flow and magnetic perturbation and currents are calculated with the MHD model and compared to the observations.

Ideally, the chemical model and fluid model should be iterated as necessary to find a steady solution. Practically, because this iterative process is time and computer resource consuming, we iterate only twice. We feel that the results represent a significant advance in modeling of Io's local interaction.

In summary, a contribution of this thesis is the development of a coupled Hall-MHD/chemical model where we compute self-consistently the magnetic and flow perturbation, the cooling of the electrons, the change of the composition, the density and the temperature of the plasma.

7. ATMOSPHERIC SCENARIOS

We have run numerical experiments with the coupled model for two atmospheric scenarios. The first one is an atomic atmosphere simply composed of O and S, with a radial profile proposed by *Khurana et al. [2011]*. We call this scenario “KK-S&O” to refer to its author and its composition. It will be used to illustrate the magnetic and flow perturbations calculated by the Hall-MHD model.

The second one is a multi-species (S, O, SO₂) atmosphere that includes three different components. These scenarios are summarized in Table 2 and will be presented in detail in the next sections.

Name	Composition	Power law index	Scale height	Equatorial density (cm ⁻³)	Polar density (cm ⁻³)
Atomic					
KK-S&O	O/S=2	-3.5	270 km	1.89 10 ⁷	0.17 10 ⁷
Multi-species					
Corona-S&O	O/S=2	-3		1.05 10 ⁶	1.05 10 ⁶
Corona-SO ₂	SO ₂	-4			
Atm-SO ₂	SO ₂		500 km	5.0 10 ⁶	0.5 10 ⁶

Table 2: The two scenarios tested in the next sections: the atomic atmosphere KK-O&S and a multi-species atmosphere that includes three components.

8. ATOMIC ATMOSPHERE: “KK-S&O”

This atmosphere is composed of S and O only. It was proposed by *Khurana et al. [2011]* in a MHD modeling of Io with an ion mass= 20 amu. Based on our experience with the chemical model, we scale their profile by 0.5. The radial profile combines a power law corona and an exponential core.

$$n(r, \Theta) = (0.1 + \cos^6 \Theta) \times 0.5 \times \left(1.1510^7 \times \left(\frac{r}{R_{Io}} \right)^{-3.5} + 2.310^7 \times e^{-\frac{(r-R_{Io})}{270}} \right)$$

in cm^{-3} with Θ = latitude and r = distance to Io's center in km.

The power law relation is inspired by the sodium density profile observed by scattering of the visible solar light (*Schneider et al., 1991*; see Section 3.3). It was already proposed in the former MHD simulations of Linker et al., 1998. Assuming that Na, S and O experience the same ejection process from the deep atmosphere (ex. ion sputtering), Na could be a tracer for the less visible S and O. The scale height of the exponential core (270 km) is reasonable considering the probable high temperature in the upper atmosphere of Io (~ 2000 K, *Strobel [1994]*). The latitudinal variation is inspired by the Lyman-alpha observations of an atmosphere concentrated at equatorial latitude, although less steep than the profile proposed by *Strobel [1994]*

The composition is poorly constrained: we will assume that this atmosphere has an O/S density ratio =2, consistent with the total dissociation of SO_2 by electron impact.

8.1 The J0 flyby in Io 's wake

The J0 flyby is a flyby towards Jupiter, in the wake of Io, close to the equatorial plane. The outbound leg of the trajectory samples the night hemisphere. At closest approach (~ 900 km), the observed flow is stagnant (~ 1 km/s), and the plasma very cold (1 eV) and very dense ($\sim 30,000 \text{ cm}^{-3}$).

To illustrate the interaction process, we first show the results of the chemical model in the XY plane in Figure 34, parallel to the equatorial plane of I_0 at the Z distance of the closest approach $\sim -0.26 R_{I_0}$.

Panel A shows the plasma density, which increases upstream and on the flanks. Panel B shows the distribution of neutrals where the night hemisphere is shaded in gray. Panel C shows the flow speed, which was extracted from the MHD results: the flow is slowed upstream and downstream, and accelerated on the flanks. Panel D shows the average ion temperature, cold directly upstream of I_0 because the pickup takes place at a local flow speed that is very low. The temperature is high on the flanks because ions are picked-up at fast flow and the gained energy accumulates along the flow lines. The jagged results upstream of I_0 appear because of the limited number of flow lines used to draw the figures. It has no effect on the results farther away and on our discussion.

Note that all panels show an empty wake similar to *Saur et al. [1999]* and already discussed in Section 5.2, because the flow lines that hit the upstream hemisphere of I_0 come out empty. *Saur et al. [2002]*, *Dols et al. [2008]* (in this thesis) showed that the high plasma density in the wake is caused by an ionization source different than the thermal plasma of the torus. Beams of hot electrons (~ 300 eV), flowing along the field lines in both directions are responsible for ionization in the wake and maybe above the poles.

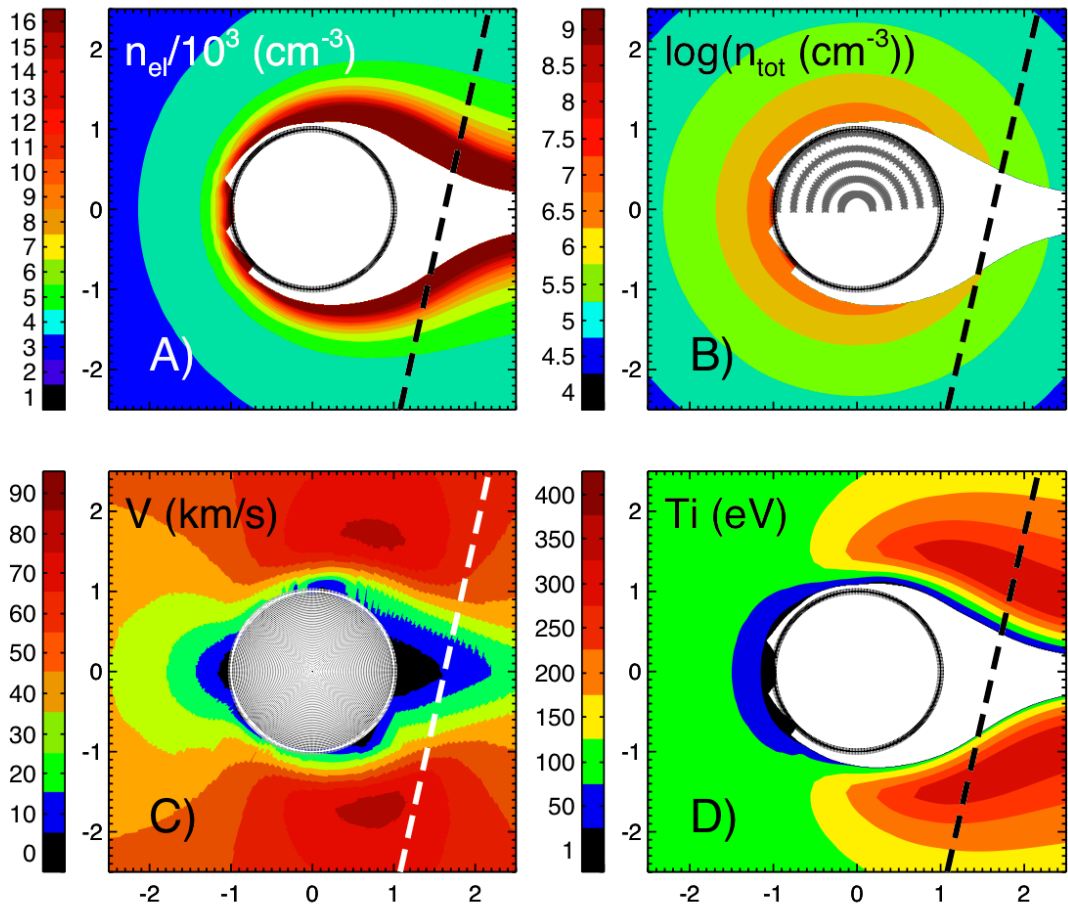


Figure 34: The plasma characteristics calculated with the chemical model in the XY plane parallel to Io's equatorial plane at distance $Z \sim -0.26 R_{Io}$. The dashed line represents the J0 trajectory. A) Plasma density. B) Neutral density. The night-side hemisphere is shaded in gray C) Flow speed extracted from the MHD simulation. D) Average ion temperature.

We now display the results extracted along the J0 flyby to compare with the observations. Figure 35 shows the flow and magnetic perturbations calculated with the Hall-MHD model.

J0: Velocity and magnetic field perturbations

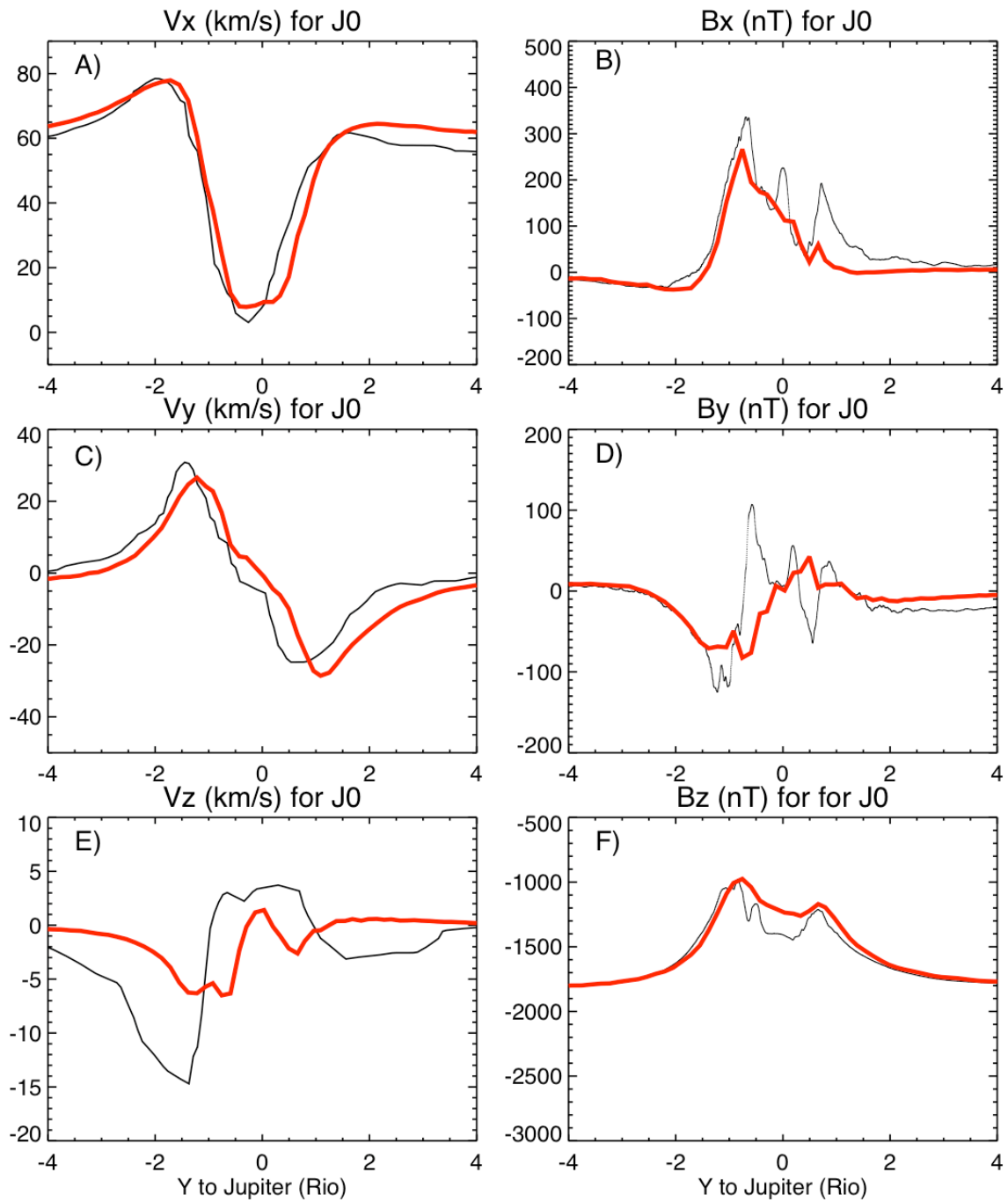


Figure 35: J0 flyby. Velocity and magnetic field perturbations. Black lines=observations, red lines= MHD model results.

The MHD results are close to the observations. B_z shows the double-peaked structure that was not well captured by previous MHD modeling (*Linker et al., 1998; Kabin et al., 2001*). *Saur et al. [2002]* claim that this double-peaked structure is caused by diamagnetic currents flowing along the wake. The doubled-peak structure would probably become deeper in our simulations if the code was run for a longer time so that the density gradients could fully develop. The magnetic components show many short scale oscillations possibly caused by ion cyclotron wave and mirror mode instabilities (*Huddleston et al., 1997*) that our MHD code cannot simulate. Our experience indicates that V_z is difficult to capture and, as it is usually small, we won't focus on this velocity component. On the outbound leg ($Y > 0$), the modeled V_x and V_y seem to extend farther from Io than the observations. As this hemisphere is in the night, it may be an indication of a partial collapse of the atmosphere. Although S and O do not condense, *Retherford et al. [2007]* showed that the FUV oxygen and sulfur emissions of Io's equatorial spots decrease in eclipse, following the probable collapse of the underlying SO₂ atmosphere.

In Figure 36, in the first four panels at the top, we display the plasma properties calculated by the MHD model: strength of the magnetic field, speed, plasma density and ion temperature. The thin black line represents the observations and the red thick ones, the model results. We add two panels at the bottom of the figure with the plasma density and average ion temperature calculated with the chemical model (thick blue line), using the MHD flow. As expected, the average ion temperature is higher than the one calculated with the MHD model because the multi-species chemistry model includes the pickup of heavy sulfur ions. We note that on the outbound leg of J0, the secondary peak in density and drop of temperature as well as the increase of temperature inside Io's orbit cannot be addressed with this modeling. The Hall effect does not provide an asymmetry large enough to explain this secondary peak. These features might be structures already present in the torus before the interaction with Io or might be better addressed with a more sophisticated model of the interaction like an hybrid simulation, which could provide more asymmetry (*Delamere, private communication*).

J0: Plasma properties

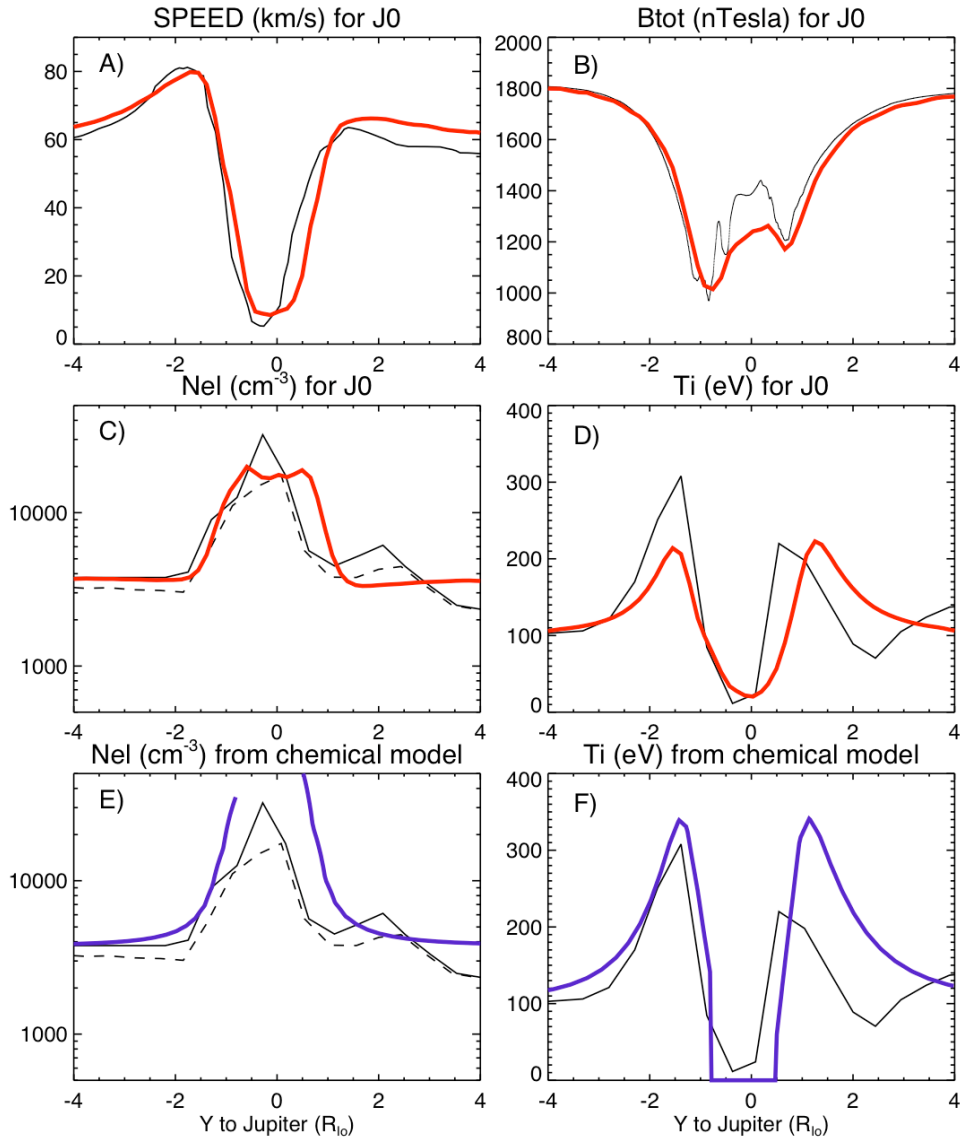


Figure 36: Plasma properties along the J0 flyby. The thin black lines represent the observations. For the plasma density, the solid black line is the PWS observations, the dashed one is PLS. The colored lines are the model results. A) speed, B) magnetic field strength. C) plasma density computed with the MHD model. D) ion temperature calculated by the MHD model. E) plasma density calculated with the Chemical model. F) Average ion temperature calculated by the chemical model.

8.2 The I24 flyby, upstream of Io

The I24 flyby samples the upstream side of Io very close to the equatorial plane. The closest approach (611 km) is close to the terminator. The plasma density ($\sim 600 \text{ cm}^{-3}$), temperature ($\sim 50 \text{ eV}$), Io's local time (10.7 LT) and the angle of the flyby in Io's frame indicate that the inbound leg far from Io ($\sim 10 R_{\text{Io}}$) was probably in the cold torus.

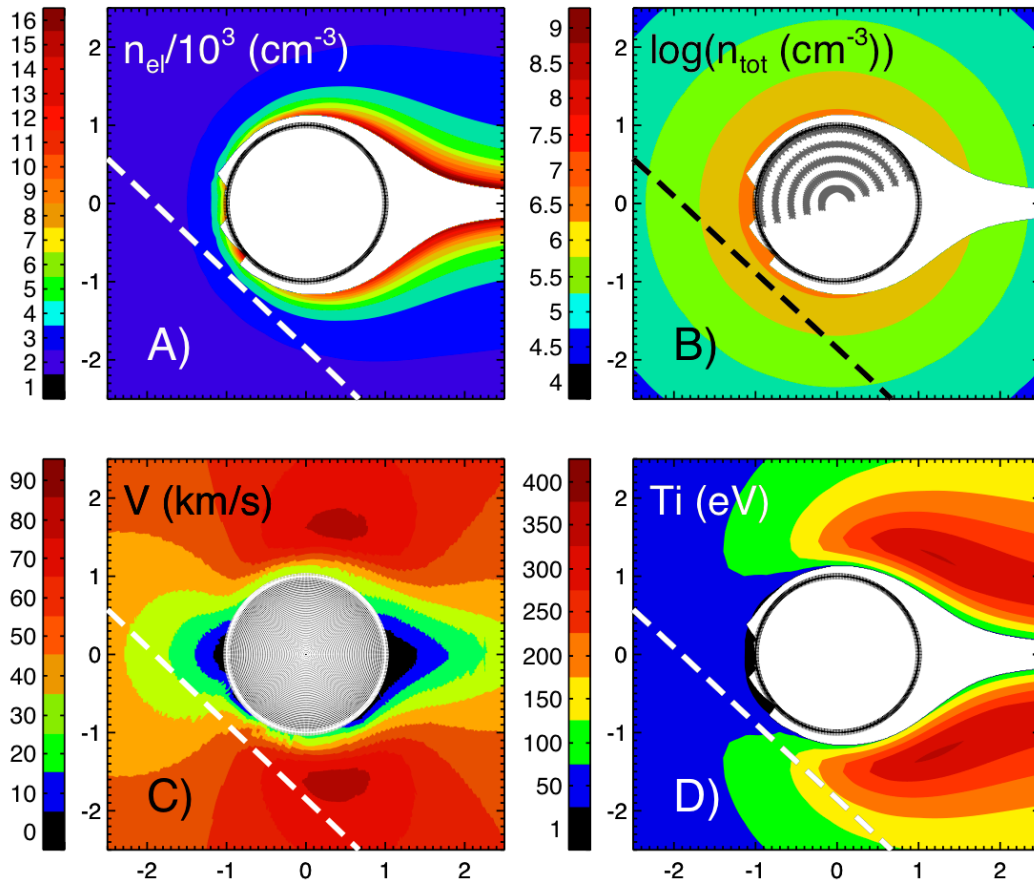


Figure 37: The I24 flyby (dashed line) in the XY plane parallel to Io's equatorial equator at $Z \sim 0.1 R_{\text{Io}}$.

I24: Velocity and magnetic field perturbations

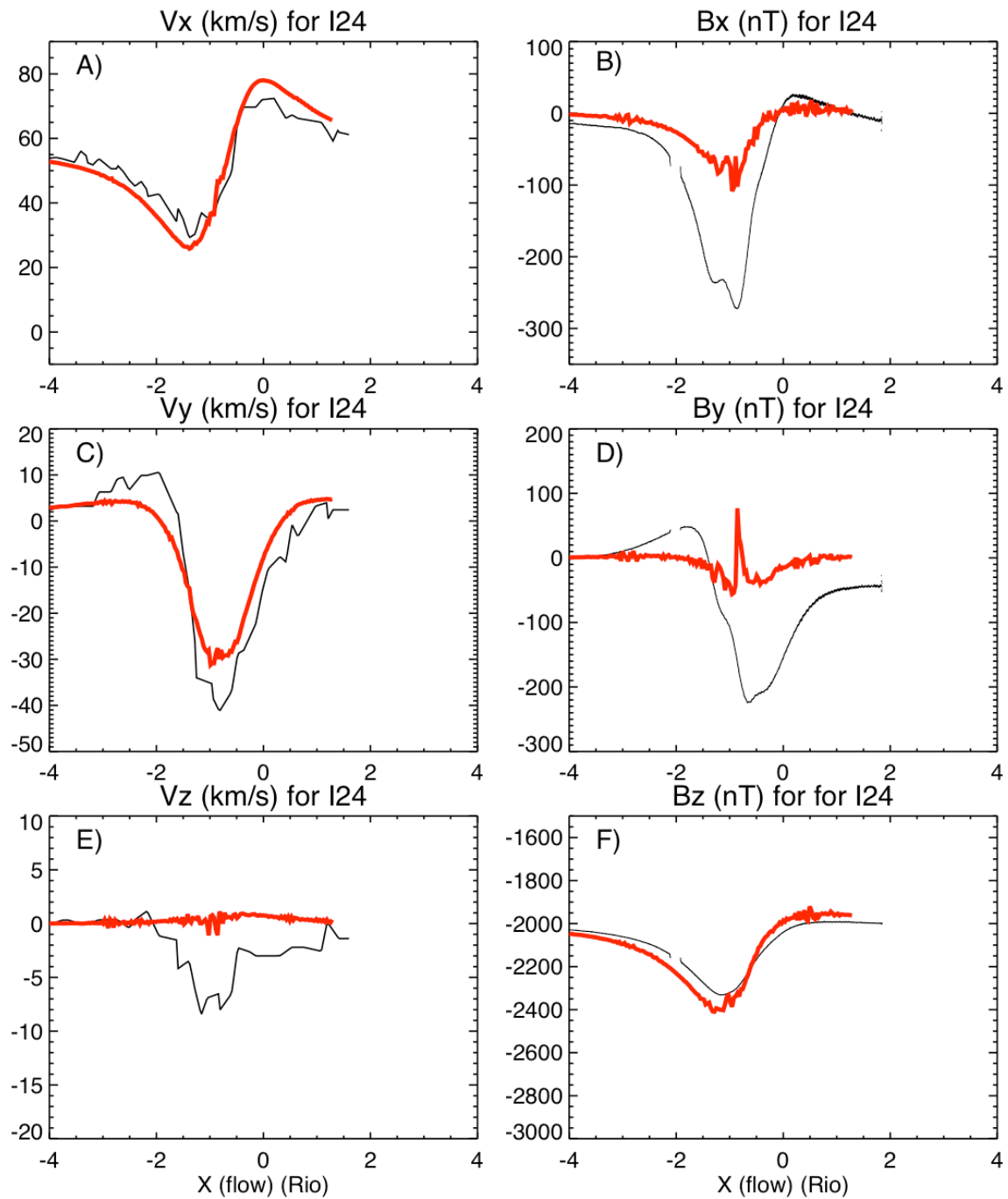


Figure 38: I24 flyby. Velocity and magnetic field perturbations from the MHD model. Observations in black, MHD results in red.

The velocity calculated seems consistent with the observations. V_y is slightly too small, which maybe the consequence of I_0 treated as a “soft” cloud of neutrals. A solid I_0 , impenetrable to the flow, might divert the incoming flow more strongly.

B_z is convincingly matched by the model results, the B_x and B_y not at all. It will be shown in Section 8.6 that the field at this latitude is perturbed by an induced dipole resulting from induced current in the magma of I_0 as suggested by *Khurana et al. [2011]*.

Figure 39 shows that the plasma density and ion temperature calculated by the models are much higher than the measurements suggest. The PWS observation does not show any plasma increase at all, while the PLS shows a slight plasma and ion temperature enhancement. This discrepancy indicates that the hypothetical atmosphere used for this simulation (KK-S&O) extends too far in the upstream hemisphere. The upstream atmosphere could be compressed by the incoming flow as suggest by *Saur et al. [2002]* or, emerging from the night, its underlying SO_2 component might not have yet fully recovered.

I24 (upstream) Plasma properties

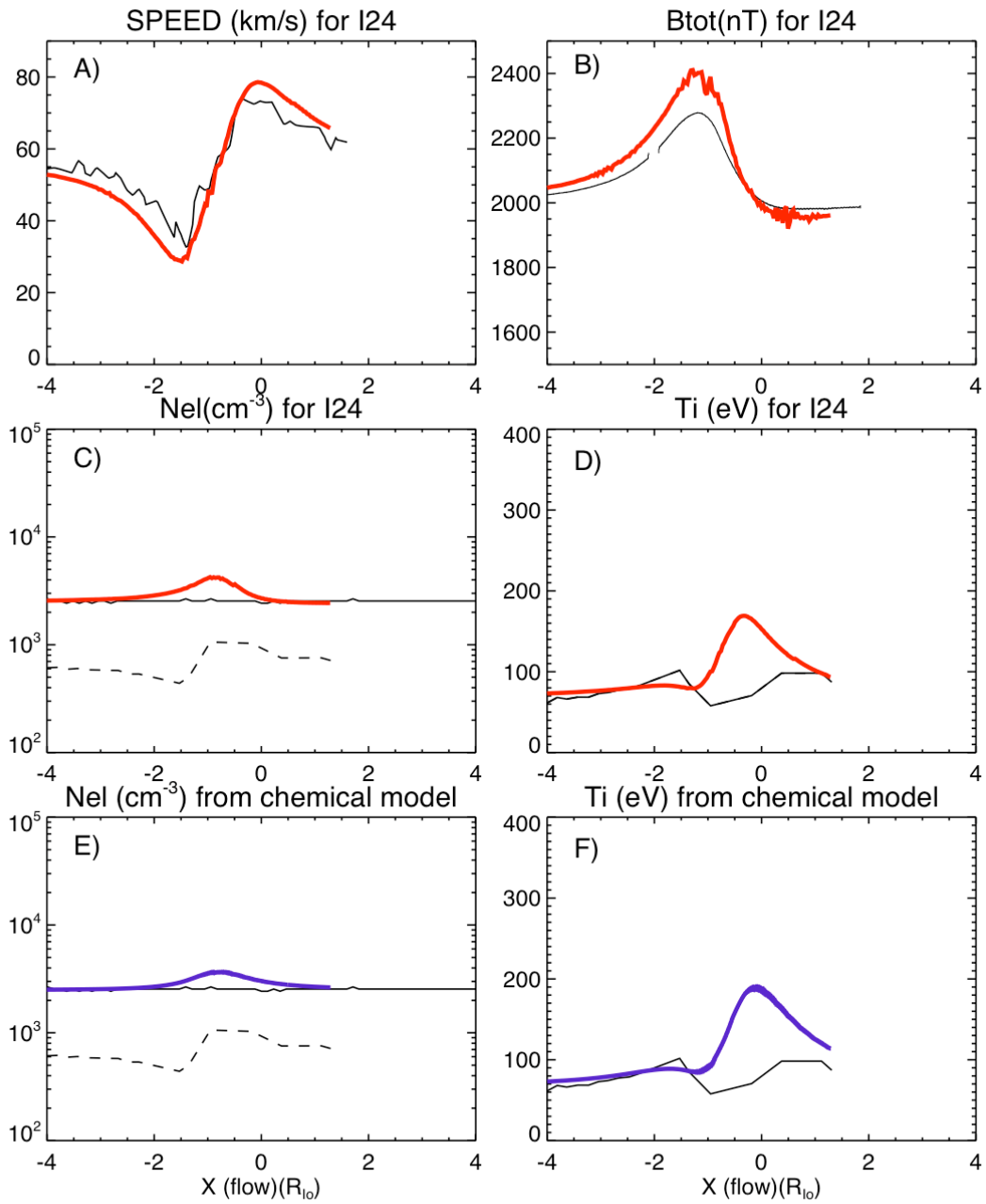


Figure 39: The I24 flyby, upstream of Io: Plasma characteristics. The observations are the black thin lines, the MHD results are in red, the chemical model results in blue.

8.3 The I27 flyby, on the anti-jovian flank

The I27 flyby is very similar to the I24 flyby. Io was at the same phase angle on its orbit (local time) and approximately at the same S_{III} longitude (see Table 1). I27 is higher above the equatorial plane (Z at closest approach $\approx 0.4 R_{Io}$) and much closer to Io at the closest approach (198 km) than I24. The closest approach is very close to the terminator and the outbound leg samples the downstream anti-jovian quadrant.

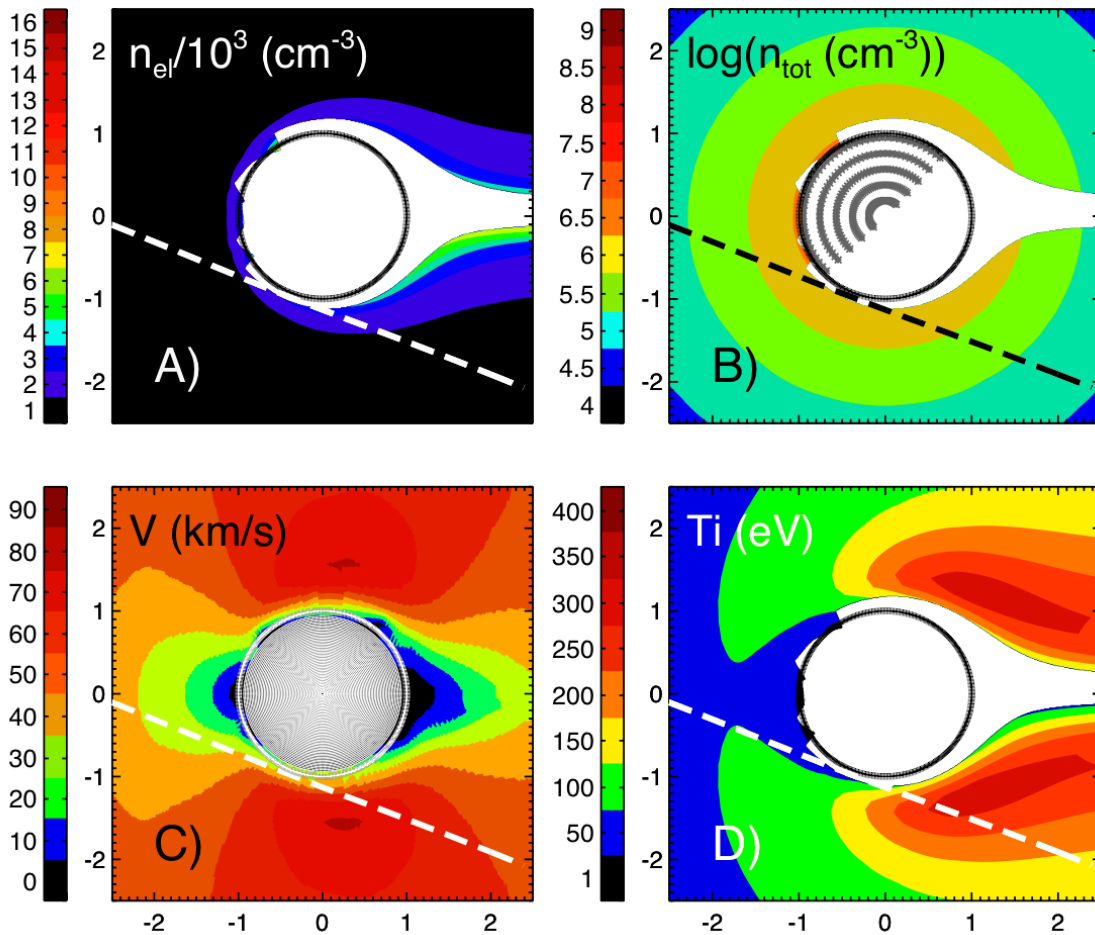


Figure 40: The I27 flyby (dashed line) and plasma characteristics in the XY plane parallel to the equatorial plane at $Z \sim 0.4 R_{Io}$, calculated by the chemical model.

I27: Velocity and magnetic field perturbations

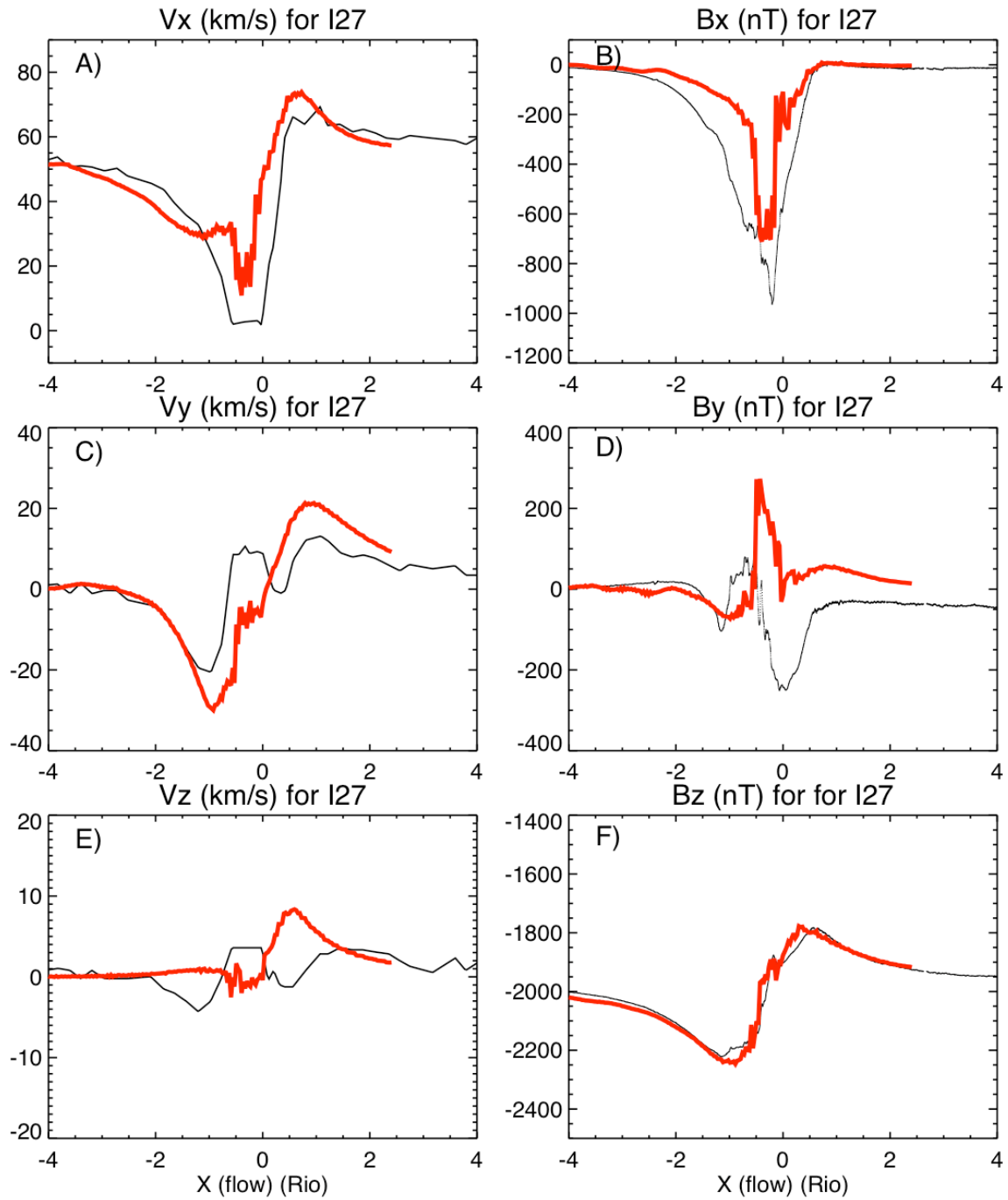


Figure 41: The I27 flyby, on the anti-jovian flank. Velocity and magnetic field perturbations.

The gross features of the observed velocity and B_z are convincingly modeled. As I27 is very similar to I24, the B_x and B_y components of the magnetic field will be explained with the inclusion of an induced dipole (Section 8.6).

Figure 42 shows the plasma properties. The high plasma density peak at closest approach on I27 ($\sim 100,000 \text{ cm}^{-3}$) was interpreted as the sampling of the bound ionosphere of Io (*Gurnett et al., 2001*). The peak plasma density is consistent with the ionospheric plasma density inferred from radio occultation by *Hinson et al. [1998]*. The atmospheric profile “KK-S&O” describes an atmosphere at a larger spatial scale and does not model accurately the sharp transition to this deep dense ionosphere.

Panels D and F display the most surprising result of this simulation. The observations show a flat temperature profile ($T_i \sim 100 \text{ eV}$), similar to the upstream plasma temperature. Both the MHD and chemical model give an ion temperature that jumps to $\sim 300 \text{ eV}$ after the closest approach. The I27 samples the downstream anti-jovian hemisphere in daylight, when the atmosphere should be fully developed. The observations do not show any sign of pickup or interaction with the atmosphere. This is a puzzling result that we will address in the Discussion section (Chapter 10.3).

I27 (anti-jovian flank): Plasma properties

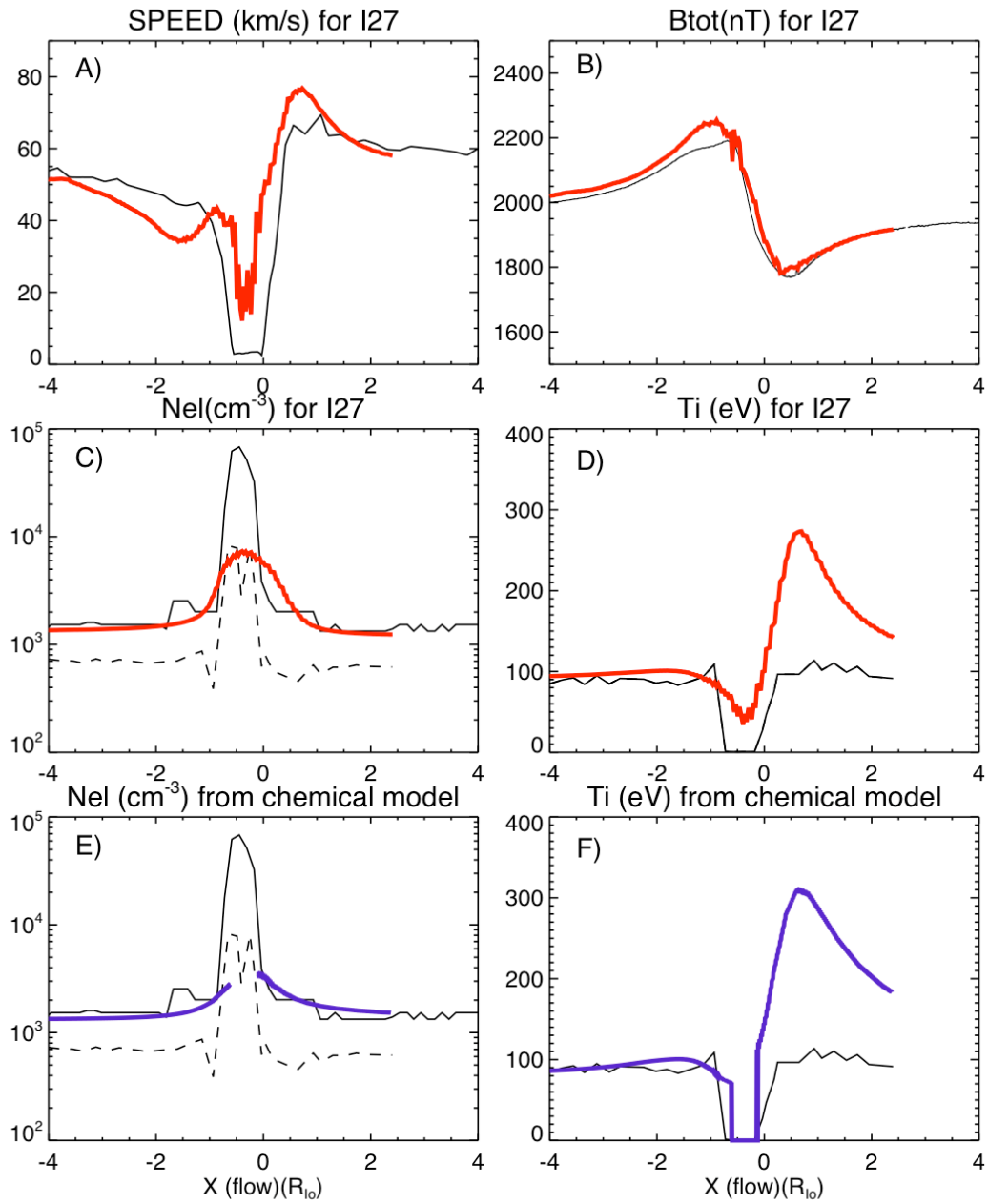


Figure 42: The I27 flyby. Plasma characteristics. Black=observations, red= MHD results, Blue= Chemical model results.

8.4 The I31 flyby, above the north pole

I31 is a flyby above the north pole of Io, at low altitude (~ 200 km) almost perfectly aligned with the flow (the X axis). GLL encountered Io on its night side, traversed the Alfvén wing where the flow is slow and the plasma is cold and dense, and emerged in the polar wake. The polar atmosphere, based on Lyman-alpha observations, is probably very thin. The surface density of the “KK-S&O” polar atmosphere is 10% of the equatorial surface density. Bidirectional field-aligned electron beams were observed in the Alfvén tube, similar to those detected in the wake (J0). These electrons are not included in the MHD simulations. Their contribution to the ionization would be difficult to evaluate as the density at the pole is not well constrained by observations.

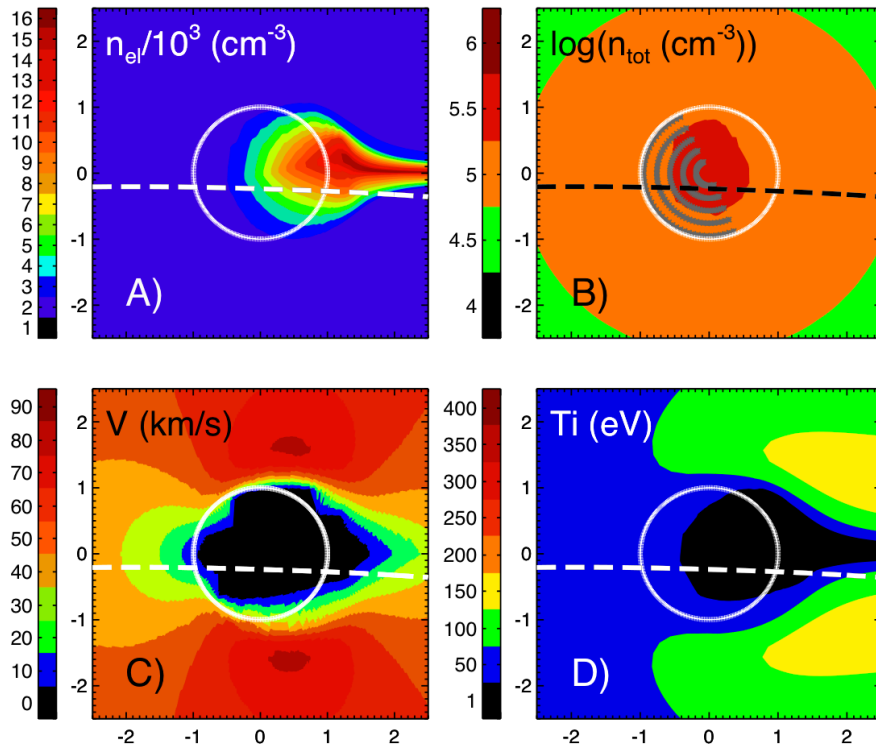


Figure 43: The 31 flyby (dashed line) above the north pole. Plasma characteristics in the XY plane parallel to Io's equator at $Z \sim 1.1 R_{Io}$.

I31: Velocity and magnetic field perturbations

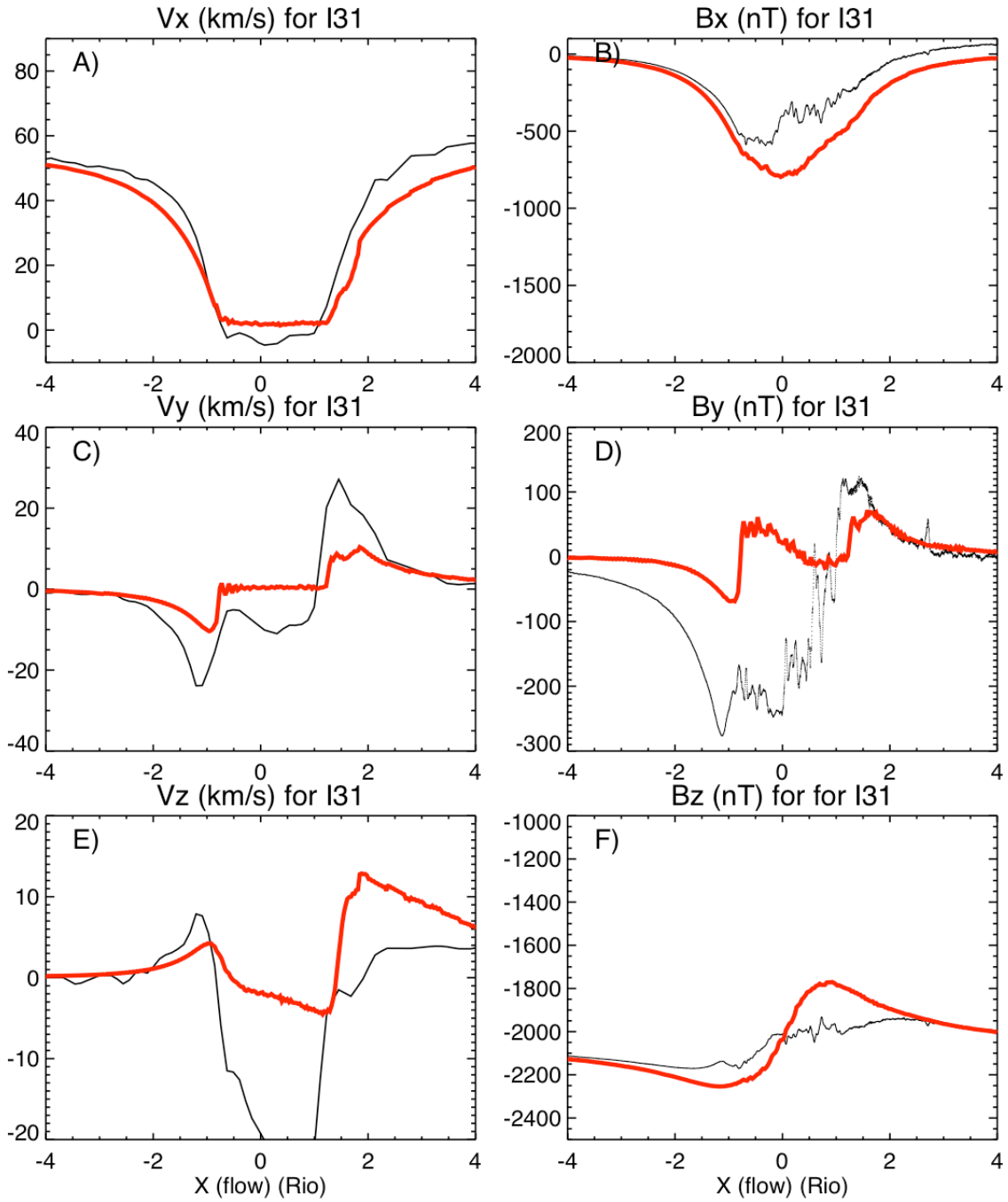


Figure 44: The 31 flyby: Velocity and magnetic field perturbations. The observations are in black, the MHD results in red.

Figure 44 shows the velocity and magnetic field perturbations. The velocity component V_x is consistent with the observations while the modeled V_y is slightly too small. Once again, we think that the lateral diversion of the plasma (V_y) would be sharper if I_0 was defined as a solid body and not as a cloud of neutrals.

The B_y perturbation is interesting: The modeled magnetic perturbation caused by the plasma interaction does not explain the large decrease of B_y . We will show in the next section that it could be explained by an induced dipole, in a direction opposite to the one needed for I24 and I27. This observation is crucial to determine the induced nature of this dipole and was not included in the publication of *Khurana et al. [2011]*.

Figure 45 (Panels D and F) shows that neither the MHD nor the chemical models capture the sudden jump of the ion temperature when GLL exits the Alfvén wing at $X \sim 1 R_{i0}$. This jump in temperature is difficult to explain in the present simulation. GLL exited the Alfvén tube in the slow wake of I_0 , inside the slow-mode wing where the temperature is low. We will propose an explanation for the model results along I31 in the Discussion section (Section 10.3), which suggests that the simplified geometry we assume here might be responsible for this discrepancy

Panel C and E show the plasma density. The chemical model does not show the steep increase of plasma density when GLL enters the Alfvén tube and calculates a plasma density too high behind the tube while the MHD results show these steep transitions. These differences might be related to the interpolation method of the MHD flow that we use to implant the flow in the chemical model. I31 shows definitely that the plasma wake observed along J0 is vertically confined to distances smaller than $1 R_{i0}$ from the equatorial plane unlike the MHD simulations in *Combi et al. [1998]* where the plasma wake flares out to polar latitude, for specific reflective boundary conditions.

In both model results, the ion temperature farther downstream at $X \sim 4 R_{i0}$ is lower (150 eV) than the observed temperature (~ 200 eV).

I31: Plasma properties

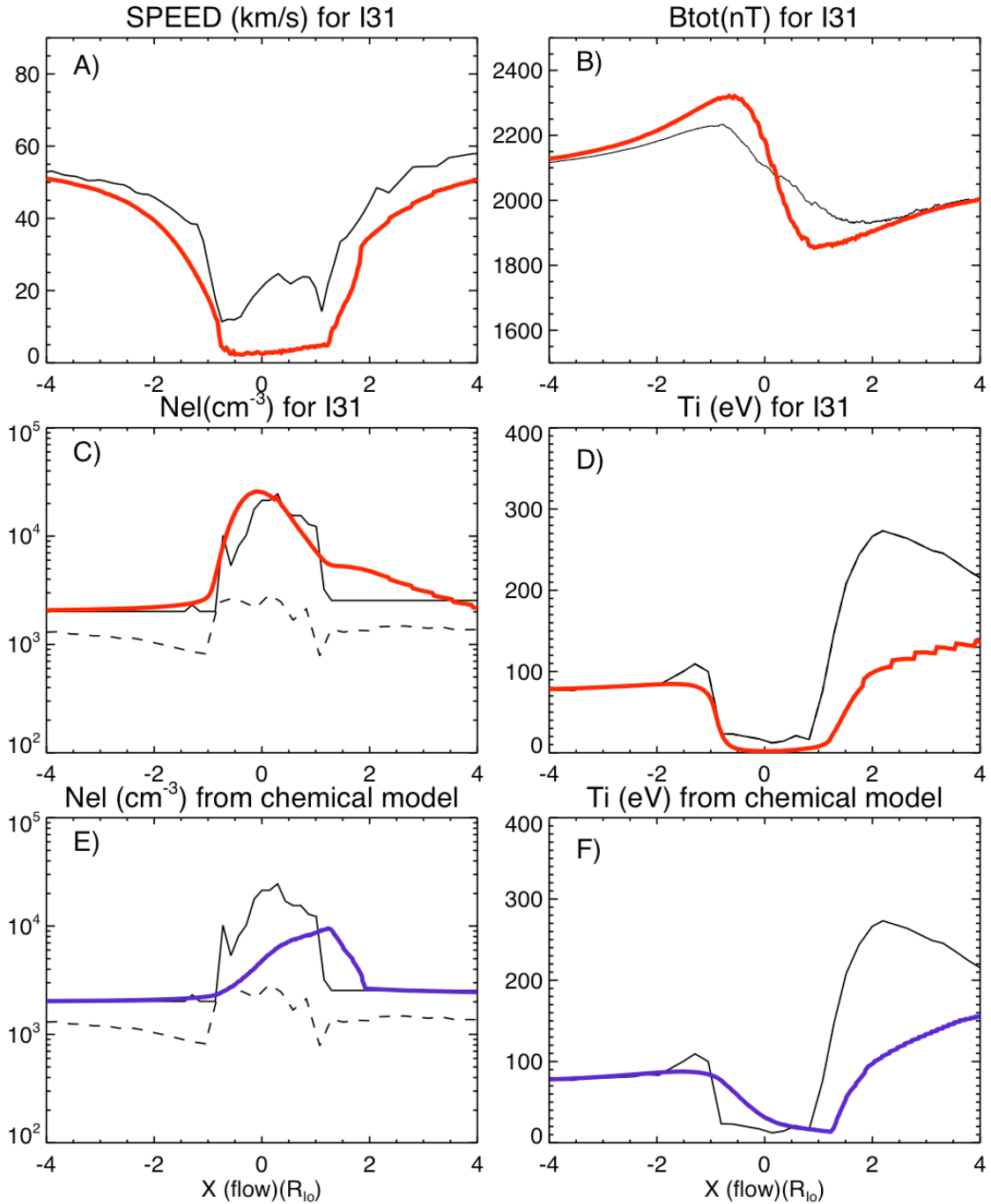


Figure 45: The 31 flyby: Plasma characteristics. Black=observations, red= MHD results, Blue= Chemical model results.

8.5 The I32 flyby, under the south pole

I32 is a flyby under the south pole, at an altitude ~ 180 km. The trajectory encounters Io on its night side and is more tilted relative to the co-rotation X direction than the I31 flyby, which was also a polar flyby.

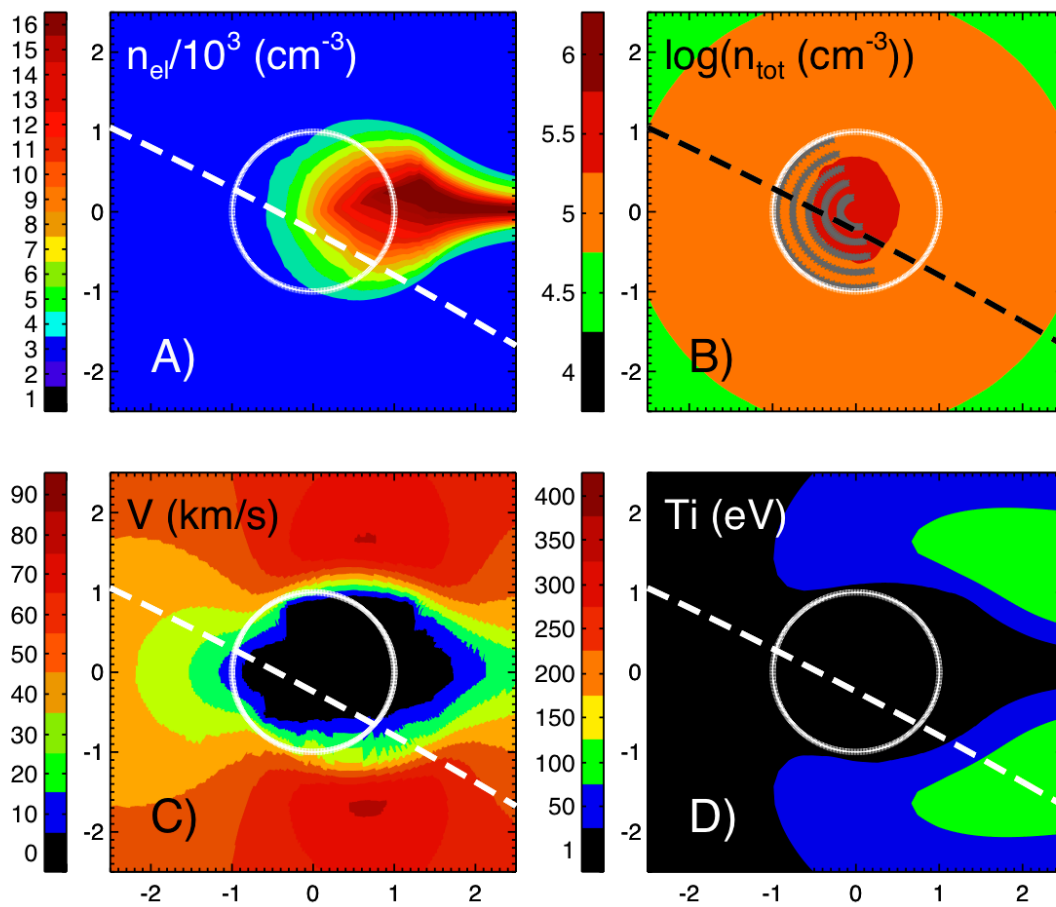


Figure 46: The I32 flyby (dashed line), under the south pole. Plasma properties calculated by the chemical model in the XY plane parallel to Io's equator at $Z \sim -1.1 R_{\text{Io}}$.

I32: Velocity and magnetic field perturbations

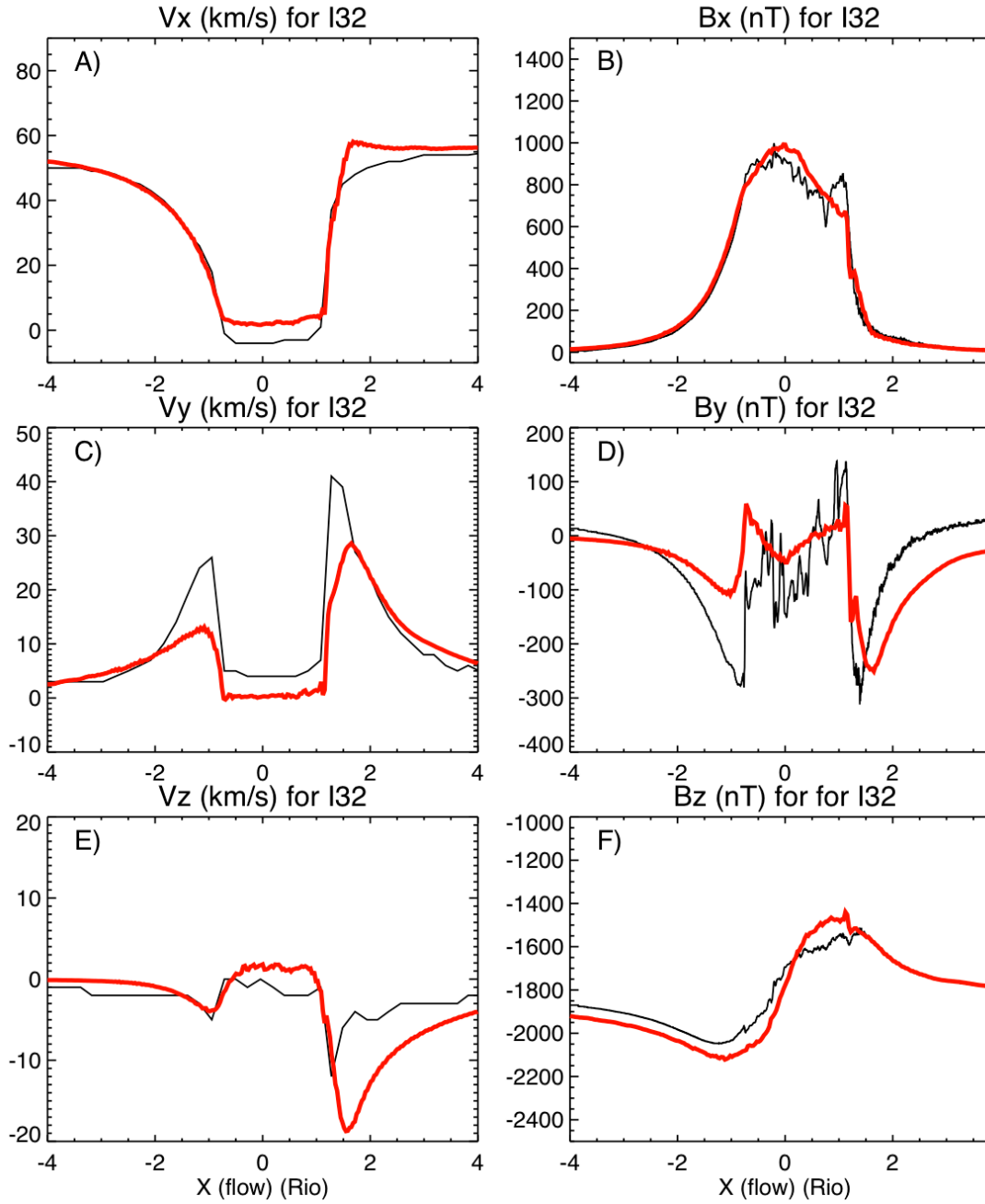


Figure 47: The I32 flyby. Velocity and magnetic field perturbations. The observations are in black, the MHD results in red.

The modeled velocity and magnetic perturbations (Figure 47) are close to the observations. V_y and B_y are not deep enough at the entrance and exit of the Alfvén tube and this shows again that our treatment of Io as a cloud of neutrals needs to be improved. Probably for the same reason, V_x is not slowed enough at the entrance of the Alfvén tube as well and consequently, B_x is not strong enough.

In Figure 48, the chemical model computes plasma density and ion temperature that are not as sharp as those calculated by the MHD model and it might be related to the way we sampled the MHD flow to insert it in the chemical model.

The atmosphere “KK-S&O” is very extended and the ion temperature profile extends far from Io on the outbound leg of the trajectory at $X \sim 4 R_{Io}$, which is consistent with the observations.

I32: Plasma properties

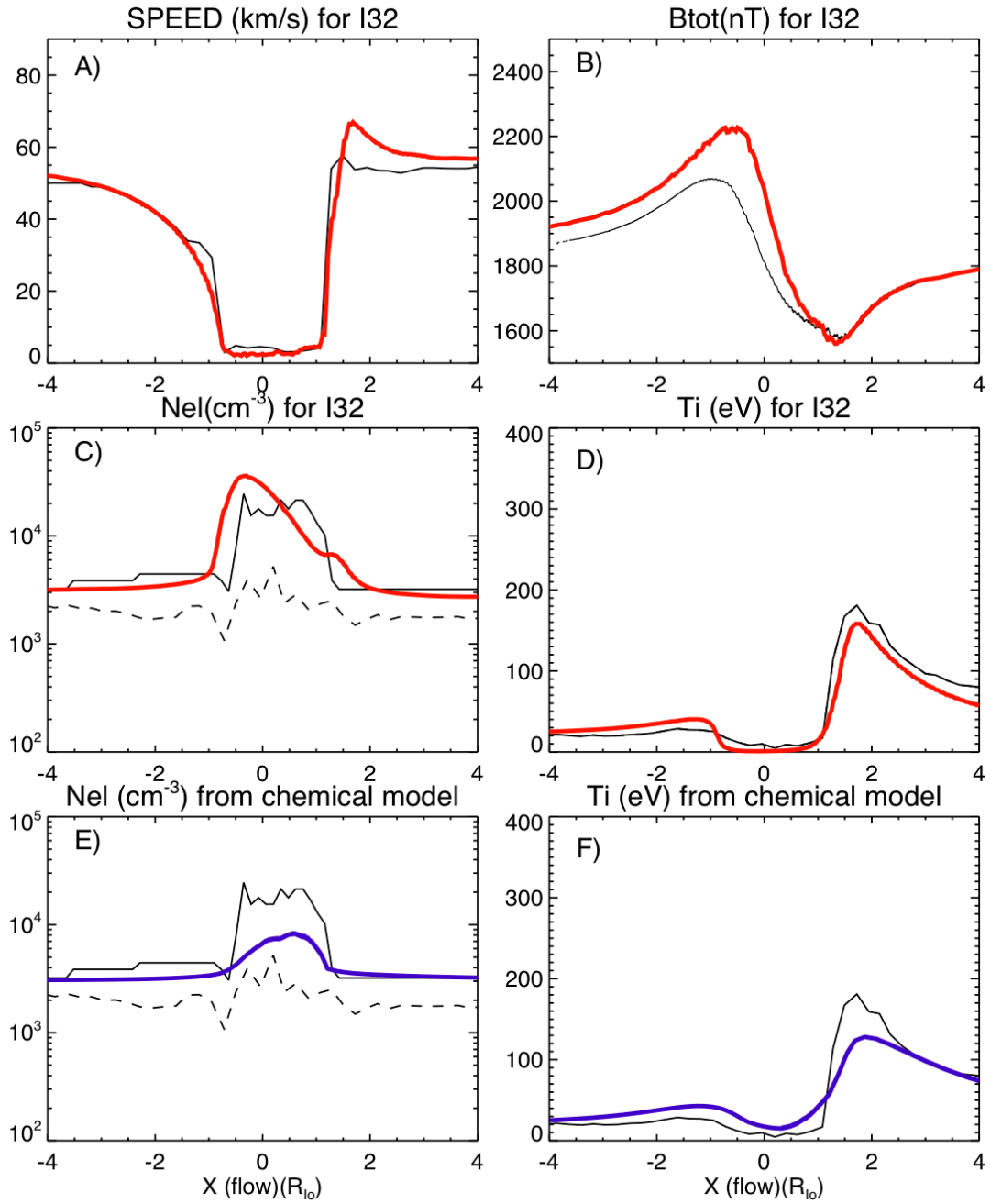


Figure 48: The 32 flyby. Plasma characteristics. Black=observations, red= MHD results, Blue= chemical model results.

8.6 Confirming the existence of an induced dipole at Io.

The simulation of B_x and B_y on I24, I27 and I31 shows that the plasma interaction cannot explain the large magnetic field variations observed along these flybys. *Khurana et al. [2011]* proposed that the I24 and I27 magnetic components could be explained by an induced dipole created by current in the conducting magma inside Io. Because of the $\sim 10^\circ$ tilt of Jupiter's magnetic dipole, Io experiences a changing background magnetic field that varies with a ~ 10 hour period. This variable magnetic flux in the body of Io creates currents in a conducting magma and these currents produce an induced magnetic field.

Ideally, a calculation of the strength of the induction based on the time variation of the background magnetic field at Io's location should be included in the MHD model to calculate self-consistently the perturbation of the flow and magnetic field along the GLL flybys. This is beyond the scope of the work presented here. We will simply illustrate its effect on the Galileo magnetometer observations by adding a dipole magnetic field to the results of our MHD simulation for I24, I27 and I31. This dipole will be close to Io's equatorial plane, with a strength ~ 300 nT at the dipole magnetic equator on Io's surface.

The flybys I32 and J0 have S_{III} longitudes that are very similar and the modeled magnetic perturbation is not improved by adding a dipole. The Jovian field variation is probably not strong enough to induce an observable magnetic field so we do not show these results.

8.6.1 Induced dipole for I24 and I27

During the I24 and I27 flybys, Io was at the same Jovian longitude and was experiencing a very similar jovian magnetic field variation. Presumably, the induced dipole field is very similar on both flybys. The I24 flyby is in Io's equatorial plane and is very sensitive to the induced dipole effect since the magnetic perturbation caused by the plasma interaction is minimum in the equatorial plane. The I27 flyby is slightly above the equatorial plane. In Figure 49 (I24) and Figure 50 (I27), the left panels show the results of B_x , B_y , B_z from the plasma interaction. The fit is poor, especially for B_y . On the right panel, we added a dipole of 300 nT, oriented in the $-Y$ anti-Jovian direction (Io longitude 197° and 180° . respectively where 0° . is towards Jupiter), slightly tilted relative to the

equatorial plane ($\sim 10^\circ$). The magnetic perturbation measurements are displayed as the thin black lines, the dipole magnetic components as green dashed lines, the modeled plasma interaction magnetic perturbation in red and the blue line represents the addition of both. It can be seen that almost all the B_y and B_x variations on I24 can be explained by the induced dipole, while B_z , because the dipole is almost in the equatorial plane, is solely explained by the plasma interaction. The conclusion is similar for I27, especially for the B_y component.

Saur et al. [2002] focused on the magnetic observations along I24 and I27 as well. They claimed that the magnetic perturbation could be explained with an asymmetric atmosphere, compressed upstream and dragged downstream by the incoming plasma. This asymmetry would create stronger horizontal currents in the downstream atmosphere of I_o compared to the upstream atmosphere and create a stronger magnetic perturbation behind I_o, consistent with Ampere's law. They support their claim of an asymmetrical atmosphere based on B_z observations and stated that they “ (...) underestimate the x and y components due in part to problems with the non-uniqueness of coordinate systems used to compare the data with our model results”. Our simulations show that the crucial observations are B_y and B_x components and an asymmetrical atmosphere will not explain the large discrepancy with the modeled magnetic perturbation caused by the plasma interaction. Nevertheless, we will support the claim of the atmospheric asymmetry, not based on the magnetometer observations but on the ion temperature and plasma density observations (see Section 10.6).

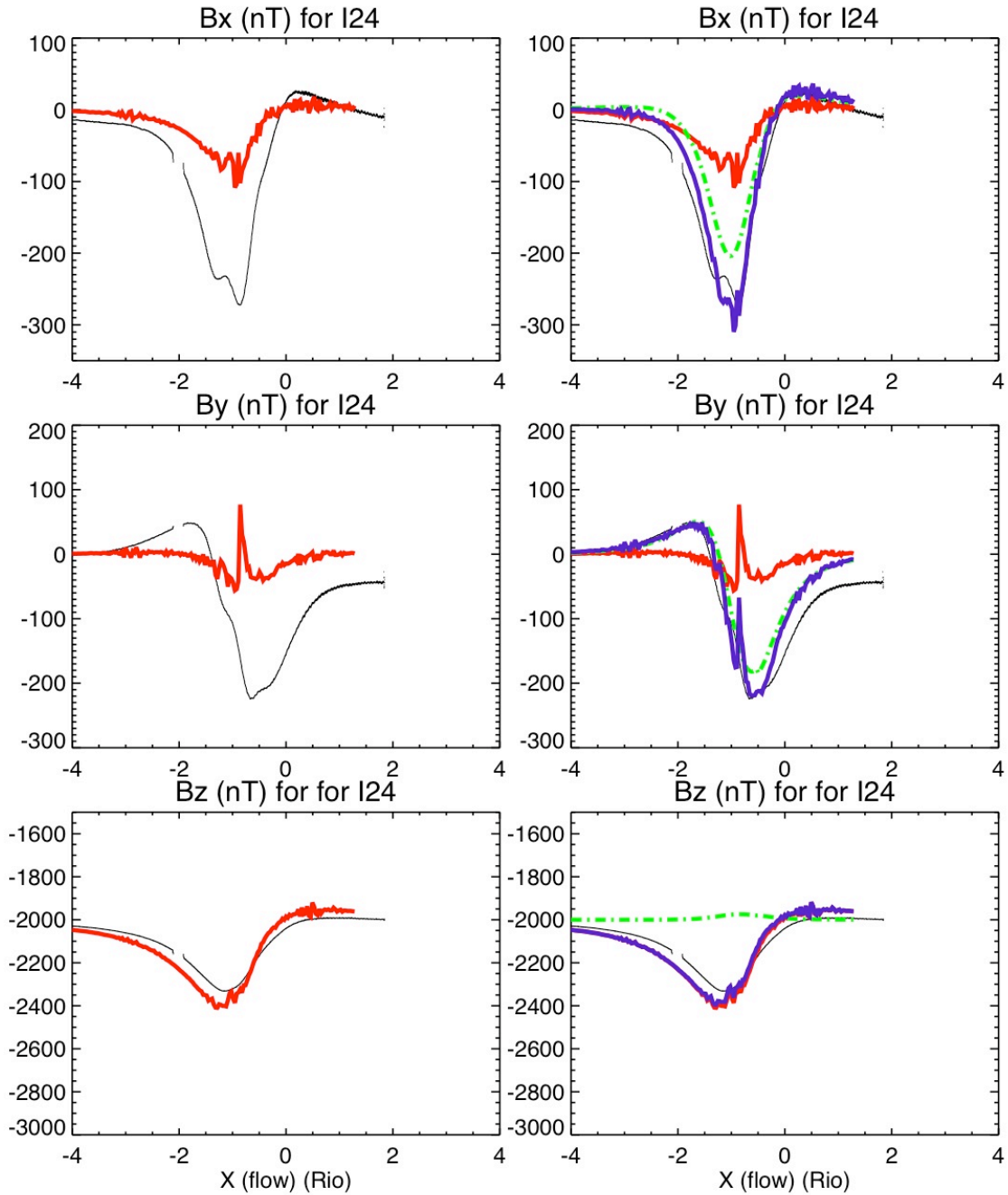


Figure 49: Components of the magnetic perturbation at Io during the I24 flyby. Black is the observations, red is the modeled plasma, green is the prescribed induced dipole and blue is the combination of the modeled plasma interaction and the induced dipole.

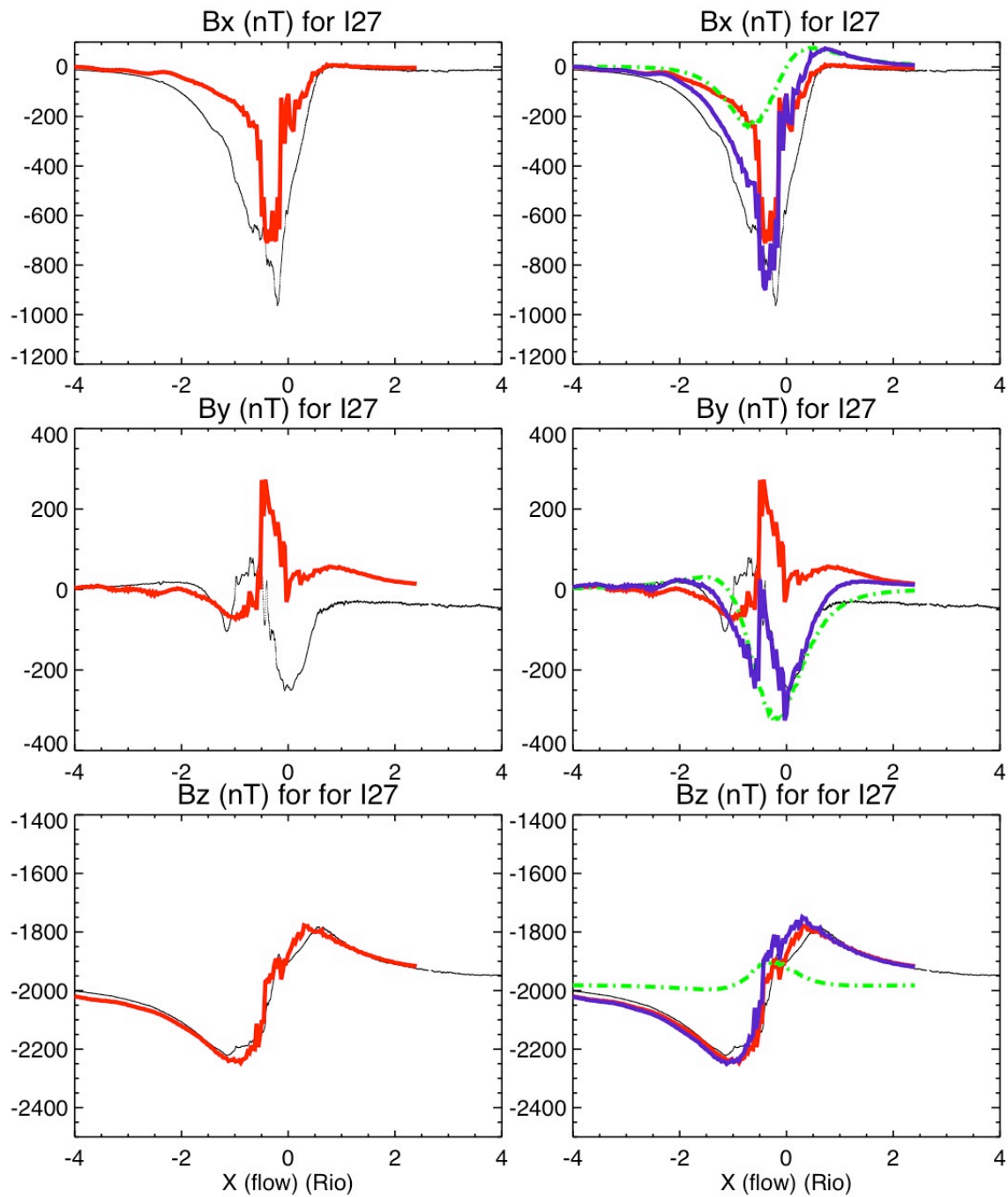


Figure 50: Components of the magnetic perturbation at Io during the I27 flyby. Black is the observations, red is the modeled plasma, green is the prescribed induced dipole and blue is the combination of the modeled plasma interaction and the induced dipole.

8.6.2 Induced dipole for I31

I31 is an important flyby because Galileo encountered Io at a S_{III} longitude very different from I24 and I27. The magnetic perturbation observed requires the addition of a ~ 300 nT dipole approximately in the Jovian direction ($Y < 0$), opposite to the direction of the induced dipole for I24 and I27. The fact that the dipole flips depending on the S_{III} longitude of Io is the crucial indication of the induced nature of this dipole compared to a permanent dipole in Io's interior. The induced dipole flips direction because, at the times of the GLL flybys, the 10° tilt of the Jovian magnetic field produces a time variation of the magnetic flux in Io in the opposite direction. Surprisingly, this important case was not shown in the *Khurana et al. [2011]* publication.

One of the contribution of this thesis is to show that the I31 flyby is an essential observation to support the existence of an induced dipole at Io.

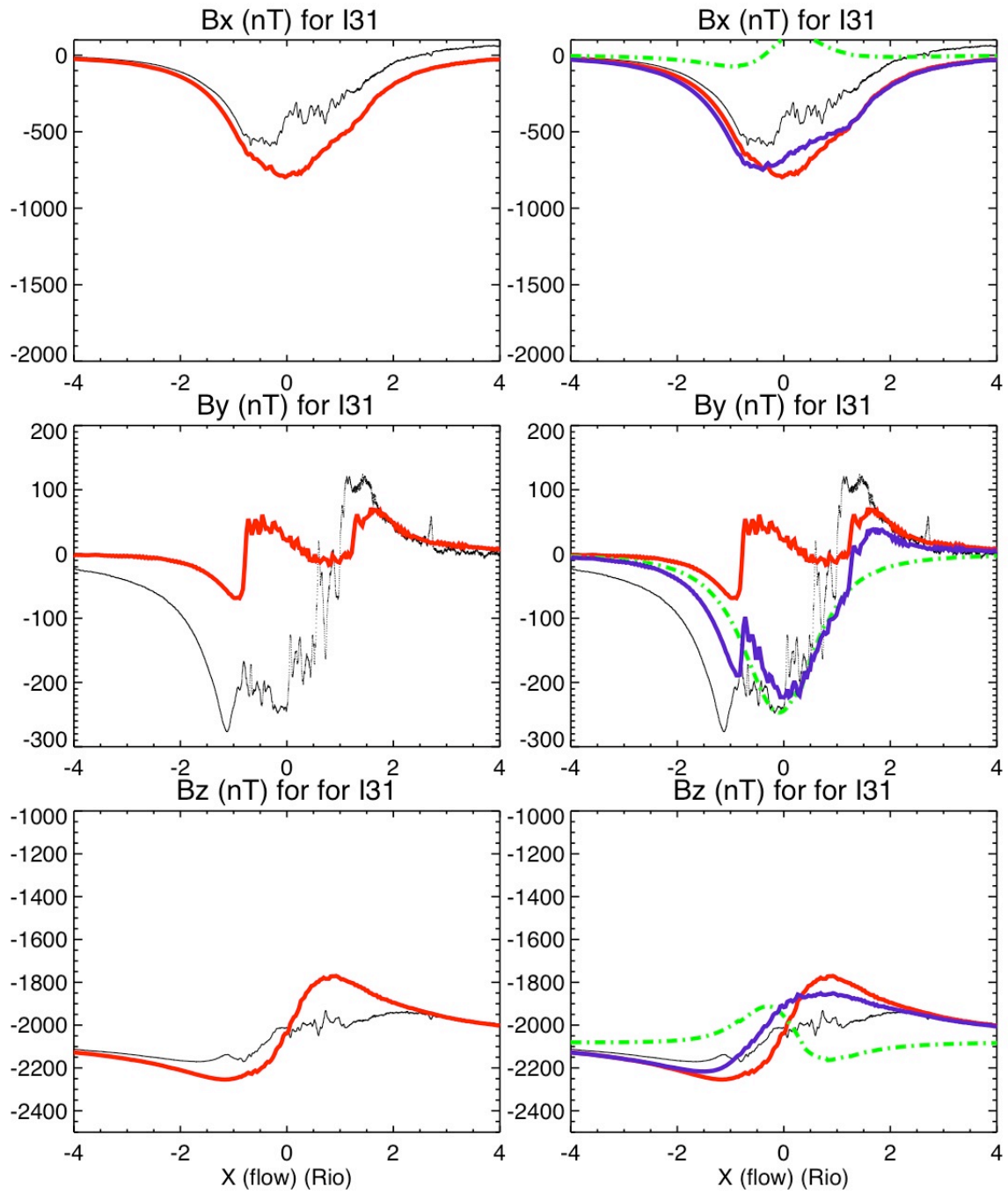


Figure 51: Components of the magnetic perturbation at Io during the I27 flyby. black is the observations, red is the modeled plasma, green is the prescribed induced dipole and blue is the combination of the modeled plasma interaction and the induced dipole.

8.7 Summary of the "KK-S&O" atmosphere

The atmosphere proposed by *Khurana et al. [2011]* was scaled by 0.5 and used in our coupled Hall-MHD/multi-species chemical model to simulate the plasma properties and flow and magnetic perturbations along the 5 GLL flybys of Io.

In general, the modeling results are close to the observations and this atmospheric profile is a good representation of the atmosphere of Io. This analysis indicates that the atmosphere is less developed on the night side (J0) but that the far atmosphere did not collapsed completely. The flyby upstream of Io indicates as well that the atmosphere is not extended upstream (scale height < 60 km).

The sudden jump of ion temperature after closest approach on the equatorial flyby I27 is currently not explained. The sudden jump after Io on I31 will be addressed in Section 10.3.

These simulations assumed that the atmosphere was composed exclusively of S and O with the density ratio $O/S=2$ while the main component of the atmosphere is thought to be SO_2 . We will discuss the consequences of such an atmosphere on the plasma composition in Section 10.4.

9. A MULTI-SPECIES ATMOSPHERE

In the previous chapter, the atmosphere was composed of S and O only with a profile based on the profile of the sodium corona observations. O, S and SO₂ might not follow the same profile as sodium, so in this chapter, we will constrain the corona profiles with actual observations. The S and O profiles will be based on the UV observations (here called “Corona-S&O”). The SO₂ corona will be based on the interpretation of the SO₂⁺ cyclotron waves observed in the wake of Io (“Corona-SO₂”). The extended SO₂ atmosphere (“Atm-SO₂”) will be prescribed as an exponential with a constant scale height (500 km) to match the ion temperature along the J0 flyby of Io. The different components of this multi-species atmosphere are shown in Figure 52 and a more detailed description of each component is given in the following paragraphs. As a comparison, we also show a profile of a dense and tightly bound SO₂ atmosphere similar to the modeling of a sublimation-sustained daylight atmosphere by *Walker et al. [2010]* (see Section 3.2.3) as well as the “KK-S&O” profile of the previous chapter .

We will change the atmosphere composition and structure in the multi-species chemical model while using the MHD flow calculated for the previous “KK-S&O” atmosphere. We acknowledge that changing the neutral profile in the chemical model while using a flow computed with a different neutral profile is a simplification but a fully self-consistent calculation would involve the development of multi-ion MHD model. Such improvement of the MHD model is postponed to future work. Although changing the atmospheric composition will affect the ion temperature and the plasma composition, Figure 52 shows that the radial neutral profile of the combined multi-species components presented in this section is not too different from the “KK-S&O” profile. Thus, using the “KK-S&O” flow is probably a reasonable simplification.

We will show, for each flyby and each atmospheric component, the electron density and ion temperature calculated with the multi-species chemical model.

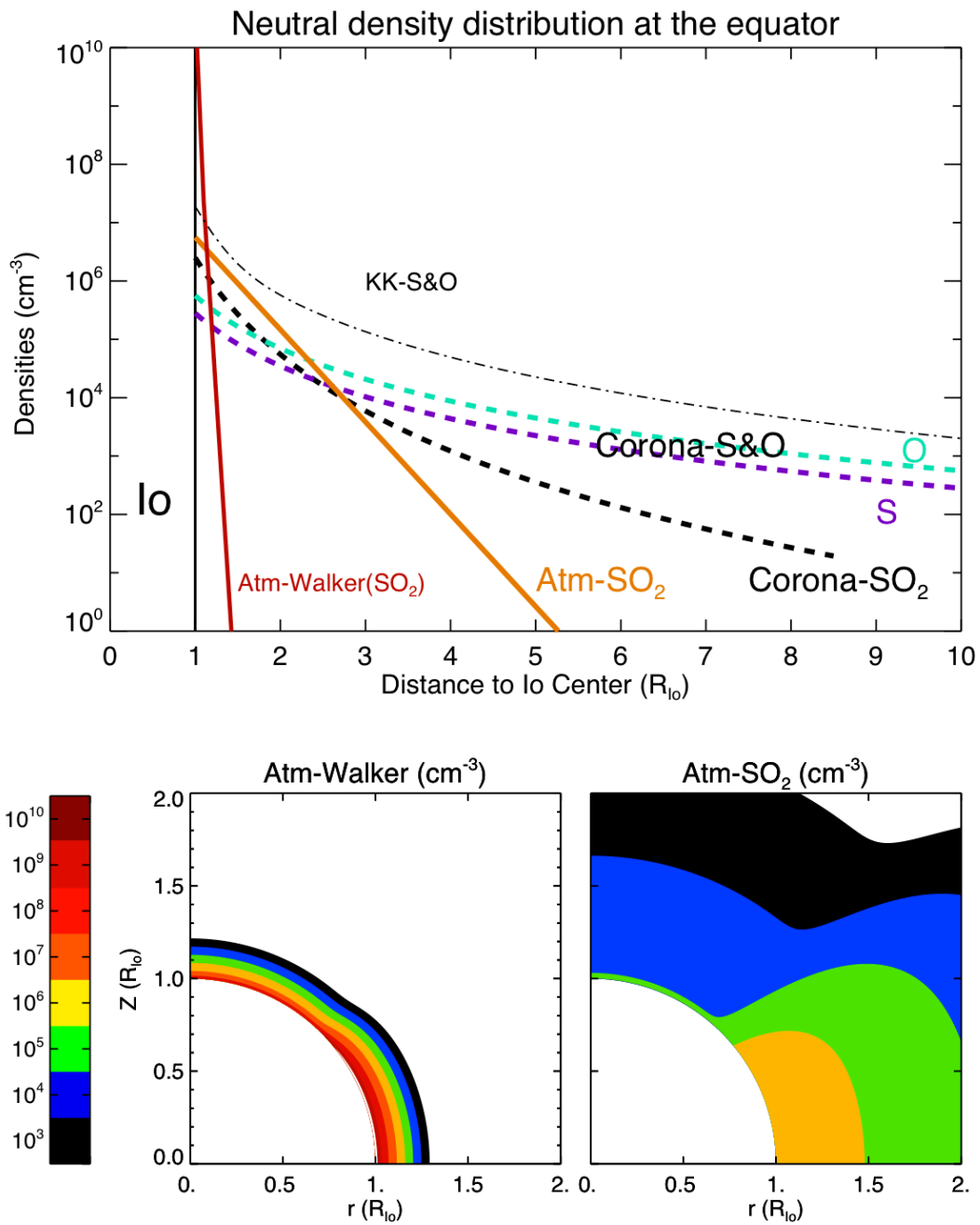


Figure 52: The different components of the multi-species atmosphere. Top: the radial profile. For comparison we added the profile of the atomic “KK-S&O” atmosphere of the previous chapter. Bottom left: A meridian section of the lower atmosphere based on the Walker et al. [2010] model. Bottom right: a meridian section of the “Atm-SO₂” component.

9.1 An atomic corona (Corona-S&O)

This profile represents an extended corona of atomic sulfur and oxygen, inspired by the UV observations of *Wolven et al. [2001]* (see Section 3.1). The UV brightness is a function of the neutral density, the electron density and the electron temperature and disentangling the three effects is difficult. The electron density and temperature certainly vary strongly close to I_0 , but we will make the simplification that the increase in brightness toward I_0 is only caused by the radial increase of the neutral density and that the electron density and temperature are constant and equal to their nominal Voyager's values $T_{ei} = 5$ eV and $n_{ei} = 2000$ cm⁻³. We prescribe a power law profile of O and S density with an index of -3 , in the range of *Wolven et al. [2001]*'s analysis when I_0 is at its largest dusk elongation (note that in *Dols et al. [2008]*, we used a power law index= -2.8 , the average of all observations for different phase angle of I_0). The UV brightness profile for O and S are similar, implying that even if the O/S ratio is unknown, it does not vary with the radial distance. Thus, we will assume a neutral S density profile similar to the O profile with an O/S ratio of 2. From the profiles described above, we calculate a density of O and S at $2 R_{I_0}$ of 1×10^5 cm⁻³ and 0.5×10^5 cm⁻³ respectively, consistent with a 50 Rayleigh (O1256Å) brightness at $2 R_{I_0}$. The resulting vertical column is $= 7.3 \cdot 10^{13}$ cm⁻² for atomic oxygen and is $= 3.7 \cdot 10^{13}$ cm⁻² for sulfur, consistent with the observational range of *Ballester [1989]*.

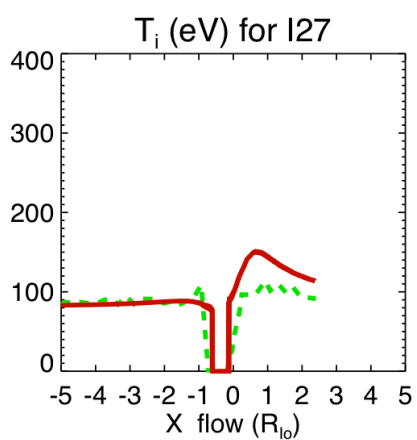
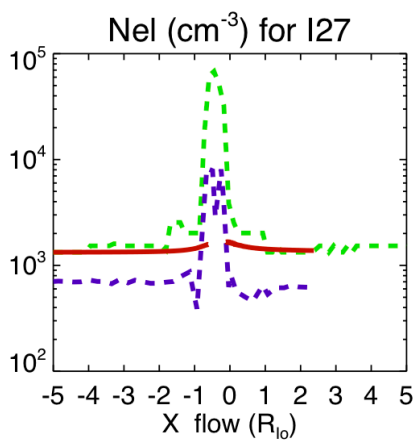
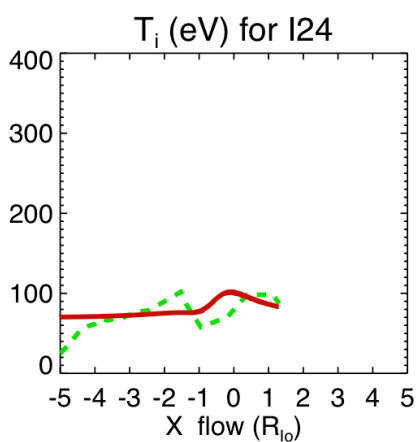
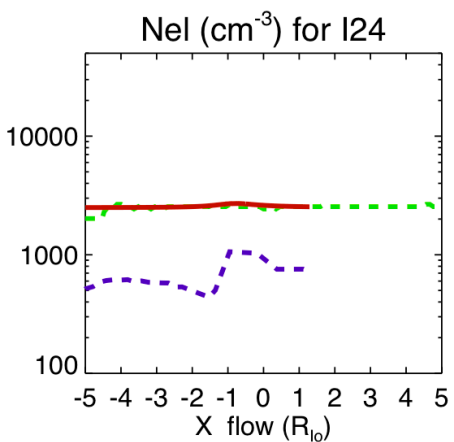
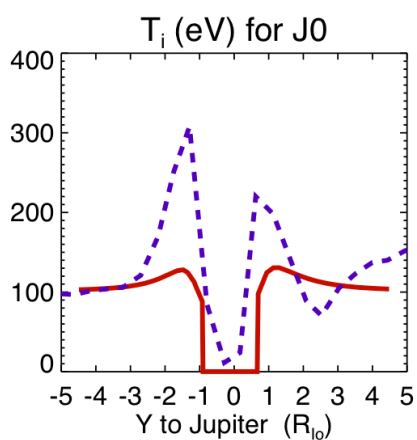
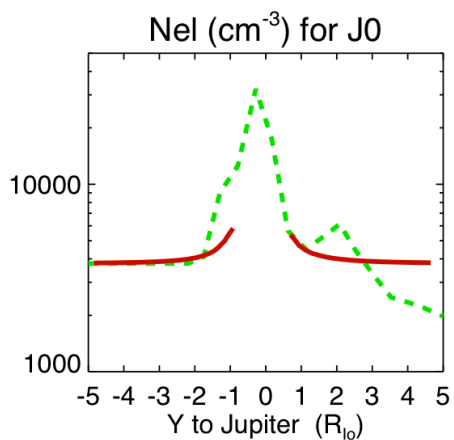
$$n_{S\&O}(r) = 5.6 \times 10^5 \times \left(\frac{R_{I_0}}{r} \right)^{-3} \text{ (cm}^{-3}\text{)}$$

with r = radial distance in km and $R_{I_0} = 1821$. km

The *Wolven* observations are made on both sides of I_0 , with the spectrometer aperture oriented northeast-southwest in jovian coordinates (see Figure 9). They show a brightness profile similar on both sides of I_0 . Thus we will assume that this corona is spherically symmetrical. This assumption is questionable as the corona radial profile depends on the process of formation of the corona. Sputtering by energetic ions, as is usually assumed for the formation of the sodium corona, is spherically symmetrical. Sputtering by thermal ions in the torus or SO₂ dissociation by electron impact would create a corona denser on the upstream side of I_0 .

Figure 53 (split over two pages) shows the plasma density and ion temperature results for each flyby using this “Corona-S&O” atmosphere:

- J0: Along the wake (J0), it is clear that some other atmospheric component close to Io is needed to explain the high plasma density and high temperature on the flanks of the wake
- I24: This corona has little effect on the plasma upstream of Io so its presence upstream of Io is neither confirmed nor refuted.
- I27: the relatively fast flow along the flanks of Io has a direct effect on the average ion temperature, even for such a thin corona. This temperature increase is not present in the observations and the I27 temperature observed by Galileo continues to be puzzling.
- I31 and I32: as the corona is spherically symmetric, S and O ionization provides a dense plasma because atomic species do not cool the electrons efficiently and the ionization persists. We made the assumption of a spherically symmetric corona while the corona might be thinner and contribute less to the plasma density above the poles than what we simulate here.
- Finally the increase of ion temperature on the outbound trajectory far from Io ($\sim 5 R_{Io}$) requires another atmospheric component or a stronger atomic corona.



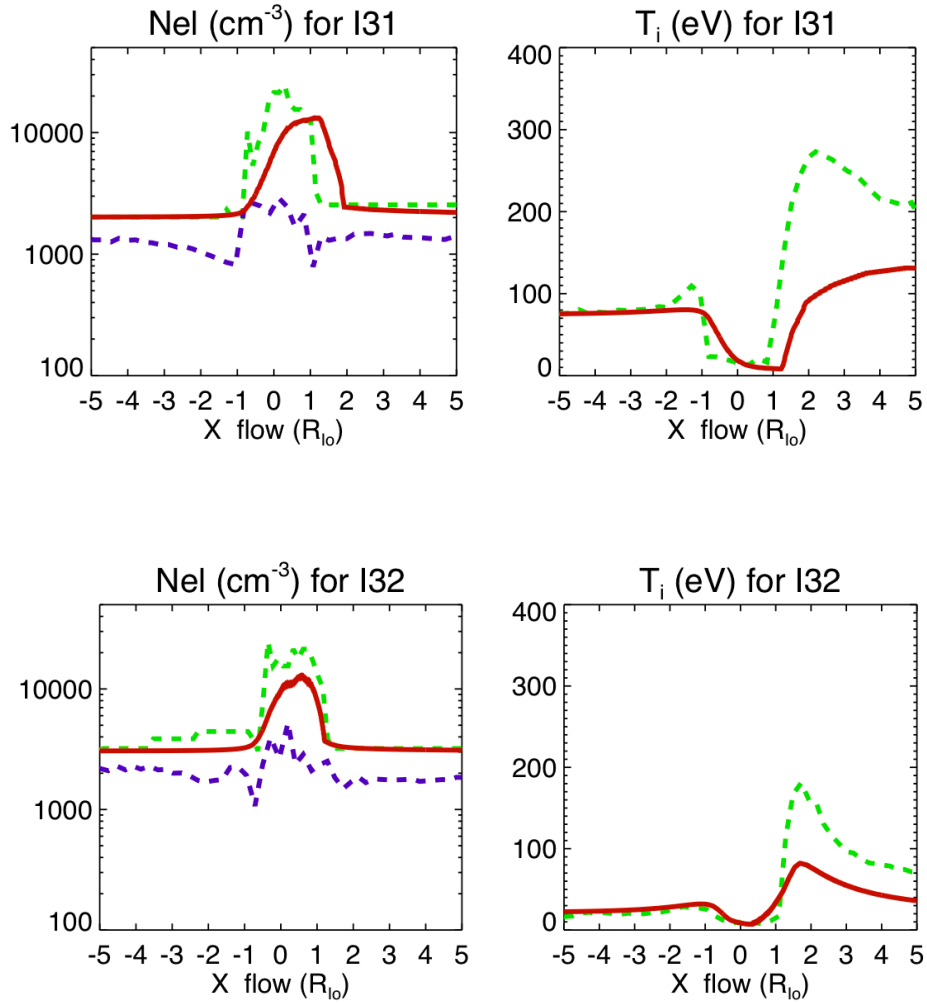


Figure 53: Electron density and average ion temperature calculated with the chemical model along each flyby. Note that the figure is split over two pages.

9.2 The SO₂ atmosphere (Atm-SO₂)

9.2.1 Radial distribution

The radial distribution of an SO₂ atmosphere close to Io (a few hundred km) is not constrained by observations. Different authors use different profiles, justified by the reasonable match of their results with the data. *Saur et al. [1999]* propose a radial hydrostatic atmosphere with a surface height scale of 100 km increasing to ~ 300 km at 2R_{Io}. The vertical column of this hypothetical atmosphere = 6 10¹⁶ cm⁻². This profile was used in *Dols et al. [2008]* attached to this thesis. In another version of their model, *Saur et al. [2002]* propose an exponential atmosphere with a smaller scale height, varying between 50 and 110 km for an equatorial vertical column ~ 2 10¹⁶ cm⁻².

We claimed in Section 3.2.3, based on the modeling of a sublimation driven atmosphere of *Walker et al. [2010]*, that most of the SO₂ column deduced from the UV observations (*Feaga et al., 2009; Jessup et al., 2004* see Section 3.2.1) can be accounted for by the integration of the SO₂ density under ~ 200 km. Thus we think that these observed columns do not constrain the extended SO₂ atmosphere (to ~ 2 R_{Io}) that we describe here.

Based on several tests of the chemical model, we propose a longitudinally symmetric exponential profile with a 500 km scale height:

$$n_{SO_2}(r) = 5 \times 10^6 \times e^{-\left(\frac{r}{500}\right)} \text{ (cm}^{-3}\text{)}$$

where r = radial distance in km, leading to a vertical column = 2.5 10¹⁴ cm⁻². We tested the Walker profile shown on Figure 52 (exponential profiles with scale heights of 10's km) and concluded that such atmospheres are too tight to contribute to the plasma density and ion temperature along the GLL flybys and thus ignore this component in the results shown below.

Sulfur monoxide (SO) is a by-product of SO₂ dissociation but it was also observed as direct ejection from a volcanic vent. As noted in Section 3.3, the interpretation of the observations is still ambiguous. In this work, we will make the

simplifying assumption that SO and SO₂ are collocated and thus assume an SO radial density profile similar to the SO₂ profile with a radial column of 10% of the SO₂ column.

9.2.2 Latitudinal distribution

The latitudinal variation of this atmosphere is based on Lyman-alpha observations (*Strobel and Wolven, 2001*):

$$n_{SO_2}(\theta) = \left(0.02 + e^{-\left(\frac{\theta}{36}\right)^6} \right)$$

with θ = latitude in degrees

The drop of density with latitude is steeper and the polar density lower than the “KK-S&O” atmosphere, as illustrated in Figure 54.

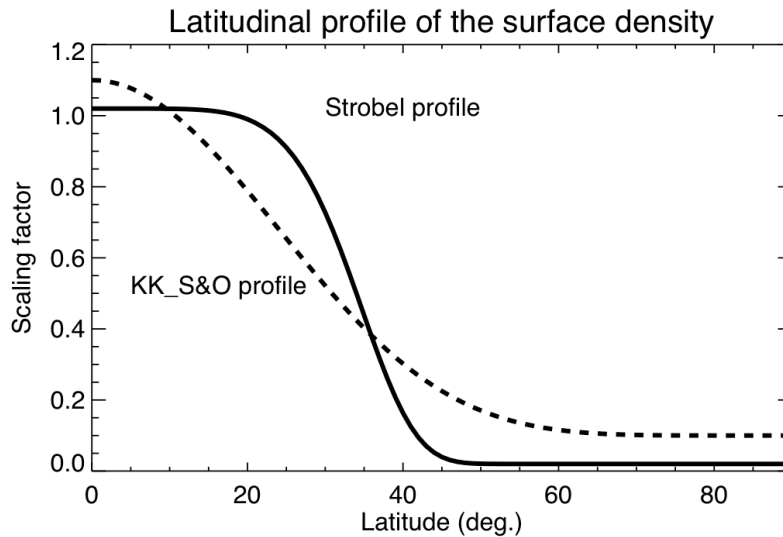


Figure 54: Latitudinal variation of surface density of the KK-S&O and Atm-SO₂ atmospheres.

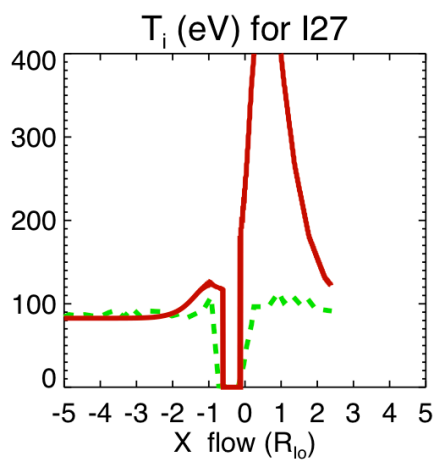
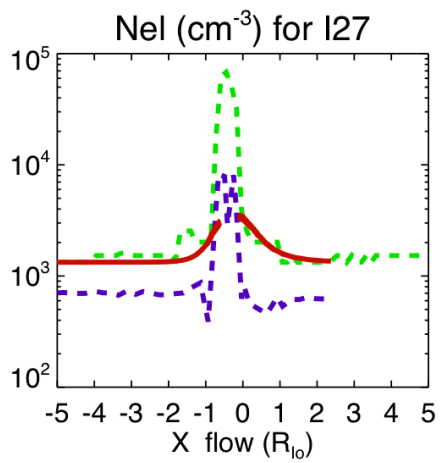
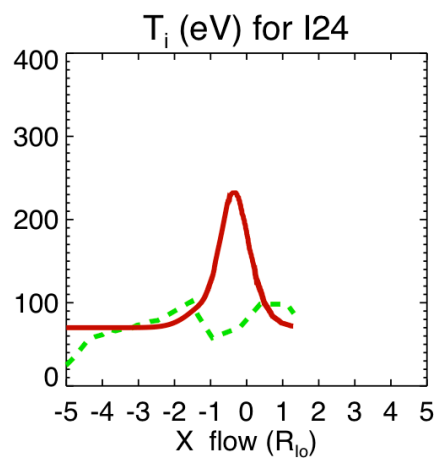
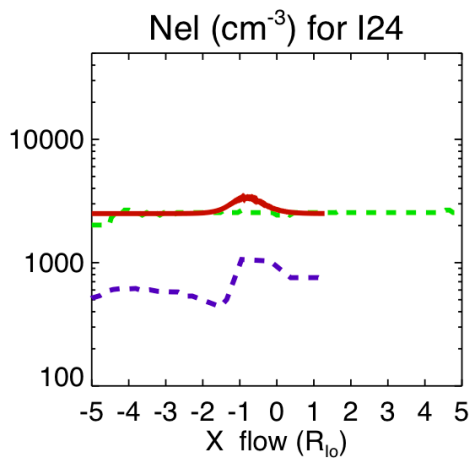
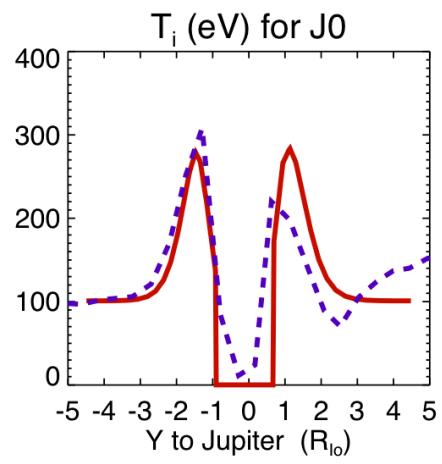
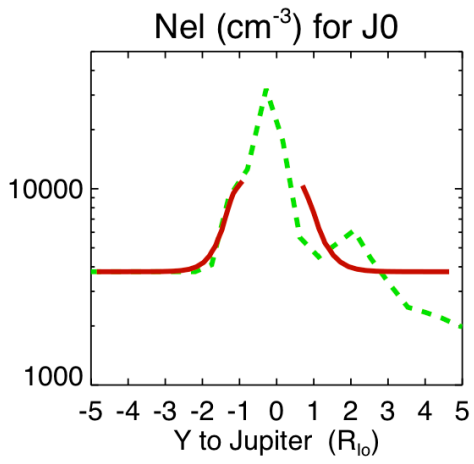
Figure 55, split over two pages, shows the plasma density and ion temperature calculated with this SO₂ atmosphere. It has a visible effect on the plasma density and temperature roughly up to 2 R_{Io} from the center of Io.

- J0:

The modeled plasma density and temperature on the anti-jovian leg of J0 is consistent with the data while it is too extended on the jovian side. This could be a consequence of the collapse of the SO₂ atmosphere during the night.

- I24:

Like the “KK-S&O” scenario, this atmosphere extends too far upstream of Io. The inbound trajectory encounters Io on its night side and the SO₂ atmosphere might have partially collapsed. But the closest approach is in daylight, at some distance from the terminator. If we follow the suggestion of *Feaga et al. [2009]* that the SO₂ daylight atmosphere is fully developed from limb to limb, such an extended atmosphere should have some effect on the plasma properties at closest approach, which is not observed. The compression hypothesis of *Saur et al. [2002]* may be an alternative explanation.



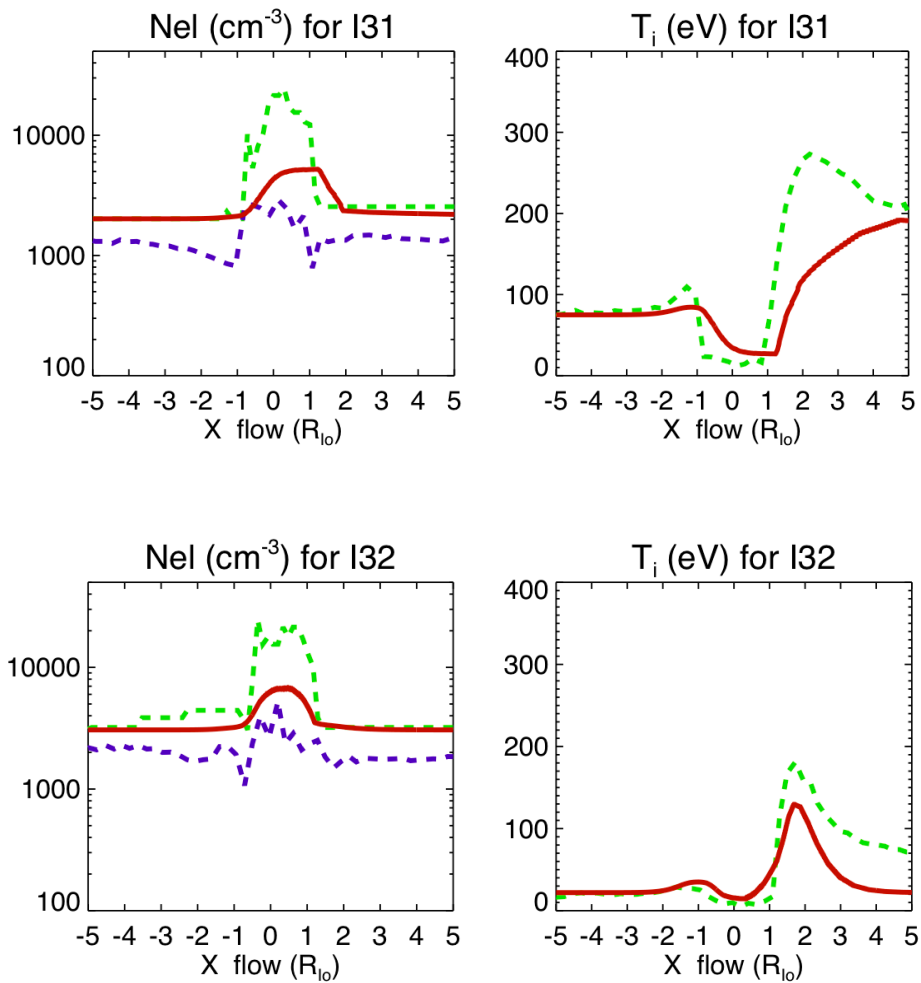


Figure 55: Electron density and average ion temperature calculated with the chemical model along each flyby for the “Atm-SO₂” atmospheric component. Note that this figure is split over two pages.

- I27:

The flat average ion temperature observed on the anti-jovian flank suggests that the atmosphere does not extend in this quadrant, which is puzzling.

- I31:

The “Atm-SO₂” scenario has very little neutral density at the pole (2% of the equatorial density), less than the “KK-S&O” atmosphere (10%). Nevertheless, the plasma density calculated at the pole is still significant. We recall that the ionization by field-aligned bi-directional electron beams detected above the poles by Galileo is not included in this model. As the polar atmosphere is very thin, these electrons might traverse the polar atmosphere without losing much of their energy. Their contribution to the plasma density and ion temperature should be evaluated in the future with a proper electron energy deposition model (*Bhardwaj and Michael, 1999*).

The ion temperature downstream of I_o increases slowly to reach the observed temperature of ~ 200K at X= 4 R_{Io}. It is slightly better than the “KK-S&O” atmosphere where the downstream temperature was reaching a plateau at 150 eV. Nevertheless, the sudden jump of ion temperature directly behind I_o that was not explained in the “KK-S&O” atmosphere is not better simulated by the pickup of heavier SO₂⁺ ions. We will propose an explanation for this discrepancy in section 10.3, based on the simplifications of our model.

In our simulations, the increased plasma density extends ~1 R_{Io} behind I_o on the outbound trajectory. In the observations, the increased plasma density is limited to the crossing of the Alfvén tube. This might be the result of our treatment of I_o as a soft obstacle: our modeled flow traverses the Alfvén wing and carries the plasma with it behind I_o while a solid obstacle would divert the flow more strongly around the Alfvén tube.

- I32:

This atmosphere is radially too limited to explain the large downstream temperature along I32 far from I_o. Another atmospheric component, such as an extended corona, is needed (see the coronae hypothesis below).

9.3 An SO₂ corona (Corona-SO₂)

Ion cyclotron wave emissions were detected by the magnetometer along the J0 flyby in the wake of Io, at distances > 900 km (Huddleston *et al.*, 1997). A lower limit on SO₂⁺ densities along this flyby was deduced from the modeling of the cyclotron emission. The absolute density is uncertain as it is model dependent. In Figure 56, on the left panel, we compare the SO₂⁺ density inferred from the ion cyclotron wave detection with the density modeled with the previous atmosphere “Atm-SO₂”. In the center of the wake, the ion cyclotron waves were masked by mirror mode instabilities and an SO₂⁺ density could not be inferred.

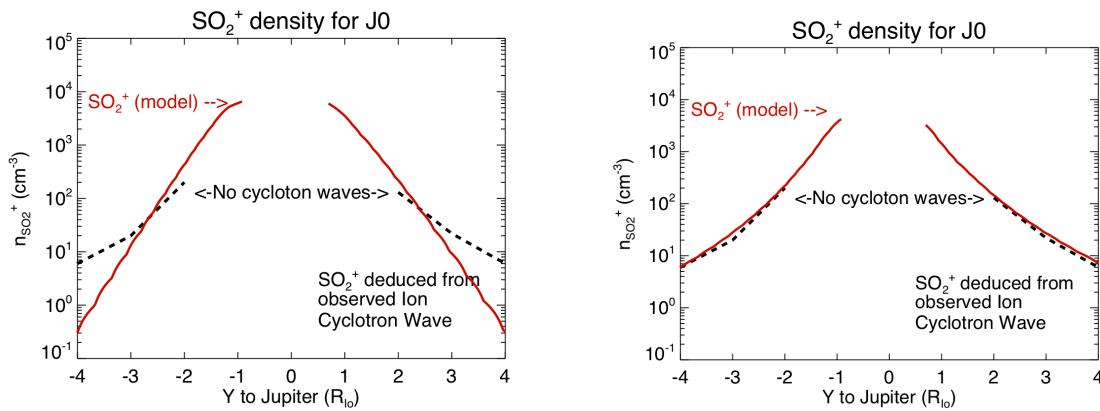


Figure 56: Comparison of the SO₂⁺ density along J0 inferred from ion cyclotron wave observation (dashed black) with the density calculated for different atmosphere scenarios (red line): Left: “Atm-SO₂” without SO₂ corona. Right: “Corona-SO₂”.

On the flanks, this atmosphere is not extended enough to match the shallow profile far from Io (~ 4R₁₀) deduced from the magnetometer observations. This observation supports the presence of a tenuous SO₂ corona extending at least 10 R₁₀ downstream of Io.

Based the poor match of “Atm-SO₂” far from I_o along J0, we propose a power law radial variation of this corona as

$$n_{SO_2}(r) = 2.5 \times \left(\frac{R_{I_o}}{r} \right)^{-5.5} \quad (\text{cm}^{-3})$$

with r = the radial distance in km and R_{I_o} = 1821. km

We assume that this SO₂ corona is spherically symmetric although its latitudinal and longitudinal distribution is probably determined by the processes responsible for its formation: a sputtering process would yield a spherically symmetric corona while a slow charge exchange process would probably confine this corona to equatorial latitudes, similar to the fast jets of sodium (*Wilson and Schneider, 1999*). On the right panel of Figure 56, we justify the choice of a power law profile by showing the good match between the SO₂⁺ density along J0 computed with this extended “Corona-SO₂ “ and the density inferred from the ion cyclotron waves.

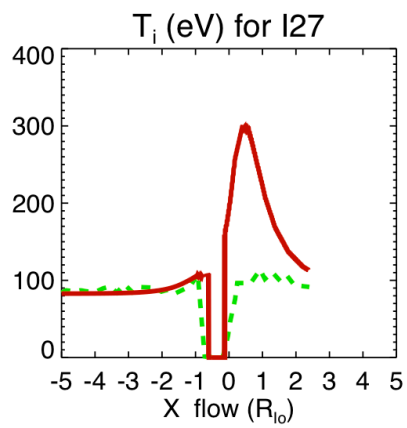
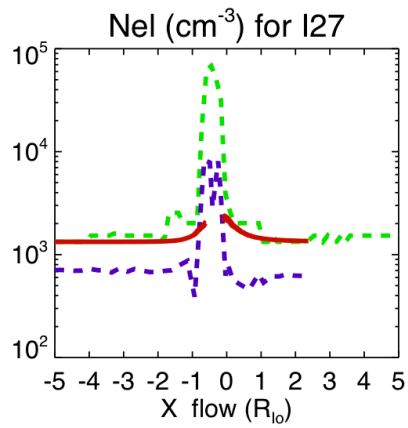
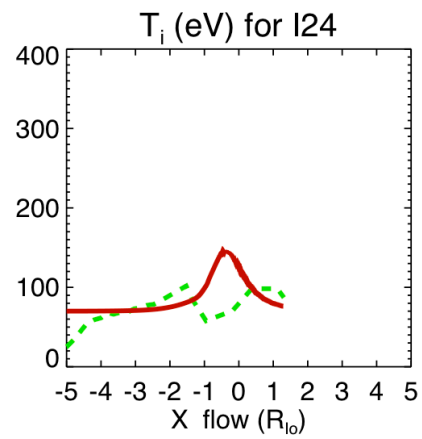
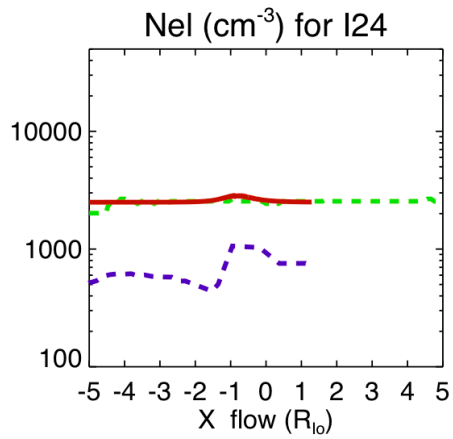
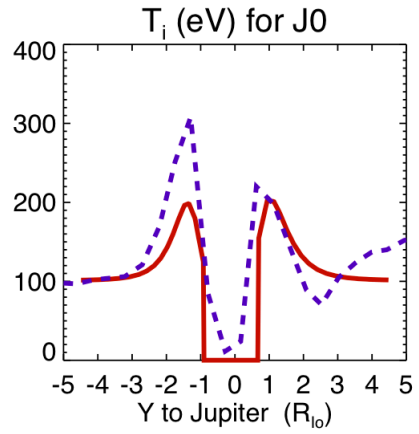
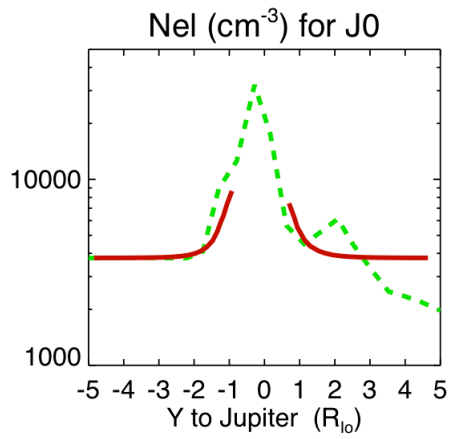
In Figure 57, split over two pages, we compare the plasma density and ion temperature calculated with the “Corona-SO₂” profile with the Galileo PLS and PWS observations along each flyby:

- J0:

This corona is not dense enough to explain the temperature peaks on the anti-jovian flanks of the wake. “Atm-SO₂” will be the major contributor to the plasma density along this flank.

- I24 and I27:

This corona increases the ion temperature upstream of I_o and along the flanks, which the data do not support. This is an indication that the SO₂ corona extends mainly downstream and not upstream. This is consistent with the ion cyclotron wave observations along I24 and I27 where waves at the SO₂⁺ gyro-frequency are observed only after closest approach (*Russell and Kivelson, 2001*).



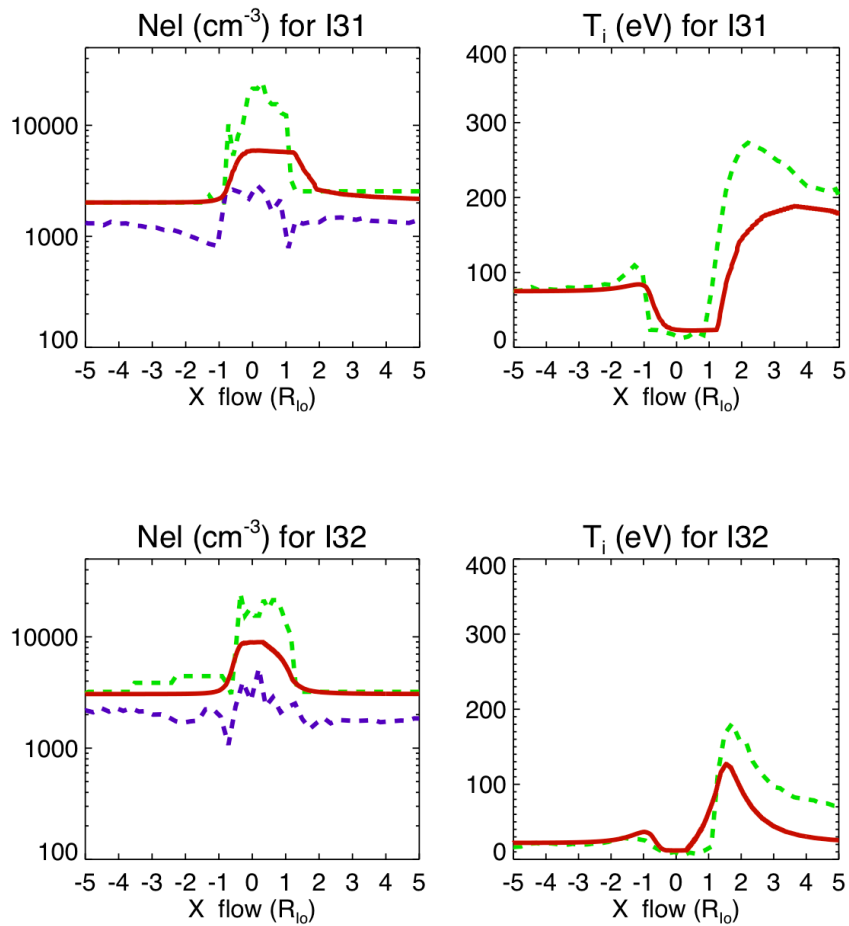


Figure 57: Electron density and average ion temperature calculated with the chemical model along each flyby for the “Corona-SO₂” atmospheric component. Note that this figure is split over two pages.

- I31:

The steep increase of temperature behind I_o on I31 is better matched by the corona than by the “Atm-SO₂”. “Corona-SO₂” is denser at polar latitudes because it is spherically symmetrical while “Atm-SO₂” is prescribed with a step decrease of SO₂ density beyond 35° of latitude.

- I32:

The contribution of this corona to the ion temperature far from Io is similar to “Atm-SO₂”. It is not dense enough, or extended enough, to explain the high temperature far from Io ($\sim 6R_{Io}$) on I32. Figure 58 shows an example of an alternative formulation of the “Corona-SO₂”. We combined “Atm-SO₂” with “Corona-S&O” and another formulation of the SO₂ corona, shallower than the power law proposed above. The SO₂ corona is prescribed as an exponential with a 4000 km scale height and a surface density $=3 \cdot 10^4 \text{ cm}^{-3}$. The ion temperature on I32 matches the observations while the profile along J0 seems too extended to match the ion cyclotron wave inference at the time of J0. This corona may be time variable or its distribution may depend on the longitude, but the main conclusion is that an extended SO₂ corona has to be present downstream of Io in order to explain the I32 ion temperature.

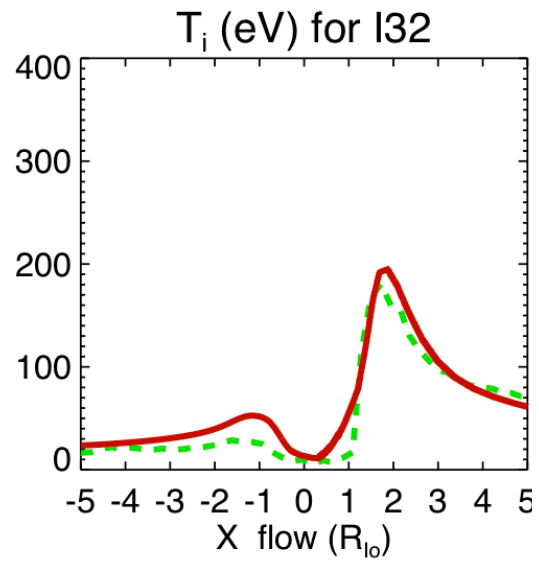
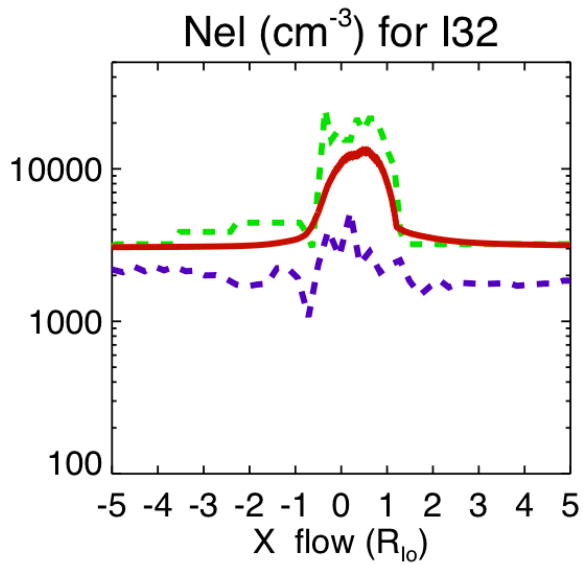
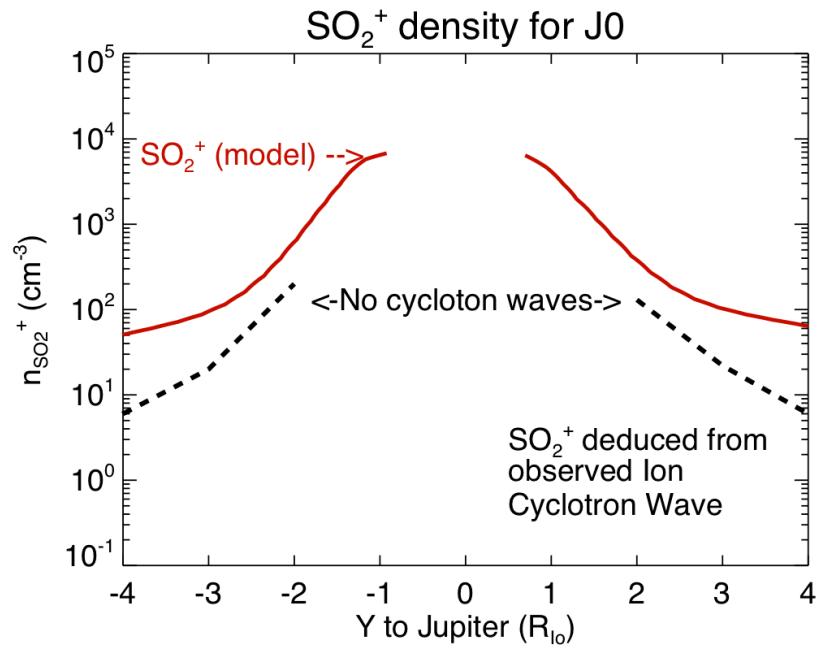


Figure 58: The exponential SO₂-corona. Top: the SO₂⁺ density along J0 compared to the density inferred from ion cyclotron wave detection. Bottom: the plasma properties along I32

10. DISCUSSION

In our proposed multi-species atmosphere, each component (the SO₂ atmosphere, the S and O corona, the SO₂ corona) plays a specific role for a specific Galileo flyby. Most of the flybys can be explained by a variable combination of all components. The temperature and density profiles of such a combination cannot be easily predicted, as it is not a simple superposition of the plasma density and temperature of each individual component. For instance, an increased SO₂ density resulting from such combination will decrease the electron temperature and reduce the ionization and pickup. We think that there is little merit at trying to define a single atmosphere that matches all flyby observations. The presentation of the effect of each atmospheric component as sensitivity experiments is sufficient to achieve the goal of demonstrating the longitudinal asymmetry of the atmosphere.

Constraining the atmosphere of Io based on the 5 Galileo flybys that cover 1995-2001 is difficult for several reasons: it is difficult to discriminate between day/night variations and longitudinal variations because there is no upstream passage on a dayside atmosphere, there is no direct sampling of the jovian downstream side of the atmosphere close to Io and there is no downstream side passage on the night-side. Furthermore we cannot definitely exclude temporal variations of the atmosphere during the Galileo mission. Finally, lack of consistency between PLS and PWS data limit their constraint on models.

First, we present global results of the coupled model for the J0 flyby. Afterwards, we discuss the problematic I27 and I31 flybys and, finally, the structure, nature and variability of Io's atmosphere.

10.1 The J0 flyby. Global results.

In this section, we present in Table 3 global (volume integrated) results for the "KK-S&O" scenario and for the simplest multi-species scenario proposed "Atm-SO₂" + "Corona-S&O". The "Corona-SO₂" component has been omitted for simplicity as we showed that it extends probably only downstream and does not have a major effect on the integrated results. The contribution of electron beams is not included but the

quantitative results based on a simplified scenario can be compared to other published results.

J0 flyby	“SO ₂ -Atm” + “Corona-S&O”	“KK-S&O”
Horizontal current through Io	11 mega-amps	11 mega-amps
Production rate of SO ₂ ⁺	1.2 10 ²⁷ s ⁻¹ = 130 kg/s	0. kg/s
Production rate of S ⁺	7.810 ²⁶ s ⁻¹ = 40 kg/s	7.8 10 ²⁷ s ⁻¹ = 425 kg/s
Production rate of O ⁺	2.010 ²⁶ s ⁻¹ = 5 kg/s	1.8 10 ²⁷ s ⁻¹ = 48 kg/s
Total ion production rate	2.1 10 ²⁷ s ⁻¹ = 175 kg/s	9.5 10 ²⁷ s ⁻¹ = 473 kg/s
SO ₂ dissociation rate	1.4 10 ²⁸ s ⁻¹ = 1500 kg/s	0. kg/s

Table 3: Global results with plasma conditions typical of the J0 flyby.

The current through Io is strong, twice as strong as the current inferred from the Voyager observations. It is consistent with the plasma density of the torus on J0 (~ 4000 cm⁻³) being denser than during Voyager encounter (2000 cm⁻³). This current is consistent with *Saur et al. [1999]* estimation (10 mega-amps).

We present in Table 3 the ion production rate for each neutral species. *Bagenal [1997]* deduced a plasma production rate = (1.75 - 5.3) 10²⁷ s⁻¹, based on the observation along J0 and some assumptions of the geometry of the interaction. Our estimation for the “KK-S&O” atmosphere is twice as large. We note that we did not include the bi-directional field-aligned electron beams that are responsible for ionization in the

downstream hemisphere of Io and for the high plasma density in the wake the wake (*Dols et al., 2008* attached to this thesis). Including this extra-ionization process would increase further the plasma production calculated for the “KK-S&O” scenario and would make it even less plausible. Our estimate for the “SO₂-Atm + Corona-S&O” falls in the range of Bagenal’s analysis and is consistent with *Saur et al. [2003]* estimation ($3 \cdot 10^{27} \text{ s}^{-1}$). The total mass-loss rate ($\sim 200 \text{ kg/s}$) is small compared to the canonical 1 ton/s required to power the torus. Consequently, most of the mass loss rate needed has to be tapped in the giant neutral clouds, not in the close vicinity of Io.

The SO₂ loss rate through dissociation is $\sim 1500 \text{ kg/s}$. If SO₂ is completely dissociated, that corresponds to 1.5 tons/sec of oxygen and sulfur neutral atoms ejected from Io. The electron impact dissociation of SO₂ results in fragments that are usually slow with an average kinetic energy $\sim 1 \text{ eV}$ (*Vatti Palle and Ajello, 2004*). These fragments can fall back on Io if their velocity is smaller than Io’s escape velocity ($\sim 2 \text{ km/s}$) or they can leave the vicinity of Io to form the S and O corona and giant clouds. It is generally accepted that the giant clouds are supplied by ion sputtering of the atmosphere of Io. We are currently in the process of modeling the trajectory of the neutrals produced by electron-impact dissociation of SO₂ to see if they can be a significant atom source for the corona and giant neutral clouds.

10.2 The O1356 Å emission

The first observations of Io’s UV auroral emissions were obtained with the STIS camera onboard the Hubble Space Telescope (*Roesler et al., 1999*). They show bright UV emissions localized on Io’s equatorial flanks as well as dimmer limb UV glow. *Retherford [2002]* proposed a morphological analysis of the oxygen emission in the OI (1356 Å) multiplet. They claimed that the auroral spots are close to the surface (50-100 km) and slightly downstream ($\sim 30^\circ$) of Io’s sub-jovian meridian (Figure 59).

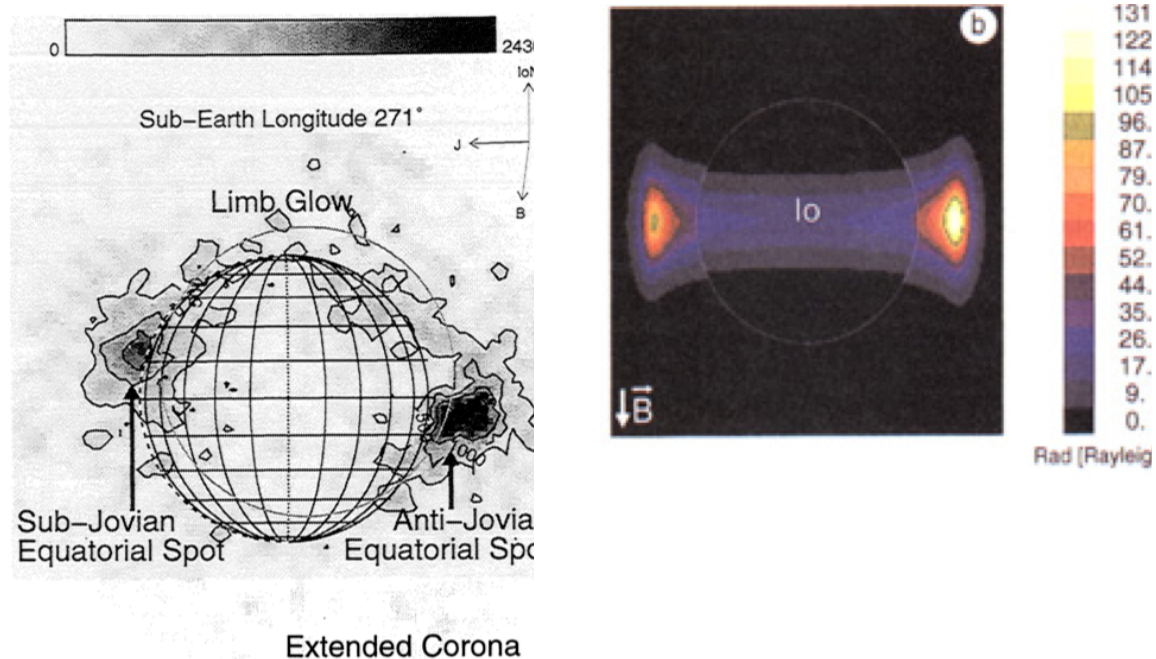


Figure 59: Left: OI (1356 Å) auroral emissions observed by the STIS camera onboard the Hubble space telescope (Retherford [2002]). Right: simulation of these auroral emissions by Saur et al. [2000].

Saur et al. [2000] simulate these OI (1356 Å) emissions with their “two-fluid” model (Figure 59) and concluded that the thermal plasma interaction with an oxygen atmosphere (in an O/SO₂ density ratio ~ 20%) could explain these bright emissions on the flanks of Io as well as their brightness asymmetry (the anti-jovian spot seems to be brighter than the sub-jovian one).

The OI (1356 Å) emission is produced by a transition from the excited metastable 3s⁵S⁰ level of the oxygen atom, ~ 9 eV above the ground level. The excitation cross section is not precisely determined by laboratory measurements.

We compute the OI (1356 Å) volumic emission rate (photon cm⁻³ s⁻¹) around Io for the “Atm-SO₂ + Corona-S&O” scenario, using an electron impact excitation cross section that is a combination of several published laboratory measurements (*Strobel, personal communication, 2007*). Like any electron impact process that depends on the electron temperature, the emission rate is localized on the upstream hemisphere of Io (Figure 60).

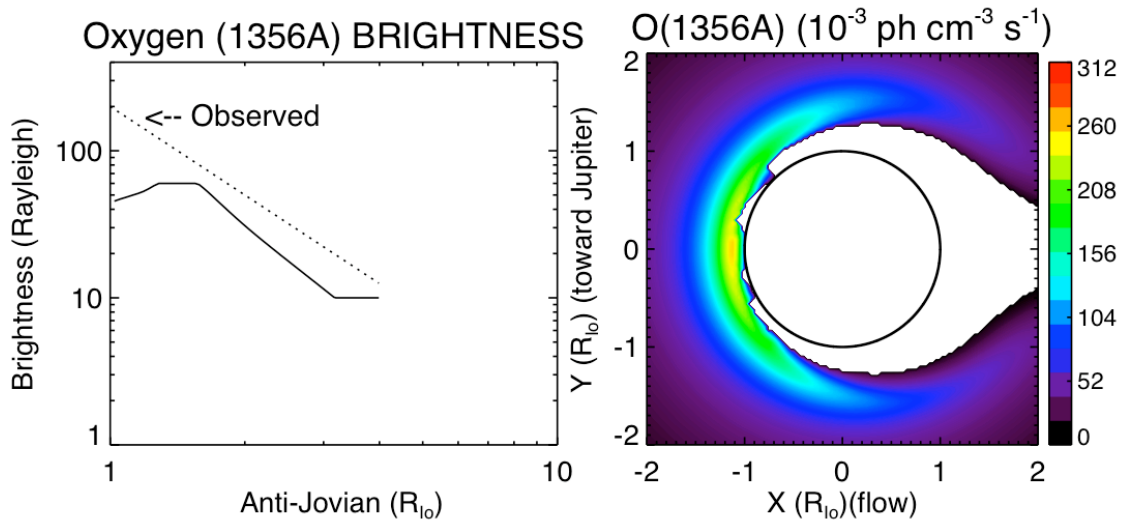


Figure 60. Right: the OI (1356 Å) volumic emission rate calculated with the chemical model. This emission is localized upstream of Io. Left: The brightness, integrated along the line of sight along the X axis, in Rayleighs. The emission follows the observed profile of Wolven et al. [2001] (dotted line, valid from 4 to 1.4 R_{Io}) and peaks at $\sim 0.3 R_{Io}$ from Io's surface.

We integrate the emission rate along a line of sight (the X axis) to simulate an actual observation at largest Western elongation. The radial brightness profile that we compute is shown in the left panel of Figure 60, with the observed power law profile from Wolven et al., 1991. We recall that the power law profile proposed by Wolven et al. is valid from 4 to 1.4 R_{Io} (see Section 3.1). As we used the observed profile to calibrate the corona density, it is no surprise that the profiles are approximately similar. Our profile is slightly lower than the observed one, probably because our cross section is different from the excitation rate coefficient at 5 eV assumed by Wolven et al. [2001]. The brightness profile peaks on the flanks of Io at a distance $\sim 0.3 R_{Io} \sim 600$ km from the surface, at much higher altitude than the observed auroral emissions. This peak is similar to the brightness peak modeled by Saur et al. [2000] and shown on the right panel of Figure 59. But this increased brightness results from the integration along the line of sight of an upstream emission, and not from localized emissions on the flank of Io, as observed.

We conclude that the thermal electrons of the torus are not responsible for the auroral emissions localized on the flanks of Io. The ~ 300 eV field-aligned electron beams could be an alternative explanation: they are observed close to Io's flanks,

downstream of Io and they would lose most of their energy in the denser part of Io's atmosphere, along the equator. These features of the beams are also typical of the features of the observed auroral spots. The emission could result from direct excitation of the oxygen component of Io's atmosphere or from dissociative excitation of SO₂. *Michael and Bhardwaj [2000]* proposed a Monte Carlo model of the energy degradation of electron beams in the SO₂ atmosphere of Io. They conclude that the 300 eV electron beams can explain the O and S emissions but the calculated ratio O(1304 Å)/O(1356 Å) is not consistent with the observations. We think that their work has not had the public impact it deserves and that it would be interesting to re-visit their calculation with improved cross sections to address not only the auroral emissions, but also the high plasma density in Io's wake and in its dense ionosphere.

10.3 I27 and I31: problematic flybys

I27 and I31 observations are not convincingly explained by our numerical experiments. For each atmospheric component, our coupled model shows a steep increase of the ion temperature after the closest approach of I27, which is not supported by the observations. Similarly, the steep increase of ion temperature on I31 directly after Io is not matched by our model results. There are several possible causes for these discrepancies.

The first possibility is to question the analysis of the PLS measurements. We have shown in Section 4.3 that the plasma density inferred from PLS and PWS are not consistent, even far from Io. We will question the plasma composition inferred from PLS measurements as well (Section 10.4).

A second possibility is the time variability of the atmosphere. We address it in Section 10.7 below. But the I27 observations would imply an almost complete disappearance of the atmosphere, which is unlikely: *Feaga et al. [2009]* claimed that the SO₂ atmosphere is quite stable as it is probably sustained by frost sublimation.

A third tentative explanation is related to the simplified geometry that we use in our model, especially for I31. In our simulations, the magnetic field is in the z direction and the I31 outbound flyby is directly in the center of the slow wake of Io, inside the slow mode wing, so pickup at the local slow velocity would not increase the average ion

temperature. *Kivelson et al. [2001]* state: “The flow of the plasma around Io is structured by the directions of the background magnetic field and the upstream co-rotation flow “. The Jovian dipole has a 10° tilt relative to the Z axis and this corresponds to $\sim 20^\circ$ inclination at the orbit of Io for the I31 flyby. A strongly tilted magnetic field would tilt the Alfvén tube in the direction of the background field lines. When the Alfvén tube is tilted toward Jupiter, the outbound leg is not in the center of the wake anymore but somewhat on the flanks of the wake, where the flow is faster and the pickup could then rapidly increase the temperature. This explanation needs to be tested both for I31 and I27. We postpone to future work the modeling of the interaction with a background magnetic field inclined relative to the Z axis but by rotating the trajectory around the X axis in the opposite direction of the background field, we can have a qualitative assessment of the effect of the background dipole tilt. Figure 61 shows the temperature along I31 for different rotations of the trajectory around the X axis. For a rotation $\sim 20^\circ$, the modeled ion temperature increases abruptly after crossing Io’s diameter, which is consistent with the observations.

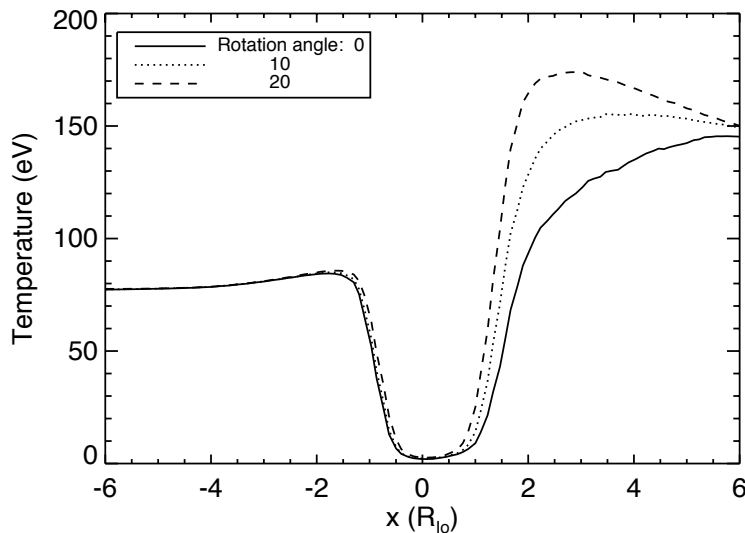


Figure 61: The ion temperature along I31 for different rotations of the trajectory around the X axis.

We think that the discrepancy between I27 and the model results would probably not be explained by a rotation of the Alfvén tube. Nevertheless, an improved version of

Hall-MHD code where the background magnetic field is not perpendicular to Io's equatorial plane is required to confirm this first qualitative investigation.

10.4 Atmospheric composition

In this section, we compare the plasma composition along J0 computed by the chemical model for the atomic atmosphere "KK-S&O" and the multi-species atmosphere combination "atm-SO₂" + "Corona-S&O" and show that both compositions are inconsistent with the composition inferred from PLS measurements by *Frank et al. [1996]*.

The "KK-S&O" atmosphere is composed of atomic species only, while SO₂ is the main component of the atmosphere. This scenario implicitly assumes that SO₂ is concentrated at very low altitude (100 km) so the interaction might not be sensitive to this low, dense atmosphere. On the other hand, as S and O are presumably produced by electron-impact dissociation of SO₂, some SO₂ density at high altitude has to be present to allow for the production of such a dense S and O atmosphere.

Our second scenario starts with an atomic corona constrained by UV observations. As this corona is not dense enough to explain the plasma density and temperature observed along the Galileo flybys, we add an SO₂ atmosphere closer to Io.

Both scenarios provide plasma density and an average ion temperature along the GLL flybys that are reasonably consistent with the observations so the composition of the extended atmosphere is not determined by these measurements. But each atmosphere leads to drastically different plasma composition.

The plasma composition at closest approach of J0 was published by *Frank et al., 1996* based on their PLS data analysis. The published mixing ratios are presented in Table 4. Note that S⁺⁺ and O⁺ have the same mass to charge ratio (16), so the species cannot be differentiated in the observations. We add in the table the torus plasma composition that we use as an initial condition in our modeling, which is consistent with the plasma composition of the canonical torus based on Voyager observations (*Bagenal, 1994*). The published composition at closest approach, compared to the torus composition, suggests a ~3 -fold increase of the minor torus ion S⁺ and a concomitant decrease of the major torus ions S⁺⁺ or O⁺.

The chemical model allows us to determine the plasma composition along J0, consistent with the atmosphere scenario “KK-S&O” and “Atm-SO₂ + Corona-S&O”. Because of the empty wake of our model results, we cannot compute the plasma composition at closest approach, but we can extrapolate the composition from the flanks of the wake to its center. Figure 62 shows the mixing ratio of the plasma along the J0 flyby, calculated with the “KK-S&O” atmosphere. Because S is easily ionized (the ionization rate coefficient at 5 eV of sulfur is ~ 10 times larger than for oxygen (see Figure 32, Section 6.3.1), the plasma on its way around Io is strongly enriched in S⁺ (8-fold) and the density of higher ionization states of S and O decreases sharply. This composition is strikingly different from the published one.

We run an experiment where we keep the radial profile of the “KK-S&O” atmosphere but change the relative contribution of O and S, to match approximately the published composition (Figure 62 and Table 4). This experiment requires an atmosphere strongly enriched in oxygen (95% of the total neutral density) : the results shown assume an O/S density ratio = 19. The O and S atmospheric species probably result from the electron-impact dissociation of SO₂. Some enrichment in O is possible and depends on the reaction path leading to complete dissociation, but such a strong enrichment would be surprising. Moreover, because oxygen atoms are more difficult to ionize (see Figure 32, Section 6.3.1) and are lighter than sulfur atoms, the plasma density and ion temperature calculated with this enriched atmosphere are not consistent with the observations.

Figure 62 and Table 4 show the composition resulting from the “Atm-SO₂+ Corona-S&O”. The center of the wake is dominated by molecular ions. The interaction depletes the impinging plasma of all atomic species and replaces them with SO₂⁺ and SO⁺. Once again, this composition is not consistent with the published one, where SO₂⁺ accounts for a mere 5% of the total composition.

		Ion mixing ratio (%)				
		Upstream		At closest approach on J0		
		Model	Published	Model		
Atmosphere	M/Q			KK-S&O O/S=2	Enriched KK-S&O O/S=19	Atm-SO ₂ + CoronaS&O O/S=2
S ⁺	32	10	30 ± 5	80	30	15
O ⁺ & S ⁺⁺	16	45 & 35	50 ± 10	20 & 3	65 & 3	4 & 1
O ⁺⁺	8	3	15 ± 5	< 0.1	< 1	< 1
S ⁺⁺⁺	10	6	NA	< 0.1	< 0.1	< 1
SO ₂ ⁺	64	0	5 ± 2	0	0	60
SO ⁺	48	0	NA	0	0	20

Table 4: Mixing ratio of different ion species at the closest approach on J0 flyby for different atmosphere scenarios, compared to the published composition of Frank et al. [1996].

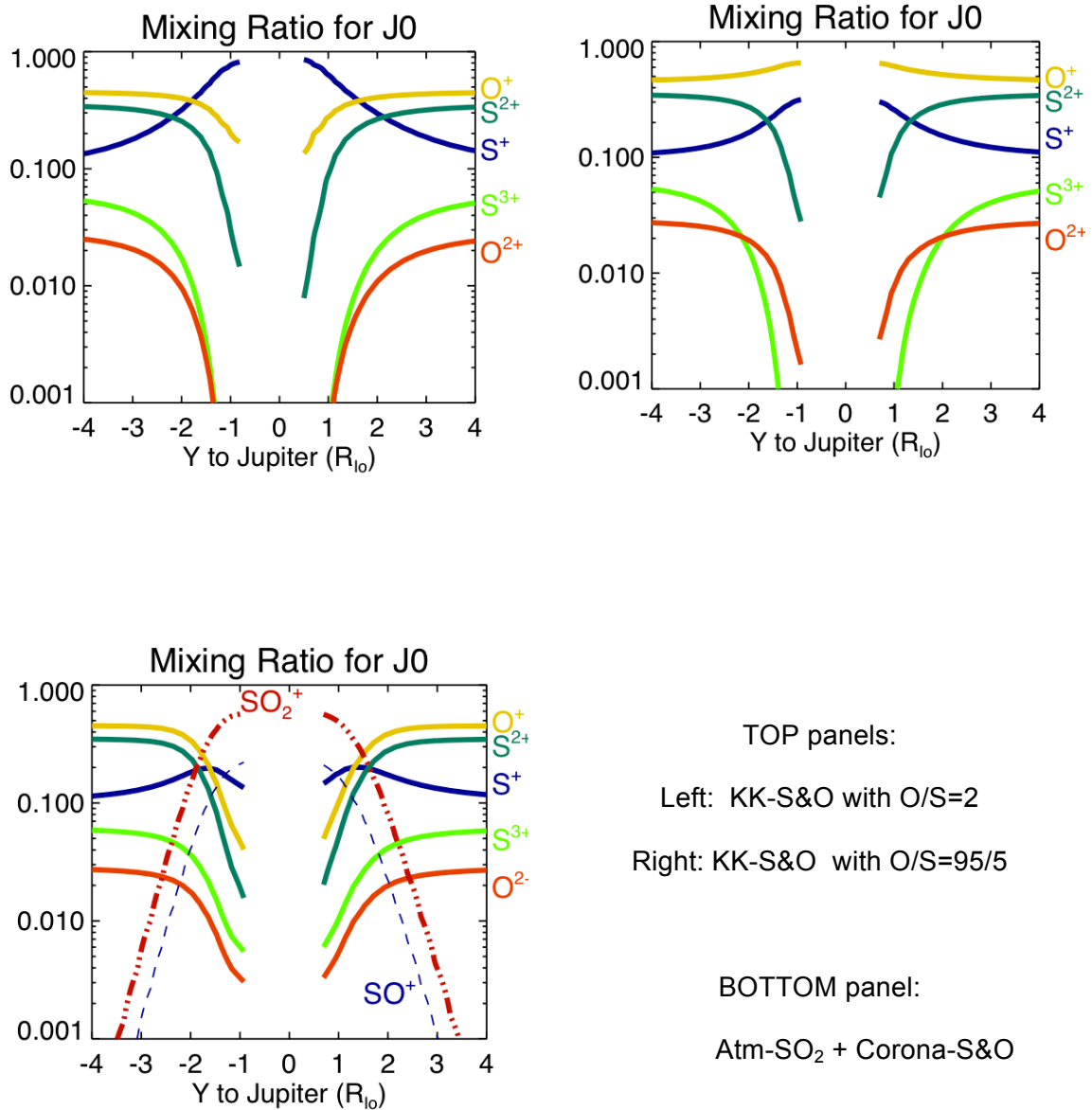


Figure 62: Mixing ratio at CA on J0 for different atmospheric scenarios listed in the bottom right panel.

The discrepancy between the composition calculated with both atmosphere scenarios and the published one may have different causes: The upstream plasma composition is time variable (*Delamere and Bagenal, 2003*) and might have been different from the one we assume here. The cross sections available might be inaccurate. For instance the ionization cross section of sulfur at 5 eV changed by a factor of ~ 10 between *Becker and Tarnovsky [1995]* and *Schreier et al. [1998]* (see fig 4 in *Delamere and Bagenal [2003]*) and the cross section for resonant charge exchange $S + S^+ \Rightarrow S^+ + S$ was re-evaluated from 29 \AA^2 to 40 \AA^2 by *McGrath and Johnson [1989]*. Another cause might simply be the interpretation of the PLS data themselves. The PLS data interpretation is difficult for several reasons: the high ion temperature in the warm torus blends the individual ion contributions in PLS measurements; the low sensitivity of the PLS instrument and the crippled spacecraft limit the completeness of the data; the non-Maxwellian nature of a pickup velocity distribution is not included in the plasma properties calculation.

Finally, the composition of the atmosphere has important consequences regarding the plasma supply to the torus. If the atmosphere is purely atomic, the ions provided by the interaction close to Io contribute directly to the plasma and energy supply to the torus. The “KK-S&O” scenario delivers $\sim 500 \text{ kg/s}$ of O and S ions to the torus. It is smaller than the canonical neutral loss rate of 1 ton/s needed to power the torus (*Delamere and Bagenal [2003]*), consistent with *Bagenal [1997]*'s analysis of the plasma flux behind Io. The rest of the mass and energy is probably provided by the giant O and S neutral clouds that extend to several R_J along the orbit of Io, but for this scenario, Io plays a direct role in the torus energetics. The hypothesis of an SO_2 atmosphere leads to radically different conclusions. Molecular ions recombine much more rapidly than atomic ions because of energy conservation consideration: the molecular recombination is followed by a rapid dissociation and the resulting neutrals can carry the extra energy of the incoming electrons. The dissociative-recombination rate of molecular ions increases when the electrons temperature is low and when the electron density is large, conditions typical of Io's wake. For example, assuming an electron temperature in the wake $\sim 1 \text{ eV}$ and a density $\sim 10,000 \text{ cm}^{-3}$, we compute a characteristic time for dissociative-recombination $\sim 1 \text{ hour}$. This recombination time is very small compared to the characteristic timescales of the torus like its rotating period ($\sim 10 \text{ hours}$), the ion energy equilibration time by coulomb collisions (several days) or the

plasma radial transport (~ 30 days). Consequently, SO_2^+ and SO^+ ions recombine, dissociate and most of them leave the torus as fast neutrals before exchanging energy with the background plasma of the torus. This implies that, in a scenario of an SO_2 atmosphere, Io provides very little mass and energy to the torus and the neutral source rate needed to power it has to be found entirely in the giant atomic clouds. The location of the ion supply to the torus is a controversial issue as reviewed by *Thomas et al. [2004]*. *Delamere and Bagenal [2003]* demonstrate that the energetics of the torus requires a pickup at corotation velocity (plus a variable contribution of hot electrons) implicitly leading to the conclusion that this pickup does not take place in the atmosphere of Io where the flow is considerably slowed, but out of the atmosphere, in the giant neutral clouds, where the flow is close to corotation.

If indeed the ions created by Io's interaction are mostly molecular, some of the most striking features of the sodium observations should be present in sulfur and oxygen as well. The fast sodium jets close to Io and the fast sodium streams all around Io's orbit result from the dissociative-recombination of sodium-bearing molecular ions (see Figure 12) (*Wilson and Schneider, 1999*). Streams and jets of S and O resulting from the dissociative recombination of SO_2^+ might be present as well. They would be more difficult to observe, as Na scatters efficiently the solar visible lines while S and O do not.

In summary, the analysis based on the chemical model presented here should motivate a re-analysis of the PLS ion composition. A contribution of this thesis is to show that the ion composition deduced from PLS observations is inconsistent with our current knowledge of the chemistry involved in the Io/Torus interaction.

10.5 Day/night asymmetry of Io's atmosphere

The I24 flyby implies an atmosphere that does not extend very far on the upstream hemisphere. It also encounters Io on its night side. In this section, we argue that the collapse of the atmosphere at night is probably not sufficient to explain the absence of interaction on I24.

The eclipse observations of Io's emission are solid support for a day/night asymmetry of the atmosphere (*Geissler et al., 1999, Retherford et al., 2007*). *Wolven et al. [2001]* observed a brightening of the O and S ultraviolet emissions of the extended

atmosphere (up to $10 R_{Io}$) after eclipse. They report that the emissions brighten by a factor 2 in the inner atmosphere ($0 < r < 2 R_{Io}$) and by 1.5 in the outer atmosphere ($2 R_{Io} < r < 4 R_{Io}$), suggesting that the outer atmosphere reacts more slowly than the inner atmosphere to a variation of solar illumination. On the modeling side, *Moore et al. [2009]* consider the atmospheric response as a function of altitude and atmospheric composition when Io enters eclipse. They show that the presence of non-condensable atmospheric species (potentially SO and O₂) form a diffusion layer near the surface that prevents rapid collapse. *Retherford [2002]* quantifies the timescales for the atmosphere collapse after ingress: ~5 minutes for the molecular atmosphere, ~ 30 minutes for the atomic atmosphere and ~280 minutes for the corona. The eclipse has a short duration while the night on Io can be locally as long as ~ 20 hours. These timescales suggest that, a priori, even the far outer atmosphere might collapse during the long night.

The J0 flyby shows a clear asymmetry of the plasma density and temperature between the night side (Jovian) of Io and the sunlit side (anti-jovian). This asymmetry may simply be interpreted as the collapse of the nightside SO₂ atmosphere. Although J0 does not sample the atmosphere directly as it is down in the wake, the plasma measurements clearly shows that the atmosphere does not collapse completely at night and is still substantial at $1.5 R_{Io}$ from Io's center. I24 and I27 inbound flybys are close to the dawn terminator and it could reasonably be argued that the sublimation atmosphere at this location is not yet fully developed because of the large local solar zenith angle. But this would not be supported by the dayside Lyman-alpha observations of *Feaga et al., 2009*, which show an absorption from limb to limb and no variation with local zenith angle. Moreover, the outbound leg of I24 that covers the upstream side of Io is clearly on the dayside and shows no sign of interaction, so the day/night asymmetry is not a sufficient explanation for the absence of interaction on this part of the flyby. In conclusion, although it is reasonable to assume that the atmosphere (inner certainly and maybe outer as well) collapses at night, J0 shows that the night outer atmosphere is still substantial at distance $\sim 1.5 R_{Io}$. The upstream atmosphere seems to be less extended than at other longitudes and the day/night asymmetry cannot be the only explanation for the plasma variations around Io.

10.6 Longitudinal asymmetry of Io's atmosphere

As the I24 flyby cannot be satisfactorily explained by a collapse of the atmosphere at night, we propose in this section that the atmosphere has a real longitudinal asymmetry.

Because Io is phase-locked in its orbit around Jupiter, longitude asymmetries could be due to either surface phenomena causing non-uniformity of the underlying atmosphere (volcanoes, frost coverage) or variations in the plasma-atmosphere interaction (upstream versus downstream, toward versus away from Jupiter). The dayside UV observations of the atmosphere strongly support a jovian/anti-jovian asymmetry of the SO₂ atmosphere: it appears denser and more extended in latitude on the anti-jovian hemisphere of Io (see Section 3.2.1). This longitudinal asymmetry might consequently be visible in the plasma interaction as well. Moreover, the observation of sodium fast jets from the anti-jovian side of Io (*Wilson and Schneider, 1999*) attributed to charge exchange in the deep anti-jovian side atmosphere of Io suggests that the interaction atmosphere/torus exhibits a jovian/anti-jovian asymmetry.

The Galileo observations discussed here suggest both an upstream/downstream and a jovian/anti-jovian asymmetry. I24 requires a less extended atmosphere upstream with a scale height smaller than ~ 60 km. J0 requires an extended atmosphere on the anti-jovian flank (scale height ~ 500 km). The I32 temperature increase far from Io implies the existence of an SO₂ corona that extends downstream to $\sim 6 R_{Io}$, which is supported by observation of ion cyclotron waves along the downstream leg of several Io flybys (*Russell et al., 2003*). There is unfortunately no daylight measurement downstream of Io on the jovian side to assess the extension of the atmosphere on this hemisphere so our discussion is limited to the downstream anti-jovian hemisphere. *Feaga et al. [2009]* claim that the SO₂ atmosphere is consistently denser and latitudinally more extended on the anti-jovian side of Io because of the asymmetry of the volcano locations. We propose that the anti-jovian downstream atmosphere is radially inflated as well. We note that the I24 downstream leg might be too far from Io to sample this quadrant. More surprisingly, this hypothetical extended atmosphere is not visible along the outbound leg of I27. This enhancement of the atmospheric density far from Io might simply be explained by the enhancement at the surface reported by *Feaga et al. [2009]* combined with diurnal variations. We would like to propose another hypothetical

explanation of this enhancement based on the observation of sodium fast jet escape from Io's atmosphere from this specific quadrant (*Wilson and Schneider, 1999*). We propose that this radial inflation of Io's atmosphere on the downstream anti-jovian far atmosphere of Io might be a natural consequence of a cascade of charge exchanges in the presence of the anti-jovian electric field in Io's orbital reference frame. Figure 10 shows a top view of the interaction of two incoming SO_2^+ ions (from the left) on "Atm- SO_2 " atmosphere of Io calculated by *Fleshman [2011]*.

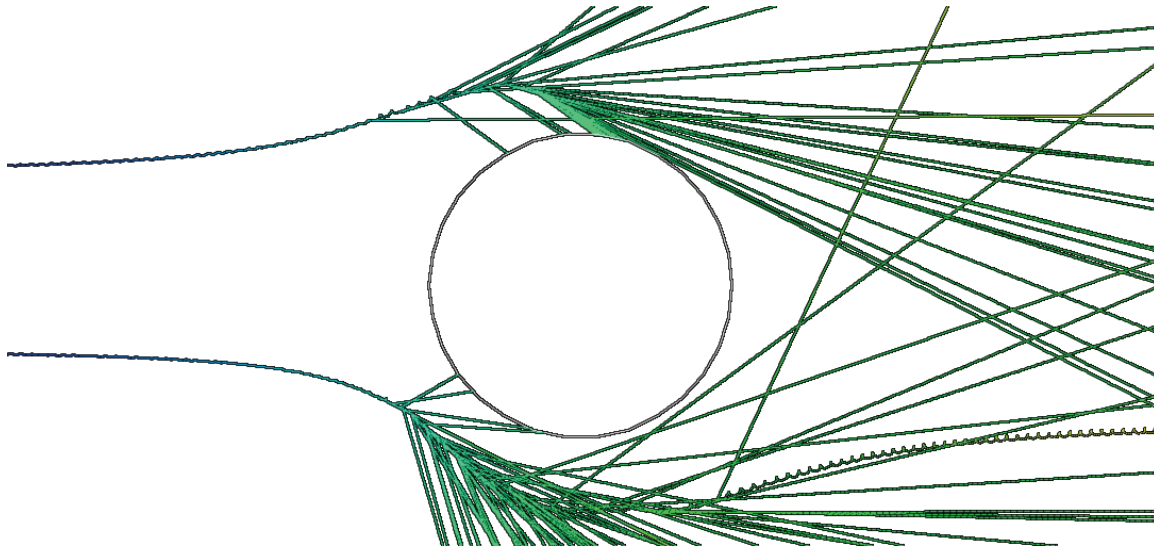


Figure 63: Two SO_2^+ ions impinging on an SO_2 atmosphere of Io. They experience a cascade of charge exchange where fast neutrals are ejected on straight paths, away from Io (Fleshman, 2011).

Jupiter is located at the top of the page. The streaming ions encounter Io's atmosphere and charge exchange with a neutral SO_2 at rest in Io's frame. The ions are suddenly neutralized and fly out of the atmosphere along straight paths with a velocity equal to the incoming ion velocity at the time of the charge exchange. In the dense part of Io's atmosphere, the charge exchange frequency $\nu_{CX} = v \times n_n \times \sigma_{CX}$ is larger than the gyro-frequency (where n_n is the neutral density, v the ion velocity, and σ_{CX} is the charge exchange cross section). This favors a charge exchange at the beginning of the gyro-cycle when the ion motion is directed toward the anti-jovian side of Io. The new ion, initially at rest in Io's frame, is picked-up by the flow and starts a gyro-motion at the local flow velocity. This new ion will later experience a new resonant charge exchange, and the cascade of charge exchanges will result in a shower of neutrals. This

preliminary simulation shows that all new neutrals are ejected downstream because of the drift velocity of the incoming ion and a larger number of neutrals are ejected in the anti-jovian direction. We suggest that this process might explain a radially extended atmosphere on the anti-jovian downstream side of Io. Any neutral ejected at the co-rotation velocity will fly rapidly out of Io's atmosphere but as the flow close to Io is strongly decelerated, some of these ions might be ejected from Io at slow velocities and might not be able to escape Io's gravitational field. The ejected neutrals may also effectively sputter the atmosphere from below (as suggested in *Wilson and Schneider, 1999*, contributing both to the SO₂ corona and the extended bound atmosphere on the anti-jovian side of Io. The idea of the charge exchange process to explain anti-jovian fast jets of sodium was originally proposed by *Schneider et al., 1991*. Na is a minor component of Io's atmosphere but the basic process is similar to the one we propose for S, O and SO₂.

An upstream/downstream asymmetry of Io's atmosphere was already proposed by *Saur et al. [2002]*. These authors prescribed an atmosphere that is compressed upstream and extended downstream because of the drag force created by the collision of the plasma and the neutral atmosphere. They support their claim based on the currents computed with their asymmetrical atmosphere and the effect of these asymmetrical currents on the magnetic field measurements upstream of Io. KK showed (and we illustrate here) that the magnetometer measurements are better explained by the presence of an induced dipole, so the magnetometer measurements are not the proper diagnostic to assess the asymmetry of the atmosphere. We claim that the ion temperature profile is a better diagnostic and we support the upstream/downstream asymmetry of the atmosphere based on our analysis of the Galileo ion temperature observations. We propose a mechanism to explain the upstream/downstream asymmetry that is not a compression/drag of the atmosphere but a natural consequence of a cascade of charge exchange.

10.7 Time variability

In this section, we discuss two flybys (I27 and J0), which trajectories intersect approximately at the same location downstream of Io. The measurements and simulation results along each flyby are very different at the crossing location. Although

Feaga et al. [2009] claim that the dayside atmosphere was mainly stable between 1997 and 2001 (which covers most of the Galileo flybys), we discuss the possibility of a time variation of the atmospheric content that may be related to a variability of Io's volcanism. We summarize our bibliographical research to assess the global volcanic activity of Io at the time of these flybys. We state from the outset that we were unable to assess consistently the global volcanic activity during GLL encounters of Io.

We note first that during the Galileo flybys of Io, the torus plasma density was comparable to the canonical Voyager torus when we consider the trajectories of the flybys in the torus structure as shown in Fig 23.18 in *Thomas et al. [2004]*, with the notable exception of J0. Compared to the Voyager epoch, the plasma density during J0 was about two times higher, modestly enhanced during I24, I25, I31 and I32 and slightly lower during I27.

We compare the J0 (Dec. 1995) and I27 (Feb. 2000) flybys. We have already discussed the 27 difficulties and speculated on the geometrical approximation of our modeling. Here we take the rhetorical view that this geometrical issue is not relevant and explore the possibility of a time variability of the interaction between Dec 1995 and Feb 2000. The two flybys sample approximately the same location in Io's wake ($X \sim 1.2 R_{Io}$, $Y \sim -1.6 R_{Io}$) as shown at the top of Figure 64 and are both close to Io's equatorial plane ($Z(J0) = -0.4 R_{Io}$; $Z(I27) = +0.4 R_{Io}$). First, we look at the GLL observations of the plasma density and average ion temperature along both flybys (bottom of Figure 64). The observations are represented by asterisks and dotted lines and the horizontal axis displays the distance to Io's center. Note that as the trajectories are different and the interaction is not spherically symmetrical, the comparison should be made only on the crossing point but we display the plasma properties on a radial distance from $1 R_{Io}$ to $3 R_{Io}$ to give a sense of the evolution along each trajectory.

The outbound leg of I27 observations shows no sign of an atmosphere/torus interaction at the crossing distance: the plasma density ($\sim 1,300 \text{ cm}^{-3}$) and average ion temperature ($\sim 100 \text{ eV}$) are comparable to the upstream values. In contrast, at the same location along the inbound leg of J0, the plasma density increases from 4,000 to 5,000 cm^{-3} while the ion temperature increases from 100 to 280 eV, which is a clear sign of an atmosphere/torus interaction. Noting that the incoming plasma density was different for J0 and I27, it might be misleading to compare the observations directly as they might depend not only on the local neutral density but on the upstream plasma density and

temperature as well. Thus, we superimpose on Figure 64 the results of our modeling for “Atm-SO₂” in solid lines for both flybys. This atmosphere hypothesis was reasonable for the downstream anti-jovian quadrant of Io’s atmosphere for J0 (Section 9.2). The density panel on the right shows that, for a similar atmosphere, the plasma density calculated at the crossing location is very dependent on the upstream plasma density. On the other hand, the model results show that the ion temperature at the crossing point is not very dependent on the incoming plasma density. Consequently, the large temperature difference observed in the data between J0 and I27 is not caused by the density of the impinging plasma but by the variation of the neutral density encountered along each flyby. This comparison, ignoring any geometrical reasons, might be interpreted as a drastic variation of the atmosphere between Dec. 1995 and Feb. 2000.

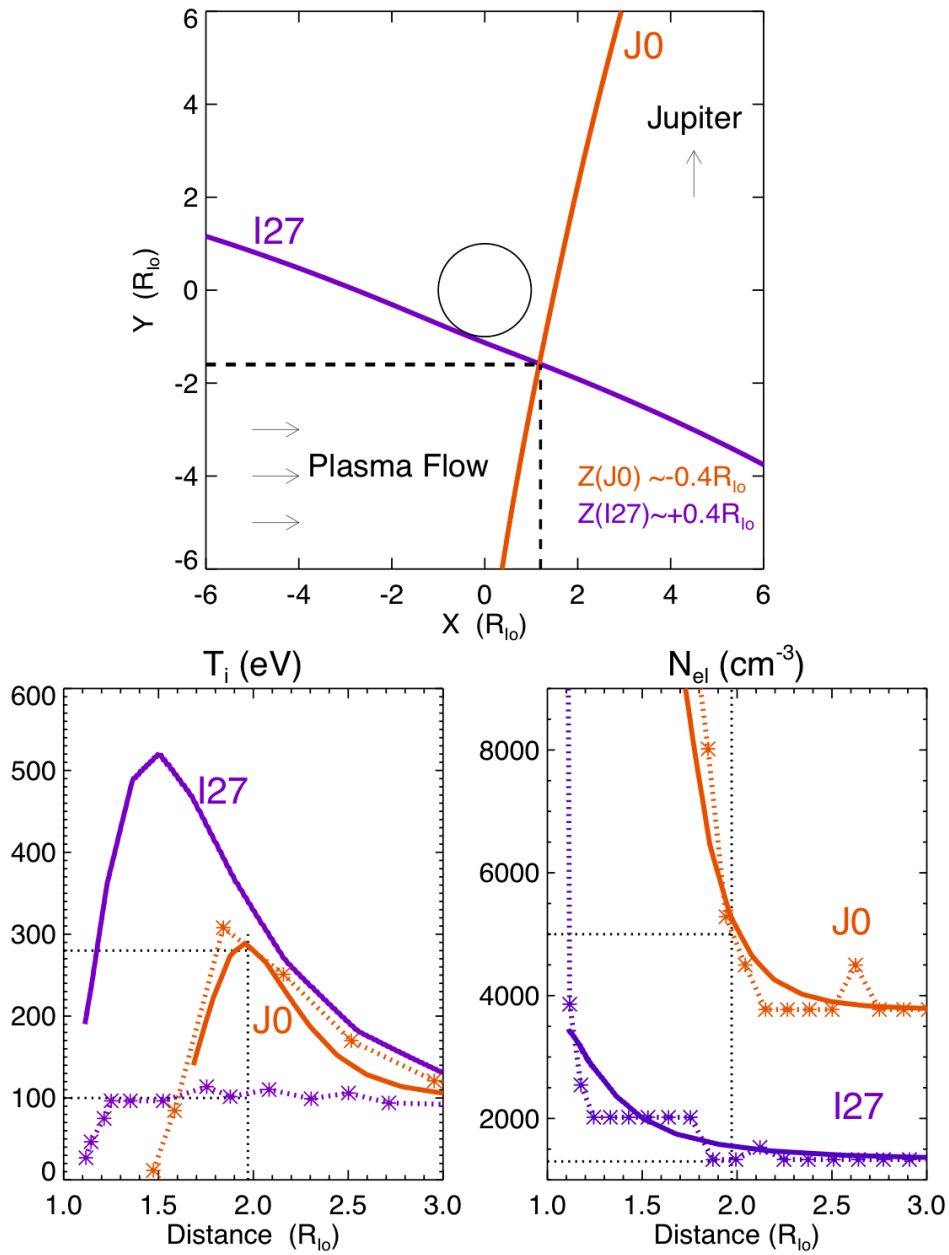


Figure 64: The comparison of the I27 and J0 flyby. Their trajectories intersect on the downstream anti-jovian hemisphere, although not at the Z altitude relative to Io's equatorial plane. On the bottom panels, we compare the observed plasma density and temperatures (dashed-star lines) with the model results (solid lines) for the "Atm-SO₂ + Corona-S&O" scenario.

Many pieces of evidence suggest that the interaction between Io's atmosphere and the torus is indeed variable in time. *Mendillo et al. [2004]* compare the brightness and global shape of the sodium nebula that extends over hundreds of jovian radii (see Figure 12). Io's volcanic activity determined from the hemispheric infrared emission. The nebula is fed by neutralization of atomic or molecular Na ions near Io and in the plasma torus and thus depends on the local interaction that we discuss here. Possible sources of sodium in the atmosphere of Io include sputtering of the Na bearing compounds on the surface or direct volcanic supply in the form of NaCl (see discussion in *McGrath et al., 2004; Lellouch et al., 2003*) They show that a bright and rectangular sodium nebula correlates with an increased volcanic activity. On the other hand, when Io's volcanic activity is low, the nebula is less bright and its shape is more diamond-like. *Mendillo et al. [2004]* convincingly demonstrate the time variability of the interaction, driven by the volcanic activity and thus the time variability of the atmospheric content. Another indication of time variability of the interaction at Io is the monitoring of dust streams by Galileo between 1996 and 2002. *Kruger et al. [2003]* calculate the Io dust emission rate from dust measurements between 13 and 30 jovian radii and show that episodes of elevated dust emission are generally in agreement with the eruption of giant plumes on Io, notably Tvashtar. Based on these dust measurements, *Delamere et al., 2004* model the plasma torus observed by Cassini between October 2000 and March 2001, which shows a significant time variability. The authors show that the torus variation can be explained if the dust emission variation is taken as a proxy of the time variation of neutral source of the torus, albeit that the neutral changes by a factor of three rather than three orders of magnitude observed for dust. Thus, a variation of the volcanic input leads to a variation of the dust in the magnetosphere and, to a lesser extent, to a variation of the atmosphere/torus interaction.

We were not able to constrain consistently the level of volcanic activity during the specific times of Galileo flybys of Io. The dust calculation of *Kruger et al. [2003]* (their Fig. 2) suggests that the I27 flyby took place during very low dust emission. A low volcanic activity might result in a thin atmosphere, and leads to a weak atmosphere/torus interaction and a low torus density.

This combination of a low torus and a thin atmosphere would reduce the importance of the charge exchange dilatation effect on the downstream anti-jovian side of Io described in Section 10.6 and could explain why I27 does not present a radially

extended atmosphere in this quadrant, in contrast to I32 and J0. The I24 and I25 flybys were also made during this period and they actually show a relatively dense torus. It is unfortunate that the I24 trajectory and the absence of ion temperature measurements on I25 do not help in constraining the downstream anti-jovian atmosphere. The sodium nebula discussion of *Mendillo et al. [2004]* unfortunately does not completely cover the Galileo epoch (except J0) but their discussion notes that the observation of a strong nebula in 1990, 1991, 1997 and 1998 were made during an eruption of a large Loki volcano and they state that Io is undoubtedly globally volcanically active on any day during a Loki eruption. Loki is a long lasting (~ 230 days) volcano and their Table 1 reports that Loki was active on November 1998. We may extrapolate that Loki was probably active one month later during the J0 flyby and that the atmosphere/torus interaction was strong, consistently with our modeling of J0. *Rathbun and Spencer [2010]* made infrared observations of volcanoes in eclipse and show that Loki was also active during the I24, I25 and I27 flybys. The argument put forth by *Mendillo et al. [2004]* says that if Loki was active during I24, I25 and I27 flybys, the plasma-atmosphere interaction should have been strong. But the Galileo plasma observations suggest that the interaction might actually have been weak so that Loki would not be a good proxy to estimate the strength of the Io/torus interaction. On the other hand, *Kruger et al. [2003]* reports low dust fluxes for the same periods. Thus the dust flux proxy of the global volcanic activity would be consistent with a low interaction during this period. This leaves us with the unsatisfying conclusion that we still lack a consistent picture of how volcanic activity on Io modifies the atmosphere, the plasma-atmosphere interaction and conditions in the torus.

11. CONCLUSIONS

The plasma interaction with Io has been a puzzle since the radio emissions first detected in the 60s. The Galileo flybys provided important constraints but left us with new puzzles. Modeling the interaction is complicated because several different pieces of physics are involved: Io's structured atmosphere, electrodynamics that modifies the field and the plasma flow, the physical chemistry of the ions and electrons interacting with the atmosphere - heating, dissociating, and ionizing atmospheric gases. Furthermore, the interaction extends well beyond the satellite - neutral clouds extending out along Io's orbit, Alfvén waves and electron beams coupling to Jupiter. We are far from developing a complete model of the interaction and must address separate components at a time.

The plasma properties along the Galileo flybys close to Io's equator have been previously modeled with reasonable success. Former models usually capture the gross features of the interaction but have inherent limitations that keep a number of issues about the interaction of Io with the plasma of the torus poorly resolved. A non-exhaustive list of these issues includes: the composition of the atmosphere, the distribution of the atmosphere in longitude, the role of electron beams in the ionization and auroral emissions in Io's atmosphere, the process of neutral escape etc. The model that we have developed addresses some of the shortcomings of previous models. It also addresses directly some of the issues listed above, pointing to directions where further research is needed.

We have developed a multi-species chemistry model that computes the change of composition, density and energy of the plasma of the torus when it encounters a prescribed atmosphere of Io. The model includes up-to-date cross sections to compute accurately the plasma production, taking into account the cooling of electrons by inelastic collisions that limits the ionization. It also computes accurately the plasma energy gain due to pickup of ions of various masses, the plasma composition, the radiative emission of the atmosphere in the oxygen 1356 Å line typical of Io's auroral emissions and the electron impact dissociation rate of SO₂. We have coupled this chemical model with a Hall-MHD model of the electromagnetic interaction, which calculates self-consistently the magnetic and plasma flow perturbations resulting from

the interaction with the atmosphere of Io. We use this model with several hypotheses about the composition and distribution of the atmosphere and compare our results with the observations made by the plasma and magnetometer instruments on board the Galileo spacecraft during five close flybys of Io.

With the coupled model, we simulate convincingly the plasma density, ion temperature, magnetic and flow perturbations along the Galileo flybys. We also compute global properties of the interaction, such as current and ion production rate. The atmospheric scenario that includes SO₂ results in a global ion production rate consistent with previous analyses published in the literature. The plasma production rate calculated with the atomic atmospheric scenario is at least two times larger than the rate deduced from the GLL/J0 observations.

We model the plasma properties for the polar flybys I31 and I32, which have never been presented in the literature before. These flybys constrain the extension of the plasma wake along the field lines to less than 1 R_{Io} from Io's equatorial plane.

We use the profiles of the average ion temperature and plasma density along each flyby as a diagnostic to constrain the longitudinal variations of the atmosphere.

We reach the following conclusions:

- 1) We conclude that the atmosphere is less extended upstream (scale height < 60 km) of Io and more extended downstream (scale height > 500 km), at least in the anti-jovian hemisphere where Galileo provided measurements. Our analysis supports the presence of an extended SO₂ corona downstream of Io and the partial collapse of Io's atmosphere at night.
- 2) We compute the plasma composition downstream of Io and show that the published composition based on the PLS measurements is inconsistent with our current knowledge of the chemistry involved in the interaction.
- 3) We show that an atmosphere dominated by SO₂ provides very little plasma and energy to the torus. We suggest that the energy supply needed to power the torus has to be provided in the giant neutral clouds of atomic O and S, which extend a few R_J along Io's orbit.
- 4) We demonstrate that ionization by the thermal plasma of the torus cannot provide the high plasma density observed in Io's wake. We show that high-energy field-

aligned electron beams observed by Galileo in the wake, on the flanks and above the poles of Io can produce this dense plasma wake.

- 5) We show that the thermal plasma of the torus cannot explain the localized UV auroral emissions observed along the flanks of Io. We suggest that the field-aligned electron beams might be responsible for these auroral emissions.
- 6) We estimate the dissociation rate of SO₂ by electron impact. If full dissociation of SO₂ is assumed, the interaction delivers ~ 1.5 tons/s of oxygen and sulfur atoms at slow speed. We suggest that this electron impact dissociation could be a significant source of neutral atoms for the S and O coronae and the giant neutral clouds that extend a few R_J along Io's orbit.
- 7) We confirm the existence of an induced dipole in the deep interior of Io. Its magnitude is ~ 300 nT at Io's surface on its magnetic equator. We demonstrate that the polar flyby I31 is crucial to assess the induced nature of this dipole because its orientation is opposite to the direction of the induced dipole during the I24 and I27 flybys.
- 8) We emphasize that the ion temperature profile along the I27 flyby on the anti-jovian flank of Io cannot be explained with this coupled model. The possible cause for this discrepancy is the time variability of Io's volcanic activity or the inaccuracy of the data analysis.
- 9) Finally, we suggest that the PLS plasma measurements should be re-analyzed based on the results presented here.

BIBLIOGRAPHY

Bagenal, F. (1994), Empirical model of the Io plasma torus: Voyager measurements, *J. Geophys. Res.*, **99**, 11043.

Bagenal, F. (1997), Ionization source near Io from Galileo wake data, *Geophys. Res. Lett.*, **24**, 2111.

Bagenal, F., T. E. Dowling, and W. B. McKinnon (2004), *Jupiter : the planet, satellites, and magnetosphere*, xi, 719 p. pp., Cambridge University Press, Cambridge, UK ; New York.

Ballester, G. E. (1989), Ultraviolet observations of the atmosphere of Io and the plasma torus Johns Hopkins Univ., Baltimore, MD.

Banks, P. M., and G. Kockarts (1973), *Aeronomy*, Part A, 14 + 430 p.; Part B, 416 + 356 p. pp., Academic Press, New York (USA).

Becker, K. H., and V. Tarnovsky (1995), Electron-impact ionization of atoms, molecules, ions and transient species, *Plasma sources science technology*, **44**, 307-315.

Bhardwaj, A., and M. Michael (1999), Monte Carlo model for electron degradation in SO₂ gas: Cross sections, Yield spectra and efficiencies, *J. Geophys. Res.*, **104**(A11), 24,713-724,728.

Bigg, E. K. (1964), Influence of the satellite Io on Jupiter's decametric emission, *Nature*, **203**, 1008.

Bonfond, B., D. Grodent, J.-C. Gérard, A. Radioti, J. Saur, and S. Jacobsen (2008), UV Io footprint leading spot: A key feature for understanding the UV Io footprint multiplicity?, *Geophys. Res. Lett.*, **35**, L05107.

Chust, T., A. Roux, W. S. Kurth, D. A. Gurnett, M. G. Kivelson, and K. K. Khurana (2005), Are Io's Alfvén wings filamented? Galileo observations, *Planetary and Space Science*, **53**, 395-412.

Clarke, J. T., J. Ajello, J. Luhmann, N. Schneider, and I. Kanik (1994), Hubble Space Telescope UV spectral observations of Io passing into eclipse, *J. Geophys. Res.*, **99**, 8387-8402.

Clarke, J. T., et al. (1996), Far-Ultraviolet Imaging of Jupiter's Aurora and the Io "Footprint", *Science*, **274**, 404.

Clarke, J. T., et al. (2002), Ultraviolet emissions from the magnetic footprints of Io, Ganymede and Europa on Jupiter, *Nature*, **415**, 997.

Combi, M. R., K. Kabin, T. I. Gombosi, and D. L. DeZeeuw (1998), Io's plasma environment during the Galileo flyby: Global three-dimensional MHD modeling with adaptive mesh refinement, *J. Geophys. Res.*, **103**, 9071.

Connerney, J. E. P. (1981), The Magnetic Field of Jupiter: A Generalized Inverse Approach, *J. Geophys. Res.*, **86**, 7679-7693.

Connerney, J. E. P., and T. Satoh (2000), The H₃⁺ ion: a remote diagnostic of the Jovian magnetosphere, *Phil. Trans. R. Soc. Lond.*, **358**, 2471.

- Delamere, P. A., D. W. Swift, and H. C. Stenbaek-Nielsen (1999), A three-dimensional hybrid code simulation of the December 1984 solar wind AMPTE release, *Geophys. Res. Lett.*, *26*, 2837–2840.
- Delamere, P. A., D. W. Swift, and H. C. Stenbaek-Nielsen (1999), A three-dimensional hybrid code simulation of the December 1984 solar wind AMPTE release, *Geophys. Res. Lett.*, *26*, 2837-+.
- Delamere, P. A., H. C. Stenbaek-Nielsen, D. W. Swift, and A. Otto (2000), Momentum transfer in the combined release and radiation effects satellite plasma injection experiments: the role of parallel electric fields, *Phys. Plasmas* *7*, 3771.
- Delamere, P. A., H. C. Stenbaek-Nielsen, and A. Otto (2002), Reduction of momentum transfer rates by parallel electric fields: a two-fluid demonstration, *Physics of Plasmas*, *9*, 3130.
- Delamere, P. A., and F. Bagenal (2003), Modeling variability of plasma conditions in the Io torus, *J. Geophys. Res.*, *109*(A10216).
- Delamere, P. A., F. Bagenal, R. Ergun, and Y.-J. Su (2003), Momentum transfer between the Io plasma wake and Jupiter's ionosphere, *J. Geophys. Res.*, *108*, 1241.
- Delamere, P. A., A. Steffl, and F. Bagenal (2004), Modeling temporal variability of plasma conditions in the Io torus during the Cassini era, *Journal of Geophysical Research (Space Physics)*, *109*, 10216.
- Delamere, P. A. (2006), Hybrid code simulations of the solar wind interaction with Comet 19P/Borrelly, *Journal of Geophysical Research (Space Physics)*, *111*(12), 217.
- Delamere, P. A. (2009), Hybrid code simulations of the solar wind interaction with Pluto, *Journal of Geophysical Research (Space Physics)*, *114*(A13), 3220.
- Dessler, A. J. (1983), *Physics of the Jovian Magnetosphere*, Cambridge University Press, Cambridge.
- Dols, V., P. A. Delamere, and F. Bagenal (2008), A multispecies chemistry model of Io's local interaction with the Plasma Torus, *Journal of Geophysical Research (Space Physics)*, *113*, 9208.
- Feaga, L. M., M. McGrath, and P. D. Feldman (2009), Io's dayside SO₂ atmosphere, *Icarus*, *201*, 570-584.
- Feldman, P. D., D. F. Strobel, H. W. Moos, K. D. Retherford, B. C. Wolven, M. A. McGrath, F. L. Roesler, R. C. Woodward, R. J. Oliverson, and G. E. Ballester (2000), Lyman-Alpha Imaging of the SO₂ Distribution on Io, *Geophys. Res. Lett.*, *27*, 1787.
- Fleshman, B. L. (2011 of Conference), The Roles of Dissociation and Velocity-Dependent Charge Exchange in Saturn's Extended Neutral Clouds, paper presented at Magnetospheres of the Outer Planets, Boston, July 11-15, 2011.
- Frank, L. A., W. R. Paterson, K. L. Ackerson, V. M. Vasyliunas, F. V. Coroniti, and S. L. Bolton (1996), Plasma observations at Io with the Galileo spacecraft, *Science*, *274*, 394.
- Frank, L. A., and W. R. Paterson (1999), Intense electron beams observed at Io with the Galileo spacecraft, *J. Geophys. Res.*, *104*, 28657.
- Geissler, P. E., A. S. McEwen, W. Ip, M. J. S. Belton, T. V. Johnson, W. H. Smyth, and A. P. Ingersoll (1999), Galileo Imaging of Atmospheric Emissions from Io, *Science*, *285*, 870-874.

- Goertz, C. K., and P. A. Deift (1973), Io's interaction with the magnetosphere, *Planet. Space Sci.*, *21*, 1399.
- Goertz, C. K. (1980), Io's interaction with the plasma torus, *J. Geophys. Res.*, *85*, 2949-2956.
- Goldreich, P., and D. Lynden-Bell (1969), Io, A Jovian unipolar inductor, *Astroph. J.*, *156*, 59.
- Grodent, D., J. H. Waite, and J.-C. Gérard (2001), A self-consistent model of the Jovian auroral thermal structure, *J Geophys Res*, *106*, 12,933-912,952.
- Gurnett, D. A., A. Persoon, and W. Kurth (2001), Electron densities near Io from Galileo plasma wave observations, *J. Geophys. Res.*, *106*, 26225.
- Hess, S. L. G., P. A. Delamere, V. Dols, B. Bonfond, and D. Swift (2010), Power transmission and particle acceleration along the Io flux tube, *Journal of Geophysical Research (Space Physics)*, *115*, 6205.
- Hinson, D. P., A. J. Kliore, F. M. Flasar, J. D. Twicken, P. J. Schinder, and R. G. Herrera (1998), Galileo radio occultation measurements of Io's ionosphere and plasma wake, *J. Geophys. Res.*
- Huddleston, D. E., R. J. Strangeway, J. Warnecke, C. T. Russell, M. G. Kivelson, and F. Bagenal (1997), Ion cyclotron waves in the Io torus during the Galileo encounter: Warm plasma dispersion analysis, *Geophys. Res. Lett*, *24*, 2143.
- Jessup, K. L., J. R. Spencer, G. E. Ballester, R. R. Howell, F. Roesler, M. Vigel, and R. Yelle (2004), The atmospheric signature of Io's Prometheus plume and anti-jovian hemisphere: evidence for a sublimation atmosphere, *Icarus*, *169*, 197-215.
- Kabin, K., M. R. Combi, T. I. Gombosi, D. L. DeZeeuw, K. C. Hansen, and K. G. Powell (2001), Io's magnetospheric interaction: an MHD model with day-night asymmetry, *Planetary and Space Science*, *49*, 337-344.
- Khurana, K. K., M. G. Kivelson, D. J. Stevenson, G. Schubert, C. T. Russell, R. J. Walker, and C. Polansky (1998), Induced magnetic fields as evidence for subsurface oceans in Europa and Callisto, *Nature*, *395*, 777-780.
- Khurana, K. K., and N. A. Tsyganenko (2002), A Global Model of Jupiter's Magnetospheric Field, *AGU Fall Meeting Abstracts*, A520+.
- Khurana, K. K., X. Jia, M. G. Kivelson, F. Nimmo, G. Schubert, and C. T. Russell (2011), Evidence of a Global Magma Ocean in Io's Interior, *Science*, *332*, 1186.
- Kivelson, M. G., K. K. Khurana, C. T. Russell, S. P. Joy, M. Volwerk, R. J. Walker, C. Zimmer, and J. A. Linker (2001), Magnetized or unmagnetized: Ambiguity persists following Galileo's encounters with Io in 1999 and 2000, *J. Geophys. Res.*, *106*, 26121-26136.
- Kruger, H., P. Geissler, M. Horanyi, A. L. Graps, S. Kempf, R. Srama, G. Moragas-Klostermeyer, R. Moissl, T. V. Johnson, and E. Grün (2003), Jovian dust streams: A monitor of Io's volcanic plume activity, *Geophys. Res. Lett*, *30*, 2101.
- Lellouch, E., D. F. Strobel, M. J. S. Belton, M. E. Summers, G. Paubert, and R. Moreno (1996), Detection of Sulfur Monoxide in Io's Atmosphere, *The Astrophysical Journal Letters*, *459*(1).

- Lellouch, E., G. Paubert, J. I. Moses, N. M. Schneider, and D. F. Strobel (2003), Volcanically emitted sodium chloride as a source for Io's neutral clouds and plasma torus, *Nature*, *421*, 45-47.
- Lellouch, E., M. A. McGrath, and K. L. Jessup (2007), Io's atmosphere, edited, pp. 231-264, Springer Praxis Books, .
- Linker, J. A., M. G. Kivelson, and R. J. Walker (1988), An MHD simulation of plasma flow past Io - Alfvén and slow mode perturbations, *Geophys. Res. Lett.*, *15*, 1311-1314.
- Linker, J. A., M. G. Kivelson, and R. J. Walker (1989), The effect of mass loading on the temperature of a flowing plasma, *Geophys. Res. Lett.*, *16*, 763-766.
- Linker, J. A., M. G. Kivelson, and R. J. Walker (1991), A three-dimensional MHD simulation of plasma flow past Io, *J. Geophys. Res.*, *96*, 21037.
- Linker, J. A., K. K. Khurana, M. G. Kivelson, and R. J. Walker (1998), MHD simulations of Io's interaction with the plasma torus, *J. Geophys. Res.*, *103*, 19867.
- Lipatov, A. S., and M. R. Combi (2006), Effects of kinetic processes in shaping Io's global plasma environment: A 3D hybrid model, *Icarus*, *180*, 412-427.
- McEwen, A. S., T. V. Johnson, D. L. Matson, and L. A. Soderblom (1988), The global distribution, abundance, and stability of SO₂, *Icarus*, *75*, 450-478.
- McGrath, M. A., and R. E. Johnson (1989), Charge exchange cross sections for the Io plasma torus, *J. Geophys. Res.*, *94*, 2677.
- McGrath, M. A., E. Lellouch, D. F. Strobel, P. D. Feldman, and R. E. Johnson (2004), Satellite atmospheres, in *Book*, edited, pp. 457-483.
- Mendillo, M., J. Wilson, J. Spencer, and J. Stansberry (2004), Io's volcanic control of Jupiter's extended neutral clouds, *Icarus*, *170*, 430-442.
- Michael, M., and A. Bhardwaj (2000), FUV emissions on Io: Role of Galileo-observed field-aligned energetic electrons, *Geophysical Research Letters* *27*(19), 3137-3140
- Moore, C. H., D. B. Goldstein, P. L. Varghese, L. M. Trafton, and B. Stewart (2009), 1-D DSMC simulation of Io's atmospheric collapse and reformation during and after eclipse, *Icarus*, *201*, 585-597.
- Moulet, A., E. Lellouch, R. Moreno, M. A. Gurwell, and C. Moore (2008), First disk-resolved millimeter observations of Io's surface and SO₂ atmosphere, *laap*, *482*, 279-292.
- Neubauer, F. M. (1980), Nonlinear standing Alfvén wave current system at Io: Theory, *J. Geophys. Res.*, *85*, 1171.
- Pearl, J., R. Hanel, V. Kunde, W. Maguire, K. Fox, S. Gupta, C. Ponnampereuma, and F. Raulin (1979), Identification of gaseous SO₂ and new upper limits for other gases on Io, *Nature*, *280*, 755.
- Piddington, J. H., and J. F. Drake (1968), Electrodynamical Effects of Jupiter's Satellite Io, *Nature*, *217*(5132), 935-937.
- Rathbun, J. A., and J. R. Spencer (2010), Ground-based observations of time variability in multiple active volcanoes on Io, *Icarus*, *209*, 625-630.
- Rees, M. H. (1989), *Physics and chemistry of the upper atmosphere*, Cambridge Univ Pr,

- Retherford, K. D. (2002), Io's aurora: HST/STIS observations, PhD thesis,
- Retherford, K. D., et al. (2007), Io's Atmospheric Response to Eclipse: UV Aurorae Observations, *Science*, *318*, 237.
- Roesler, F. L., H. W. Moos, R. J. Oliverson, R. C. W. Jr, D. K. Retherford, F. Scherb, M. A. McGrath, W. H. Smyth, P. D. Feldman, and D. F. Strobel (1999), Far UV imaging spectroscopy of Io's atmosphere with HST/STIS, *Science*, *283*, 353.
- Russell, C. T., and M. G. Kivelson (2001), Evidence for sulfur dioxide, sulfur monoxide, and hydrogen sulfide in the Io exosphere, *J. Geophys. Res.*, *106*(33), 267–233.
- Russell, C. T., X. Blanco-Cano, Y. L. Wang, and M. G. Kivelson (2003), Ion cyclotron waves at Io: Implications for the temporal variation of Io's atmosphere, *Planet. Space Sci.*, *51*(14-15), 937-944.
- Saur, J., F. M. Neubauer, D. F. Strobel, and M. E. Summers (1999), Three-dimensional plasma simulation of Io's interaction with the Io plasma torus: Asymmetric plasma flow, *J. Geophys. Res.*, *104*, 25105-25126.
- Saur, J., F. M. Neubauer, D. F. Strobel, and M. E. Summers (2000), Io's ultraviolet aurora: Remote sensing Io's interaction, *Geophys. Res. Lett.*, *27*, 2893.
- Saur, J., F. M. Neubauer, D. F. Strobel, and M. E. Summers (2002), Interpretation of Galileo's Io plasma and field observations: I0, I24, and I27 flybys and close polar passes, *Journal of Geophysical Research (Space Physics)*, *107*, 5-1.
- Saur, J., D. F. Strobel, F. M. Neubauer, and M. E. Summers (2003), The ion mass loading rate at Io, *Icarus*, *163*, 456-468.
- Saur, J., F. M. Neubauer, J. E. P. Connerney, P. Zarka, and M. G. Kivelson (2004), Plasma interaction of Io with its plasma torus, in *Book*, edited, pp. 537-560.
- Saur, J., and D. F. Strobel (2004), Relative contributions of sublimation and volcanoes to Io's atmosphere inferred from its plasma interaction during solar eclipse, *Icarus*, *171*, 411-420.
- Schneider, N. M., J. K. Wilson, J. T. Trauger, D. I. Brown, R. W. Evans, and D. E. Shemansky (1991), Molecular origin of Io's fast sodium, *Science*, *253*, 1394-1397.
- Schreier, R., A. Eviatar, and V. M. Vasylunas (1998), A two-dimensional model of plasma transport and chemistry in the Jovian magnetosphere, *J. Geophys. Res.*, *103*, 19,901-919,913.
- Shemansky, D. E., and B. R. Sandel (1980), Radial Dependence of the Io Plasma Torus Spectrum in the EUV, *Bulletin of the American Astronomical Society*, *12*, 674.
- Sittler, E. C., and D. F. Strobel (1987), Io plasma torus electrons: Voyager 1, *J. Geophys. Res.*, *92*, 5741.
- Spencer, J. R., E. Lellouch, M. J. Richter, M. A. López-Valverde, K. Lea Jessup, T. K. Greathouse, and J.-M. Flaud (2005), Mid-infrared detection of large longitudinal asymmetries in Io's SO₂ atmosphere, *Icarus*, *176*, 283-304.
- Spencer, J. R., et al. (2007), Io Volcanism Seen by New Horizons: A Major Eruption of the Tvashtar Volcano, *Science*, *318*(5848), 240-243
- Strobel, D. F., and B. C. Wolven (2001), The Atmosphere of Io: Abundances and Sources of Sulfur Dioxide and Atomic Hydrogen, *Apss*, *277*, 271-287.

- Strobel, D. F., X. Zhu, and M. F. Summers (1994), On the vertical thermal structure of Io's atmosphere, *Icarus*, *111*, 18-30.
- Swift, D. W. (1995), Use of a hybrid code to model the Earth's Magnetosphere, *Geophys. Res. Lett.*, *22*, 311.
- Swift, D. W. (1996), Use of a hybrid code for Global-scale plasma simulation, *J. Comput. Phys.*, *126*, 109.
- Thomas, N., F. Bagenal, T. W. Hill, and J. K. Wilson (2004), The Io neutral clouds and plasma torus, in *Jupiter. The planet, satellites and magnetosphere*, edited by T. E. D. Fran Bagenal, William B. McKinnon. , pp. 561-591, Cambridge planetary science,, Cambridge, UK.
- Tsang, C. C., J. R. Spencer, E. Lellouch, M. J. Richer, M. A. Lopez-Valverde, and T. K. Greathouse (2010 of Conference), Density and temperature of Io's atmosphere from Mid-infrared observations, 2001 to 2010: continued evidence for inflation as perihelion approaches, paper presented at American Astronomical Society, DPS meeting
- Vatti Palle, P., and J. Ajello (2004), High-resolution far ultraviolet spectrum of electron-excited SO₂, *J. Geophys. Res.*, *109*, A02310.
- Walker, A. C., S. L. Gratiy, D. B. Goldstein, C. H. Moore, P. L. Varghese, L. M. Trafton, D. A. Levin, and B. Stewart (2010), A comprehensive numerical simulation of Io's sublimation-driven atmosphere, *Icarus*, *207*(1), 409-432.
- Williams, D. J., B. Mauk, R. E. McEntire, E. C. Roelof, S. M. Krimigis, T. P. Armstrong, B. Wilken, J. G. Roederer, T. A. Fritz, and L. J. Lanzerotti (1996), Energetic Electron Beams Measured at Io, *Bulletin of the American Astronomical Society*, *28*, 1055.
- Wilson, J. K., and N. M. Schneider (1999), Io's sodium directional feature: Evidence for ionospheric escape, *J. Geophys. Res.*, *104*, 16567-16584.
- Wolven, B. C., H. W. Moos, K. D. Retherford, P. D. Feldman, D. F. Strobel, W. H. Smyth, and F. L. Roesler (2001), Emission profiles of neutral oxygen and sulfur in Io's exospheric corona, *J. Geophys. Res.*, *106*, 26155.
- Wong, M. C., and R. E. Johnson (1996), A three-dimensional azimuthally symmetric model atmosphere for Io 1. Photochemistry and the accumulation of a nightside atmosphere, *J. Geophys. Res.*, *101*, 23243-23060.